

INMATEH -

**AGRICULTURAL
ENGINEERING**

JANUARY - APRIL

No liability is assumed by the editorial staff for the content of scientific papers and opinions published in this volume. They represent the author's point of view

Editorial

The National Institute of Research-Development for Machines and Installations designed to Agriculture and Food Industry - INMA Bucharest has the oldest and most prestigious research activity in the field of agricultural machinery and mechanizing technologies in Romania.

Short History

- ✓ *In 1927, the first research Center for Agricultural Machinery in Agricultural Research Institute of Romania - ICAR (Establishing Law was published in O.D. no. 97/05.05.1927) was established;*
- ✓ *In 1930, was founded The Testing Department of Agricultural Machinery and Tools by transforming Agricultural Research Centre of ICAR- that founded the science of methodologies and experimental techniques in the field (Decision no. 2000/1930 of ICAR Manager - GHEORGHE IONESCU ȘIȘEȘTI);*
- ✓ *In 1952, was established the Research Institute for Mechanization and Electrification of Agriculture - ICMA Băneasa, by transforming the Department of Agricultural Machines and Tools Testing;*
- ✓ *In 1979, the Research Institute of Scientific and Technological Engineering for Agricultural Machinery and Tools - ICSITMUA was founded - subordinated to Ministry of Machine Building Industry - MICM, by unifying ICMA subordinated to MAA with ICPMA subordinated to MICM;*
- ✓ *In 1996 the National Institute of Research-Development for Machines and Installations designed to Agriculture and Food Industry - INMA was founded - according to G.D. no.1308/25.11.1996, by reorganizing ICSITMUA, G.D no. 1308/1996 coordinated by the Ministry of Education and Research G.D. no. 823/2004;*
- ✓ *In 2008 INMA has been accredited to carry out research and developing activities financed from public funds under G.D. no. 551/2007, Decision of the National Authority for Scientific Research - ANCSno. 9634/2008.*

As a result of widening the spectrum of communication, dissemination and implementation of scientific research results, in 2000 was founded the institute magazine, issued under the name of SCIENTIFIC PAPERS (INMATEH), ISSN 1583 – 1019.

*Starting with volume 30, no. 1/2010, the magazine changed its name to INMATEH - *Agricultural Engineering*, appearing both in print format (ISSN 2068 - 4215), and online (ISSN online: 2068 - 2239). The magazine is bilingual, being published in Romanian and English, with a rhythm of three issues / year: January-April, May-August, September-December and is recognized by CNSIS - with B⁺ category. Published articles are from the field of AGRICULTURAL ENGINEERING: technologies and technical equipment for agriculture and food industry, ecological agriculture, renewable energy, machinery testing, environment, transport in agriculture etc. and are evaluated by specialists inside the country and abroad, in mentioned domains.*

*Technical level and performance processes, technology and machinery for agriculture and food industry increasing, according to national requirements and European and international regulations, as well as exploitation of renewable resources in terms of efficiency, life, health and environment protection represent referential elements for the magazine „INMATEH - *Agricultural Engineering*”.*

We are thankful to all readers, publishers and assessors.

Editor in chief,

Ph. D. Eng. Vladut Nicolae-Valentin

Managing Editorial Board - INMA Bucharest**Editor in Chief****VLADUȚ Nicolae-Valentin**

General Manager, Ph.D.Eng, SR I

E-mail: inmatehjournal@gmail.com**Executive Editor****POPA Lucreția**

Ph.D.Eng, SR I

Assistant Editor**MATACHE Mihai-Gabriel**

Ph.D.Eng, SR I

Logistic support, database**MURARU Virgil, Ph.D.Eng, SR I****ȚICU Tania, techn.****Scientific Secretary****Cârdei Petre, math.****Official translators****RADU Daniela-Cristina, Prof.English, French****Editorial Board**

- Acad. Prof. Ph.D. TABĂRA Valeriu - Romania, President of ASAS - Academy of Agricultural and Forestry Sciences "Gheorghe Ionescu Șişești";
- Ph.D. BOGOESCU Marian - Romania, Vicepresident of ASAS - Academy of Agricultural and Forestry Sciences "Gheorghe Ionescu Șişești";
- Hon.Prof.Ph.D.Eng. PIRNA Ion - Romania, President of the Department of Agricultural Mechanization of ASAS - Academy of Agricultural and Forestry Sciences "Gheorghe Ionescu Șişești";
- Ph.D. Eng. NICOLESCU C. Mihai - Romania, Scientific General Secretary of the ASAS-Academy of Agricultural and Forestry Sciences "Gheorghe Ionescu Șişești";
- Assoc.Prof. Ph.D. Eng. BELC Nastasia - Romania, IBA Bucharest;
- Ph.D. Eng. BUȚU Alina - Romania, INSB Bucharest;
- Prof. Ph.D. Eng. PARASCHIV Gigel - Romania, P.U. Bucharest;
- Prof. Ph.D.Eng. BIRIȘ Sorin - Romania, P.U. Bucharest;
- Prof. Ph.D. Eng. VLASE Sorin - Romania, "Transilvania" University Brașov;
- Prof. Ph.D.Eng. BURNETE Nicolae - Romania, Technical University Cluj Napoca;
- Prof. Ph.D. Eng. FILIP Nicolae - Romania, Technical University Cluj Napoca;
- Prof. Ph.D. Eng. VOICU Gheorghe - Romania, P.U. Bucharest;
- Prof. Ph.D. Eng. GERGEN Iosif - Romania, USAMVB Timișoara;
- Prof. Ph.D. Eng. ȚENU Ioan - Romania, USAMV Iași;
- Assoc.Prof.Ph.D.Eng. BUNGESCU Sorin - Romania, USAMVB Timișoara;
- Prof. Ph.D.Eng. FENYVESI László - Hungary, Hungarian Institute of Agricultural Engineering Godolo;
- Assist.Prof.Ph.D.Eng. BILANDZIJIA Nikola - Croatia, University of Zagreb;
- Ph.D. BIOCCA Marcello - Italy Agricultural Research Council, Agricultural Engineering Research Unit;
- Prof.Ph.D.Eng. MIHAILOV Nikolay - Bulgaria, University of Rousse;
- Assoc.Prof.Ph.D.Eng. ATANASOV At. - Bulgaria, University of Rousse;
- Assoc.Prof. Ph.D. ERTEKIN Can - Turkey, Akdeniz University Antalya;
- Prof. Ph.D.Sc. Eng. VARTUKAPTEINIS Kaspars - Latvia, Latvia University of Agriculture, Institute of Agricultural Machinery;
- ir. HUYGHEBAERT Bruno - Belgium, Walloon Agricultural Research Center CRA-W;
- Prof.Ph.D. Eng. FABBRO Dal Inacio Maria - Brazil, Campinas State University;
- Prof. Ph.D. Eng. DE WRACHIEN Daniele - Italy, State University of Milan;
- Prof. Ph.D.Guanxin YAO - P.R.China, Along Agriculture R&D Technology and Management Consulting Co., Ltd;
- Prof. Ph.D. Eng. GONZÁLEZ Omar - Republic of Cuba, Central University "Marta Abreu" de las Villas;
- Assist. Prof.Dr. KABAŞ Önder –Turkey, Akdeniz University.
- Asist.Prof.Dr. SELVİ Kemal Çağatay - Turkey, Ondokuz Mayıs University.

In the present, *INMATEH - Agricultural Engineering* journal is indexed in the next international databases:
 ELSEVIER /SciVerse SCOPUS, CLARIVATE ANALYTICS' WEB OF SCIENCE- Emerging Sources Citation Index (ESCI),
 ULRICHS Web: Global Serials Directory, CABI, SCPIO, Index COPERNICUS International,
 EBSCO Publishing, Elektronische Zeitschriftenbibliothek

INMATEH - Agricultural Engineering**vol. 54, no.1 / 2018**

NATIONAL INSTITUTE OF RESEARCH-DEVELOPMENT FOR MACHINES AND
 INSTALLATIONS DESIGNED TO AGRICULTURE AND FOOD INDUSTRY -
 INMA Bucharest

6 Ion Ionescu de la Brad Blvd., sector 1, Bucharest

Three issues per year,
 e-ISSN: 2068 – 2239
 p-ISSN: 2068 – 4215

Edited by: INMA Bucharest

Copyright: INMA Bucharest / Romania

CONTENT

		Pag.
1.	<p>ASPECTS REGARDING THE COMPRESSION RESISTANCE OF GEOSYNTHETICS USED IN BUILDING MUNICIPAL SOLID WASTE LANDFILLS / ASPECTE PRIVIND REZISTENȚA LA COMPRESIUNE A GEOSINTETICELOR UTILIZATE ÎN CONSTRUCȚIA DEPOZITELOR DE DEȘEURI MUNICIPALE</p> <p>Prof. Ph.D. Eng. Voicu Gh.^{*1)}, As. Ph.D. Eng. Toma M.L.¹⁾, Lect. Ph.D. Eng. Tudor P.¹⁾, Lect. Ph.D. Eng. Ipate G.¹⁾, Ph.D.Stud. Ștefan V.²⁾</p> <p>¹⁾University "Politehnica" of Bucharest, Faculty of Biotechnical Systems Engineering/Romania; ²⁾ National Institute of Research - Development for Machines and Installations Designed to Agriculture and Food Industry - INMA Bucharest</p>	7
2.	<p>JUSTIFICATION OF RATIONAL PARAMETERS OF A PNEUMOCONVEYOR SCREW FEEDER / ОБГРУНТУВАННЯ РАЦІОНАЛЬНИХ ПАРАМЕТРІВ ЖИВИЛЬНИКА ПНЕВМО-ШНЕКОВОГО ТРАНСПОРТЕРА</p> <p>Prof. Ph.D. Eng. Baranovsky V.M.¹⁾, Prof. Ph.D. Eng. Hevko R.B.²⁾, Assoc. Prof. Ph.D. Eng. Dzyura V.O.¹⁾, Ph.D. Eng. Klendii O.M.³⁾, Assoc. Prof. Ph.D. Eng. Klendii M.B.³⁾, Eng. Romanovsky R.M.¹⁾</p> <p>¹⁾Ternopil Ivan Pul'uj National Technical University; ²⁾Ternopil National Economical University / Ukraine; ³⁾Separated Subdivision of National University of Life and Environmental Sciences of Ukraine Berezhanly Agrotechnical Institute / Ukraine</p>	15
3.	<p>ENGINEERING MANAGEMENT OF VIBRATING MACHINES FOR TARGETED MECHANICAL ACTIVATION OF PREMIX COMPONENTS / ІНЖЕНЕРНИЙ МЕНЕДЖМЕНТ ВІБРАЦІЙНИХ МАШИН ДЛЯ ЦІЛЬОВОЇ МЕХАНОАКТИВАЦІЇ КОМПОНЕНТІВ ПРЕМІКСУ</p> <p>Assoc. Prof. Ph. D. Eng. Yanovych V., Assoc. Prof. Ph. D. Econ. Honcharuk T., Assoc. Prof. Ph. D. Econ. Honcharuk I., Assoc. Prof. Ph.D. Ped. Kovalova K.</p> <p>Vinnitsia National Agrarian University, Vinnitsia / Ukrainian</p>	25
4.	<p>EFFECTS OF MATURITY TIME ON SOME MECHANICAL PROPERTIES OF BEEF TYPE TOMATO FOR TRANSPORTATION / TAŞIMA İÇİN OLGUNLAŞMA ZAMANIN BEEF TİPİ DOMATESİN BAZI MEKANİK ÖZELLİKLERİ ÜZERİNE ETKİSİ</p> <p>Ph.D. Kabaş O.^{*1)}, Ph. D. Eng. Kabaş A.²⁾, Ph.D. Ünal İ.¹⁾</p> <p>¹⁾Akdeniz University, Vocational School of Technical Science, Machinery Department / Turkey ²⁾Akdeniz University, Vocational School of Technical Science, Department of Organic Farming / Turkey</p>	33
5.	<p>VERIFICATION OF STRESS BY FEM ANALYSIS / MECHANICAL TESTING OF AGRICULTURAL MOBILE AGGREGATES COUPLING DEVICES / VERIFICAREA SOLICITĂRILOR PRIN ANALIZA MEF / TESTAREA MECANICĂ A DISPOZITIVELOR DE CUPLARE ALE AGREGATELOR AGRICOLE MOBILE</p> <p>Phd. Eng. Vlăduț V.¹⁾, Prof.PhD.Eng. Maican E.²⁾, PhD.Eng. Apostol L.³⁾, Lect. PhD. Eng.Ungureanu N.²⁾, Eng. Dumitru I.¹⁾, Eng. Oprescu R.¹⁾</p> <p>¹⁾INMA Bucharest / Romania; ²⁾University "POLITEHNICA" Bucharest / Romania; ³⁾IBA Bucharest / Romania</p>	39
6.	<p>WIRELESS MEASUREMENT AND CONTROL SYSTEM OF CARBON DIOXIDE USING INFRARED SENSOR IN GREENHOUSE ENVIRONMENT / 基于红外传感器的温室二氧化碳无线监测和控制系统的研制</p> <p>Ph.D. Bin Li¹⁾, Stud. Jitong Wang¹⁾, Prof. Yao-Dan Chi¹⁾, Prof. Xiaotian Yang^{*1)}, Prof. Yiding Wang²⁾</p> <p>¹⁾ Institute of Electrical & Computer, Jilin Jianzhu University, Changchun 130012 / China ²⁾ State Key Laboratory on Integrated Optoelectronics, College of Electronic Science and Engineering, Jilin University / China</p>	47
7.	<p>SOLAR THERMAL SYSTEM SIMULATION OF PEANUT DRYING DEVICE BASED ON TRNSYS / 基于 TRNSYS 的花生干燥装置太阳能集热系统研究</p> <p>As. M.S.Stud. Eng. Chao Wang^{1,2)}, M.S.Stud. Eng. GuoLiang Zhang^{1,2)}, M.S.Stud. Eng. Liu Yang^{1,2)}, A/Prof. M.S. Eng. ChuanYang Zhang^{*1,2)}</p> <p>¹⁾ Mechanical & Electronic Engineering, Shandong Agricultural University, Taian / China; ²⁾ Shandong Provincial Key Laboratory of Horticultural Machinery and Equipment, Shandong Agricultural University, Taian / China</p>	55

		Pag.
8.	<p>ANALYTICAL RESEARCH RESULTS OF THE COMBINED ROOT DIGGER / РЕЗУЛЬТАТИ АНАЛІТИЧНИХ ДОСЛІДЖЕНЬ КОМБІНОВАНОГО КОПАЧА КОРЕНЕПЛОДІВ As. Prof. Ph.D. Eng. Herasymchuk H. A.¹⁾, Prof. Ph.D. Eng. Baranovsky V. M.²⁾, As. Prof. Ph.D. Eng. Herasymchuk O. O.¹⁾, Ph.D. Eng. Pastushenko A.S.³⁾ ¹⁾ Lutsk National Technical University, Lvivska str., 75, Lutsk / Ukraine ²⁾ Ternopil Ivan Puluj National Technical University, Ruska str., 56, Ternopil / Ukraine ³⁾ Mykolayiv National Agrarian University, Georgiy Gongadze str., 9, Mykolaiv / Ukraine</p>	63
9.	<p>DESIGN AND TEST OF AN ALL FEED AXIAL FLOW SAME DIAMETER DIFFERENTIAL SPEED THRESHER / 全喂入纵轴流同径不同速脱粒分离装置设计与试验 Prof. M.S. Wang Jinshuang¹⁾, Prof. Ph.D. Li Hua²⁾, P.G. Yuan Jianbo³⁾, Prof. M.S. Ma Guang^{1*)}, Prof. M.S. Xiong Yongsen¹⁾ ¹⁾ Jinhua Polytechnic, Jinhua / China; ²⁾ College of Engineering, Nanjing Agricultural University, Nanjing / China; ³⁾ Nanjing Tech University, Nanjing / China</p>	73
10.	<p>INFLUENCE OF TECHNOLOGICAL PARAMETERS OF PSEUDOFUIDIZED LAYER GRAIN DRYER ON THE GRAIN DRYING QUALITY / ВЛИЯНИЕ ТЕХНОЛОГИЧЕСКИХ ПАРАМЕТРОВ ЗЕРНОСУШИЛКИ ПСЕВДООЖИЖЕННОГО СЛОЯ НА КАЧЕСТВО СУШКИ ЗЕРНА Prof. Ph.D. Eng.Sc. Kuznetsov Y.A.¹⁾, Assoc. Prof. D.Eng.Sc. Volzhentsev A.V.¹⁾, Prof. Ph.D. Eng.Sc. Kolomeichenko A.V.¹⁾, Prof. Ph.D. Phil.Sc. Kalashnikova L.V.²⁾ ¹⁾ Orel State Agrarian University "N.V. Parakhin" / Russia ²⁾ Orel State University "I.S. Turgenev" / Russia</p>	81
11.	<p>THEORETICAL RESEARCHES OF COOLING PROCESS REGULARITY OF THE GRAIN MATERIAL IN THE LAYER / ТЕОРЕТИЧНІ ДОСЛІДЖЕННЯ ЗАКОНОМІРНОСТЕЙ ПРОЦЕСУ ОХОЛОДЖЕННЯ ЗЕРНОВОГО МАТЕРІАЛУ В ШАРІ Prof. Ph.D. Kotov B.I.¹⁾, Ph.D. Spirin A.B.¹⁾, Ph.D. Tverdokhlib I.V.¹⁾, Ph.D. Polyevoda Y.A.¹⁾, Ph.D. Hryshchenko V.O.²⁾, Ph.D. Kalinichenko R.A.²⁾ ¹⁾ Vinnytsia National Agrarian University / Ukraine</p>	87
12.	<p>MODELING OF MECHANICAL AND TECHNOLOGICAL PROCESSES OF THE AGRICULTURAL INDUSTRY / МОДЕЛЮВАННЯ МЕХАНІЧНИХ ТА ТЕХНОЛОГІЧНИХ ПРОЦЕСІВ СІЛЬСЬКОГОСПОДАРСЬКОЇ ПРОМИСЛОВОСТІ Ph.D. Aliev E.B.¹⁾, Ph.D. Bandura V.M.²⁾, Ph.D. Pryshliak V.M.²⁾, Ph.D. Yaropud V.M.²⁾, Ph.D. Trukhanska O.O.²⁾ ¹⁾ Institute of Oilseed Crops of the NAAS / Ukraine, ²⁾ Vinnitsa National Agrarian University / Ukraine</p>	95
13.	<p>MODELLING OF THE HYDRO-MECHANICAL MIXER PARAMETERS / МОДЕЛЮВАННЯ ПАРАМЕТРІВ ГІДРОМЕХАНІЧНОЇ МІШАЛКИ Doctor of technical sciences Golub G.A.¹⁾, Doctor of technical sciences Kukharets S.M.²⁾, Ph.D. Eng. Chuba V.V.¹⁾, Ph.D. Eng. Pavlenko M.Y.¹⁾, Ph.D. Eng. Yarosh Y.D.²⁾ ¹⁾ National University of Life and Environmental Sciences of Ukraine / Ukraine, ²⁾ Zhytomyr National Agroecological University / Ukraine</p>	105
14.	<p>THE LONG-TERM ASSESSMENT OF MISCANTHUS × GIGANTHEUS CULTIVATION IN THE FOREST-STEPPE ZONE OF UKRAINE / БАГАТОРІЧНА ОЦІНКА ВИРОЩУВАННЯ MISCANTHUS × GIGANTHEUS У ЛІСОСТЕОВІЙ ЗОНІ УКРАЇНИ Dr. Ph.D. Biol.Sci.Kvak V.¹⁾, Assoc. Prof. Ph.D. Biol.Sci.Stefanovska T.²⁾, Prof. Ph.D. Biol.Sci. Pidlisnyuk V.³⁾, Ph.D. Stud. Alasmay Z.⁴⁾, Prof. Ph.D. Agri.Sci. Kharytonov M.⁵⁾ ¹⁾ Institute of Bioenergy Crops and Sugar Beets of the NAAS of Ukraine ; ²⁾ National University of Life and Environmental Sciences of Ukraine; ³⁾ Jan Evangelista Purkyně University in Ústí nad Labem; ⁴⁾ Kansas State University; ⁵⁾ Dnipro State Agrarian and Economic University</p>	113
15.	<p>OPTIMIZATION OF THE WORKING PERFORMANCE OF HALF-FEEDING PEANUT PICKING DEVICE BASED ON RESPONSE SURFACE METHODOLOGY / 基于响应曲面法的半喂入式花生摘果装置作业性能优化 Prof. Ph.D. Hu Z.C.^{*)}, Prof. Ph.D. LV X.L.²⁾, A.Prof. M.S. Peng B.L.¹⁾, A.Prof. M.S. Wu F.¹⁾, M.S. Yu Z.Y.¹⁾ ¹⁾ Nanjing Research Institute for Agricultural Mechanization Ministry of Agriculture, Nanjing/China ²⁾ Colleges of Machinery and Automotive Engineering, Chuzhou University Anhui / China</p>	121

		Pag.
16.	<p>RESEARCH ON THE PHOTOELECTRONIC SEPARATOR SEED SUPPLY BLOCK FOR OIL CROPS / ДОСЛІДЖЕННЯ БЛОКА П ОДАЧІ ФОТОЕЛЕКТРОННОГО СЕПАРАТОРА НАСІННЯ ОЛІЙНИХ КУЛЬТУР</p> <p>Prof. Ph.D. Eng. Shevchenko I.A, Ph.D. Eng. Aliev E.B. Institute of Oilseed Crops NAAS, Zaporizhzhia / Ukraine</p>	129
17.	<p>RESEARCH ON THE TURNING ABILITY OF A TWO- MACHINE AGGREGATE / ИССЛЕДОВАНИЕ РАЗВОРАЧИВАЕМОСТИ ПОСЕВНОГО ДВУХМАШИННОГО АГРЕГАТА</p> <p>Prof. Ph.D. Eng. Bulgakov V.¹⁾, Ph.D. Eng. Ivanovs S.²⁾, Prof. Ph.D. Eng. Nadykto V.³⁾, Ph.D. Eng. Kuvachov V.³⁾, Ph.D. Eng. Masalabov V.³⁾</p> <p>¹⁾National University of Life and Environmental Sciences of Ukraine / Ukraine, ²⁾Latvia University of Agriculture / Latvia; ³⁾Tavria State Agrotechnological University / Ukraine</p>	139
18.	<p>DEVELOPMENT OF SCIENTIFIC FOUNDATIONS OF INNOVATIVE TECHNOLOGIES FOR PRODUCTION OF BEST FIBERS FOR SPECIAL PURPOSES / РАЗРАБОТКА НАУЧНЫХ ОСНОВ ИННОВАЦИОННЫХ ТЕХНОЛОГИЙ ДЛЯ ПОЛУЧЕНИЯ ЛУБЯНЫХ ВОЛОКОН ЦЕЛЕВОГО НАЗНАЧЕНИЯ</p> <p>Ph.D. Researcher Kruglyj D.,¹⁾ Ph.D. doctoral student Boyko G.,²⁾ Prof. Ph.D. Eng. Klevtsov K.²⁾,</p> <p>¹⁾Kherson National Technical University, Department of Scientific Research, Kherson / Ukraine; ²⁾Kherson National Technical University, Faculty of Integrated Technologies & Commodity Science / Ukraine</p>	147
19.	<p>DEVELOPMENT OF A PNEUMATIC SCREW CONVEYER DESIGN AND SUBSTANTIATION OF ITS PARAMETERS / РОЗРОБКА КОНСТРУКЦІЇ ПНЕВМО-ШНЕКОВОГО ТРАНСПОРТЕРА ТА ОБГРУНТУВАННЯ ЙОГО ПАРАМЕТРІВ</p> <p>Prof. Ph.D. Eng. Hevko R.B.¹⁾, Prof. Ph.D. Eng. Strishenets O.M.²⁾, Prof. Ph.D. Eng. Lyashuk O.L.³⁾, Assoc. Prof. Ph.D. Eng. Tkachenko I.G.³⁾, Assoc. Ph.D. Eng. Klendii O.M.⁴⁾, Assoc. Prof. Ph.D. Eng. Dzyura V.O.³⁾,</p> <p>¹⁾Ternopil National Economical University / Ukraine; ²⁾Lesya Ukrainka Eastern European National University / Ukraine; ³⁾Ternopil Ivan Puluj National Technical University / Ukraine; ⁴⁾Separated Subdivision of National University of Life and Environmental Sciences of Ukraine Berezhany Agrotechnical Institute / Ukraine</p>	153
20.	<p>JUSTIFICATION OF THE CULTIVATOR SWEEP AND STRENGTHENING ELEMENTS ON THE WORKING SURFACE / ОБГРУНТУВАННЯ ПАРАМЕТРІВ КУЛЬТИВАТОРНОЇ ЛАПИ ТА ЕЛЕМЕНТІВ ЗМІЦНЕННЯ ЇЇ НА РОБОЧІЙ ПОВЕРХНІ</p> <p>Prof. Ph.D. Eng. Kobets A.S., Lect. Ph.D. Eng., Pugach A.M., Prof. Ph.D. Agri.Sci. Kharytonov M.M. Dnipro State Agrarian and Economics University, Faculty of Agrarian Engineering / Ukraine</p>	161

ASPECTS REGARDING THE COMPRESSION RESISTANCE OF GEOSYNTHETICS USED IN BUILDING MUNICIPAL SOLID WASTE LANDFILLS

ASPECTE PRIVIND REZISTENȚA LA COMPRESIUNE A GEOSINTETICELOR UTILIZATE ÎN CONSTRUCȚIA DEPOZITELOR DE DEȘEURI MUNICIPALE

Prof. Ph.D. Eng. Voicu Gh.*¹⁾, As. Ph.D. Eng. Toma M.L.¹⁾,
Lect. Ph.D. Eng. Tudor P.¹⁾, Lect. Ph.D. Eng. Ipate G.¹⁾, Ph.D.Stud.Eng. Ștefan V.²⁾

¹⁾University "Politehnica" of Bucharest, Faculty of Biotechnical Systems Engineering/Romania;

²⁾ National Institute of Research - Development for Machines and Installations Designed
to Agriculture and Food Industry - INMA Bucharest

Tel: 0724715585; E-mail: ghvoicu_2005@yahoo.com

Keywords: geosynthetics, deformation-force curve, loading-unloading, regression laws, correlation coefficient

ABSTRACT

Choosing the physical characteristics of geosynthetics used in the construction of municipal waste landfills must be carried out according to the functions they must fulfil - sealing, filtration, protection. Since the geomembranes are subjected to significant compressive stress, and tearing by sticking against hard objects, experimental determinations are necessary to be made both in laboratory and in-situ for the determination of its resistance over time. The protection of the geomembranes shall be carried out, usually with geotextile, and its characteristics must also be established by experimental determinations. The results of measurements of the laboratory tests carried out both on a membrane of HDPE and a nonwoven PP geotextile, and the values of their deformation according to the pressing force led to the identification of the best correlate experimental data by regression curve analysis are presented in this paper.

REZUMAT

Alegerea caracteristicilor fizice ale geosinteticelor utilizate în construcția depozitelor ecologice de deșeur menajere trebuie efectuată în funcție de funcțiile pe care trebuie să le îndeplinească – etanșare, filtrare, protecție. Având în vedere că geomembranele sunt supuse unor solicitări importante de compresie, dar și de rupere prin înțepare cu obiecte contondente, este necesar a fi efectuate determinări experimentale, atât în laborator, cât și in-situ, pentru stabilirea rezistenței acestora în timp. Protecția geomembranelor se realizează, de obicei, cu geotextil, iar caracteristicile acestuia trebuie, de asemenea, stabilite prin determinări experimentale. În lucrare se prezintă rezultatele unor determinări de laborator efectuate, atât pe o geomembrană din HDPE, cât și pe un geotextil nețesut din PP, iar valorile deformației acestora în funcție de forța de apăsare au condus la identificarea prin analiză de regresie a curbei de variație care corelează cel mai bine datele experimentale.

INTRODUCTION

In the municipal landfill construction, but also for land improvement works, geosynthetics are materials with a wide use and can perform several functions: sealing, filtration, drainage, protection, stability slopes etc. (Giroud et al, 1992; Koerner R.M., 1998; Mandal J.N., 2014; Richardson and Zhao, 2009; Zornberg and Christopher, 1999).

Geosynthetics are materials made from polymers or polymer additives with various components for characteristics diversification and properties improvement. They can replace many conventional materials, with the same performance, showing guaranteed uniform properties over the entire surface. They are easy to apply, with reduced labour and costs, contributing to significant savings in materials and energy, but they also reduce the impact of construction on the environment. They also can work under load immediately after installation, and their price is comparable to the price of conventional materials.

However, geosynthetics are sensitive to contact with traditional materials (hard and tough) because they are, in general, thin and lightweight materials, thus can be easily damaged due to the specialized structure, which makes them usable only for the purpose for which they were designed and tested in laboratory and field. They are often sensitive to UV radiation and presents an aging phenomenon more pronounced than traditional materials (Narejo et al, 1996).

The main polymers used for obtaining geosynthetics are:

- polypropylene (PP, 0.895 – 0.910 g/cm³, melting temperature 155 – 175°C);
- low (LDPE), medium (MDPE) and high density (HDPE) polyethylene;
- polyester (PES, density 1.38 g/cm³, shrinkage in hot water 5–9%);
- polyamide (PA);
- polyvinyl chloride (PVC, 1.38–1.55 / 1.16–1.35 g/cm³).

Of all geosynthetics, geomembranes and geotextiles are largely employed in municipal landfills construction and beyond. In general, geomembranes act as a barrier (seal), while geotextiles have the role to protect the membrane or act as a drainage (*Wilson-Fahmy et al, 1996; Narejo et al, 1996; Koerner et al, 1996; Rowe R.K., 2012*).



Fig. 1 – Examples of geomembrane and protection geotextile utilisation in the construction of waste landfills

The protective properties, thickness and type of material that geosynthetics are made off, significantly require a rational design method.

In the works mentioned above, the authors present the theoretical approach of thinning the membrane in contact with the rounded edges of the stone layer beneath it, using the theory of membrane tension and results of laboratory experiments using a special apparatus and stone or truncated push con, during short and long periods of time. Theoretical study conducted for the geomembrane with or without geotextile protection shows the need for a material protection when membrane is applied. Furthermore, the authors show that the characteristics of the protuberant object and of the protection material are important in designing structures with geomembranes (*Wilson-Fahmy et al, 1996*).

In the experiments, high density polythene (HDPE) with 1.5 mm thickness (yield load 23 kN/m, 18% yield strain, puncture load 0.44 kN according to ASTM D 4885) and various non-woven textile, with different specific weights (per unit area) were tested. Using the results of the testing program, a design methodology for determination of the geotextile's necessary specific mass to geomembrane's puncture protection for a certain safety coefficient or vice versa has been developed (*Narejo et al, 1996*). Thus, it was found that the puncture resistance of geomembranes increases with increasing mass per unit area of the geotextile protection for all of the prominent bodies heights. Increasing the protuberances height decreases the geomembrane's perforation resistance, regardless of geotextile protection's specific mass, puncture resistance is inversely proportional to the square of the protrusion's height. Particularly important is the protuberance's shape, the puncture resistance of subrounded stones or rounded was two, respectively four times higher than the puncture resistance using the cornerstones (sharp). Also, the puncture resistance of a geomembrane laid on a bed of stones is two times higher than laid on the isolated rocks of the same height with the previously ones. At the same time, the membrane puncture resistance decreases with time and the time impact is more pronounced with decreasing specific weight of the geotextile protection and increase the protuberance height underneath the membrane.

The maximum permissible pressure on the geomembrane, depending on the height of a single protuberance underneath the geomembrane may be determined by the relation:

$$p_{adm} = 450 \frac{M_{gtx}}{H^2} \geq 50 \text{ kPa} \quad (1)$$

where M_{gtx} is the specific mass of the geotextile protection (g/m²) and H is protuberance's height (mm).

Minimum pressure of 50 kN corresponds to a failure pressure of a 1.5 mm thickness HDPE geomembrane, without any protective material (Narejo *et al*, 1996).

Therefore, the puncture resistance of the geomembrane determine required characteristics of the protection material, both in the case of coatings and to the construction of the landfill's bed foundation. Tests carried out in accordance with ASTM D5514, on a 1 mm PVC geomembrane lead to failure water pressure much higher than for the 1.5 mm HDPE membrane, (Marcotte *et al*, 2009). PVC geomembrane offers better advantages as a hydraulic barrier in designing leachate collection system, including puncture resistance is the most important. For example, under hydrostatic conditions, the disposition of PVC geomembrane on layers of 20 - 100 mm packed angular gravel has presented a decline of the minimum failure pressure when the particle diameter increases. The bottom line is that abrasion is probably the predominant factor for puncture resistance of PVC geomembranes. The authors' recommendation is to test the geomembranes with real granular materials for test results to be as conclusive as possible. Also, testing and analysis of protective geotextiles demonstrated that the use of a non-woven needle-punched geotextile with a specific mass of 270 g/m² increase of the burst pressure of the 1 mm PVC membrane up to 800 kPa, which is ten times higher than the value of allowable pressure calculated for a 1.5 mm HDPE membrane protected with a 550 g/m² geotextile. Moreover, the HDPE membrane requires a direct contact only with fine granular materials to prevent punctures while PVC geomembrane may be used over layers of coarser granular material.

Other works covering the geomembranes and geotextiles resistance are HAXO and Kamp, 1990; Peggs I., 1990; Koerner, 1998 Blond and Elie, 2006; Jones and Clarke, 2007; Bacas *et al*, 2011; Lin *et al*, 2012 ; Qiang *et al*, 2013; Voicu Gh., 2016.

The results of pre-compression tests performed on a HDPE geomembrane without geotextile protection to relatively small pressure forces (up to 20 N), but also on a geotextile protection using pressure devices with cylindrical or spherical roller bearings in order to identify mathematical relationship between loading force and deformation, both for loading and unloading, and energy hysteresis are presented in this paper. Experimental data are tested with known mathematical relationships and best mathematical equation that correlates the experimental data is established.

MATERIALS AND METHODS

Measurements were carried out in the specialized laboratory of the Department of Biotechnical Systems from the University "Politehnica" of Bucharest, materials used in the experiments being purchased from Chiajna waste landfill, Ilfov County. The thickness of the HDPE geomembrane was 3 mm, and the unit weight of the geotextile was 500 g/m² and thickness 4.7 mm, obtained from non-woven polypropylene yarns.

Laboratory bench (shown in Figure 2) has been specially adapted for the compression experimental tests on geosynthetics used, being provided with a rigid support plate (8), on which were placed 100 × 100 mm square tiles of geosynthetics material (9). The hold itself (10) has been either a roll steel cylinder with a diameter of 8.1 or 11.3 mm, or metal spherical ball with a 13.4 mm diameter, reinforced with a top plate (3'), which comes into contact with an external digital comparator (5). Between the metal plates (3 and 3') there is a connecting rod (12) connected to a flexible wire (11) passing over two pulleys (6) and a balancing weight (7) to the left end. On the top plate (3') can be placed different weights (4), whose pressure force is transmitted through the stiffened chain elements (3'-12-3-10) on the geosynthetics material (10). For puncture resistance of the membrane was used a 20° metal tip cone, using the same device.

Experimental determinations were performed by reading the geosynthetics material strain at different weights added to the stand's upper plate (3'), until a predefined force is reached and also on return, by reducing the pressure weight. No determinations were made at discharge for a longer relaxation time of the material. Relaxation time was estimated at about one minute (how long until weights were unloaded from the upper plate (3')).

Further on, the values obtained for the material deformation were processed in analysis program Microcall Origin, by plotting data points and regression analysis with different mathematical functions and the regression curves were plotted to identify the best variation law of deformation as a function of pressure force (at loading - unloading).

Mathematical functions used in the regression analysis are:

- linear function:

$$y = ax + b \quad (2)$$

- power function:

$$y = a x^b \tag{3}$$

- exponential function:

$$y = a + b \cdot \exp\left(-\frac{x}{c}\right) \tag{4}$$

- logistic function:

$$y = b + \frac{a-b}{1+\left(\frac{x}{c}\right)^d} \tag{5}$$

Estimated calculations were made to determine the energy dissipated in the material.

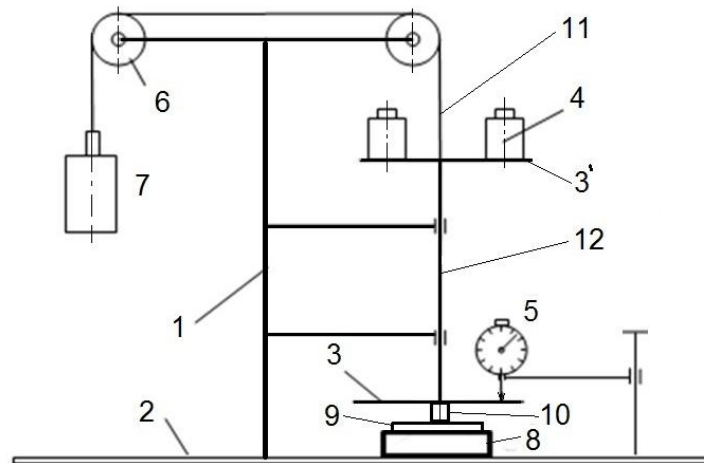


Fig. 2 – Principled layout of the laboratory stand used in experimental tests

1 – support with rod and arms; 2 – support plate; 3 – pressure plate; 4 – weights; 5 – external comparator; 6 – pulleys; 7 – balancing weight; 8 – rigid metal plate; 9 – geomembrane (geotextile); 10 – pressure ball (or roller); 11 – connection thread; 12 – rod

RESULTS

The results obtained for values of deformation according to the strength load are shown in Table 1.

Table 1

Geosynthetics deformation values (in mm) for several different devices and pressure forces

Mass, N	4.7 mm PP Geotextile				Geomembrane HDPE, 3 mm							
	8.1 mm Roll		11.3 mm Roll		8.1 mm Roll		11.3 mm Roll		φ 13.4 mm Ball		Edge	
	Pressure	Return	Pressure	Return	Pressure	Return	Pressure	Return	Pressure	Return	Pressure	Return
0	0	1.05	0	1.40	0	0.02	0	0.14	0	0.21	0	0.67
1.36	0.01	1.23	0.16	1.60	0	0.04	0.01	0.21	0.01	0.30	0.09	0.72
2.68	0.04	1.30	0.42	1.70	0.01	0.05	0.04	0.24	0.04	0.38	0.15	0.76
3.99	0.25	1.38	0.65	1.80	0.02	0.05	0.06	0.28	0.08	0.43	0.24	0.78
5.31	0.41	1.43	0.82	1.85	0.03	0.06	0.08	0.31	0.15	0.48	0.32	0.79
6.64	0.60	1.49	0.98	1.90	0.04	0.06	0.10	0.33	0.21	0.52	0.40	0.80
7.96	0.75	1.52	1.15	1.94	0.05	0.07	0.14	0.34	0.29	0.55	0.46	0.81
9.27	0.81	1.54	1.25	1.97	0.05	0.07	0.17	0.35	0.34	0.58	0.51	0.81
10.58	1.01	1.55	1.39	1.99	0.06	0.08	0.22	0.35	0.39	0.62	0.54	0.81
11.91	1.09	1.58	1.50	2.00	0.06	0.08	0.24	0.36	0.45	0.63	0.58	0.81
13.21	1.20	1.60	1.60	2.01	0.07	0.08	0.27	0.37	0.49	0.63	0.61	0.81
14.55	1.32	1.61	1.69	2.02	0.07	0.09	0.29	0.37	0.55	0.65	0.68	0.81
15.88	1.40	1.62	1.78	2.03	0.08	0.09	0.32	0.38	0.58	0.65	0.74	0.81
17.18	1.49	1.62	1.93	2.03	0.09	0.10	0.34	0.38	0.63	0.66	0.78	0.81
18.50	1.62	1.62	2.03	2.03	0.09	0.10	0.36	0.39	0.64	0.67	0.81	0.81
19.51					0.10	0.10	0.38	0.39	0.66	0.67		
20.28					0.10	0.10	0.39	0.39	0.67	0.67		

The curves of geosynthetics deformation, on loading and unloading, depending on the pressure force were plotted based on experimental data from Table 1. The arrangement of data points, together with the variation curves drawn by regression analysis are shown in Figures 3 and 4.

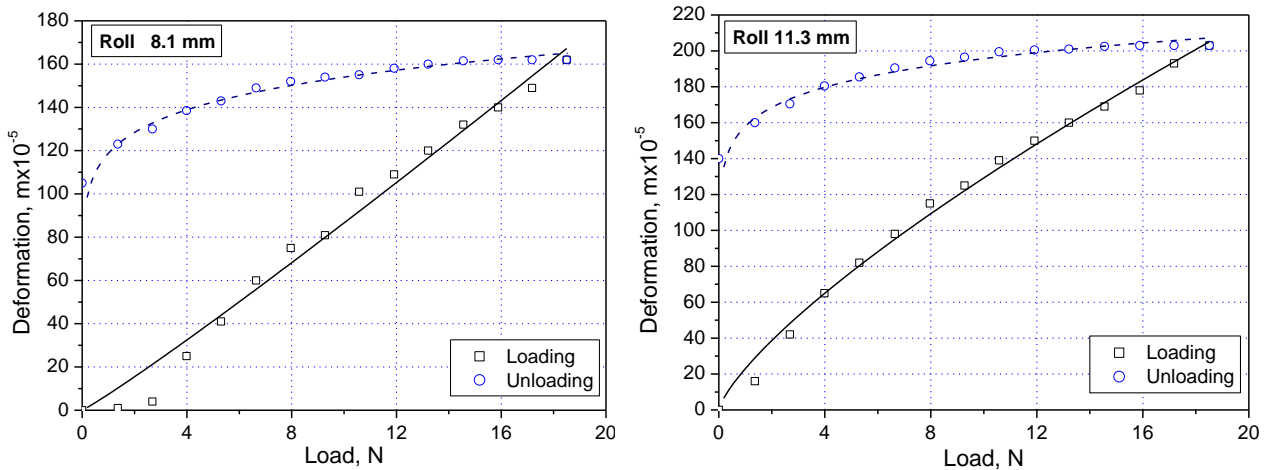


Fig. 3 – The variation of the geotextile deformation curves, as a function of the pressure force, on loading and unloading, for two diameters of the cylindrical roll press

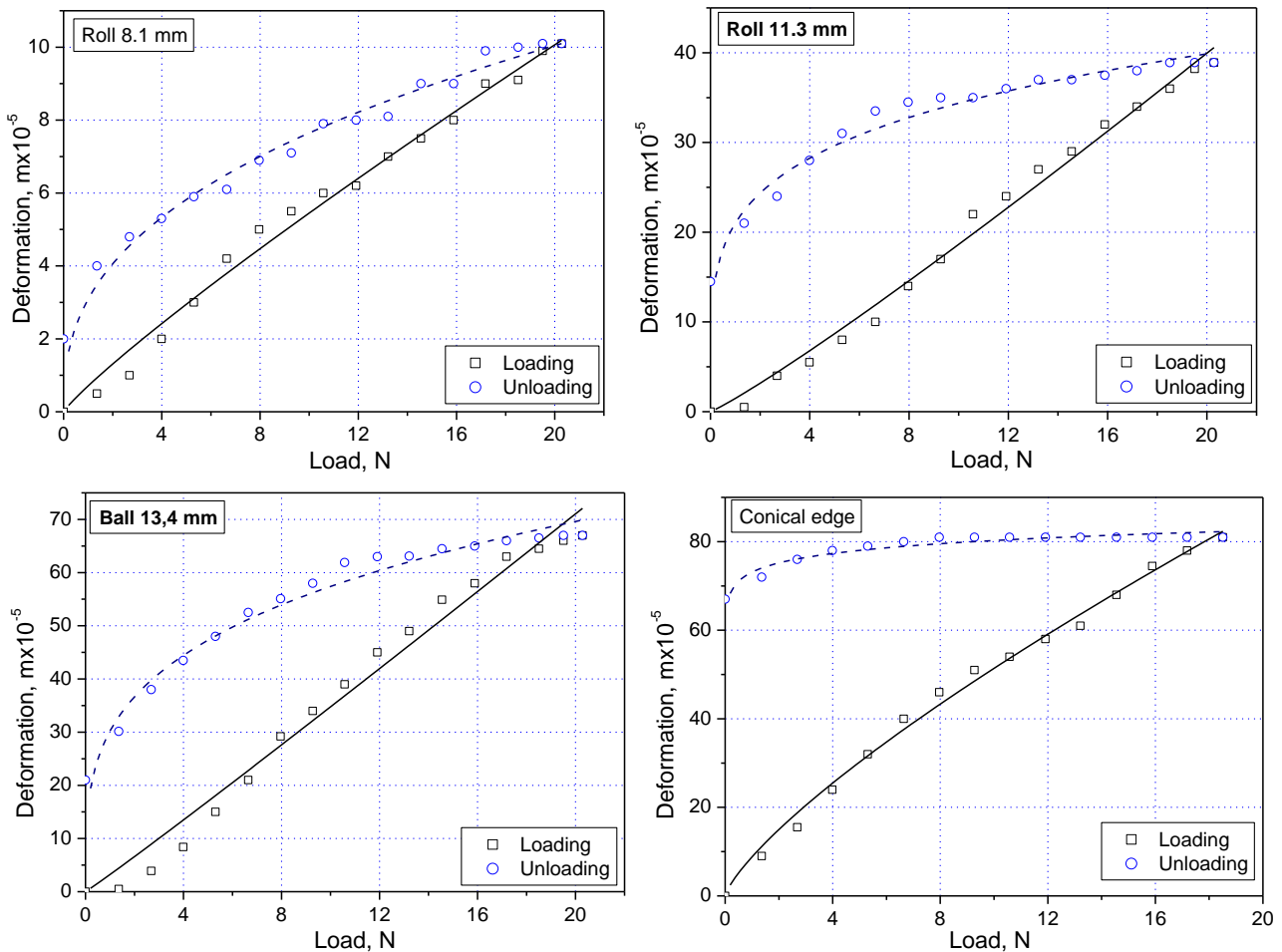


Fig. 4 – The variation curves for geomembrane deformation, depending on the pressure force, on loading and unloading, for different types of work systems (rolls, ball, conical edge)

From the analysis of experimental data and plotted variation curves, it can be seen that the unload takes place on a route different from loading, which indicates that some of the strain remains stored in the material and it can be resorbed after shorter or longer periods of time. Thus, there is the possibility of material thinning and if testing continues, the material can no longer return to the initial form. This thinning inevitably leads to stretching and wrinkling of the material, which induce other types of stresses, together

with the existence of an additional weight (waste or drainage material or coating) above the material.

Thus, the deformation is elastic-plastic deformation with a higher degree of recovery from the membrane, especially when cylindrical rollers are used. For geotextile protection, the strain was more pronounced as compared to geomembrane, for the same load, and return much smaller, which means that the coefficient of elasticity is also smaller.

Instead, membrane recovery was much smaller when using the conical tip, possibly due to its retention by material and its friction with the material.

Also, it can be said that a part of the energy consumed for deformation remains in the material, manifested as hysteresis both in case of deformation and consumption of the energy needed for deformation. This phenomenon occurs both for geosynthetics protection and for sealing geomembrane, but less obvious in case of the last one, for loading values used in the paper, but with a greater influence on geomembranes.

Energy stored in material (called lost or dissipated energy) can be determined by measuring the surface area between the two curves (loading - unloading). In the paper, the energy dissipation was calculated with Mathcad software, based on equations derived from regression analysis, as a difference between surface areas under the curves of unloading and loading, from the 0 N load to the load mentioned in Table 1 (18.50 N, respectively 20.28 N) for each one of the experimental samples.

If the energy dissipation for the geotextile lies between $(1255-1354) \cdot 10^{-5}$ N·m, in case of the geomembrane, dissipated energy lies between $(37.2-395.9) \cdot 10^{-5}$ N·m, depending on the type and shape of the pressure device (roller or ball). However, there are slight differences depending on the mathematical relation used (Eq. 2-5). Thus, the calculation error between the values of the dissipated energy calculated by the linear equation (1) and the logistic function (4) lies between 0.15–7.58%, as shown in Table 3:

$$\varepsilon = \frac{E_{linear} - E_{logistic}}{E_{logistic}} \cdot 100 \text{ (\%)} \quad (6)$$

From regression analysis of experimental data with mathematical functions mentioned above resulted the values of the equations coefficients and of the correlation coefficient R² and they are shown in Table 2.

Table 2
The coefficients values of the regression functions (2-5) and of the correlation coefficient R² for strain - strength variation curves of the experimental tests on PP geotextile and HDPE geomembrane

Equation	Loading / Unloading	Geotextile, roll $\phi 8.1$ mm					Geotextile, roll $\phi 11.3$ mm				
		a	b	c	d	R ²	a	b	c	d	R ²
Eq.2	Loading	0.095	-0.076	-	-	0.988	0.107	0.168	-	-	0.976
	Unloading	0.026	1.237	-	-	0.813	0.027	1.631	-	-	0.759
Eq.3	Loading	0.074	1.070	-	-	0.980	0.230	0.750	-	-	0.992
	Unloading	1.188	0.113	-	-	0.983	1.580	1.766	-	-	0.968
Eq.4	Loading	$6.6 \cdot 10^6$	$-6.6 \cdot 10^6$	$7 \cdot 10^6$	-	0.986	2.9512	-2.9712	16.446	-	0.998
	Unloading	1.6358	-0.5697	4.972	-	0.995	2.0395	-0.631	4.161	-	0.999
Eq.5	Loading	-0.0372	2.4744	13.146	1.718	0.995	-0.0211	4.311	21.247	1.044	0.998
	Unloading	1.0527	1.7753	4.604	1.022	0.996	1.4026	2.123	3.289	1.208	0.997
		Geomembrane, roll $\phi 8.1$ mm					Geomembrane, roll $\phi 11.3$ mm				
		a	b	c	d	R ²	a	b	c	d	R ²
Eq.2	Loading	0.005	0.0026	-	-	0.985	0.021	-0.018	-	-	0.993
	Unloading	0.0035	0.036	-	-	0.951	0.0095	0.228	-	-	0.786
Eq.3	Loading	0.007	0.886	-	-	0.987	0.015	1.100	-	-	0.990
	Unloading	0.031	0.394	-	-	0.979	0.210	0.214	-	-	0.955
Eq.4	Loading	0.1258	-0.0989	14.562	-	0.980	$-2.68 \cdot 10^4$	$2.68 \cdot 10^4$	$-1.3 \cdot 10^6$	-	0.992
	Unloading	$-1.456 \cdot 10^4$	$1.456 \cdot 10^4$	$-2.91 \cdot 10^5$	-	0.983	0.3883	0.2417	4.938	-	0.993
Eq.5	Loading	-0.0017	0.2316	25.621	1.172	0.992	0.0029	0.6539	16.393	1.784	0.998
	Unloading	0.021	27.833	$4.92 \cdot 10^5$	0.577	0.991	0.1461	0.419	3.950	1.250	0.993
		Geomembrane, ball $\phi 13.4$ mm					Geomembrane, conical edge				
		a	b	c	d	R ²	a	b	c	d	R ²
Eq.2	Loading	0.037	-0.026	-	-	0.985	0.043	0.064	-	-	0.980
	Unloading	0.0196	0.340	-	-	0.839	0.0053	0.738	-	-	0.581
Eq.3	Loading	0.032	1.032	-	-	0.978	0.088	0.766	-	-	0.995
	Unloading	0.302	0.279	-	-	0.969	0.731	0.040	-	-	0.992

Equation	Loading / Unloading	Geotextile, roll $\phi 8.1$ mm					Geotextile, roll $\phi 11.3$ mm				
		a	b	c	d	R ²	a	b	c	d	R ²
Eq.4	Loading	$-1.07 \cdot 10^5$	$1.07 \cdot 10^5$	$2.89 \cdot 10^6$	-	0.983	1.3052	-1.3044	19.377	-	0.996
	Unloading	0.6912	-0.4832	6.209	-	0.998	0.8119	-0.144	2.698	-	0.996
Eq.5	Loading	-0.0039	0.915	11.983	1.995	0.999	-0.0041	2.2752	34.055	0.976	0.995
	Unloading	0.213	0.7559	5.171	1.287	0.997	0.6704	0.8153	2.017	1.773	0.995

Analysing the data in Table 2, it is clear that the mathematical function that has the best correlation with the experimental data is the logistic function for which the values of the correlation coefficient R² are higher (over 0.992 in all analysed cases). However, all four functions used in the regression analysis shows very high values of the correlation coefficient.

Table 3

The dissipated energy (N·m) and the calculation error based on the mathematical relationship used

	Nonwoven geotextile		HDPE geomembrane		
	Small roll	Big roll	Small roll	Big roll	Ball
Dissipated energy (N·m)					
By the linear equation (2)	1255×10^{-5}	1354×10^{-5}	37.16×10^{-5}	269.35×10^{-5}	380.19×10^{-5}
By the logistic equation (5)	1271×10^{-5}	1352×10^{-5}	38.55×10^{-5}	291.45×10^{-5}	395.92×10^{-5}
Calculation error ε (%)	1.26	0.15	3.60	7.58	3.97

CONCLUSIONS

Geotextiles are widely used in the construction of waste landfills. Among them, the HDPE geomembranes are especially used for sealing the bottom and for the final coating of the deposit. These geomembranes are sensitive to mechanical actions of the weights acting on them and of the blunt bodies inside the materials with which they are in contact. Therefore, protective geotextiles are used for their protection, whose mass per unit area is chosen depending on the specific type of land.

Therefore, the compressive strength of the two geosynthetics is particularly important and needs to be determined, both in the field and in the laboratory, whether the manufacturer's technical features are known or not.

Several conclusions result from our measurements, such as:

- geosynthetics deformation under the action of compressive stresses is an elastic-plastic deformation between 1.6 – 2 mm for the pressure forces of 185 – 360 kPa in case of 4.7 mm protective geotextiles and a weight of 500 g/m²;
- geomembrane deformation is much smaller compared with geotextile, with values of about 0.10 – 0.40 mm, for pressure forces of 205 – 398 kPa;
- the recovery degree of the geotextile (after about 1 minute) is much smaller compared to that of the geomembrane, in our determinations is in the range of 65 – 70% for the geotextile and 20 – 36% for the geomembrane, depending on the loading force and pressure device used;
- the shape of the pressure device on geosynthetics material is very important and, thus, of the objects with which it comes into contact, being transposed into different loading pressure of the various contact surfaces for the same loading degree;
- when using of a spherical ball-type pressure device, the penetration depth into the material has been much higher for the geomembrane compared to cylindrical-type pressure devices (about 1.7 – 6.7 times over);
- the return of geosynthetics material deformation occurs on a curve other than the loading one, due to its elastic-plastic behaviour, which results in the manifestation of the hysteresis phenomenon; lost or dissipated energy in the material is much higher for the geotextile, between 3 – 30 times over, in comparison with the geomembrane, at the same loading degree;
- both loading and recovery of the material has not necessarily a linear trajectory, but being closer to it in case of loading, when the deformation is approximately proportional to the pressure force; the regression analysis with the linear function showed a correlation coefficient R² over 0.980 at loading and between 0.759 – 0.951 at unloading, for all samples, except in tests with the conical tip;

- the mathematical function with the best correlation of the experimental data was logistic function, which showed a correlation coefficient $R^2 \geq 0.991$, both for loading and unloading curves;
- utilisation of the linear and logistic functions in regression analysis leads to errors in the verification of the dissipated energy in the material from 0.15% to 7.58%, which shows that it is very important to choose the proper law of variation of the deformation depending on the pressure force, in order to estimate the dissipated energy.

Therefore, knowing the strength characteristics of geosynthetics is particularly important for designers and builders of ecological landfills, thus the success in operation is consistent with the environmental protection laws, and the data presented in our paper can be particularly useful in this sense.

REFERENCES

- [1] Bacas B.M.; Konietzky H.; Berini J.C.; Sagaseta C., (2011), A new constitutive model for textured geomembrane/geotextile interfaces, *Geotextiles and Geomembranes*, Vol.29, pp.137–148;
- [2] Blond E., Elie G., (2006), Interface shear-strength properties of textured polyethylene geomembranes, viewed, *59th Canadian Geotechnical Conference*, Vancouver, Canada;
- [3] Giroud J.P., Badu-Tweneboah K., Bonaparte R., (1992), Rate of leakage through a composite liner due to geomembrane defects, *Geotextiles and geomembranes*, Vol.11, Iss.1, pp.1-28, Elsevier Sci Ltd, Kidlington, Oxford, England;
- [4] Jones C.J.F.P., Clarke D., (2007), The residual strength of geosynthetic reinforcement subjected to accelerated creep testing and simulated seismic events, *Geotextiles and Geomembranes*, Vol.25, pp.155–169;
- [5] Koerner R.M., (1998), *Designing with geosynthetics*, Prentice Hall Publishing Co., Englewood Cliffs, NJ.;
- [6] Koerner R.M., Wilson-Fahmy R.F. and Narejo D., (1996), Puncture protection of geomembranes, Part III: Examples, *Geosynthetics International*, Vol. 3, no. 5, pp. 655-675;
- [7] Lin W.A., Zhang H.W., Zhan L.T., Chen Y.M., (2012), Large-scale ramp model tests on geomembrane/geotextile interface, *Chinese Journal of Geotechnical Engineering*, Vol.34, pp.1950–1956, Nanjing HuJu, China;
- [8] Mandal J.N., (2014), *Geosynthetics engineering: in theory and practice*, Department of Civil Engineering, IIT Bombay Course;
- [9] Marcotte M., Denis R., Blond É., (2009), Design algorithm for the puncture resistance of pvc geomembranes for heap leach pads, *Proceedings of the Second Middle East Geosynthetics Conference*, Dubai, UAE, http://www.solmax.com/wp-content/uploads/2012/08/4_PVC-PunctureResistance.pdf
- [10] Narejo D., Koerner R.M. and Wilson-Fahmy R.F., (1996), Puncture Protection of Geomembranes Part II: Experimental", *Geosynthetics International*, Vol. 3, No. 5, pp. 629-653;
- [11] Peggs Ian, (1990), Destructive testing of polyethylene geomembrane seams: Various methods to evaluate seam strength, *Geotextiles and Geomembranes*, Vol.9(4-6), pp.405-414;
- [12] Qiang Xue, Qian Zhang, Zhen-Ze Li, Kai Xiao, (2013), The tension and puncture properties of HDPE geomembrane under the corrosion of leachate, *Materials*, Vol.6, pp.4109-4121, Basel, Switzerland;
- [13] Richardson G.N., Zhao A., (2009), Geosynthetic fundamentals in landfill design, *Proc. of Int. Symp. on Geoenvironmental Eng.*, ISGE2009, Hangzhou, China;
- [14] Rowe R.K., (2012), Short- and long-term leakage through composite liners, *The 7th Arthur Casagrande Lecture, Canadian Geotechnical Journal*, Vol. 49, iss.2, pp.141-169;
- [15] Voicu Gh., (2016), *Ecological storage engineering of solid waste (Ingineria depozitarii ecologice a deseurilor solide)*, Ed. Politehnica Press, Bucuresti;
- [16] Wilson-Fahmy R.F., Narejo D., Koerner R.M., (1996), Puncture Protection of Geomembranes, Part I: Theory, *Geosynthetics International*, Vol. 3, no. 5, pp. 605-628, ICE Publishing, Inst Civil Engineers, Westminster, England;
- [17] Zornberg J.G., Christopher B.R., (1999), Geosynthetics, *The Handbook of Groundwater Engineering*, pp.37-1 – 37-36, CRC Press, Taylor & Francis Group, Abingdon, USA.

JUSTIFICATION OF RATIONAL PARAMETERS OF A PNEUMOCONVEYOR SCREW FEEDER

/

ОБГРУНТУВАННЯ РАЦІОНАЛЬНИХ ПАРАМЕТРІВ ЖИВИЛЬНИКА ПНЕВМО- ШНЕКОВОГО ТРАНСПОРТЕРА

Prof. Ph.D. Eng. Baranovsky V.M.¹⁾, Prof. Ph.D. Eng. Hevko R.B.²⁾, Assoc. Prof. Ph.D. Eng. Dzyura V.O.¹⁾,
Ph.D. Eng. Klendii O.M.³⁾, Assoc. Prof. Ph.D. Eng. Klendii M.B.³⁾, Eng. Romanovsky R.M.¹⁾

¹⁾Ternopil Ivan Pul'uj National Technical University; ²⁾Ternopil National Economical University / Ukraine; ³⁾Separated Subdivision of
National University of Life and Environmental Sciences of Ukraine Berezhaný Agrotechnical Institute / Ukraine

E-mail: klendii_o@ukr.net

Keywords: feeder, pneumoconveyor screw, loose material, curvilinear route

ABSTRACT

The article presents the justification of rational parameters of the operating parts of a pneumoconveyor screw. The dependences of pressure screw efficiency on the change in design and kinematic parameters and process variables of a screw and on loose material characteristics have been considered. In addition, general analysis of the choice substantiation of a feeder pressure screw diameter and the cross-sectional area of a hopper loading opening, which provides the required efficiency of a pneumoconveyor screw, has been conducted.

РЕЗЮМЕ

В статті наведено обґрунтування раціональних параметрів робочих органів пневмо-шнекового транспортера. Представлено залежності продуктивності напірного шнека від зміни конструктивно-кінематичних і технологічних параметрів шнека та властивостей сипкого матеріалу. Також проведено обґрунтування вибору діаметра напірного шнека живильника та площі поперечного перерізу завантажувального отвору бункера, при якому буде забезпечуватися необхідна продуктивність пневмо-шнекового транспортера.

INTRODUCTION

The conducted analysis on the state of current technologies and the review of recent scientific and patent literature, which cover the design of machinery and mechanisms for conveying loose materials along curvilinear routes (Lyashuk O.L., et.al., 2015; Rogatynska O. et.al., 2015; Rohatynskiy R.M. et.al., 2016) shows that they satisfy most of the requirements to a certain extent, but most of the designed operating parts of conveyers perform not only translational axial movement of material, but they also perform rotary motion, which causes material damage and reduces the efficiency of such mechanisms. This paper is the follow-on study to the work, covered in papers (Hevko R.B. et.al., 2009; Hevko R.B. et.al., 2014; Hevko R.B. and Klendiy O.M., 2014; Hevko R.B. et.al., 2016), and is aimed at improving the efficiency of pneumoconveyor screw in order to provide loose material flow along technological lines of various space configurations applying power-operated material feed by means of a screw feeder and additional pneumatic reinforcement. The developed designs of pneumoconveyor screws have been patented (Hevko R.B. et.al., 2011; Halka R.I., 2001; Hevko R.B. et.al., 2012). When doing theoretical research, we were based on the approaches set out in the work (Voityuk V.M., 2005).

MATERIALS AND METHODS

In order to formalize loose material transportation process and further substantiate the rational parameters of a pneumoconveyor screw operating elements, let us consider its flow-sheet, presented in Fig.1.

The main system points of a pneumoconveyor screw are: a screw feeder 1 and a pneumoconveyor screw 2. A screw feeder consists of a loading hopper 3, which has a loading opener 4 in its underflow and a screw 5, which is made in the form of an axle 6 with spiral flights 7. A pneumoconveyor consists of a pneumatic nozzle section 8 and a pneumatic pipeline 9.

The technological process is the following. Loose material from a loading hopper 3 of a screw feeder 1 is emptied on a screw 5 through a loading opening 4. Screw flights 7 convey loose material to the outlet

end of a screw and further to the initial pneumoconveyor 2 coverage. By means of high-pressure air, a pneumoconveyor transports loose material through a pneumatic nozzle section 8 into a pneumatic pipeline 9. In order to provide effective transportation of loose materials in a flexible casing (it is not shown in Fig.1), the guides, which are equally-spaced on a circle of a nozzle, are directed along with material movement. Thus, the process of material transportation is provided due to its forced feed by a feeder and further pneumatic pressure.

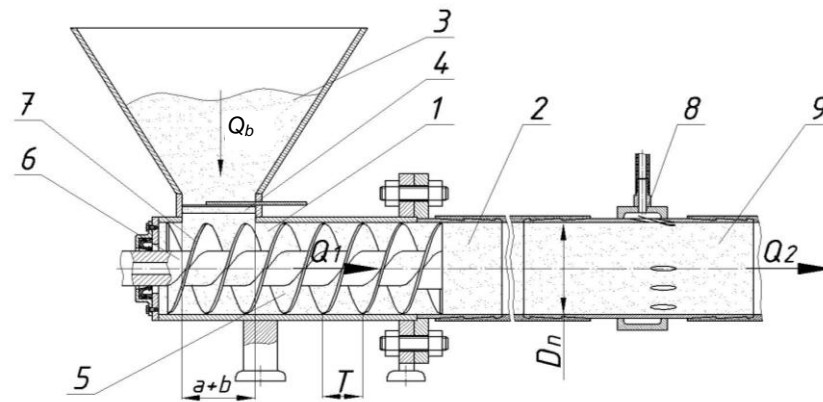


Fig.1 - A technological process flow-sheet of pneumoconveyor screw operation

1 –screw feeder; 2 –pneumoconveyor; 3 –loading hopper; 4 –loading opener; 5 –screw; 6 – screw axle; 7 –screw flight; 8 –pneumatic nozzle section; 9 –pneumatic pipeline

To formalize the pneumoconveyor screw operation, let us assume the following:

- cross sectional area of a loading opening is rectangular in shape and its sides equal to a, b ;
- patterns of loose material movement in a loading hopper are given by overall patterns of loose materials free outflow from a tank; here, material consumption through a loading opening is done in the process of its flowing down into a funnel at an angle of a natural slope before the height breakdown time of a dynamic unloading bridge;
- loose material consumption through a loading opening to screw flights in total is not less than the screw efficiency.

Justification of the operating elements parameters of a pneumoconveyor screw is based on the analysis of the technological material flow along the surface of the main element of a screw feeder structure. Design and kinematic parameters of a screw and dimensional specifications of a pneumoconveyor screw, which is formed by a pneumatic nozzle section and a pneumatic pipeline, have been interrelated based on the analytical analysis of the required capacity or design efficiency of a pneumoconveyor screw.

In total, the efficiency of a pneumoconveyor screw is regulated by the efficiency of its last basic block, namely, by the efficiency of a pneumatic conveyor, which, in its turn, is functionally dependent on the efficiency of a screw and, respectively, on loose material consumption through the opening of a loading hopper.

Let us set cross-sectional area of a loading opening 4 by S_o (sm^2); loose material consumption through opening 4 or per-second feeding of loose material to the flights 7 of a screw 5 is denoted by Q_b (kg/s); Q_1 (kg/s) stands for screw efficiency; pneumoconveyor efficiency is denoted by Q_2 (kg/s).

Then, it is possible to provide efficient operation of a pneumoconveyor screw under the following condition:

$$Q_b \leq Q_1 \leq Q_2 \quad (1)$$

According to (Voityuk V.M., 2005), loose material consumption Q_b (kg/s) through a hopper opening and the made assumption are determined from the following formula:

$$Q_b = \frac{1.47k_n \rho S_o^4 \sqrt{r_z}}{\sqrt{f}} \quad (2)$$

where: k_n – coefficient of resistance; ρ – bulk weight of loose material, kg/sm^3 ; r_z – composite radius of the opening, m; f – coefficient of internal friction.

In a general case of load transportation, in order to determine the efficiency of screw conveyers Q the following dependences are used:

$$Q = \rho F V_c \quad (3)$$

where: F – cross-sectional area of material flow, m^2 ; V_c average velocity of flow, m/s; ρ – load bulk weight, kg/m^3 .

Here, the cross-sectional area of material flow F is determined from the flow area of a screw F_n and space filling coefficient of a trough φ_k , or

$$Q = 0.25\pi\varphi_k V_c \gamma (D^2 - d^2) \quad (4)$$

where: φ_k – space filling coefficient of a screw; D – screw diameter, m; d – diameter of a screw beater, m.

In this case, average velocity V_c of axial movement of loose material by a pressure screw can be rationally determined using a correction coefficient, which takes into account V_c reduction relative to theoretical velocity of axial movement of screw flights V_m , or slip coefficient k_k , which regulates the reduction in the design capacity of a pressure screw as consequence of the friction of loose material particles on the surface of its constructional elements

$$V_c = V_m k_k = \frac{T'\omega}{2\pi} k_k = \frac{T'k_k}{2\pi} \frac{d\varphi}{dt} = 0,5k_k [Dtg(45^\circ - 0,5\alpha_k) - \delta_n] \frac{d\varphi}{dt} \quad (5)$$

where T' is determined as the difference between the last pressure flight pitch T_n and its thickness; $\beta' = 45^\circ - 0,5\alpha_k$ – a helix angle of the last pressure flight screw, deg.; α_k – angle of friction from loose material slipping on helical surface of a flight screw, deg.; δ_n – thickness of the last pressure flight screw, m.

Then, according to (4) and (5), the efficiency of a pressure screw is determined by the following formula

$$Q_1 = 0.125\pi\varphi_k k_k \rho (D^2 - d^2) [Dtg(45^\circ - 0,5\alpha_k) - \delta_n] \frac{d\varphi}{dt} \quad (6)$$

The efficiency of screw conveyers depends to a great extent on the value of a space filling coefficient of a pressure screw φ_k , which is one of the main criterion (together with screw diameter and its angular velocity). That is why, when calculating the desired maximum capacity of a pressure screw it is important to take into account the volume of flights in the overall space of a screw.

For this purpose, let us introduce the coefficient, which is denoted as k_z ; here k_z is formulated as the relation of the effective volume with the overall volume of a pressure screw inter-flight space, namely:

$$k_z = V_k / V_n; V_k = V_n - V_z, \text{ or } k_z = 1 - V_z / V_n \quad (7)$$

where V_k – volume of inter-flight space, m^3 ; $V_n = F_n l_n$ – overall volume of inter-flight space, m^3 ; $F_n = 0,25(D^2 - d^2)$ – cross-sectional area of a screw, m^2 ; l_n – length of a pressure pump, m; $V_z = V'_z z_n$ – overall space occupied by flights, m^3 ; $V'_z = F_z l_z$ – volume, which is occupied by the flights of one screw entry, m^3 ; $F_z = \delta_n h_n$ – cross-sectional area of a flight screw blade, m^2 ; l_z – length of a helical line over mean screw diameter, m; $h_n = 0,5(D - d)$ – height of a flight screw blade, m; z_n – number of screw entries, pc.

The length of a helical line over mean screw diameter l_z is determined by the following dependence:

$$l_z = \frac{\pi n (D + d)}{2T} \cos \arctg \frac{2T}{D + d} = \frac{0,5l_n (D + d)}{Dtg\beta} \cos \arctg \frac{2\pi Dtg\beta}{D + d} \quad (8)$$

Then, taking into consideration (7) and (8), after transformation and simplification, the coefficient k_z

is determined by the following formula:

$$k_z = 1 - \frac{\delta_n z_n}{D \operatorname{tg}(45^\circ - 0.5\alpha_k)} \cos \operatorname{arctg} \frac{2\pi D \operatorname{tg}(45^\circ - 0.5\alpha_k)}{D + d} \quad (9)$$

Taking into account k_z , actual value of a space filling coefficient of a pressure screw φ_{kz} is determined as $\varphi_{kz} = \varphi_k k_z$, or

$$\varphi_{kz} = \left[1 - \frac{\delta_n z_n}{D \operatorname{tg}(45^\circ - 0.5\alpha_k)} \cos \operatorname{arctg} \frac{2\pi D \operatorname{tg}(45^\circ - 0.5\alpha_k)}{D + d} \right] \varphi_k \quad (10)$$

In fact, in the process of practical implementation of loose material transportation by a screw, the value of a space filling coefficient of a pressure screw φ_{kz} is not constant and mainly depends on the uniformity of granular loose material flow from a loading hopper and on other factors as well, for example on dimensional features of material, its moisture content, ability of firming material particles during their conveying by a screw and so on.

A slip coefficient k_k depends on many factors, such as a helix angle of flights winding, a screw diameter, a coefficient of loose material compacting by a screw, etc. and is determined by the following formula:

$$k_k = k_\beta k_y \quad (11)$$

where k_β , k_y – respectively, the coefficients, which show the influence of a helix angle β' over a mean radius of the last pressure flight screw, compacting coefficient of a screw and a screw diameter D on a slip coefficient k_k .

Having substituted the values from formulas (10) and (11), in (6) we obtain a dependence needed for determination of the required design efficiency Q_1 (kg/s) of a pressure screw:

$$Q_1 = 0.125\pi\varphi_k k_\beta k_y \rho (D^2 - d^2) \left[D \operatorname{tg}(45^\circ - 0.5\alpha_k) - \delta_n \right] \times \left[1 - \frac{\delta_n z_n}{D \operatorname{tg}(45^\circ - 0.5\alpha_k)} \cos \operatorname{arctg} \frac{2\pi D \operatorname{tg}(45^\circ - 0.5\alpha_k)}{D + d} \right] \frac{d\varphi}{dt} \quad (12)$$

For practical implementation, when calculating design efficiency of a pressure screw Q_1' (kg/s), taking into consideration, that $\frac{d\varphi}{dt} = \omega = \frac{\pi n}{30}$, where n – rotation frequency of a screw (rpm), the dependence (12) may be written as:

$$Q_1' = 0.25\pi^2 n \varphi_k k_\beta k_y \rho (D^2 - d^2) \left[D \operatorname{tg}(45^\circ - 0.5\alpha_k) - \delta_n \right] \times \left[1 - \frac{\delta_n z_n}{D \operatorname{tg}(45^\circ - 0.5\alpha_k)} \cos \operatorname{arctg} \frac{2\pi D \operatorname{tg}(45^\circ - 0.5\alpha_k)}{D + d} \right] \quad (13)$$

or, when determining Q_1'' (t/h), it may be written as:

$$Q_1'' = 0.015\pi^2 n \varphi_k k_\beta k_y \rho (D^2 - d^2) \left[D \operatorname{tg}(45^\circ - 0.5\alpha_k) - \delta_n \right] \times \left[1 - \frac{\delta_n z_n}{D \operatorname{tg}(45^\circ - 0.5\alpha_k)} \cos \operatorname{arctg} \frac{2\pi D \operatorname{tg}(45^\circ - 0.5\alpha_k)}{D + d} \right] \quad (14)$$

RESULTS

Change dependences of pressure screw efficiency Q_1'' on its diameter D and rotation frequency of a screw n as functional $Q_1'' = f(D, n)$ at $\varphi_k = 1$, $k_\beta = 0.8$; $k_y = 1.3$; $d = 0.5D$, $\alpha_k = 0.522$ rad $z = 1$, $\delta = 0.02$ m, $\rho = 1300$ kg/m³ and on bulk material weight ρ and rotation frequency of a screw n as functional $Q_1'' = f(\rho, n)$ for $D = 0.15$ m have been graphed (according to 14) in the form of surfaces and their two-dimensional sections, which are illustrated in Fig. 2 and Fig. 3 respectively.

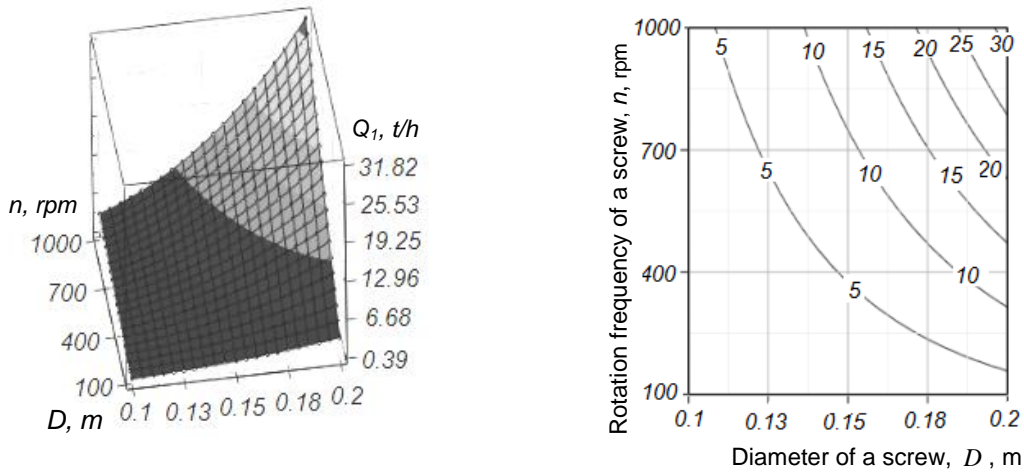


Fig. 2 - Change dependence of pressure screw efficiency Q_1'' on its diameter D and rotation frequency of a screw n as functional $Q_1'' = f(D, n)$

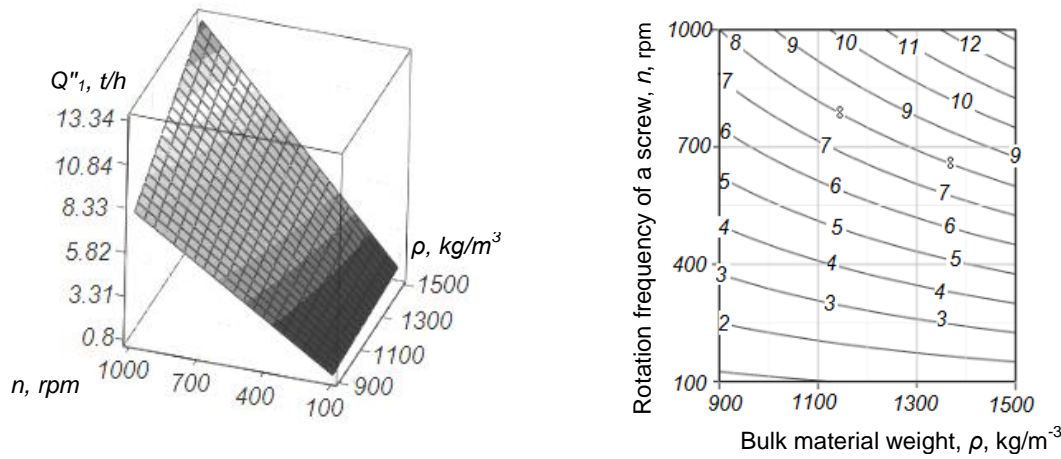


Fig. 3 - Change dependence of pressure screw efficiency Q_1'' on bulk material weight ρ and rotation frequency of a screw n as functional $Q_1'' = f(\rho, n)$

The analysis of the surfaces reveals, that pressure screw efficiency Q_1'' changes within the range of 0.4...32 (t/h) depending on the change in design and kinematic parameters and process variables of a screw and on loose material characteristics within the following limits: screw diameter $D=0.1...0.2$ (m); rotation frequency of a screw $n=100...1000$ (rpm); bulk material weight $\rho = 900...1500$ (kg/m³).

General tendency of the change in pressure screw efficiency Q_1'' depending on rotation frequency of a screw n at specified limits of screw diameter D variation and at $\rho=1300$ kg/m³ is represented by characteristic curves in Fig. 4, a, and depending on bulk material weight ρ within the specified variation limits of rotation frequency of a screw n and at $D=0.15$ m is represented by characteristic curves, which are shown in Fig.4, b. The change in pressure screw efficiency Q_1'' depending on rotation frequency of a screw n and bulk weight of loose material ρ is described by a linear function and is of directly proportional character. The main values of Q_1'' are within the range of $Q_1'' = 1.2...28.6$ and $Q_1'' = 2.3...11.9$ (t/h).

In order to determine the required design diameter D (cm) of a pressure screw, the values of which provide transportation of loose material, which comes from a loading opening 4 of a hopper 5 of a screw feeder 1, let us write condition (1) according to (12) as:

$$Q_b \leq 0.125\pi\varphi_k k_\beta k_\gamma \rho (D^2 - d^2) [D \operatorname{tg}(45^\circ - 0.5\alpha_k) - \delta_n] \times \left[1 - \frac{\delta_n z_n}{D \operatorname{tg}(45^\circ - 0.5\alpha_k)} \cos \operatorname{arctg} \frac{2\pi D \operatorname{tg}(45^\circ - 0.5\alpha_k)}{D + d} \right] \frac{d\varphi}{dt} \quad (15)$$

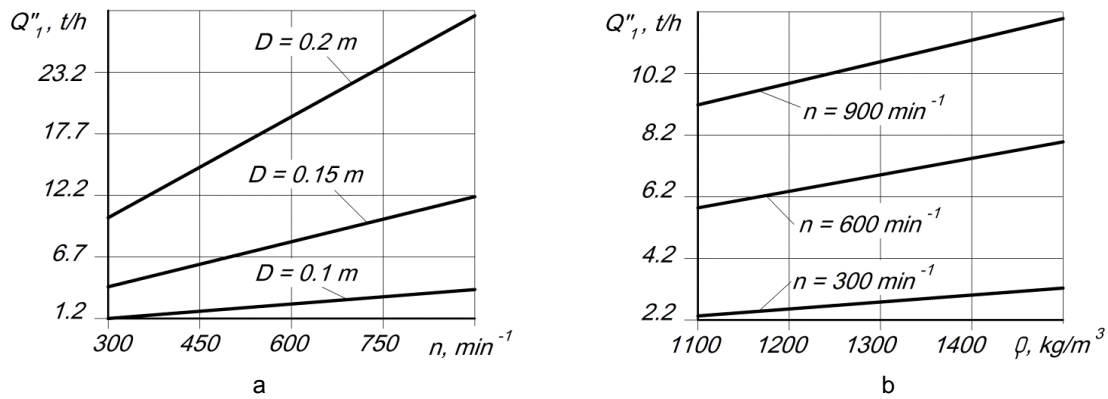


Fig. 4 - Change dependence of pressure screw efficiency Q_1'' :

a – on rotation frequency n of a screw at $\rho=1300 \text{ kg/m}^3$ as functional $Q_1'' = f(n)$;

b – on bulk material weight ρ at $D=0.15 \text{ m}$ as functional $Q_1'' = f(\rho)$

After transformation (15) and according to (2), (9) we obtain:

$$D^3 \text{tg} \beta - D^2 \delta_n - D d^2 \text{tg} \beta + d^2 \delta_n - \frac{1.47 k_n S_o^4 \sqrt{r_z}}{A \sqrt{f} \frac{d\varphi}{dt}} \geq 0 \tag{16}$$

where $A = 0.125 \pi \rho_k k_\beta k_y k_z$.

According to formula (9), the value of coefficient k_z has been determined in relation to the number of screw entries z_n , at design values $\delta_n = 0,002 \text{ m}$, $d = 0,45D$ and $\beta = 0.26 \text{ rad}$ (Table 1).

Table 1

Value of coefficient k_z depending on pressure screw design parameters

Number of entries	1			2		
	12	16	20	12	16	20
Screw diameter, m						
k_z	0.999	0.996	0.992	0.988	0.984	0.979

The obtained dependence (16) is the equation of the third degree relative to the diameter D of a pressure screw. Firstly, let us reduce it to a canonical form by dividing each term of the dependence by $\text{tg} \beta$.

$$D^3 - D^2 \frac{\delta_n}{\text{tg} \beta} - D d^2 + d^2 \frac{\delta_n}{\text{tg} \beta} - \frac{1.47 k_n S_o^4 \sqrt{r_z}}{A \text{tg} \beta \sqrt{f} \frac{d\varphi}{dt}} \geq 0 \tag{17}$$

Let us set the following in equation (17) $r = -\frac{\delta_n}{\text{tg} \beta}$; $s = -d^2$; $t = \frac{1}{\text{tg} \beta} \left(d^2 \delta_n - \frac{1.47 k_n S_o^4 \sqrt{r_z}}{A \sqrt{f} \frac{d\varphi}{dt}} \right)$ and let us

replace unknown $y = D + (r/3)$, here canonical form of the equation is brought into a reduced equation by the replacement of $D = y - (r/3)$, where $p = \frac{3s - r^2}{3}$, $q = \frac{2r^3}{27} - \frac{rs}{3} + t$, according to (Hevko R.B. et.al., 2016).

Here, we obtain:

$$\left. \begin{aligned} D^3 + rD^2 + sD + t &\geq 0; & y^3 + py + q &\geq 0; \\ p &= \frac{\delta_n^2}{3 \text{tg}^2 \beta} - d^2; & q &= \frac{2}{3 \text{tg} \beta} \left(d^2 \delta_n - \frac{2.2 k_n S_o^4 \sqrt{r_z}}{A \sqrt{f} \frac{d\varphi}{dt}} - \frac{\delta_n^3}{9 \text{tg}^2 \beta} \right) \end{aligned} \right\} \tag{18}$$

Let us determine the discriminant D' of the reduced cubic equation (18), here

$$D' = (p/3)^3 + (q/2)^2 = \frac{1}{9tg^2\beta} \left[\frac{1}{3} \left(\frac{\delta_n^2}{3} - d^2tg^2\beta \right)^3 + \frac{1}{2} \left(d^2\delta_n - \frac{2.2k_n S_o^4 \sqrt{r_z}}{A\sqrt{f} \frac{d\varphi}{dt}} - \frac{\delta_n^3}{9tg^2\beta} \right)^2 \right] > 0 \quad (19)$$

That is to say, in this case equation (18) possesses one real solution of unknown in a reduced cubic equation $y^3 + py + q \geq 0$.

The reduced cubic equation $y^3 + py + q \geq 0$ in unknown y is solved using Cardano formula and taking into account that the discriminant D' of the canonical form of cubic equation (18) $D^3 + rD^2 + sD + t \geq 0$ is greater than zero, that is to say $D' > 0$, we obtain one real solution of unknown y by the expression $y = u + v$, where $u = \sqrt[3]{-(q/2) + \sqrt{D'}}$, $v = \sqrt[3]{-(q/2) - \sqrt{D'}}$, that is to say

$$y \geq \frac{1}{\sqrt[3]{3tg\beta}} \left(\sqrt[3]{ \frac{1}{3} \left(\frac{\delta_n^2}{3} - d^2tg^2\beta \right)^3 + 0.5 \left(d^2\delta_n - \frac{2.2k_n S_o^4 \sqrt{r_z}}{A\sqrt{f} \frac{d\varphi}{dt}} - \frac{\delta_n^3}{9tg^2\beta} \right)^2 } - d^2\delta_n + \frac{2.2k_n S_o^4 \sqrt{r_z}}{A\sqrt{f} \frac{d\varphi}{dt}} + \frac{\delta_n^3}{9tg^2\beta} } + \sqrt[3]{ \frac{2.2k_n S_o^4 \sqrt{r_z}}{A\sqrt{f} \frac{d\varphi}{dt}} + \frac{\delta_n^3}{9tg^2\beta} - d^2\delta_n - \sqrt[3]{ - \frac{1}{3} \left(\frac{\delta_n^2}{3} - d^2tg^2\beta \right)^3 + 0.5 \left(d^2\delta_n - \frac{2.2k_n S_o^4 \sqrt{r_z}}{A\sqrt{f} \frac{d\varphi}{dt}} - \frac{\delta_n^3}{9tg^2\beta} \right)^2 } } \right) \quad (20)$$

Using inverse substitution of value $D = y - (r/3)$ into inequality (18), taking into consideration dependence (20), and substituting value A , after corresponding calculations, let us determine a design value of the required diameter of a pressure screw D (cm) of a feeder:

$$*D \geq \frac{1}{\sqrt[3]{3tg\beta}} \left(\sqrt[3]{ \frac{1}{3} \left(\frac{\delta_n^2}{3} - d^2tg^2\beta \right)^3 + 0.5 \left(d^2\delta_n - \frac{528k_n S_o^4 \sqrt{r_z}}{\pi^2 n \varphi_k k_\beta k_y k_z \sqrt{f}} - \frac{\delta_n^3}{9tg^2\beta} \right)^2 } - d^2\delta_n + \frac{528k_n S_o^4 \sqrt{r_z}}{\pi^2 n \varphi_k k_\beta k_y k_z \sqrt{f}} + \frac{\delta_n^3}{9tg^2\beta} } + \sqrt[3]{ \frac{528k_n S_o^4 \sqrt{r_z}}{\pi^2 n \varphi_k k_\beta k_y k_z \sqrt{f}} + \frac{\delta_n^3}{9tg^2\beta} - d^2\delta_n - \sqrt[3]{ - \frac{1}{3} \left(\frac{\delta_n^2}{3} - d^2tg^2\beta \right)^3 + 0.5 \left(d^2\delta_n - \frac{528k_n S_o^4 \sqrt{r_z}}{\pi^2 n \varphi_k k_\beta k_y k_z \sqrt{f}} - \frac{\delta_n^3}{9tg^2\beta} \right)^2 } } \right) + \frac{\delta_n}{3tg\beta} \quad (21)$$

The obtained equation (21) describes a change in the required design diameter D of a feeder pressure screw depending on design parameters of a hopper loading opening, process parameters of a screw and loose material characteristics and the process of its transportation.

In order to determine the required design diameter D of a feeder pressure screw, the surface of change dependence of D and its two-dimensional section on the cross-sectional area S_o of a hopper loading opening of a screw feeder and rotation frequency of a screw n have been constructed in the form of a functional $D = f(S_o, n)$ (Fig. 5) and the surface of change dependence of D and its two-dimensional section on rotation frequency of a screw n and a helix angle β have been constructed in the form of a functional $D = f(n, \beta)$ (Fig. 6) at average values $f = 0.5$, $d = 0.01$ m, $k_z = 0.984$ (Table 1.), $\beta = \pi/12$

deg.

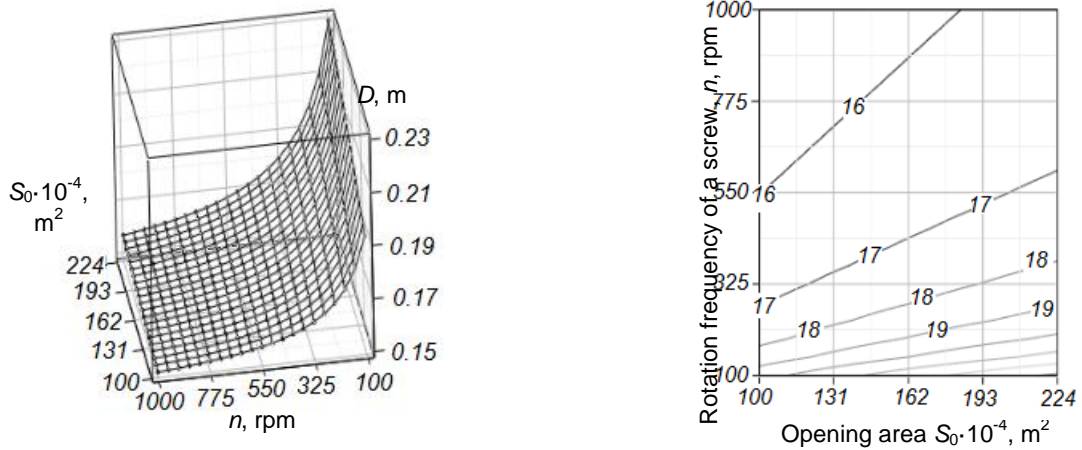


Fig. 5 - Change dependence of a screw diameter D on opening area S_o and rotation frequency of a screw n as a functional $D = f(S_o, n)$

The analysis of the presented surfaces and their two-dimensional sections of the dependences $D = f(S_o, n)$ and $D = f(n, \beta)$ shows that with the increase in rotation frequency of a screw n from 100 to 1000 min^{-1} (Fig. 6) and a helix angle β from $\pi/18$ rad (or 10 deg) to $\pi/9$ rad (or 20 deg) the diameter D of conveyor pressure screw decreases and is within the range of $D = 0.15 \dots 0.36$ (m), which is also confirmed by characteristic curves $D = f(n)$ and $D = f(\beta)$, which are represented in Fig. 7.

Besides, diameter D change of a pressure screw depending on the change of the cross-sectional area S_o of a hopper opening is of minor nature, here, when S_o increases from 100 to 224 cm^2 (Fig. 5, 7, a), increment $\Delta D \cong 0.01 \dots 0.02$ m

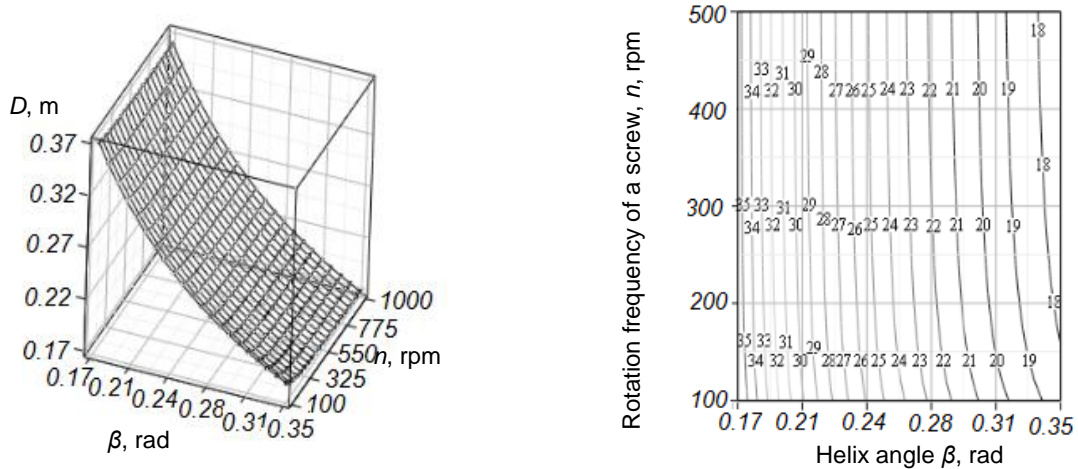


Fig. 6 - Change dependence of a screw diameter D on rotation frequency of a screw n and a helix angle β as a functional $D = f(n, \beta)$

The conducted general analysis of the justification of a pressure screw feeder diameter D has shown that design values of D are within the range of $D = 0.15 \dots 0.36$ (m) at variations of rotation frequency of a screw being $100 \leq n \leq 1000$ (rpm) and a helix angle being $0.17 \leq \beta \leq 0.34$ (rad).

The required cross-sectional area S_o of a loading opening of a hopper, at which the desired efficiency of a screw feeder can be obtained, is determined from equation (16)

$$S_o \leq \frac{A\sqrt{f}(D^3 \text{tg} \beta - D^2 \delta_n - Dd^2 \text{tg} \beta + d^2 \delta_n) \frac{d\varphi}{dt}}{1.47k_n^4 \sqrt{r_z}} \quad (22)$$

or

$$S_o \leq \frac{0.003\pi^2 n \varphi_k k_\beta k_y k_z \sqrt{f} (D^3 \operatorname{tg} \beta - D^2 \delta_n - D d^2 \operatorname{tg} \beta + d^2 \delta_n)}{k_n^4 \sqrt[4]{r_z}} \quad (23)$$

or according to (1), (2)

$$S_o \leq \frac{Q_1 \sqrt{f}}{1.47 \rho k_n^4 \sqrt[4]{r_z}} \quad (24)$$

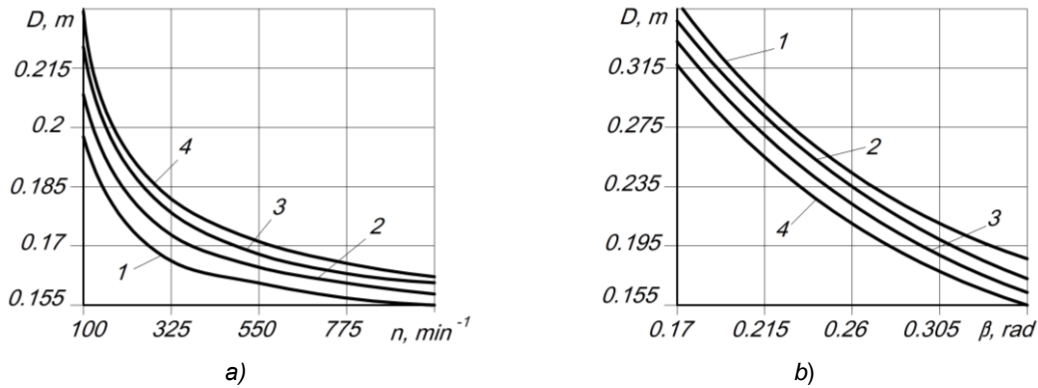


Fig. 7 - Dependence of screw diameter change D

a – on rotation frequency of a screw n at $\beta = \pi / 12$ rad as a functional $D = f(n)$, 1, 2, 3, 4 – respectively, $S_o = 100, 140, 180, 220$ (10^{-4} m^2); b – on a helix angle β at $S_o = 160 \cdot 10^{-4} \text{ m}^2$ as a functional $D = f(\beta)$, 1, 2, 3, 4 – respectively, $n = 400, 700, 1000$ (rpm¹)

According to equations (23) and (24), change dependence of the cross-sectional area S_o of a feeder hopper loading opening on screw efficiency Q_1 and a screw diameter D , the limits of which are determined from the previous analysis, has been constructed (Fig. 8).

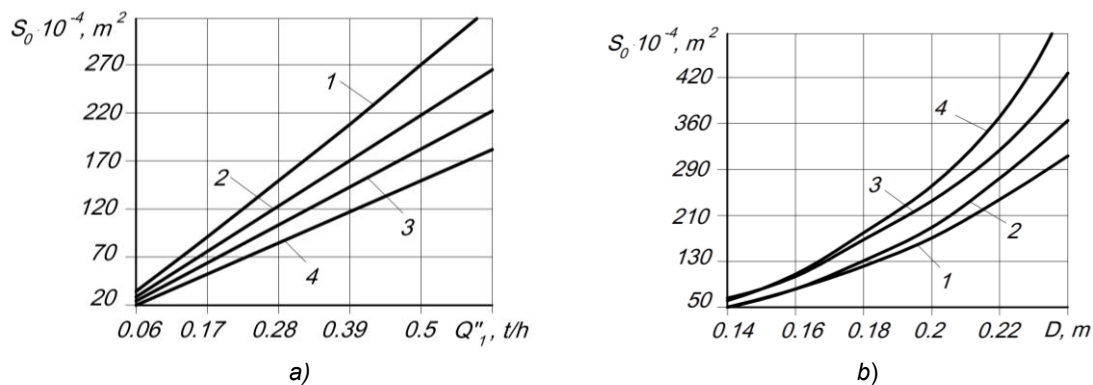


Fig. 8 - Change dependence of loading opening area S_o

a – on screw efficiency Q_1 , 1, 2, 3, 4 – at $\rho = 900; 1100; 1300; 1500 \text{ kg/m}^3$ respectively;
 b – on screw diameter D , at $n = 100, 300, 700, 1000 \text{ rpm}$ respectively

The cross-sectional area S_o of an opening, which provides the required loose material consumption through the feeder hopper loading opening of pneumoconveyor screw, is within the range of $70 \dots 250$ (10^{-4} m^2) and provides designed screw capacity within the limits of $2,0 \dots 9,0 \text{ t/h}$ (Fig. 8, a). At screw diameter variation within the range of $D = 0,15 \dots 0,22$ (m), cross-sectional area S_o of an opening should be approximately from 70 to 350 (10^{-4} m^2) (Fig. 8, b).

CONCLUSIONS

Based on the conducted constructive and technological analysis of a pressure pump operation process and under the condition of provided technological effectiveness of pneumoconveyor screw, a mathematical model, which describes a change in operation efficiency and loose material consumption through a screw feeder hopper depending on design and kinematic parameters and process variables of a screw and on loose material characteristics, has been obtained.

It has been determined that screw feeder efficiency Q_1 changes within the range of 0.4...32 (t/h) depending on process variations within the following limits: a screw diameter $D= 0.1...0.2$ (m); rotation frequency of a screw $n = 100...1000$ (min^{-1}); bulk weight of loose material $\rho= 900...1500$ (kg/m^3). A change in feeder efficiency Q_1'' depending on its rotation frequency and bulk weight of loose material ρ is described by a linear function and is of directly proportional character, while the values of Q_1'' are within the range of $Q_1'' = 1.2...28.6$ and $Q_1'' = 2.3...11.9$ (t/h).

Under the condition of proper operation of a screw feeder, the dependence for determining the required screw diameter, which can provide loose material consumption from a hopper to a screw has been developed. Here, it has been determined that the values of D are within the limits of $D= 0.15...0.36$ (m) at the variations of screw rotation frequency being $100 \leq n \leq 1000$ (rpm) and screw helix angle being $0.17 \leq \beta \leq 0.34$ (rad).

The cross-sectional area of a feeder hopper opening S_0 should be within the limits of 70...250 (10^{-4} m^2) and it provides the required screw efficiency within the range of 0.1...0.5 t/h. At diameter change within the limits of $D= 0.15...0.22$ (m), cross-sectional area S_0 of an opening should range from 70 to 350 (10^{-4} m^2).

REFERENCES

- [1] Halka R.I., Hevko R.B., Nazar I.I., Hevko I.B., Malanchyn A.M. Bezpalko A.P., (2001) – Screw Pneumatic Conveyer (Шнековий пневматичний транспортер), *Patent № 34329A Ukraine*, МПК В65G 53/48;
- [2] Hevko R.B., Dzyura V.O., Romanovsky R.M., (2009) – Designing of pneumo-mechanical conveyer for loose materials (Проектування пневмо-механічного транспортера сипких матеріалів), *Bulletin of I.Pyliui Ternopil State Technical University (Вісник Тернопільського державного технічного університету)*, Vol 14, no 4, pp.84-88, Ternopil/ Ukraine;
- [3] Hevko R.B., Dzyura V.O., Romanovsky R.M., (2014) – Mathematical model of the pneumatic-screw conveyor screw mechanism operation, *INMATEH-Agricultural Engineering*, vol.44, no.3, pp.103-110, Bucharest/Romania;
- [4] Hevko R.B., Klendiy O.M., (2014) – The investigation of the process of a screw conveyer safety device actuation, *INMATEH: Agricultural Engineering*, vol.42, no.1, pp.55-60, Bucharest/Romania;
- [5] Hevko R.B., Klendiy M.B., Klendii O.M., (2016), Investigation of a transfer branch of a flexible screw conveyer, *INMATEH: Agricultural Engineering*, vol.48. no.1, pp.29-34, Bucharest/Romania;
- [6] Hevko R.B., Rozum R.I., Klendiy O.M., (2016) – *Development of design and investigation of operation processes of loading pipes of screw conveyors*, *INMATEH: Agricultural engineering*, vol.50, no.3, pp.89-96, Bucharest/Romania;
- [7] Hevko R.B., Shynkaryk M.I., Vozniuk S.V., (2012) – Screw Conveyer (Гвинтовий конвеєр), *Patent № 68113 Ukraine*, МПК В65G 33/14;
- [8] Hevko R.B., Vitrovyi A.O., Dzyura V.O., Romanovsky R.M., (2011) – Pneumatic Mechanical Conveyer (Пневмомеханічний транспортер), *Patent № 61567 Ukraine*, МПК В65G 53/00;
- [9] Lyashuk O.L., Rogatynska O.R., Serilko D.L., (2015) - Modelling of the vertical screw conveyer loading, *INMATEH-Agricultural Engineering*. vol. 45, no 1, pp. 87-94, Bucharest/Romania;
- [10] Rogatynska O., Liashuk O., Peleshok T., Liubachivskiy R., (2015) - Investigation of the Process of Loose Material Transportation by Means of Inclined Screw Conveyers (Дослідження процесу транспортування сипкого вантажу похилими гвинтовими конвеєрами), *Bulletin of I.Pyliui Ternopil National Technical University (Вісник Тернопільського національного технічного університету ім. І.Пулюя)*, Vol.79, pp. 137-143, Ternopil/Ukraine;
- [11] Rohatynskiy R.M., Diachun A.I., Varian A.R., (2016) - Investigation of Kinematics of Grain Material in a Screw Conveyor with a Rotating Casing (Дослідження кінематики зернового матеріалу у гвинтовому конвеєрі із обертовим кожухом). *Bulletin of Kharkiv Petro Vasylenko National Technical University of Agriculture №168 (Вісник Харківського національного технічного університету сільського господарства імені Петра Василенка №168)*, pp.24-31, Kharkiv / Ukraine;
- [12] Voitiuk D.H., Baranovskyi V.M., Bulhakov V.M. and other, (2005) - *Agricultural Machinery. Foundations of Theory and Calculations: textbook (Сільськогосподарські машини. Основи теорії та розрахунку: підручник)*, Vyshcha Osvita (Вища освіта), 446 p., Kyiv / Ukraine.

ENGINEERING MANAGEMENT OF VIBRATING MACHINES FOR TARGETED MECHANICAL ACTIVATION OF PREMIX COMPONENTS**ІНЖЕНЕРНИЙ МЕНЕДЖМЕНТ ВІБРАЦІЙНИХ МАШИН ДЛЯ ЦІЛЬОВОЇ МЕХАНОАКТИВАЦІЇ КОМПОНЕНТІВ ПРЕМІКСУ**

Assoc. Prof. Ph. D. Eng. Yanovych V., Assoc. Prof. Ph. D. Econ. Honcharuk T.,
Assoc. Prof. Ph. D. Econ. Honcharuk I., Assoc. Prof. Ph.D. Ped. Kovalova K.
Vinnytsia National Agrarian University, Vinnytsia / Ukrainian
Tel: +38(097)12-78-638; E-mail: Yanovichvitaliy@i.ua

Keywords: vibration equipment, premix components, mechanical activation

ABSTRACT

The article shows the technological scheme and the implementation of structural vibration equipment for complex processing of bulk premix ingredients in the manufacturing of high active premix based on natural ingredients. To intensify the process of dissolution of premix ingredients by biologically active environment and to minimize the time for reaching their maximum concentration in the body, it is proposed to carry out targeted mechanical activation, which allows increasing the dispersion of the material significantly, generating more soluble polymorphic modifications with the active destruction of the crystal lattice of the treated material to its full amorphization.

РЕЗЮМЕ

В статті відображено технологічні схеми та конструктивну реалізацію вібраційних машин для комплексної обробки сипких компонентів преміксу при виробництві високоактивних сумішей на основі природних інгредієнтів. Для інтенсифікації процесу засвоєння компонентів біологічно активним середовищем та мінімізації часу для досягнення їх максимальної концентрації в організмі, пропонується здійснювати цільову механоактивацію, що надає можливість значно збільшити дисперсність оброблюваного матеріалу, генеруючи більш розчинні поліморфні модифікації за умови активної деструкції кристалічної решітки оброблюваної сировини до повної її аморфізації.

INTRODUCTION

One of the most important areas of research in physical chemistry is to link the reactivity of the reagents with their structure and conditions of the chemical reaction. Increasing solubility dosage forms is one of the most important issues, as 40% of premix substances are difficult to solubilise, and of newly synthesized substances up to 60% have low solubility in water and aqueous solutions.

Nowadays a recognized fact for solid-phase reagents is that the reactivity depends on their structure, including the presence of different kinds of micro defects. Among the methods for acquiring this condition with substantial degradation of the crystalline material is grating target mechanical activation, which received wide development as a way to regulate the reactivity of solid materials that come in a variety of chemical reactions.

MATERIALS AND METHODS

Growing consumer demand for premix particulate mixture of natural origin and benefits of their use cause expansion of industrial dosage forms production data (see fig.1).

One of the most important stages of the production process of premix compounds is grinding plant with gradual sifting and bringing it to a smooth consistency with additional premix ingredients by mixing. Last comes to the production as shallow dispersive loose bulks (Shakhtshneider T.P., 2013; Chueshov V.I., Hladuh E.V., Saiko I.V., 2012).

Crumbly premix mixture is the basic foundation for the production of granules of drugs, the consumption of which is the oral method and mostly depends on the parameters of the drug - physical and chemical properties of raw speed of absorption and time to reach maximum concentration in the organism (Sydorenko I.I., Kushnir A.Y., Baidzhanov S. M., 2015).

During the last three decades one of the most important criteria for assessing the quality characteristics of oral medical facilities became their capacity for absorption by which a system of bio premix classification was made, based on the latest solubility in the liquid and the permeability degree of the active substance in the intestine wall.

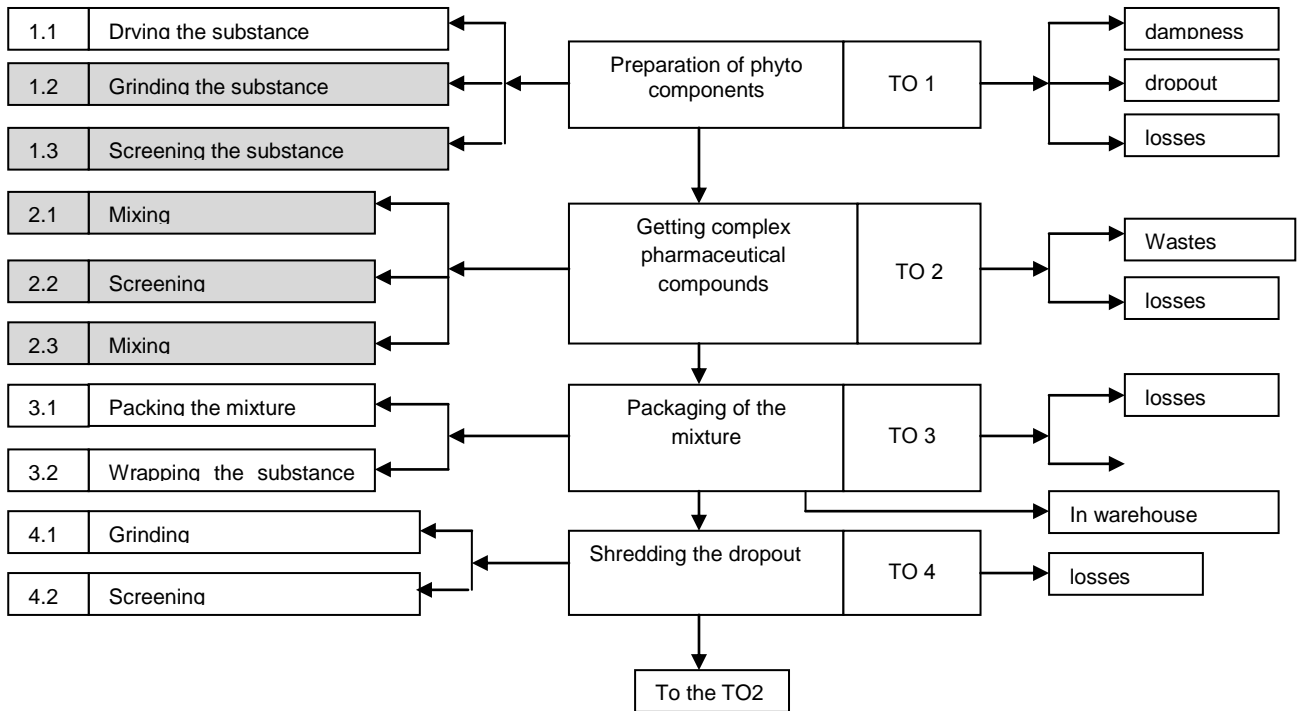


Fig. 1 - Technological scheme of complex premix compounds

The rate of dissolution of the raw material is characterized by the Neuees-Whitney equation (1):

$$\frac{dC}{dT} = SD(C_s - C) / h \quad (1)$$

where - $\frac{dC}{dT}$ the rate of dissolution; S - dissolution of the surface area; D - diffusion coefficient; C_s - solubility substance; C - substance concentration at the time t , h - the thickness of the diffusion layer adjacent to the surface of the solvent.

The analysis of the equation led to the conclusion that the intensification of the drugs dissolution process is possible for a significant increase in the dispersion of the material and consequently the contacting area of substance or by reducing the thickness of the diffusion layer (*Cheney M.L., Weyna N., Shan M., Hanna L., Wojtas M.J., 2010*).

The solubility of solids is a complex process that combines integrated communications gap between the ions, atoms or molecules in the structure of soluble material and requires significant energy costs.

The higher the binding energy between the particles of the material, the better.

Simultaneously goes the interaction of particles with a solvent that is accompanied by the release of energy. The energy intensity of the process comprehensively reflects the total energy expenditure associated with the destruction of the molecular lattice, for intensive transfer of the active substance molecules in the solution, and as a result solvation energy and entropy increases in the local system (2):

$$\Delta H_{\text{solubility}} = \Delta H_{\text{destruction}} + \Delta H_{\text{solvation}} \quad (2)$$

This equation shows that the molecular switch in solution can be intensified as a result of targeted destruction of the crystal lattice of a solid, and as a result its complete amorphization.

As plant material for experimental treatment valerian root and mix herbs were chosen (see fig.2.).

A promising experimental drug for the treatment of aluminum silicate glauconite was used (see fig.3.), which meets all the requirements to immune sorbents: inertia with respect to biological agents; stability properties over a wide range; it is not destroyed when exposed to microorganisms; high sorption capacity; ability to covalent binding ligand as in the initial state as in the modification.



Fig. 2 - The plant material before and after grinding

a,b – valerian root before and after grinding; c, d – gathering herbs before and after grinding



Fig. 3 - glauconite before and after grinding

a – glauconite before grinding; b – glauconite after grinding

RESULTS

The current technology of bulk premix compounds, based on plant material has several disadvantages, one of which is energy intensive phased implementation process, separation and mixing of premix ingredients phytocomponents in separate powder mass (Lavrova L.Y., 2013; Nadutiy V.P., Titov A.A., 2017).

To address these deficiencies a vibrocentrifugal shredder was developed (Dudnikov A.A., Belovod A.I., Pasyuta A.G., 2015); it combines elements of a ball mill, mixer and sieve separator that provides oscillating and rotating movements in two perpendicular planes.

Schematic diagram of vibrocentrifugal disintegrator and its constructive realization are shown in fig. 4.

Vibrocentrifugal shredder includes frame 1 and two main structural paths that are driven into motion by electrical engine 2; they are interconnected by drive shaft 3, open bevel gear 4 and wedge-belt transmission system 5.

The internal circuit of the disintegrator is composed of three-chambered working container 6, sieve elements 7 and grinding bodies 8, pipes 9, 10, 11 respectively for supplying and discharging technology environment, imbalance 12 to generate power imbalance systems elastic elements 13 between the container and the rim 14, drive shaft rim 15 is placed on the support 16 nodes.

The external circuit includes the disintegrator hoop 14 with its drive shaft 15 that leads to the rotation of the motor 2 through 5 wedge-belt gear axis 17 and open bevel gear 4. The carrier 18 is driven through the hollow drive shaft 19, which, with the help of wedge-belt through transmission 20 is connected to the motor 2.

This design works as follows: after the required amount of raw materials is downloaded in the corresponding proportions in the chamber for grinding and mixing, we switch on the electric motor 2, 6 and drive the container carrier 18.

The torque from the electric motor 2 through the wedge-belt gear 5 and bevel gear 4 creates rotation of the rim 14 and of the imbalance 12 and drives 18 relative to the perpendicular axes. Rotating of the imbalance leads to spatial fluctuations of spring-loaded three-chambered drum 6 together with the loaded raw materials and grinding bodies 8 in the form of metal balls or ceramic elements. This leads to the crushing of the treated mass.

With decreasing particle size of the crushed material under the influence of centrifugal forces and alternating loads through sieve surface, their classification by size is performed: the particle diameter equal to or smaller than sieve openings fall in the mixing compartment, others go to re-grinding.

This combination of technology and the intensification of structural factors make it possible to significantly increase the destruction degree of particles with subsequent mixing of additional components, making complex effect on the work environment.

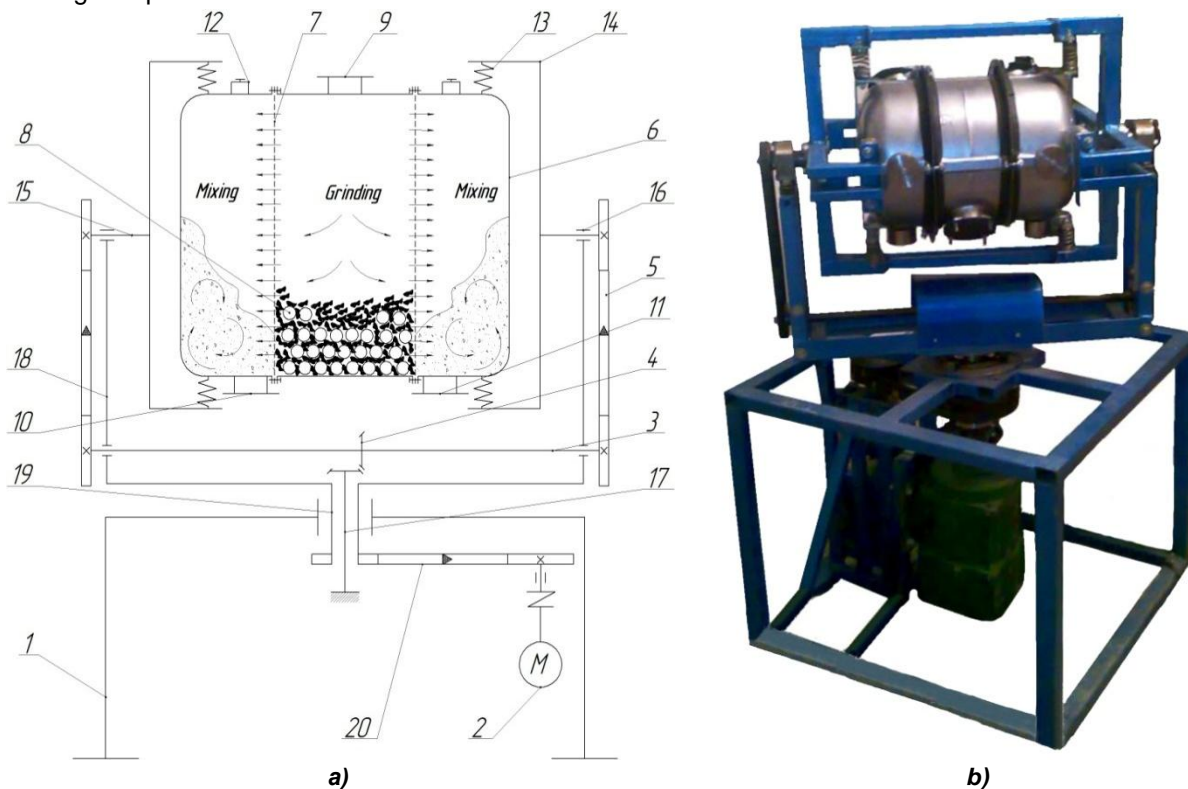


Fig. 4 - Vibrocentrifugal disintegrator for the production of premix mixtures:

a) schematic diagram; b) constructive realization;

1 - bed; 2 - electric; 3, 15, 19 - drive shafts; 4 - conical transmission; 5, 20 - wedge-belt transmission; 6 - three-chambered container; 7 - sieve elements; 8 - crushing balls; 9, 10, 11 - pipes; 12 - unbalanced weight; 13 - elastic elements; 14 - hoop; 16 - bearing components; 17 - axis; 18 - drives

Modern trends in premix complex based on implementing highly efficient methods to change the substance structure are based on the facts that they provide the process of mechanical activation, which is characterized by a significant increase in the dispersion of the material and helps generating more soluble polymorphs. This process intensifies the distribution of drugs in the media, but also contributes to a significant degradation of the material crystal lattice to its full amorphization.

This technological effect is advisable to use for the production of entero- and immunosorbent glauconite powder, which makes it possible to intensify the process of binding and separation of blood antibodies or antigens.

Glauconite, a natural aluminosilicate meets all the requirements to immunosorbents: inertia with respect to biological agents; stability of properties over a wide range; it is not subject to destruction when exposed to microorganisms; high sorption capacity; ability to covalent binding ligand in the initial state and in the modified one.

Based on the analysis of manufacturing processes and design schemes of existing equipment for the fine grinding process (Poluljakh D. A, 2017; Kuzo I.V., Lanets O.S., Gursky V.M., Shpak Y.V., 2015), the vibratory mill was developed, which implements the idea of superfine grinding of glauconitic material and it provides significant activation of the newly formed particles surface.

Schematic diagram of a vibrating mill volume fluctuations and its constructive realization are shown in fig. 5.

The vibrating mill contains two main structural contours, which are driven by an electric motor 1, which are interconnected by elastic elements 2, 3, bearing units 4, 5, and a spindle 6, with an angle of inclination θ which is regulated by screws 7.

Such rotating technological movement of the mill's executive body makes it possible to significantly increase the force influence of the crushing balls on the processing material, and as a result it helps increasing the productivity and quality of the specified process.

The inner contour of the mill is composed of: elastic coupling 8 and a kinematic drive shaft 9 with eccentricity e and balancing masses 10 to create a combined power and momentary imbalance of the system.

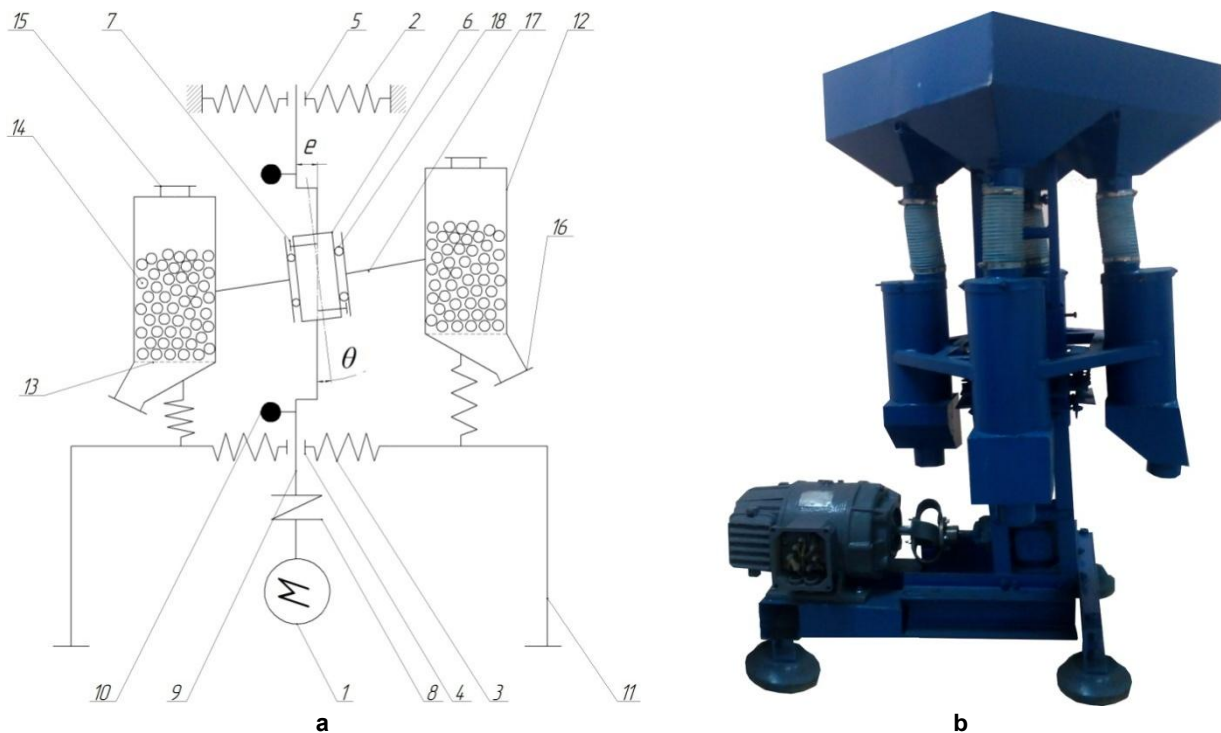


Fig. 5 - Vibration mill for glauconite

a) schematic diagram; b) constructive realization; 1 - electric motor; 2, 3 - elastic elements 4,5 - bearing assemblies; 6 - gyrations sleeve; 7 - adjusting bolts 8 - elastic sleeve; 9 - kinematic drive shaft; 10 - balancing weight; 11-frame; 12 - cylindrical container; 13 separation elements; 14 - crushing balls; 15 16 - pipes for loading and unloading the surface of the material; 17 - drive platform; 18 - bearing.

The outer contour of the mill contains the frame 11, cylindrical container 12 with perforating elements 13 and 14 crushing balls, pipes 15, 16 for loading and unloading of the surface of the material, the drive platform 17 and bearing 18.

Vibration mill works as follows:

If you put the motor 1 torque with the help of elastic sleeve 8 it will transmit to the kinematic drive shaft 9 with eccentricity e and balancing masses 10 by rotation which is rolling the bearing 18 to relatively graceful sleeve 6 forcing through the drive platform 17 at the same time to carry out horizontal vibrations and graceful movement of spring-loaded cylindrical containers 12 together with 14 manufacturing crushing balls material that is continuously supplied through pipes 15 and as a result of crushing balls 14 force through pipes 16 is discharged from the mill.

The proposed construction implements the idea of a combined interaction of the containers vibration motion with the possibility to realize the milling process, which is provided by the highly dynamic condition of the crushing balls.

Today, one of the most common dosage forms in the world are forms for pre-oral usage, most of which are in the solid state and their active interaction with the body starts as a result of dissolution of premix ingredients and subsequent penetration of the active substance through the mucous membrane of the gastrointestinal tract.

The analysis considered approach shows that significant reduction in particle size, more soluble polymorphs, and distribution of drugs and the destruction of the crystal lattice of the complete amorphization may be implemented with the help of energy-mechanical and chemical processing methods of premix raw materials that can be implemented by energy-mechanical processing methods of premix substances (Shakhtshneider T.P., 2013).

This task can be implemented by creating vibrating mills, including plant material, which is provided by oscillating movement of preconceived milling blends of camera that are performed in two parallel placed

cylindrical containers placed at an angle to the horizontal pipe that connects the transition to the effective transport of the crushed plant matter (Solona O.V., Yanovych V.P., 2016).

Fig.6 presents a schematic diagram and the implementation of mill structural vibration for plant material

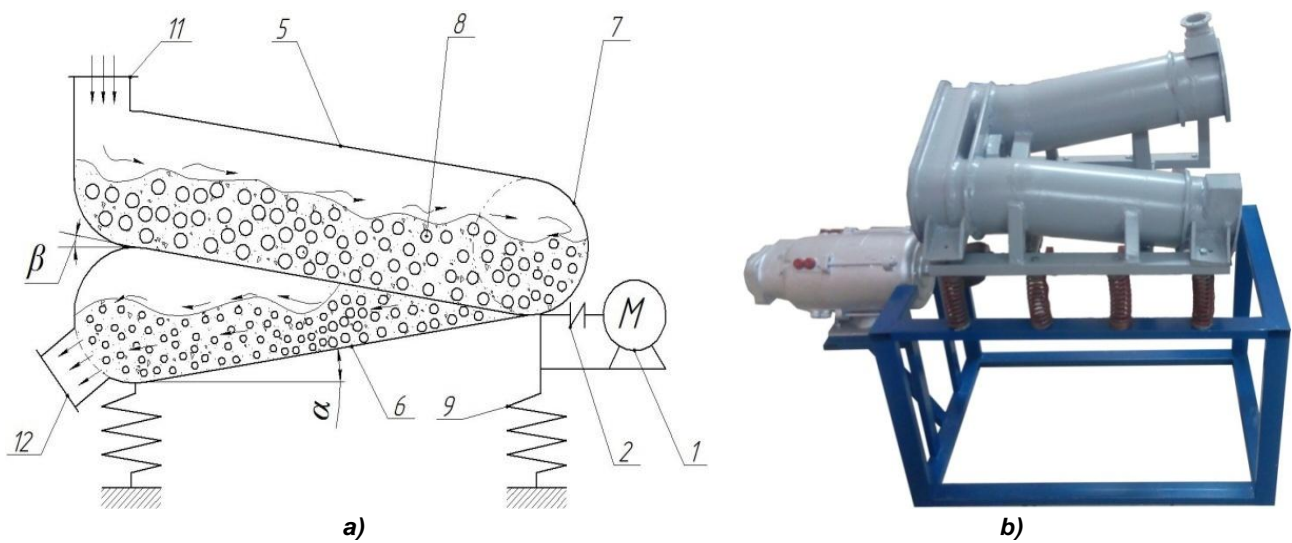


Fig. 6 - Vibrating mill for plant material

a) schematic diagram; b) constructive realization; 1 - electric motor; 2 - flexible coupling; 3 - a power shaft; 4 - imbalance; 5,6 - cylindrical container; 5, 8 - transitional tubes; 8 – crushing balls; 9 - elastic elements; 10 - crosspiece; 11, 12 - tubes for supplying and discharging the treated material

Vibrating electric mill that has 1, 2 elastic coupling, connected to the drive shaft 3 on which is placed imbalance 4 of the grinding chamber performed as two parallel cylindrical containers 5, 6 placed at an angle α and β to the horizon, which joined the transitional pipe 7 and complete crushing balls 8, the elastic elements 9, arms 10 tubes 11 and 12 respectively for feeding and unloading material.

Vibration mill works as follows: the motor 1 through flexible coupling 2, transmits the torque to the drive shaft 3 with imbalance 4, by rotation as tightly as traverse 10 is placed and it creates a combined power and vibration of unbalanced milling mixture made of cylindrical containers 5, 6 and transition pipe 7, that in their turn are filled with crushing balls 8 and helical milling chamber. Processing material which is continuously supplied through the loading pipe 11 is actively grained as a result of force of crushing balls 8 in spiral trajectories and it is transported to the pipe 12 to unloading out of the vibration mill.

This type of fluctuation of the pouring medium provided by the working chamber can significantly increase the effect of process capacity and the transport speed of the filler, as well as increase the productivity and quality of the intended process.

To activate the mechanical auxiliary components tablet form (lactose, talc) vibratory mill was developed, in which by changing the design of drive mechanism, the intensification of material grinding is achieved and quality milling of weight minimize energy consumption (Chueshov V.I., Hladuh E.V., Saiko I.V., 2012).

Schematic diagram of angular oscillation of vibration mill is shown in fig. 7.a, and there is its constructive realization in fig. 7.b.

The vibrating mill contains an electric motor 1, an elastic coupling 2, a drive shaft 3 which has imbalance 4, which in turn, through the bearing unit 5, is mounted locally to the rod 6 at the prop side end of which is counterbalanced 7, spring-loaded grinding chambers 8 are connected by traversing 9 and equilibrium on the central axis 10, which is located on the racks 11, the pipes 12 and 13, respectively, for feeding and unloading.

If you switch on the motor torque 1 through elastic coupling 2 it is transmitted to the drive shaft 3 of imbalance 4, its rotation leads to the creation of a combined power and torque imbalance of the rod 6, which is a consequence of moving the central fastening and inertial influence counterweight 7, it causes the appearance of angular oscillations, as a result traverse connection 9 through the central axis 10, which are transmitted to the spring-loaded grinding chamber 8.

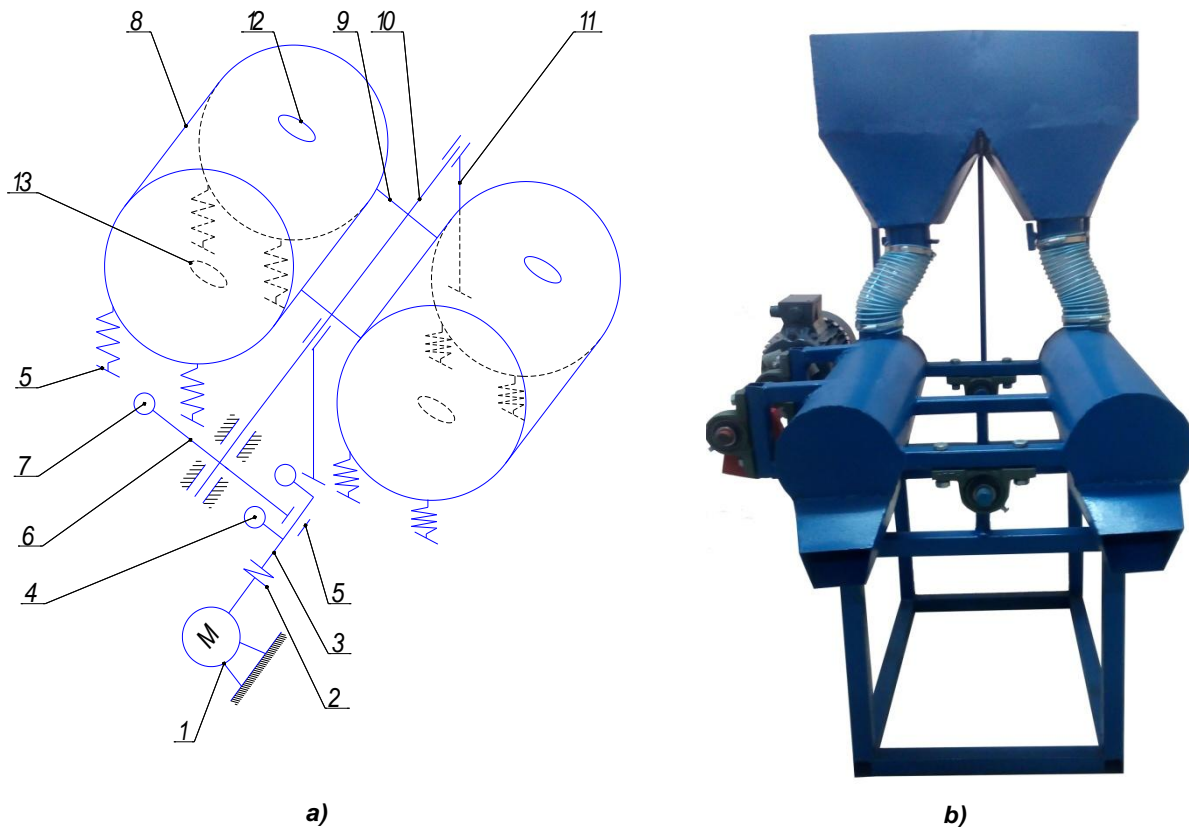


Fig. 7 - Vibration mill of volume oscillations

a) schematic diagram; b) constructive realization;

1 - electric motor; 2 - elastic sleeve; 3 - drive shaft; 4 - imbalances; 5 - bearing assembly; 6 - pole;
7 - counterweight; 8 - spring-loaded grinding chamber; 9 - arms; 10 - axis; 11 - racks;
12 13 - pipes respectively for feeding and unloading process environment

Such oscillating technological movement of the mill's executive bodies makes it possible to significantly increase the force influence of the crushing balls on the processing material, and as a result it helps increasing the productivity and quality of the specified process.

CONCLUSION

Based on the analysis of the technological features of manufacturing premix bulk mixtures based on natural substances the following means were elaborated:

- Vibro-central shredder for complex implementation processes of crushing, separation of premix ingredients, which combines elements of a ball mill, mixer and sieve separator that provide oscillating and rotating movements in two perpendicular planes;
- Vibratory mill for the production of mechanically activated entero - and immunosorbent glauconitic powder application which makes it possible to significantly increase the degree of destruction of natural aluminum silicate particles with substantial degradation of its molecular structure, and consequently to increase its solubility and absorption of the active substance in the body;
- Vibratory mill for plant material, which provided a significant degradation of the material during its processing by activating sorption properties of the original product;
- Vibratory mill for mechanical activation of auxiliary components of tablet form (lactose, talc) which, by changing the design of drive mechanism, is achieved by intensifying the process of material grinding and the quality of the milling machine by minimizing energy consumption.

REFERENCES

- [1] Cheney M.L., Weyna N., Shan M., Hanna L., Wojtas M.J., (2010), Supramolecular architectures of meloxicam carboxylic acid cocrystals, a crystal engineering case study, *Cryst. Growth Des.* Vol. 10, pp. 4401-4413;

- [2] Chueshov V.I., Hladuh E.V., Saiko I.V., (2012), Industrial technology of drugs, *National University of Pharmacy, Kharkiv / Ukraine*;
- [3] Dudnikov A.A., Belovod A.I., Pasyuta A.G., (2015), Relationship parameters of vibration processing quality of the surface layer, *Vibration in engineering and technology*, №2(78), pp. 70-74;
- [4] Kuzo I.V., Lanets O.S., Gursky V.M., Shpak Y.V., (2015), Choice of optimization criteria and resilient power parameters of vibro-impact resonance machines, *Vibration in engineering and technology*, №3 (79), pp. 28-37;
- [5] Lavrova L.Y., (2013), Mechano-activated organic powder and organoleptic quality of semi-finished biscuit, *Confectionery production*, № 3, pp.18–19;
- [6] Nadutiy V.P., Titov A.A., (2017), Analysis of influence of loose mining rocks compactibility on the process of their deformation between flat surfaces of disintegrators, *Vibration in engineering and technology*, №1(84), pp. 29-34;
- [7] Poluljakh D. A, (2017), Determination of coal hydro-mechanical screening parameters on the combined cone form sifting surface, *Vibration in engineering and technology*, №1(84), pp. 68-75;
- [8] Shakhtshneider T.P., (2013), *Effect of mechanical influences on the physicochemical properties of drugs*, PhD dissertation, Novosibirsk / Russia;
- [9] Solona O.V., Yanovych V.P., (2016), *Vibration mill*, UA, Patent № 109539;
- [10] Sydorenko I.I., Kushnir A.Y., Baidzhanov S. M., (2015), Elastic characteristics of nonlinear elastic devices with the expansion of the mechanical structure, *Vibration in engineering and technology*, №2(78), pp. 56-63.

EFFECTS OF MATURITY TIME ON SOME MECHANICAL PROPERTIES OF BEEF TYPE TOMATO FOR TRANSPORTATION

TAŞIMA İÇİN OLGUNLAŞMA ZAMANININ BEEF TİPİ DOMATESİN BAZI MEKANİK ÖZELLİKLERİ ÜZERİNE ETKİSİ

Ph.D. Kabas O.^{*1)}, Ph. D. Eng. Kabaş A.²⁾, Ph.D. Ünal İ.¹⁾

¹⁾Akdeniz University, Vocational School of Technical Science, Department of Machinery, Antalya / Turkey

²⁾Akdeniz University, Vocational School of Technical Science, Department of Organic Farming, Antalya / Turkey

Tel: +902423106769; E-mail: okabas@akdeniz.edu.tr

Keywords: maturity, puncture, colour, properties

ABSTRACT

Effect of maturity time as colour on mechanical properties is important for long way transportation. In this research, some physical and mechanical properties of beef tomato (Tybeef) grown in the Antalya region were determined based on the puncture tests. The tests were carried out at four maturity stages namely green, light pink, pink and red colour. Size and sphericity were measured using the standard methods. Surface colour of tomatoes were determined using a colorimeter and the mechanical properties such as puncture force and stress, puncture energy, deformation, strength and elastic modulus by texture analyser. The puncture force and energy values were found different at 5% probability level for all the maturity stages. Deformation, failure stress and toughness values were found different at 1% probability level for all the maturity stages. Statistically, there is no difference in the modulus of elasticity values for all the maturity stages. In conclusion, it was found that $L^*/a^*/b^*$ and C^*/h colour parameter can be a good index for evaluating mechanical properties of beef tomato.

ÖZET

Uzun yol taşımacılığı için renk olarak olgunlaşma zamanının mekanik özellikleri üzerine etkisinin bilinmesi oldukça önemlidir. Bu çalışmada Antalya bölgesinde yetişen beef tipi (Tybeef) domates çeşidinin bazı fiziksel özellikleri ve delinme testi temel alınarak mekanik özellikleri belirlenmiştir. Denemeler 4 farklı olgunlaşma zamanı olan yeşil, açık pembe, pembe ve kırmızı renk domateslerde yürütülmüştür. Boyutlar ve küresellik standart metotlar kullanılarak ölçülmüştür. Domateslerin renkleri kolormetre cihazı ile delinme kuvveti, dayanım, delinme enerjisi, deformasyon ve elastikiyet modülü gibi mekanik özellikler ise tekstür analiz cihazı ile ölçülmüştür. Tüm olgunluk düzeyleri için delinme kuvveti ve enerji değerleri istatistiksel olarak %5 önem seviyesinde önemli bulunmuştur. Ayrıca Deformasyon, gerilme ve dayanım değerleri ise istatistiksel olarak %1 önem seviyesinde önemli bulunmuştur. Elastikiyet modülü değerlerinde ise olgunluk düzeyleri için istatistiksel bir fark saptanmamıştır. Sonuç olarak $L^*/a^*/b^*$ ve C^*/h gibi renk parametrelerinin beef tipi domatesin mekanik özelliklerinin değerlendirilmesinde iyi bir gösterge olabileceği saptanmıştır.

INTRODUCTION

Tomato (*Lycopersicon esculentum*) is classified under subfamily of the Solanaceae. It (*Lycopersicon esculentum* Mill.) is a self-fertile vegetable and one of the most popular vegetable crops grown all over the world. It has a high amount of vitamin A and C, calcium, potassium and particularly lycopene which prevents people against heart disease and cancer (Karacali I., 1990; Rao and Agarwal, 2000). Additionally, tomato fruit is one of the most consumed vegetables used as fresh, dried or processed for human nutrition and is of secondary importance in its family (Delina and Mahendran, 2009).

The quality for agricultural products is generally evaluated under three attributes: texture, colour and taste. Texture and colour are the most important factors that are determining the quality of tomatoes (Tijkens and Evelo, 1994). Especially, the colour is an extremely important characteristic for tomato quality. The mechanical properties of agricultural products are most conveniently measured by compression testing. From this curve, a number of mechanical properties can be determined such as maximum force to rupture or puncture, energy, stiffness and deformation (Fischer et al., 1969).

Considering that low quality depends on the damages occurred during harvest and postharvest processes, it is quite important to know textural properties of tomato to provide it to the market with minimum damage (Batu A., 2004). The distance to the market plays an important role to determine the harvesting time. If the market is close, the tomato can be harvested when their colour is red; on the contrary, if the market is far, they must be harvested at an early maturity stage. From this point of view, the colour is the preferential determining component (Ince et al., 2016). However, changes of Tybeef F1 tomato cultivar's textural properties depending on the maturity stage must be known.

Many studies focused on the results of the mechanization of tomato harvest, postharvest and grading with respect to different types of mechanical damage (Hatton and Reeder, 1963; Sargent et al., 1989). In a research, the factors that determine the puncture injury during handling were characterized (Desmet et al., 2003). Therefore, many researchers' studies on the textural properties of tomato have been published and different methods have been used such as image processing, nuclear magnetic resonance, ultrasonic technique, visible/near infrared and near infrared spectroscopy, which cannot measure the food texture directly (Sirisomboon et al., 2012; Syahrir et al., 2009).

For this reason, the aim of this study is to investigate the effects of maturity stages (green, light pink, pink and red) on puncture force, deformation, toughness, failure stress, puncture energy and modulus of elasticity of Tybeef F1 variety.

MATERIALS AND METHODS

The beef tomato variety used for all the experiments in this research was Tybeef F1. This variety of tomato was grown and harvested in the greenhouse of the Batı Akdeniz Agriculture Research Institute at Kocayatak, Antalya, Turkey on the 20th April, 2016.

The 45 samples were randomly selected from the harvested tomatoes of Tybeef F1. All analyses were carried out at a room temperature of 20–21°C during the laboratory tests. All tests were made at Medicinal and Aromatic Plants Central Laboratory of Batı Akdeniz Agriculture Research Institute in a texture analysis device.

To determine the average size of the tomato fruits, two linear dimensions (length (L) and diameter (D)) were measured by using a digital caliper with accuracy of 0.01 mm, and the samples mass was determined with an electronic balance of 0.1 g accuracy. The geometric diameter was calculated by considering Eq. (1), (Mohsenin N.N., 1986):

$$D_g = (LD^2) \quad (1)$$

where: D_g - geometric diameter, L - length, D-diameter (all in mm).

The sphericity, ϕ (%) and surface area S (mm^2) were calculated by considering Eqs. (2) and (3), respectively (Mohsenin N.N., 1986):

$$\phi = \frac{D_g}{L} \times 100 \quad (2)$$

$$S = \pi D_g^2 \quad (3)$$

where: ϕ - sphericity (%), S – surface area (mm^2), D_g - geometric diameter, L – length

To determine the mechanical properties of the three tomato varieties in the compressive tests, a biologic material test device was used (Fig. 1). A curve-ended cylindrical probe 2 mm in diameter was used to compress the fruit at 10 mm/min loading velocity during all the tests (Anonymous, 1984).



Fig. 1 - Texture analysis device and puncture test

As shown in Figure 2, a typical force-deformation curve was obtained as the result of puncture test. The puncture force, deformation, failure stress were determined by force-deformation curve while puncture energy was obtained by measuring the area under the force-deformation curve.

Hardness (Q) was calculated by dividing the puncture force (F) by the deformation to the puncture point (D), (Sirisomboon *et al.*, 2007):

$$Q = \frac{F}{D} \quad (4)$$

The modulus of elasticity E in newton per square millimetre of the fruits test was calculated using Boussinesq techniques as follows (Mohsenin N.N., 1986):

$$E = F(1 - \lambda^2)/d \cdot \Delta D \cdot r \quad (5)$$

where E is the modulus of elasticity in compression, F is the compressive force, λ is the Poisson ratio, ΔD is the deformation, d is the diameter of the cylindrical probe (2 mm) and r is the radius of the fruit curvature.

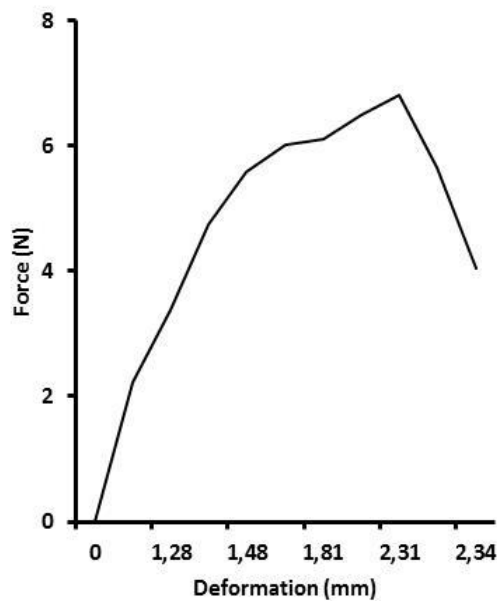


Fig. 2 - Typical force-deformation curve obtained in puncture test for Tybeef (light pink)

The maturities of tomatoes were categorized as green, light pink, pink and red according to their colours. For this purpose, Minolta CR-300 chromometer color measurement device was used (Fig 3). Hue and chroma were also determined (Sirisomboon *et al.*, 2007).

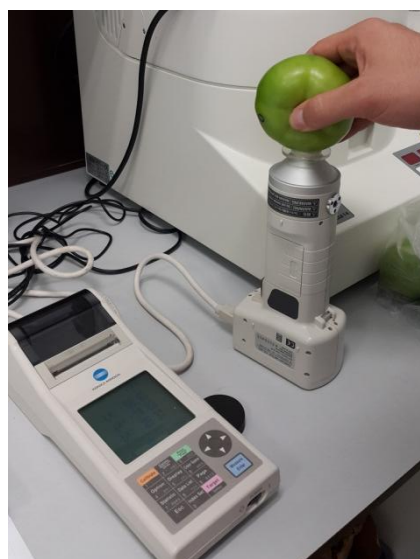


Fig. 3 - Chromometer for color measurement

RESULTS

The data on color and physical properties of Tybeef F1 tomato cultivars are shown in Tables 1 and 2. Also, a summary of the descriptive statistics of the various physical dimensions is shown in Table 1.

Table 1

Measured physical parameters of Tybeef F1			
	Min	Max	Average
Mass (g)	289.14	364.11	334.40±8.190
Diameter (mm)	77.34	102.17	88.92±0.651
Length (mm)	60.83	91.08	75.84±0.673
Geometric diameter(mm)	71.67	96.48	80.60±0.420
Sphericity (%)	91.15	121.67	106.58±0.911
Surface area (mm ²)	19435.27	26736.48	20425.61±215.784

Dimensions of Tybeef tomato varied from 77.34 to 102.17 mm in diameter, 60.83 to 91.08 mm in length and 71.67 to 96.48 mm in geometric diameter, with average values of 88.92, 75.84, and 80.60 mm, respectively. The importance of dimensions is in determining the aperture size of machines, particularly in the separation of materials as mentioned by Mohsenin (*Mohsenin N.N., 1986*). The importance of sphericity is in determining the fruit shape. The average sphericity of tomato was 106.58 %; the sphericity is reported by Mohsenin in the range of 32-1 (%) (*Mohsenin N.N., 1986*). The surface area of Tybeef F1 varied from 19435.27 to 26736.48 cm² with mean values of 20425.61 cm².

Table 2

Color properties of Tybeef F1					
	L*	a*	b*	C*	h
Green	56.60	-14.18	26.96	30.46	117.75
Light pink	49.51	12.50	28.87	31.87	67.56
Pink	46.44	21.59	31.22	38.18	55.64
Red	42.89	27.99	33.52	41.15	49.01

The skin color (L*, a*, b*, C*,h) mean values of Tybeef F1 tomato variety are presented in Table 2. The average values of L*, a*, b*, C*, h for green maturity stage are 56.60, -14.18, 26.96, 30.46 and 117.75, respectively. The average values of L*, a*, b*, C*, h are 49.51, 12.50, 28.87, 31.87 and 67.56, respectively in light pink tomato. Also, for pink skin colour, they are 46.44, 21.59, 31.22, 38.18 and 55.64 and for red skin, 42.89, 27.99, 33.52, 41.15 and 49.01, respectively.

The mean of puncture force, deformation, failure stress, toughness, puncture energy and modulus of elasticity of Tybeef tomato depending on the maturity stage and the descriptive statistics of the various mechanical properties are presented in (Table 3)

Table 3

Effect of maturity time on Mechanical Properties of Tybeef					
	Green	Light Pink	Pink	Red	Sign. level
Puncture Force (N)	10.39 ^a	6.15 ^b	4.86 ^c	4.16 ^d	**
Deformation (mm)	1.43 ^c	2.39 ^b	2.5 ^b	3.16 ^a	*
Failure stress (N/mm ²)	4.30 ^a	3.91 ^b	2.83 ^c	2.75 ^c	*
Toughness (N/mm)	5.87 ^a	4.27 ^b	3.74 ^c	3.53 ^c	*
Puncture energy (Nmm)	50.66 ^d	65.485 ^c	85.94 ^b	122.62 ^a	**
Modulus of elasticity (N/mm ²)	0.26	0.31	0.29	0.28	ns

All data represent the mean of three replications with 45 determinations.

ab Letters indicate the statistical difference in rows.

* Significant levels at 1%.

** Significant levels at 5%.

ns, not significant.

As seen in Table 3, the puncture force, failure stress and toughness values decreased as fruit maturity increased and deformation and puncture energy values increased as the maturity decreased.

The average puncture force values were 10.39, 6.15, 4.86 and 4.16 N for green, light pink, pink and red, respectively. The highest value of puncture force was found in the green maturity stage. The mean deformation values for green, light pink, pink and red maturity stages were 1.43, 2.39, 2.50 and 3.16 respectively, so the deformation values were the highest for red colour and the lowest for green colour. Also, the mean failure stress values for maturity stages were 4.30, 3.91, 2.83 and 2.75 from green to red colour so the failure stress values were the highest for green colour and the lowest for red colour. The average for toughness values for green, light pink, pink and red maturity stages were 5.87, 4.27, 3.74 and 3.53 respectively. The highest toughness was obtained in the green maturity stage. The mean modulus of elasticity values for green, light pink, pink and red maturity stages were about 0.26, 0.31, 0.29 and 0.28 respectively, so the modulus of elasticity values were the highest for light pink colour and the lowest for green colour (Fig 4).

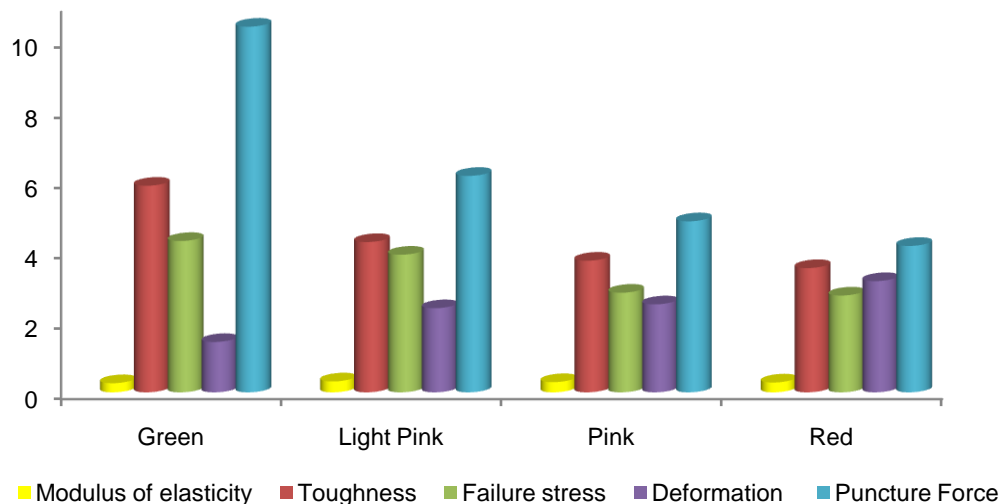


Fig.4. Average values of some mechanical properties for all maturity time

For all maturity stages, the highest puncture energy was obtained for red colour as 122.62 Nmm and the lowest value was found for green colour as 50.66 Nmm (Fig. 5).

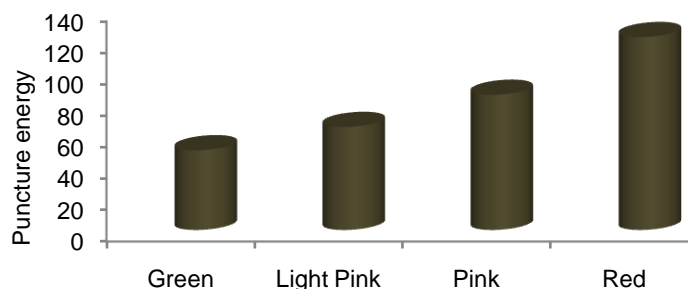


Fig.4. Average values of some mechanical properties for all maturity time

The puncture force values were found different at 5% probability level for all the maturity stages. Also, similarly, the puncture energy values were found different at 5% probability level for all the maturity stages. Similar results have also been reported (*Ince et al., 2016*). Deformation, failure stress and toughness values were found different at 1% probability level for all the maturity stages. Statistically, there is no difference in modulus of elasticity values for all the maturity stages.

Deformation of fruit changes based on the properties of biological materials. It depends on the structure of biological material and cells' pores (*Persson S., 1987*). Deformation increased as the maturity of fruit increased. This result verified the softening of the tomato fruit. While deformation values for pink and

light pink maturity stages were in the same group statically, however, the modulus of elasticity did not show any statically difference for all maturity stages. Similar results have also been reported (Ince *et al.*, 2016).

Also, failure stress and toughness decreased as the maturity of fruit increased. We can say that ripe fruit might be damaged more due to its soft texture compared to unripe fruit under the same force. While failure stress and toughness values for pink and red maturity stages were in the same group statistically.

CONCLUSION

In this study, some mechanical properties (puncture force, deformation, modulus of elastic, puncture energy, failure stress and toughness) of Tybeef F1 tomato variety were determined as affected by maturity stage. Puncture force, failure stress and toughness decreased with the increase in maturity stage. On the contrary, deformation and puncture energy increased as the maturity of fruit increased. Also, the modulus of elasticity did not show any statistic difference for all maturity stages. According to the test results, puncture force and energy are more sensitive textural mechanical parameters related to the maturity stage.

ACKNOWLEDGMENT

This study was supported by the Scientific Research Fund of Akdeniz University and Bati Akdeniz Agricultural Research Institute Antalya, Turkey.

REFERENCES

- [1] Batu A., (2004), Determination of acceptable firmness and color values of tomatoes, *Journal of Food Engineering*, Vol.61, Issue 3, pp.471–475;
- [2] Delina E.F., Mahendran T., (2009), Physico-chemical properties of mature green tomatoes (*Lycopersicon esculentum*) coated with pectin during storage and ripening, *Tropical Agricultural Research and Extension*, Vol.12, Issue 2, pp.41-45;
- [3] Desmet M., Lammertyn J., Scheerlinck N., Verlinden B.E., Nicolai, B.M., (2003), Determination of puncture injury susceptibility of tomatoes, *Postharvest Biol. Technol.*, Vol. 27, pp. 293–303;
- [4] Fischer R.R., Elbe J.H.V., Schuler R.T., Bruhn H.D., Moore J.D., (1969), Some physical properties of sour cherries, *Transaction of ASAE*, Vol.12, pp.175–179;
- [5] Hatton T.T., Reeder W.F., (1963), Effect of field and packinghouse handling on bruising of Florida tomatoes, *Florida. State Horticultural Society*, Vol.76, pp. 301–304;
- [6] Ince A., Cevik M.Y., Vursavus K.K., (2016), Effects of maturity stages on textural mechanical properties of Tomato, *International Journal of Agricultural and Biological Engineering*, Vol. 9, Issue 6, pp.200-206;
- [7] Karacali I., (1990), *The storage and handling of horticultural crops*. Ege University Agricultural Faculty Press, p. 368;
- [8] Mohsenin N.N., (1986), *Physical Properties of Plant and Animal Materials*. Gordon and Breach Press, New York, 750 p.;
- [9] Persson S., (1987), Mechanics of cutting plant material. *ASAE Publications*, Michigan, 280 p;
- [10] Rao A. V., Agarwal S., (2000), Role of antioxidant lycopene in cancer and heart disease, *The Journal of the American College of Nutrition*, Vol.19, pp.563-569;
- [11] Sargent S.A., Brecht J.K., Zoellner J.J., (1989), Assessment of mechanical damage in tomato packing lines, *ASAE/CSAE Meeting*, paper No. 89-6060, pp.174-181;
- [12] Sirisomboon P., Kitchaiya P., Pholpho T., Mahuttanyavanitch W., (2007), Physical and mechanical properties of *Jatropha curcas* L. fruits, nuts and kernels, *Journal of Food Engineering*, Vol.97, pp.201-207;
- [13] Sirisomboon P., Tanaka M., Kojima T., (2012), Evaluation of tomato textural mechanical properties, *Journal of Food Engineering*, Vol. 111, Issue 4, pp. 618–624;
- [14] Syahrir W.M., Suryanti A., ConnsynnC., (2009), Color grading in tomato maturity estimator using image processing technique, *International Conference on Computer Science and Information Technology (ICCSIT)*, 276 p.;
- [15] Tijskens L. M. M., Evelo R. W., (1994), Modelling colour of tomatoes during postharvest storage, *Postharvest Biology and Technology*, Vol.4, pp.85-89;
- [16] *** (1984), *Compression test of food materials of convex shape*, In Agricultural Engineers Yearbook, American Society of Agricultural Engineers, ASAE S368.2.

VERIFICATION OF STRESS BY FEM ANALYSIS / MECHANICAL TESTING OF AGRICULTURAL MOBILE AGGREGATES COUPLING DEVICES

/

VERIFICAREA SOLICITĂRILOR PRIN ANALIZA MEF / TESTAREA MECANICĂ A DISPOZITIVELOR DE CUPLARE ALE AGREGATELOR AGRICOLE MOBILE

Phd. Eng. Vlăduț V.¹⁾, Prof.PhD.Eng. Maican E.²⁾, PhD.Eng. Apostol L.^{*3)}, Lect. Ph.D. Eng.Ungureanu N.²⁾,
Eng. Dumitru I.¹⁾, Eng. Oprescu R.¹⁾

¹⁾INMA Bucharest / Romania; ²⁾University "POLITEHNICA" Bucharest / Romania; ³⁾IBA Bucharest / Romania;
Tel: 0740.001.473; E-mail*: aposto_livia@yahoo.com

Keywords: *aggregate, coupling, analysis, stresses, forces, meshing*

ABSTRACT

The coupling devices must be checked for the resistance they provide during the movement of a mobile aggregate (tractor + trailer or agricultural machine), which can be done by a finite element analysis (SOLIDWORKS Simulation, CATIA, ANSYS, etc.) or by testing in service or, the fastest, in simulated and accelerated mode on special installations. The paper presents the results obtained by finite element analysis of a 55 HP tractor draught bar (after meshing the model), determining the most stressed points and the maximum risk areas where breaks will occur, respectively after performing the tests in static and dynamic mode (in case of fatigue) on the simulated and accelerated test installation to determine if deformations or breaking result from stresses.

REZUMAT

Dispozitivele de cuplare trebuie verificate din punct de vedere al rezistenței pe care o asigură în timpul deplasării unui agregat mobil (tractor + remorcă sau mașină agricolă), verificare ce se poate realiza printr-o analiză cu element finit (SOLIDWORKS Simulare, CATIA, ANSYS, etc.) sau prin testări în exploatare sau, cel mai rapid, în regim simulat și accelerat pe instalații speciale. Lucrarea prezintă rezultatele obținute prin analiza cu element finit a unei bare de tracțiune a unui tractor de 55 CP (după discretizarea modelului), determinându-se punctele solicitate cel mai puternic și zonele de risc maxim unde vor apărea rupturile, respectiv după testarea în regim static și dinamic (la oboseală) pe instalația de încercări în regim simulat și accelerat, pentru a determina dacă în urma solicitărilor apar deformații sau rupturi.

INTRODUCTION

The coupling devices for tractor - agricultural machine / trailer unit are designed in different types, depending on the towing / towing mass, the type of machine / towed gear, the angle under which it engages, etc. Analysis of the operation of coupling devices for agricultural aggregates (tractor-agricultural machinery) aims to identify the optimal coupling and to determine the optimal operation, in the case of normal and / or critical stresses, by simulated and accelerated tests, respectively in exploitation on uneven soils, to identify its critical areas (Finite Element Analysis - FEM) (Birîș, 1999; Blumenfeld, 1995).

The optimization of the coupling can be achieved taking into account the results of this analysis, which will lead to optimal operation and increase of the service life, under safety conditions for the operator, but especially for the participants to the traffic.

Tractors, trailers and their couplings (draught / coupling devices) must comply with certain technical and mechanical requirements for the safety of public road transport in Romania and to be allowed into circulation (Ormenișan, 2014).

When developing new types of coupling systems for tractors, trailers and agricultural machinery all technical conditions must comply with the European standards in order to increase the degree of interchangeability and safety in circulation. This is one of the main reasons for studying these devices, having in view due the multiple accidents caused by inadequate coupling systems (on tractors or farm tractors, respectively between tractors and farm tractors), which are not carried out in compliance with certain specifications about traffic safety (Andrei et al., 2006; Zatocilová et al., 2014).

Particularly for the coupling systems of tractors and trailer trucks intended for operation in the agricultural or forestry sector, the condition which implies that they must be carried out and meet the same rules is based on the need to couple between them all machinery of the same type existing on the European and Romanian market and, on the other hand, to the fact that these coupling systems have safety features in operation and mostly during road traffic.

For most machinery and equipment used in agriculture and forestry there is a freedom of expression in terms of their development (constructive, functional, etc.) (Maican E. et al., 2018). Nevertheless, for the coupling systems, which are the elements that contribute to the safety in operation and circulation, severe conditions are demanded by internal and European manufacturing regulations, functional parameters, mounting conditions etc., which all the mentioned factors must comply with (Stoica, 2001).

In Romania, like in other European countries, road traffic in particular changes on a year-to-year basis and from country to country, depending on the increase of the motoring index, the state of the road network, the level of economic development of the country in general and in particular of the car transport (Iordache, 2011).

Despite the variety of measures taken to organize and improve road traffic, road safety is still far from being satisfactory, with a large number of road accidents resulting in serious material damage and even more, in losses of life. Although their participation to public traffic is occasional, the agricultural and forestry transport (represented by tractor-trailer systems or agricultural machinery) has an important role in these accidents (Bodea, 2008).

Most of these accidents are due to unsuitable general technical conditions or failures in the safety components of the involved agricultural or forestry machinery, including the coupling systems. Another important factor that can lead to incidents and road accidents is the fact that some tractors and agricultural machinery are not provided with the appropriate coupling systems (Cândea et al., 2008).

MATERIALS AND METHODS

The experimental research for FEM analysis of the draught bar was carried out in the *SOLIDWORKS Simulation* (Fig.1) and testing of a coupling device resistance from the U650M tractor was carried out on a draught bar (Fig. 2), which was tested in static and dynamic regime on a Hidropuls-type installation (Fig. 3).

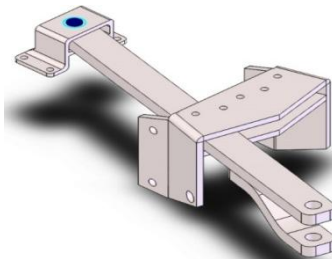


Fig. 1 - Model: Rel-1.0 used for the analysis

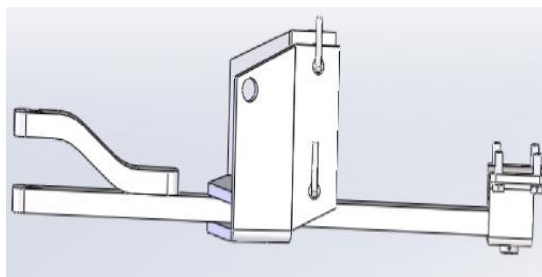


Fig. 2 – Draught bar mounted for the experiments

Verification of the coupling devices (static and dynamic) is achieved on specialized installation for testing in simulated and accelerated regime, type Hidropuls (Fig. 3), where they are mounted in the same position in which they are used during operation. Determination of forces and stresses in the coupling devices must take into account the shape, dimensions and technical conditions imposed on their aggregation devices, for each type of coupling system being provided in the legislation (directives, regulations, standards etc.), the conditions which they must meet and respect.



Fig. 3 – Testing installation in simulated and accelerated regime, Hidropuls type

RESULTS

Nonlinear static analysis of draught bar – *longitudinal stress*

Type of analysis: *Nonlinear- Static*

Table 1

Reaction forces

Selection mode	M.U.	Sum X	Sum Y	Sum Z	Resultant
Entire Model	N	-250	6.31357e-007	-2.8424e-005	250

Table 2

Moment of reaction

Selection mode	M.U.	Sum X	Sum Y	Sum Z	Resultant
Entire Model	N.m	0	0	0	0

Table 3

Obtained results

Name	Type	Min	Max
Stress	VON: von Mises stress at step no.: 10 (1 sec.)	3.009e-002N/mm ² (MPa) Node: 52818	2.360e+002N/mm ² (MPa) Node: 48787
<p>Rel-1.0-Nonlinear-Stress-Stress_Ensemble</p>			
<p>Rel-1.0-Nonlinear-Stress-Stress 1_1</p>		<p>Rel-1.0-Nonlinear-Stress-Stress 1_2</p>	
<p>Rel-1.0-Nonlinear-Stress-Stress 1_3</p>		<p>Rel-1.0-Nonlinear-Stress-Stress 1_4</p>	

Table 3 (continuation)

Name	Type	Min	Max
Displacement	URES: Displacement resultant at step no.: 10 (1 sec.)	0.000e+000mm Node: 12293	3.340e+000mm Node: 8276
<p>Rel-1.0-Nonlinear-Displacement-Displacement_Ensemble</p>			
<p>Rel-1.0-Nonlinear-Displacement-Displacement 1_1 Rel-1.0-Nonlinear-Displacement-Displacement 1_2</p>			
<p>Rel-1.0-Nonlinear-Displacement-Displacement 1_3 Rel-1.0-Nonlinear-Displacement-Displacement 1_4</p>			

Name	Type	Min	Max
Strain	ESTRN: Equivalent stress at step no.: 10 (1 sec.)	9.236e-008 Element: 56359	1.496e-003 Element: 24502
<p>Rel-1.0-Nonlinear-Strain-Strain1</p>			

Nonlinear static analysis of draught bar - Nonlinear stress in curve

Table 4

Reaction forces

Selection set	Units	Sum X	Sum Y	Sum Z	Resultant
Entire Model	N	-242.994	6.87689e-006	-58.7709	250

Reaction Moments

Selection set	Units	Sum X	Sum Y	Sum Z	Resultant
Entire Model	N.m	0	0	0	0

Table 5

Study Results

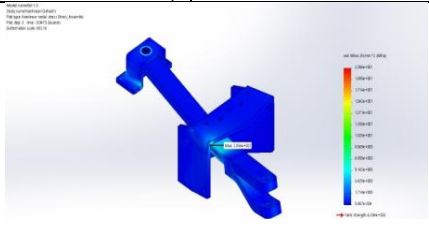
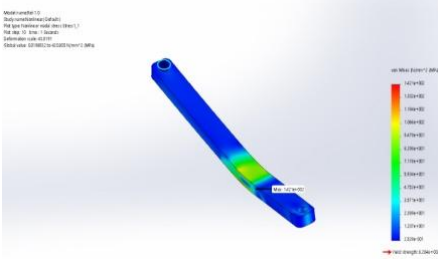
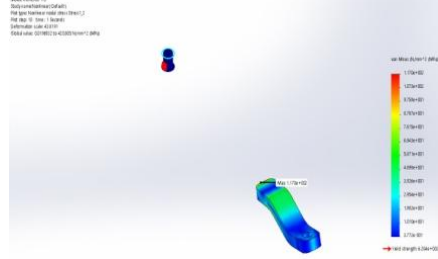
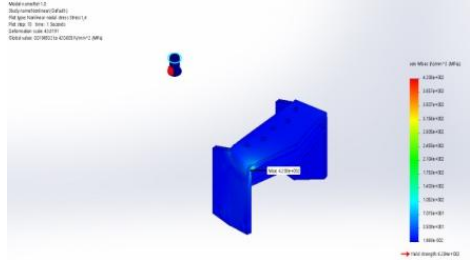
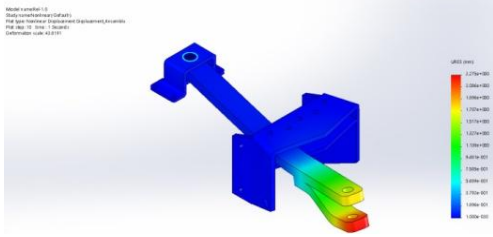
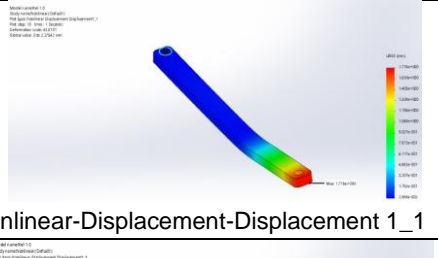
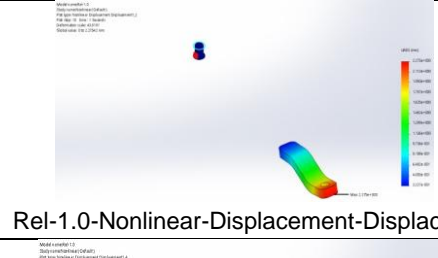
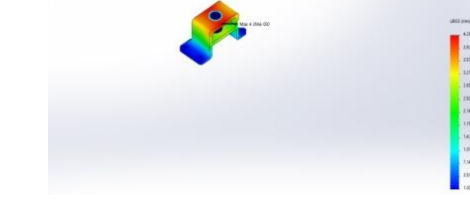
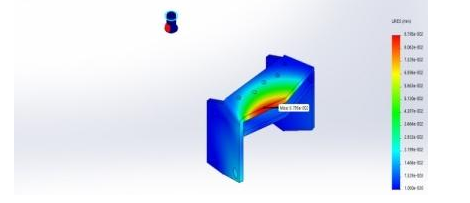
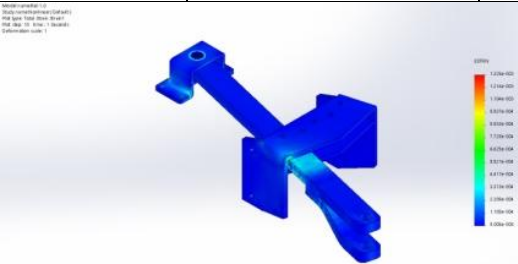
Name	Type	Min	Max
Stress_Ensemble	VON: von Mises Stress at Step no: 3 (0.0475 seconds)	8.867e-004 N/mm ² (MPa) Node: 49337	2.056e+001 N/ mm ² (MPa) Node: 62193
 <p>Rel-1.0-Nonlinear-Stress-Stress_Ensemble</p>			
Stress	VON: von Mises Stress at Step no: 10 (1 seconds)	1.969e-002 N/ mm ² (MPa) Node: 49337	4.208e+002 N/ mm ² (MPa) Node: 62193
 <p>Rel-1.0-Nonlinear-Stress-Stress1_1</p>		 <p>Rel-1.0-Nonlinear-Stress-Stress1_2</p>	
 <p>Rel-1.0-Nonlinear-Stress-Stress1_3</p>		 <p>Rel-1.0-Nonlinear-Stress-Stress1_4</p>	
Displacement	URES: Resultant Displacement at Step no: 10 (1 seconds)	0.000e+000mm Node: 12176	2.275e+000mm Node: 8211
 <p>Rel-1.0-Nonlinear-Displacement-Displacement_Ensemble</p>			
 <p>Rel-1.0-Nonlinear-Displacement-Displacement 1_1</p>		 <p>Rel-1.0-Nonlinear-Displacement-Displacement 1_2</p>	
 <p>Rel-1.0-Nonlinear-Displacement-Displacement 1_3</p>		 <p>Rel-1.0-Nonlinear-Displacement-Displacement 1_4</p>	

Table 5 (continuation)

Name	Type	Min	Max
Strain	ESTRN: Equivalent Strain at Step no: 10 (1 seconds)	9.005e-008 Element: 26676	1.325e-003 Element: 30722



Rel-1.0-Nonlinear-Strain-Strain1

Data processing - static tests

Static tests were carried out at INMA Bucharest on a specialized installation (Hidropuls), with the towing device and any tractor coupling component attached to a rigid structure by means of the same components used for mounting on the tractor body (Fig. 4).



Fig. 4 - Mounting on the Hidropuls installation for the static test of the draught bar

Equipment for measuring and control used to record loads and applied moments must be of high precision: applied loads ± 50 daN; moments ± 0.01 mm.

During the test, the deformation of the coupling device must not exceed 10% of the maximum elastic deformation observed. Verification was performed after removal of the load and return to the initial load of 500 daN.

$$\begin{aligned}
 MT &= 1450 \text{ kg} = 1422.45 \text{ daN}; & MR &= 1500 \text{ kg} = 1471.50 \text{ daN}; \\
 D &= 25 \text{ kN} = 2500 \text{ daN}; & S &= 7 \text{ kN} = 700 \text{ daN}.
 \end{aligned}$$

where:

MT - total permissible tractor mass, from a technical point of view;

MR - total permissible mass of the towed vehicle, from a technical point of view;

D - mathematically determined force (the components of the horizontal force on the longitudinal axis of the vehicle);

S - static load of the draught bar (component of the vertical forces on the road).

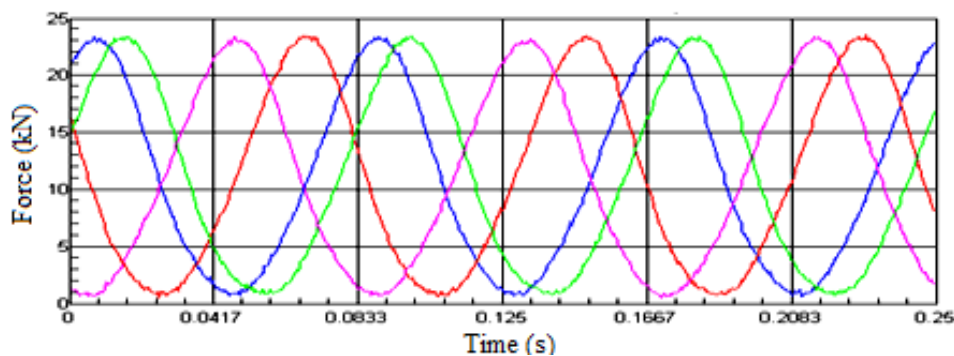


Fig. 5 - Force-time diagram for the static test of the draught bar on the Hidropuls installation

Data processing - dynamic tests

In dynamic tests, the resistance of the mechanical coupling system (draught bar) was established by alternating traction at a specialized stand (Hidropuls installation).

This dynamic method describes the fatigue test which applies to the entire draught bar, respectively, when the draught bar, equipped with all the components required for installation, is mounted and tested on the Hidropuls.

Alternate forces have been applied sinusoidally, from the longest possible distance (by alternate towing and / or lifting), to a load cycle determined by the material involved, during which no cracks or wear must occur.

The horizontal force components on the longitudinal axis of the vehicle, and the components of the vertical force, formed the basis of the load to be subjected to the test. However, the components of horizontal force at right angles to the longitudinal axis of the vehicle, as well as the moments are of secondary importance, therefore they have not been considered.

The horizontal force components on the longitudinal axis of the vehicle are expressed by a mathematically determined force, D .

$$D = g \cdot (M_T \cdot M_R) / (M_T + M_R) \quad (1)$$

The technically acceptable load masses specified by the manufacturer on this traction unit are: $M_T = 1450 \text{ kg} = 1422.45 \text{ daN}$; $M_R = 1500 \text{ kg} = 1471.50 \text{ daN}$; $D = 25 \text{ kN} = 2500 \text{ daN}$; $S = 7 \text{ kN} = 700 \text{ daN}$.

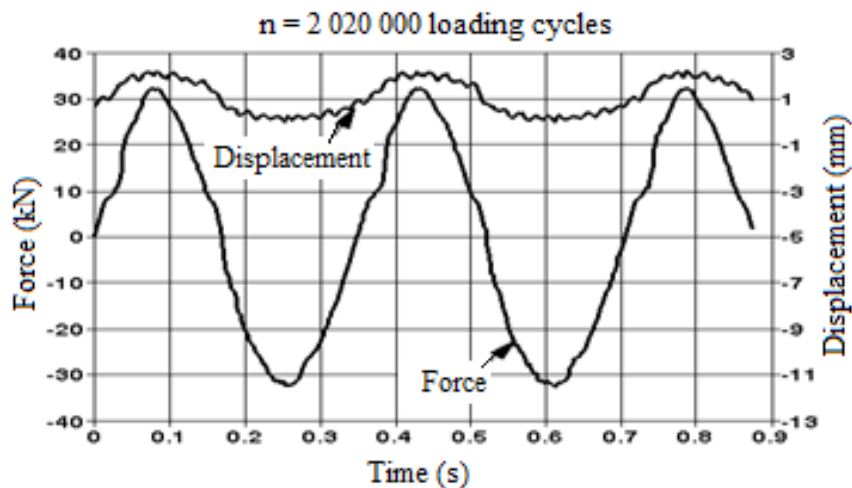


Fig. 6 - Diagram force-time and movement-time (in the horizontal direction)

CONCLUSIONS

For non-linear static analysis of the draught bar - longitudinal stress, the highest stresses occur in the hinge area of the bar between the two fixation elements at the engine chassis, respectively in the coupling bolt between the tractor and the trailer, which is why they must be optimized in the sense of choosing a quality material, with a good coefficient of elasticity that will allow taking over some shocks that occur in the case of passing over pits, etc. and which can cause shearing of the bolt or articulation elements.

For non-linear stresses in the curve, the highest stresses occur as in the case of longitudinal stresses, in the hinge areas of the bar at the engine chassis, respectively in the coupling bolt between tractor and trailer, but they are larger in the first coupling bolt in the fixation element to the chassis and the front and rear parts of the bar (against the bolt), which implies a reinforcement (optimization) of this area.

Data obtained and processed after the testing in static and dynamic regime show that the draught bar did not break when more than 2000000 cycles (2020000 cycles) of stress - in dynamic regime were applied, with a maximum displacement at a horizontal plane of $\pm 1.12 \text{ mm}$ which corresponded to a force of $\pm 32.27 \text{ kN}$ and a maximum displacement at the vertical plane of $\pm 0.48 \text{ mm}$ which corresponded to a force of $\pm 10.19 \text{ kN}$, respectively at a force equal to 1.5 times the permitted towable mass in the case of static load, without any visible deformation, rupture or other visible damage.

REFERENCES

- [1] Andrei I., Cârdei P., Gângu V., Muraru V., Popa C., Păunescu D., (2006), Resistance analysis of the coupling system between tractor and trailer. *SCIENTIFIC PAPERS – INMATEH*, vol. 2, pp. 105-112;
- [2] Biriş S., (1999), Finite Element Method - Applications in the construction of agricultural machinery. *PRINTECH Publishing*, Bucharest, Romania;
- [3] Blumenfeld M., (1995), Introduction in the finite element method. *Technical Publishing*, Bucharest, Romania;
- [4] Bodea C., (2008), Theoretical and experimental studies on couplings between tractor and trailer. Doctoral thesis, *University "Transilvania" Braşov*, Romania;
- [5] Cârdea A., Bodea M., Bria N., Andrei I., (2008), Kinematic and dynamic analysis of the spherical coupling as a coupling body between tractor and semi-trailer. *Scientific Papers – INMATEH*, no. 3/2008, pp.77-86;
- [6] Iordache S., (2011), Study of technical conditions for tractor + agricultural equipment units to be admitted into road circulation on public roads. Doctoral thesis, Craiova, Romania;
- [7] Maican E., Biriş S.Şt., Persu C., Duţu M., Matache M., Iordache S., Alfianu C., (2018), Nonlinear impact resistance simulation of a newly designed roof from an agricultural tractor cabin, *46th Symposium "Actual Tasks on Agricultural Engineering"*, Opatija, Croatia, pp. 231-238;
- [8] Ormenişan N., (2014), Theoretical and experimental research on the influence of automatic control systems of tractor suspension mechanisms on the dynamics and power of ploughing aggregates. *Doctoral thesis, University „Transilvania”, Braşov*, Romania;
- [9] Stoica C., (2001), Studies and research on mechanical links between towed and not towed vehicles. *Doctoral thesis, University „Transilvania”, Braşov*, Romania;
- [10] Zatocilová A., Koutny´ D., Paloušek D., Brandejs J., (2014), Experimental Verification of Deformation Behaviour of Towing Hitch by Optical Measurement Method. *Brno University of Technology*, Brno, Czech Republic.

WIRELESS MEASUREMENT AND CONTROL SYSTEM OF CARBON DIOXIDE USING INFRARED SENSOR IN GREENHOUSE ENVIRONMENT

基于红外传感器的温室二氧化碳无线监测和控制系统研制

Ph.D. Bin Li¹⁾, Stud. Jitong Wang¹⁾, Prof. Yao-Dan Chi¹⁾, Prof. Xiaotian Yang^{*1)}, Prof. Yiding Wang²⁾

¹⁾ Institute of Electrical & Computer, Jilin Jianzhu University, Changchun 130012 / China

²⁾ State Key Laboratory on Integrated Optoelectronics, College of Electronic Science and Engineering, Jilin University / China

Tel: +86-043184566184; E-mail: 870731919@qq.com

Keywords: Greenhouse, Carbon dioxide detection, Infrared gas sensor, Wireless communication

ABSTRACT

A carbon dioxide detecting and controlling system has been experimentally established in a greenhouse located in northern China. The developed system consists of several major parts including wireless infrared gas sensor node, wireless receiver and CO₂ concentration controller with pure CO₂ cylinder. The wireless infrared gas sensor was developed for real time detection of CO₂ which is essential for plant photosynthesis. Digitalized data of concentration can be received by the wireless receiver which connects to a laptop installed developed LabVIEW program. Ambient CO₂ concentration can be controlled automatically by the concentration controller based on fuzzy PID algorithm. Experiments demonstrate that the stability fluctuation of detection results is less than 2.2%. The fluctuation of ambient CO₂ concentration under automatic control is less than 60 ppm which proves good efficiency of the system. The proposed CO₂ detecting and controlling system is suitable for precision management of key factors along with temperature, humidity and luminance in greenhouse for optimal production.

摘要

研制了用于温室环境的二氧化碳气体的测控系统。研制的系统主要分为几个部分，包括无线红外检测节点、无线接收器和用于控制二氧化碳气瓶的控制器。二氧化碳作为植物光合作用的重要要素，可以通过研制的无线红外检测节点进行实时检测。检测的浓度信息可以通过数字量的形式无线发送给研制的无线接收器，无线接收器连接温室旁控制室内的电脑，该电脑安装了基于 LabVIEW 平台开发的软件。环境中二氧化碳浓度可以通过模糊 PID 算法由二氧化碳控制器进行调控。实验证明检测结果的波动不大于 2.2%。二氧化碳浓度在设定值范围内波动不超过 60ppm，显示了较好的测控精度。本文提出的二氧化碳测控系统适用于研究温室作物增产和优产，在检测二氧化碳浓度的同时，还可以检测温室内的温度、湿度和光照度。

INTRODUCTION

In recent years, greenhouse has been developed and improved world widely. According to reports, the total area of greenhouse had been increased more than 2 million hm² in China (Jianing et al. 2016; Jianing et al. 2016). Meanwhile, the demand of modern technologies and technical equipment are increasingly required in greenhouse environment. Production of greenhouse can be increased and the quality can be optimized by taking advantage of the modern techniques, including sensors, signal transmission, signal processing, and control strategy and algorithm (Malaver et al. 2015; Serodio et al. 2001; Gutierrez et al. 2014). These technologies effectively promote the development of modern greenhouse by quantification of key factors, decreasing the complexity of environment and increase the efficiency of signal processing. Among the applicable techniques, sensors and sensing techniques have been reported by many groups (Somov et al. 2013; Somov et al. 2014; Salker et al. 2005; Misra et al. 2004) for achieving accuracy real time detection of key factors in greenhouse. Also, control and management of key factors such as temperature, humidity and luminance in greenhouse have been reported experimentally (Hwang et al. 2010; Ma et al. 2015).

Carbon dioxide is essential for plants photosynthesis and is also studied by many researchers (Yauda et al. 2012). Carbon dioxide concentration can be detected by CO₂ sensors which are developed in different sensing principles (Ren et al. 2014). Detection and fertilization of CO₂ is significant to plant growth management in greenhouse. Compared to traditional sensors, photo-electrical sensors have been reported widely in recent years due to their advantages including high-sensitivity, fast response time, non-intrusive

nature, wide sensing range and long lifespan (Ritobrata et al. 2013; Charles et al. 2014). Therefore, photo-electrical CO₂ sensors are adopted in the developed system.

In this paper, a CO₂ detecting and controlling system has been experimentally established along with other key factors including temperature, humidity and luminance. These sensors have been controlled by the developed circuits and are integrated as a sensor node in the system. Considering the wiring difficulty in greenhouse environment, wireless communication has been adopted in the system by using the 433 MHz communication frequency. CO₂ fertilization can be performed by the developed CO₂ controller. Design details of sensor node, CO₂ controller and circuits are introduced firstly. Then, sensing and testing experiments of the system with discussion will be demonstrated.

MATERIALS AND METHODS

System structure

The proposed CO₂ measurement and control system consists of developed software and hardware. The structure diagram is shown in Figure 1. As shown in the figure, the developed sensor node is placed in the greenhouse and it is responsible for sensing key factors including CO₂, luminance, temperature and humidity. The detected data can be transmitted to a developed wireless receiver which connects to a laptop in the adjacent control room by wireless communication. Detected data can be shown and be stored in the laptop. In the greenhouse, there is also a CO₂ controller that is able to control the open/close of a CO₂ cylinder for gas fertilization. The CO₂ controller can be controlled by the sensor node or the laptop by wireless communication. Considering the difficulty of wiring power cables and signal cables in greenhouse environment, wireless communication is desirable for the duty of signal transmission. Besides, water proof of the sensor node is also considered and is performed to avoid circuit damage caused by the moisture condensation in greenhouse.

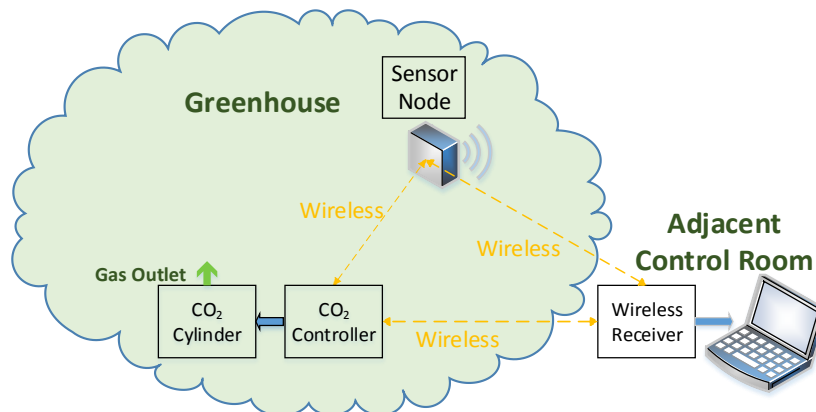


Fig.1 - Structure diagram of the developed system in the greenhouse

Wireless sensor node

The wireless sensor node was developed for monitoring real time ambient factors including CO₂ concentration, temperature, humidity and luminance. The function diagram of the sensor node is shown in Figure 2.

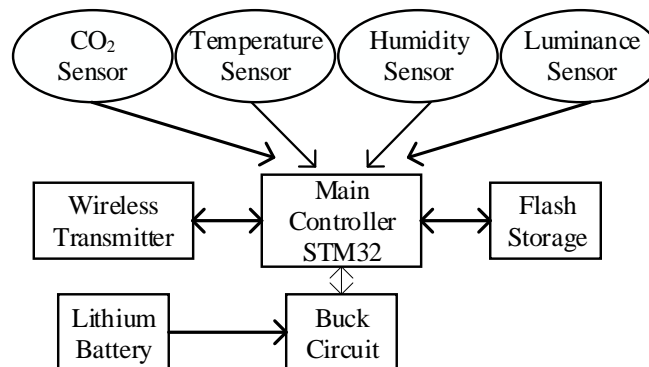


Fig. 2 - Function diagram of the developed sensor node

The main controller is a surface mounted microchip (STM32F103R). It is a 32-bit chip with a maximum CPU speed of 72 MHz. The main controller is responsible for signal processing of the sensor node. It is connected with the individual sensors and a wireless module (Si4463). The circuit is powered by a lithium battery that consists of four serially connected 18650 batteries. A buck circuit board was developed to convert voltage and the output voltage is set as 5 V. The main controller stores data in a 64-M flash chip (W25Q64BV). In order to guarantee the wireless communication quality, an amplifier chip (RFX2401C) was applied to enhance signal strength. Therefore, collected data can be sent to the wireless receiver and the CO₂ controller.

Sensors and signal receiver

The CO₂ sensor applied in this system is a compact infrared sensor based on the Beer-Lambert Law. Compared to the general chemical sensors, it has a larger detection range which is 0 to 10⁴ ppm. The sensing precision is about 30 ppm. The photo of CO₂ sensor is shown in Figure 3 (b). The temperature and humidity sensors are combined together and it is shown in Figure 3 (b) as well. It can be buried in the soil to detect the temperature and humidity in underground as shown in Figure 3 (a). It can also detect the ambient air temperature and humidity. The detection accuracy is about 0.5 °C of temperature and 1.8% of humidity. The luminance sensor is embedded on the panel of the developed sensor node. This luminance sensor has a low driving current of 0.7 mA and its accuracy is about 0.054 Lux. The three sensors are connected with the main controller of the sensor node.

Wireless communication has been adopted in this system to avoid high expense instalment of telecommunication infrastructures. Wireless communication is flexible, fault-tolerant and simpler to implement in greenhouse. The wireless module is also shown in Figure 2 (b). Compared to WIFI and Bluetooth, the applied 433 MHz communication wireless module has a better penetration that is suitable for the greenhouse environment because the transmission can be guaranteed considering the inevitable plant shelter. This is a key advantage of this signal transmission method in greenhouse environment.

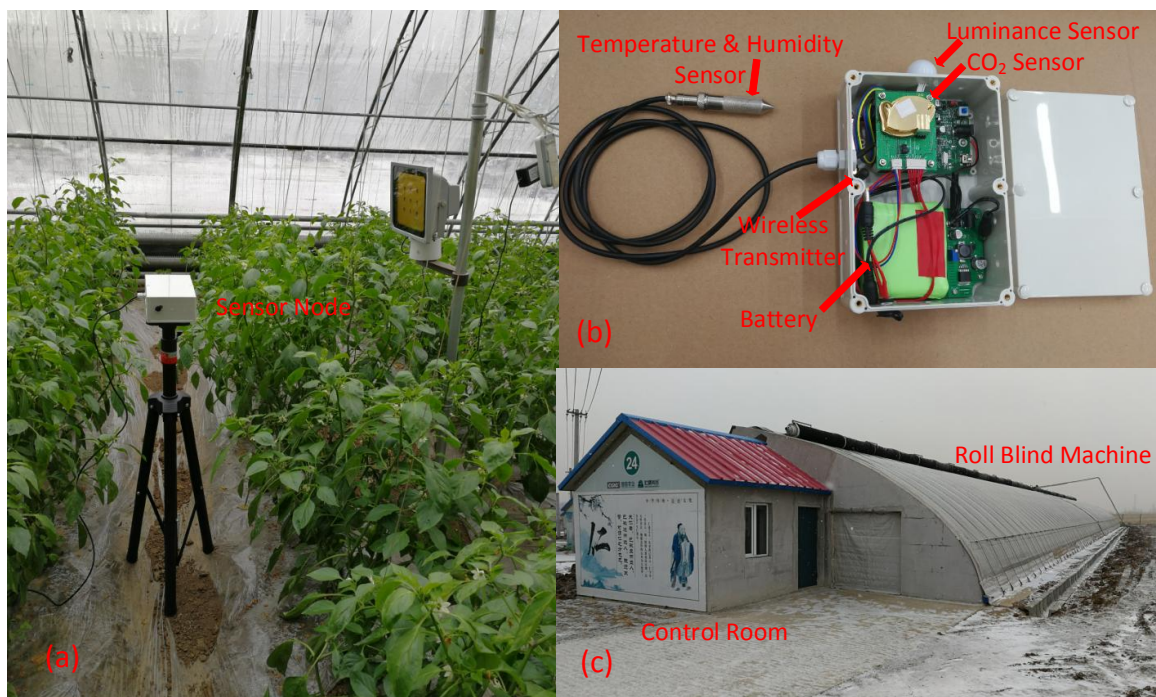


Fig. 3 - Photo of the sensor node working in the greenhouse (a), the inside view of the developed sensor node (b) and the outside view of the greenhouse (c)

Concentration controller and developed software

The CO₂ concentration can be increased to a desired level by a CO₂ controller. It consists of wireless module and an electromagnetic valve (SONGLE). The CO₂ cylinder can be opened by the electromagnetic valve to increase gas concentration. Fuzzy PID algorithm has been adopted in the system to calculate the compensation of CO₂ concentration. The duty circle of driving circuit of the electromagnetic valve is flexible and the minimum switching period is set as 5 seconds.

A monitoring GUI (graphic user interface) based on LabVIEW platform was developed and is shown in Figure 4. The received data can be stored in the laptop and the curve can be shown in separate windows. The detected CO₂ concentration, temperature, humidity and luminance data are sent from the sensor node and can be received by the wireless receiver which is connected to the laptop. The received data can be stored in separately created files in the laptop. These files can be opened by using Excel. As shown in Figure 4, the received data are separately shown in a window with a pull-down menu. The function of choosing sensor nodes has been developed for future experiments that involving multiple developed sensor nodes. The column on the right side of the software is the configuration zone of the serial ports including the communication baud rate, stop bit and byte counting etc.

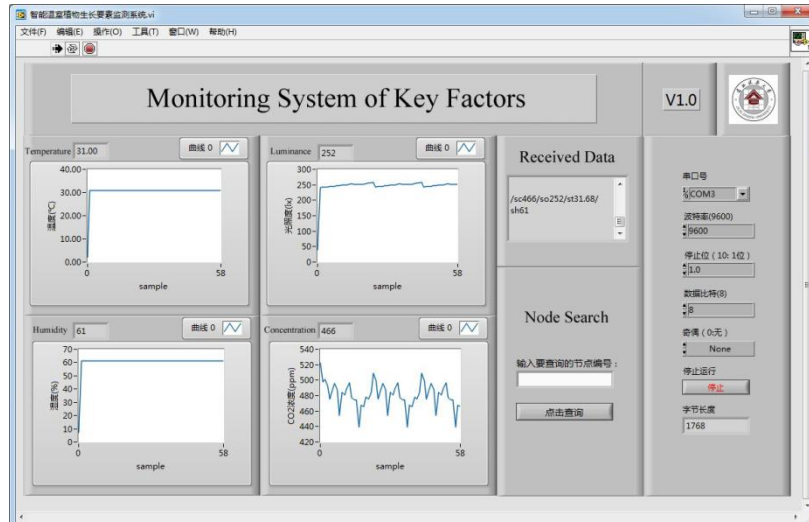


Fig. 4 - Developed monitoring system based on LabVIEW platform

RESULTS

Performance test of gas sensor

The developed sensor node was tested in laboratory in order to evaluate its sensing performance. Standard gas samples were flushed into a gas cell by a mass flow meter. Two standard gas samples of 1000 ppm and 600 ppm were tested separately and the results are shown in Figure 5. In a total period of 1,000 seconds the stability tests were carried out. For the 1000 ppm gas sample, the maximum and minimum detected values were 1017 ppm and 978 ppm respectively. The relative error can be calculated as 2.2%. The fluctuation of detected concentration is slightly smaller for the 600 ppm standard gas sample. The maximum and minimum concentrations are 619 ppm and 584 ppm respectively. The relative error can be obtained as 1.9%. The detected results demonstrated acceptable sensing performance.

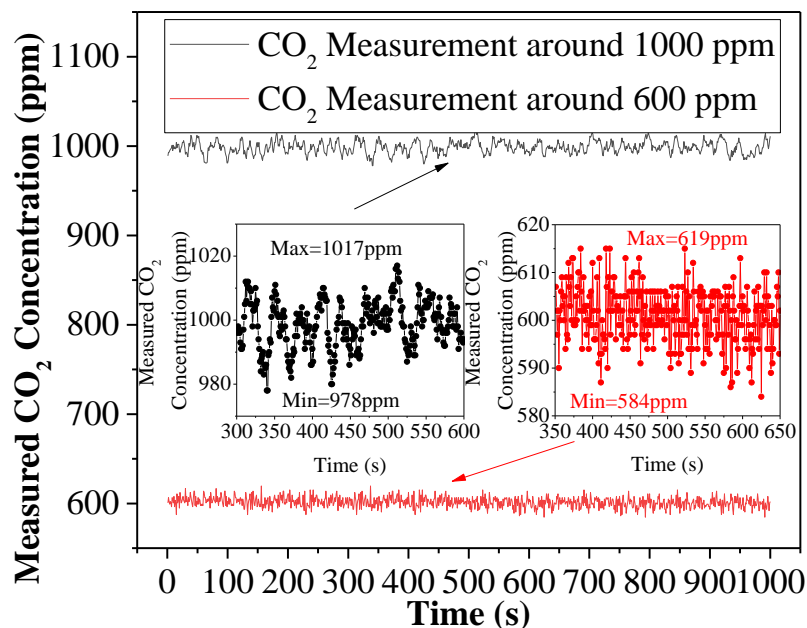


Fig. 5 - Stability tests of the developed sensor node

Wireless network test

The wireless communication tests were carried out in order to evaluate the wireless transmission performance. The greenhouse occupies a total area of 640 m². The developed sensor node was placed about 1 m height from ground. The RSSI (received signal strength indication) and package loss rate were measured experimentally and are shown in Figure 6 (a) and Figure 6 (b). As shown in Figure 6 (a), the RSSI value decreases with the increasing of the distance. The RSSI value is in the range from -25 dBm to -60 dBm when the distance between the sensor node and the wireless receiver is less than 20 meters. Then, the RSSI value slowly decreases with the increase of the distance. The RSSI value located in the range from -80 dBm to -90 dBm when the distance increased to 80 -100 m. As shown in Figure 6 (a), the main trend of RSSI value is decreasing while the distance is increased. Then, the package loss rate was tested as shown in Figure 6 (b). It can be seen that the package loss rate remains zero while the distance increases from 0 m to 28 m between the sender, which is the sensor node, and the receiver. Then, the package loss rate increases with the increase of the distance. The loss rate reaches about 2.1% when the distance is 80 meters. If the sent data is not correctly received, the sender will send again until the receiver successfully captures the data and answers the sender. This process not only wastes time but also consumes more power which will shorten the usage time of the battery. From the experiments, the RSSI value and package loss rate demonstrate that the wireless communication is reliable and suitable for the developed system.

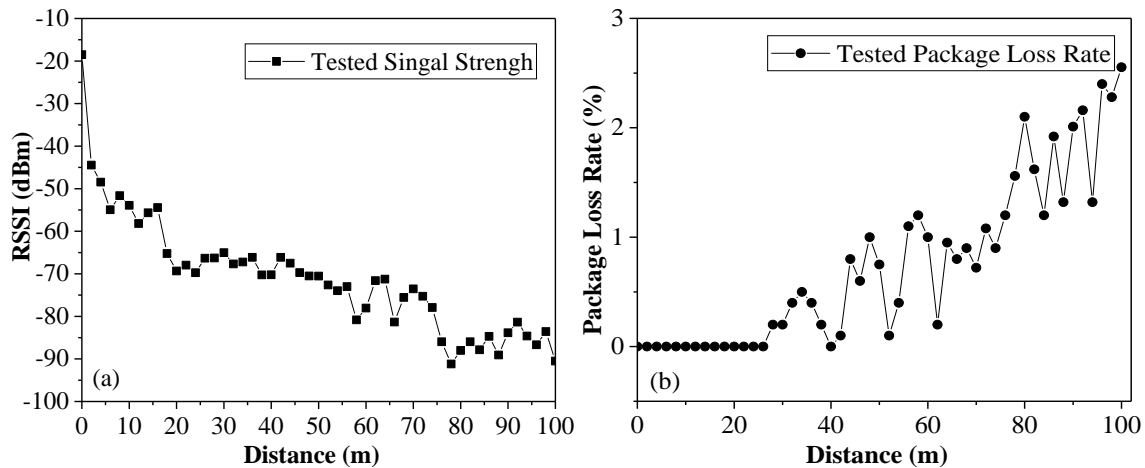


Fig. 6 - Tests of RSSI (a) and package loss rate (b) for the wireless communication in greenhouse

Concentration measurement

The developed system was deployed in a greenhouse with the length of 80 meters. The sensor node, CO₂ controller and CO₂ cylinder were placed in the greenhouse. The laptop was located in the adjacent control room which is shown in Figure 3 (c). A 24-hours detection experiment was carried out as shown in Figure 7. In Figure 7, it can be seen that the CO₂ concentration and temperature in the greenhouse were detected as shown. The CO₂ concentration was detected every 30 seconds from 12:00 at noon and the experiment ends at 11:59:30 the next day.

The CO₂ concentration decreases from the beginning of the experiment due to the photosynthesis effect. In a photosynthesis process, CO₂ is absorbed by the plants and is converted into chemical energy. In this way, CO₂ can be realised as an important fuel of plants. As shown in Figure 7, the CO₂ concentration decreases from 300 ppm at 12:00 to 130 ppm at 3:30. It is essential to realise that the roll blind machine for greenhouse starts to work at about 3:30 for thermal insulation because the outside of the greenhouse gets dark. The surface of greenhouse that faces towards the sun is covered at about 3:30. Therefore, the photosynthesis process in the greenhouse is dramatically slowed and the decrease of CO₂ concentration is interrupted. Then, the CO₂ concentration starts to increase because the greenhouse cannot be entirely sealed. The CO₂ concentration increases due to the air exchange between the inside and outside of the greenhouse. The increase will be continued until the roll blind machine rolls up the covering the next morning. Then, the CO₂ concentration starts to fall again caused by the photosynthesis.

It can be seen that CO₂ concentration is in a circulation in the total 24-hours experiments. This is caused by the resist of air-exchange by the greenhouse which is good for warm keeping. In Figure 7, the temperature is shown as the red curve. It can be seen that the trend of the temperature and CO₂ concentration is opposite. The temperature in the greenhouse increases in the process of photosynthesis

due to the strong sunshine. The temperature starts to decrease at 3:30 when the rolling blind machine cover the surface of the greenhouse. Without the heating effect of sunshine, the temperature decreases continually until the roll blind machine rolls up the covering the next morning. According to the experiment, it can be realized that the CO₂ concentration fertilization is necessary to compensate the concentration drop caused by photosynthesis and air-exchange resist of the greenhouse. Therefore, a reasonable CO₂ fertilization is desired to compensate the CO₂ concentration which is important for photosynthesis.

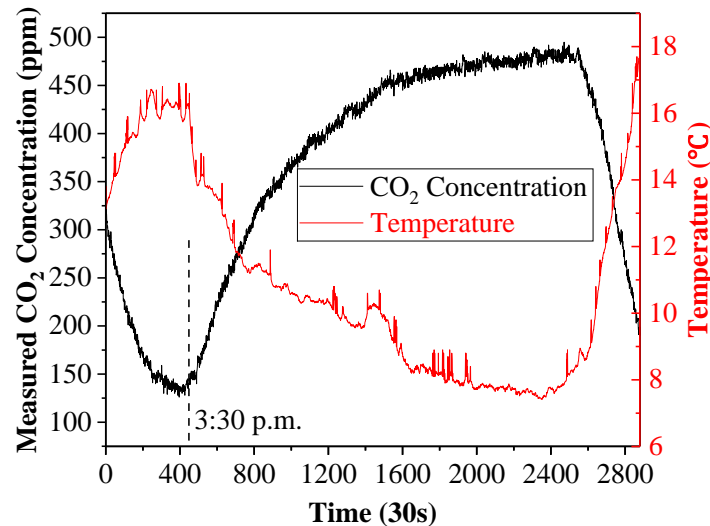


Fig. 7 - Detection of CO₂ concentration and temperature in the greenhouse in a period of 24 hours

The humidity and luminance tests were also carried out by using the developed system. The humidity decreases in the photosynthesis process as shown in Figure 8 (a). The humidity in the greenhouse increases and remains at a high level in the night. Its peak value can be 89% during the night. On the other side, the luminance in the greenhouse is affected by the roll blind machine directly as shown in Figure 8 (b). During the period when the greenhouse is covered, the luminance drops to zero in the figure. It can be seen that the machine rolls up the covering at about 7:00 a.m. because the luminance value starts to increase in the figure. The luminance value dramatically raises when the sunshine covers the greenhouse. The humidity and luminance are both impacted by human activities and can be controlled to a large extent. The luminance can be supplied by artificial light source in the night and the related experiments will be carried out in the future studies.

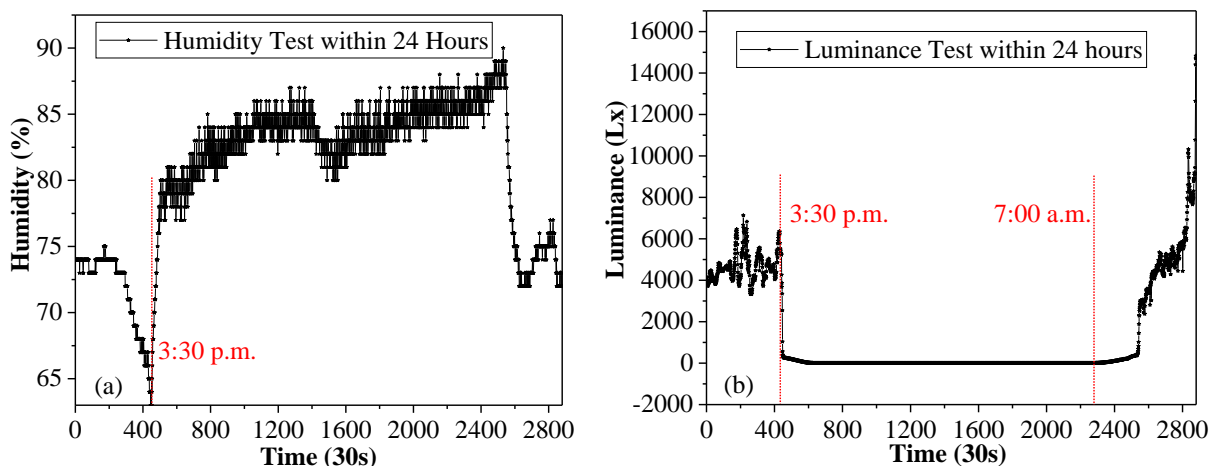


Fig. 8 - Detection of humidity (a) and luminance (b) in the greenhouse in a period of 24 hours

Test of CO₂ concentration control

The CO₂ compensation experiment was carried out to evaluate the control performance of the developed system. The results are shown in Figure 9. As shown in the figure, the total experimental period can be divided into four parts from T₀ to T₃. In the first period of time, T₀, the CO₂ concentration remains at a constant level of about 690 ppm without photosynthesis. Then, the CO₂ concentration starts to decrease in the T₁ period due to the photosynthesis effect. In this stage, the CO₂ cylinder is closed and the concentration

is without control or human impact. After setting a target concentration at 1000 ppm, the CO₂ cylinder is opened by the electromagnetic valve via wireless control. The pure CO₂ gas slowly permeate in the greenhouse in the T2 period. It can be seen from the figure that the most fluctuated period lasts approximately 1 hour. This period of time can be shortened by setting a larger flow speed of the CO₂ cylinder or adjusting the PID control strategy. Finally, the CO₂ concentration remains constant around 1000 ppm which is the target point in the T3 period. The maximum fluctuation of concentration is less than 60 ppm. It can be seen that the CO₂ concentration can be effectively regulated by the system during the period from T0 to T3.

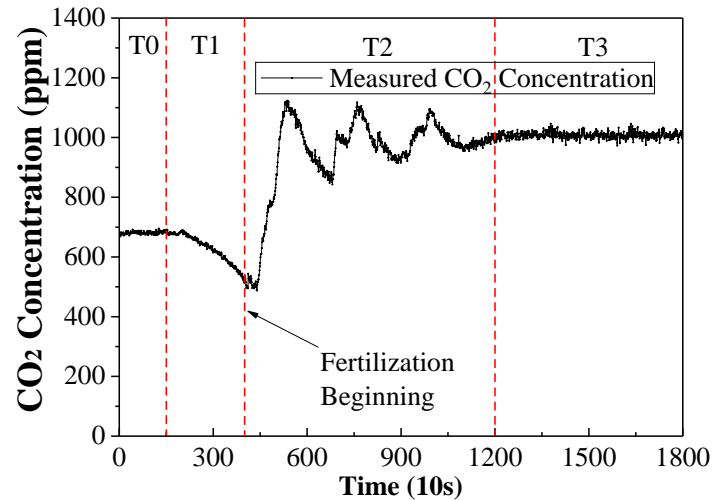


Fig.9 - Experiment of CO₂ concentration control in the greenhouse at 1000 ppm

CONCLUSIONS

A carbon dioxide detecting and controlling system has been proposed. This system has been experimentally applied in a greenhouse in northern China. The developed system consists of several major parts including a sensor node, a wireless receiver and a CO₂ concentration controller with pure CO₂ cylinder. The sensor node is wireless communicated with other parts and an infrared CO₂ sensor is embedded in it. The wireless infrared gas sensor was developed for real-time CO₂ detection which is essential for plant photosynthesis. Collected data of concentration can be received by the wireless receiver which connects to a laptop installed developed LabVIEW program. In the greenhouse, CO₂ concentration can be controlled automatically by the concentration controller based on fuzzy PID algorithm. According to the experiments, the fluctuation of detection results is less than 2.2%. The fluctuation of CO₂ concentration under automatic control in the greenhouse is less than 60 ppm which proves good performance of the system. In addition, the proposed CO₂ detecting and controlling system is also capable to detect temperature, humidity and luminance in the greenhouse. The proposed system can be applied for researching optimal production in greenhouse environment. Multiple sensor nodes will be studied in the future in order to be applied in larger greenhouses.

ACKNOWLEDGEMENT

The authors wish to express their gratitude to the National Natural Science Foundation of China (No. 51672103), Jilin Jianzhu University (2017G11011), the National Key Technology R&D Program of the Ministry of Science and Technology of China, the Education Department of Jilin Province of China, and the State Key Laboratory of Integrated Optoelectronics, Jilin University for their generous support of this work.

REFERENCES

- [1] Charles M. Wynn, Stephen Palmacci, Michelle L. Clark et al., (2014), High-sensitivity detection of trace gases using dynamic photo-acoustic spectroscopy, *Optical Engineering*, Vol.53, 021103, Bellingham/U.S.A.;
- [2] Gutierrez J., Villa-medina J. F. et al, (2014), Automated irrigation system using a wireless sensor network and GPRS module, *IEEE Transactions on Instrumentation and Measurement*, Vol.62, Issue 1, pp.166-176, Ottawa/Canada;

- [3] Hwang J., Shin C., Yoe H., (2010), A wireless sensor network-based ubiquitous paprika growth management system, *Sensors*, Vol.10, pp.11566-11589, Basel/Switzerland;
- [4] Jianing Wang, Lingjiao Zheng, Xintao Niu et al., (2016), Mid-infrared absorption-spectroscopy-based carbon dioxide sensor network in greenhouse agriculture: development and deployment, *Applied Optics*, Vol. 55, Issue 25, pp.7029-7036, Washington, D.C./U.S.A.;
- [5] Jianing Wang, Xintao Niu, Lingjiao Zheng et al., (2016), Wireless Mid-Infrared Spectroscopy Sensor Network for Automatic Carbon Dioxide Fertilization in a Greenhouse Environment, *Sensors*, Vol.16, pp. 1941-1960, Basel/Switzerland;
- [6] Ma X., Liu S., Gao Q.Z. et al., (2015), Effectiveness of gaseous CO₂ fertilizer application in China's greenhouse between 1982 and 2010. *Journal of CO₂ Utilization*, Vol.11, pp.63-66, London/U.K.;
- [7] Malaver A., Motta N., Corke P., et al., (2015), Development and integration of a solar powered unmanned aerial vehicle and a wireless sensor network to monitor greenhouse gases, *Sensors*, Vol.15, pp.4072-2096, Basel/Switzerland;
- [8] Misra S. C. K., Mathur P., Srivastava B. K., (2004), Vacuum-deposited nanocrystalline polyaniline thin film sensors for detection of carbon monoxide, *Sensors and Actuators B*, Vol.114, pp.30-35, London/U.K.;
- [9] Ritobrata Sur, Kai Sun, Jay B. Jeffries et al., (2014), TDLAS- based sensors for in situ measurement of syngas composition in a pressurized, oxygen-blown, entrained flow coal gasifier, *Applied Physics B*, Vol.116, pp.33-42, Berlin/Germany;
- [10] Salker A. V., Choi N. J., Kwak J. H. et al., (2005), Thick films of In, Bi and metal oxides impregnated in LaCoO₃ perovskite as carbon monoxide sensor, *Sensors and Actuators B*, Vol.106, pp.461-467, London/U.K.;
- [11] Serodio C., Cunha J. B., Morais R. et al., (2001), A networked platform for agricultural management systems, *Computers and Electronics in Agriculture*, Vol.31, pp.75-90, London/U.K.;
- [12] Somov A., Baranov A., Spirjakin D., et al. (2013), Development and evaluation of a wireless sensor network for methane leak detection, *Sensors and Actuators A*, Vol.202, pp.217-225, London/U.K.;
- [13] Somov A., Baranov A., Spirjakin D. et al. (2014), A wireless sensor-actuator system for hazardous gases detection and control, *Sensors and Actuators A*, Vol.202, pp.217-225, London/U.K.;
- [14] Wei Ren, Wehze Jiang, Nancy P. Sanchez, et al., (2014), Hydrogen peroxide detection with quartz-enhanced photo acoustic spectroscopy using a distributed feedback quantum cascade laser, *Applied Physics Letters*, Vol.104, 041117, U.S.A.;
- [15] Yasuda T., Yonemura S., Tani A., (2012), Comparison of the characteristics of small commercial NDIR CO₂ sensor models and development of a portable CO₂ measurement device, *Sensors*, Vol.12, pp.3641-3655, Basel/Switzerland.

SOLAR THERMAL SYSTEM SIMULATION OF PEANUT DRYING DEVICE BASED ON TRNSYS

基于 TRNSYS 的花生干燥装置太阳能集热系统研究

As. M.S.Stud. Eng. Chao Wang^{1,2)}, M.S.Stud. Eng. GuoLiang Zhang^{1,2)}, M.S.Stud. Eng. Liu Yang^{1,2)},
A/Prof. M.S. Eng. ChuanYang Zhang^{*1,2)}

¹⁾ Mechanical & Electronic Engineering, Shandong Agricultural University, Taian / China; ²⁾ Shandong Provincial Key Laboratory of Horticultural Machinery and Equipment, Shandong Agricultural University, Taian / China
Tel: 05388246103; *Email: chuanyangzhang@163.com

Keywords: peanut drying, drying chamber, heat collector, TRNSYS

ABSTRACT

In order to solve the problems of natural drying peanut with long drying cycle, huge resource and vulnerable to pollution, a solar drying peanut device taking solar energy as the main energy source and electric energy as the auxiliary energy source is designed. The working principle, device structure, drying chamber and heat collector are also studied. The heat collector performance of solar collector system is simulated by utilizing TRNSYS. The simulation results show that the total solar heat collector inclined surface radiation, temperature of solar collector, and electric auxiliary heating rate and water layer changes with time.

摘要

为了解决花生传统自然晾晒干燥存在干燥周期长、晾晒场资源需求巨大、易受污染等问题，设计了一种以太阳能为主要能源、电能为辅助能源的太阳能干燥花生装置，并对其工作原理、装置结构、干燥室及集热器进行了相应的研究。利用 TRNSYS 软件对太阳能干燥花生装置集热系统的集热性能进行了仿真，仿真结果分别显示了太阳能集热器倾斜面日总辐射量、太阳能集热器出口温度、电辅助加热率和水箱不同层随时间的变化。

INTRODUCTION

China is a big country of peanut cultivation. According to the statistics of the United Nations Food and Agriculture Organization, in recent years, the output value of peanut in China has reached about 40% of the world with first ranking (Yan Jian-Chun et al. 2013; FAOSTAT 2012). At present, peanut drying in China is still mainly artificial, although it does not require inputting additional energy and the long drying period, huge area demand and weather conditions cause greater dependence. It has been unable to meet the development requirements of peanut industry in China. Solar drying refers to a drying operation using solar drying devices and solar radiation. Presently, the research and development of solar drying technology has made it possible to use solar energy for peanuts drying effectively.

The test place of solar peanut drying plant is Taishan District, Tai'an, Shandong Province, where, the annual radiation is 4806.72 MJ/(m²a) and the sunshine duration is 2668 hours. Thereby, it has good solar energy utilization conditions.

MATERIALS AND METHODS

Design scheme of solar drying peanut

Combined with the advantages of various solar drying equipments and in view of the actual needs of peanut drying, we have developed a drying system using solar energy. The system combines solar energy with electric heating equipment for applying heat, which mainly dries the peanuts. Taking peanuts as an example, the design of a single loading capacity is 50-100 kg; the drying time is 20 hours and the power of the electric heating device is selected as 3 kW. The solar energy drying peanut equipment is used as small-sized drying equipment, and the following requirements should be met (Lahnine L et al. 2016):

- (1) Solar drying equipment has compact structure and small footprint;
- (2) The material heating method is normal-pressure heat drying, and the drying temperature is controlled within 34°C-52 °C;
- (3) Good continuous drying operation: the use of solar energy and electric heating device, ensure material continuous drying;

- (4) Drying chamber uniform distribution of air: air uniform design in the drying room, improve the uniformity of air flow drying chamber;
- (5) Reasonable use of the drying chamber space: to ensure the loading of 50-100 kg, simple material loading is required.

1.1 The basic mechanism

We design peanut solar drying system with hot water according to the requirements mentioned above. The system is mainly composed of heat collecting system, drying system and control system. The basic structure of the solar drying system with hot water is shown in Fig.1

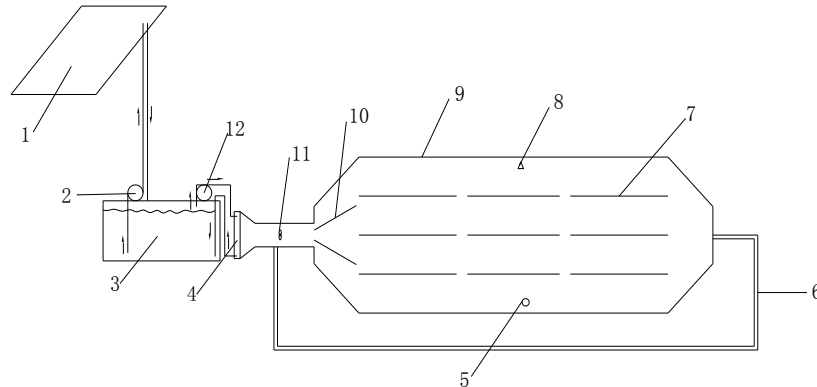


Fig. 1 - Schematic diagram of peanut drying system using solar water heating
 1 - heat collector; 2 - heat collector circulation pump; 3 - water storage tank; 4 - heat exchanger;
 5 - humidity sensor; 6 - circulation duct; 7 - material tray; 8 - temperature sensors; 9 - drying room;
 10 - plate; 11 - blower; 12 - heat exchanger circulating pump

The heat collecting system consists of solar collector, water tank and electric heating device. The drying system is mainly composed of drying chamber, a fan and a windshield material tray. The control system includes temperature and humidity control and air volume control. Under the influence of the control system, heat collecting system supplies energy to input drying system meeting the needs of the drying system, which can improve the drying efficiency.

1.2 Working principle

Working principle of the drying system is that it heats the water through the heat collector during daytime and the hot water is circulated by a pump to the water storage tank. The tank and the drying chamber are connected through the heat exchanger transferring collected heat to the drying chamber, which is used in drying peanut. When the outside cold air is driven by the blower at the left of the drying chamber, the cold air is heated by the heat exchanger into the drying chamber for increasing peanuts temperature. The surface of the peanut is vaporized, lowering the moisture content of the peanut (FAOSTAT, 2012). In the drying process, the drying room temperature drops to a predetermined temperature; when solar energy is not enough, the electric heating device in the water tank operates to add the required heat to the drying chamber in order to maintain continuous drying. The storage tank electric heating device stops working when the indoor temperature is higher than a predetermined temperature.

1.3 Design of the drying room

The drying room is designed to dry peanuts; we have to consider the drying characteristics of peanut firstly, such as the initial moisture content and maximum allowable temperature. Secondly, the drying chamber not only achieves the heat and moisture transfer of hot air and peanut, it also needs a reasonable way of material bearing and releasing. The space can be fully utilized; the heat and water exchange can be fully carried out. At the same time, the convenience of the system operation and the access of materials are also considered (Aktaş M.et al. 2016; Liu Mingle 2015).

In order to be compatible with and solve the above-mentioned problems, the solar drying chamber adopts horizontal box structure; the drying room is a total of 1.2 m height, 2.1 m long and 1.4 m wide. Left end of the drying chamber is provided with a conical inlet; the right end is provided with a conical air outlet; the middle part of the drying chamber is a cuboid and the drying chamber side is provided with a door. As material access, the drying chamber is divided into 3 layers; each layer is provided with 3 material trays (Zi Rou et al. 2011). The drying chamber structure diagram is shown in Fig.1.

1.4 Design of the heat collector system

The heat collector system is an important part of the solar drying peanut system. Electric heating device is composed of a solar collector and water tank. The performance of heat collector of the solar drying device has a great influence on the solar drying peanut effect.

1.4.1 Calculation of collector area

Solar collector and solar drying device of peanut are installed in Tai'an, Shandong province. The peanut harvest from late September to early October and the daily average temperature is 25 °C. The average daily solar radiation amount reaches 12.23×10^3 kJ/m².

(1) Calculation of total area of direct system heat collector (*Xie Shan-Zhu and Di Nan 2015*)

$$A_c = \frac{Q_w C_w (t_{end} - t_i) f}{J_t \eta_{cd} (1 - \eta_L)} \quad (1)$$

A_c - the total area of the collector, m² ;

Q_w - the average daily water consumption, kg;

t_{end} - water temperature, K;

C_w - constant pressure heat capacity of water, 4.187 kJ/(kg·K);

t_i - the initial temperature of water, K;

f - solar fraction, GB range of value for 0.3~0.8;

J_t - the local daily average collector heating surface radiation, kJ/m²;

η_{cd} - the collector efficiency throughout the day, GB range of value from 0.4 to 0.55;

η_L - the pipeline and storage tank heat loss rate, range of value from 0.15 to 0.2.

(2) Indirect type system of the total area of the collector

$$A_{in} = A_c \left(1 + \frac{F_R U_L \bullet A_c}{U_{hx} \bullet A_{hx}} \right) \quad (2)$$

A_{in} - indirect heating system of the solar collector area, m²

A_c - total area of solar collector in direct heating system, m²

$F_R U_L$ - total heat loss coefficient of collector, W/(m²·K), Flat plate solar collector from 4 to 6W/(m²·K);

U_{hx} --the heat loss coefficient of heat exchanger, W/(m²·K)

A_{hx} —heat exchanger area, m²;

The solar water heating system in this design adopts indirect systems and by the formula (1) and (2) we calculated the solar collector area of 5.99 m².

1.4.2 Collector installation

The project uses P-J-F-80/1.70/0.70-L type flat plate collector; the single collector area is 1.7 m². As peanut collector area of the solar drying system necessary is 5.99 m², we select the 4 flat-plate collectors.

In order to make the solar collector to obtain the maximum heat, we need to select an optimum installation angle of solar collector. The installation of solar collector should not be less than 0.5 m in the ground level; the collector day lighting surface angle is the local latitude 5 degrees, and not less than 30 degrees (*Li Bian-Sheng et al 2011*). The location of Tai'an latitude is: 113.13 degrees longitude, 36.18 degrees latitude. In the installation process, the heat collector should be installed in accordance with the best angle, select the tilt angle of 36 degrees, the gap at 5 degrees up and down, in order to obtain the best solar thermal effect. The installation of solar collector is shown in Fig.2.

1.5 Design of the water storage tank

The water tank is one of the most important parts of the solar heat collector system, as a storage device for hot and cold water. It should have good insulation properties. The water capacity, water tank insulation, shape, structure and material will directly affect the performance and operation of the solar collector system.

The volume of the water storage tank is related to the area of solar collector, the general per square meter solar collector area, tank volume needed for 40-100 liters, usually recommended by the proportion of heat exchanger area per square meter of the sun set corresponding to the 75 liters storage tank volume (*Guan Qiao-Li 2009*). The collector area is 6.8 m², therefore, the volume of the storage tank should be 510 liters, and the volume of the storage tank is 750 liters.



Fig. 2 - Collector installation schematic

2. Simulation of the solar heating system using TRNSYS

2.1 TRNSYS Introduction

TRNSYS (Transient System Simulation) software was originally developed by Solar Energy laboratories Wisconsin-Madison University (SEL) and improved under the joint study of the European Institute gradually. TRNSYS simulation program that simulates solar system includes two parts: photoelectric and light. It includes a heat collector, water tank, water pump, auxiliary heater and other dozens of commonly used components. It can simulate the hot water, heating, refrigeration, air conditioning room and heat pump (Liu Sheng-Yong *et al.* 2001).

2.2 Simulation model of solar collector system

Pic.1 is built in TRNSYS solar collector system component integration diagram, the simulation object for the flat plate collector forced circulation, water supply system with constant temperature control, solar energy as the main energy water heating, electric heating device, auxiliary heating, to maintain the water temperature at 60 degrees Celsius (Wang An-Jian *et al.* 2014).

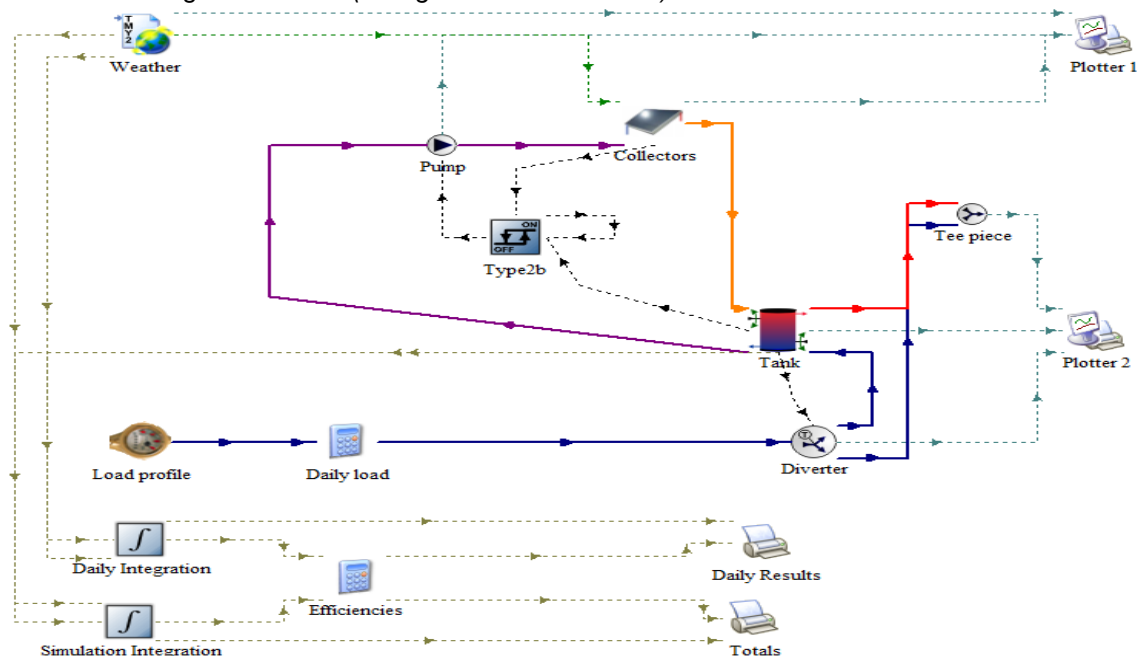


Fig.3 - Pic.1 Simulation model of solar heat collector system

The typical meteorological year is a set of meteorological parameters consisting of 8760 hours of hourly meteorological data, including dry, wet bulb temperature, solar radiation, and wind speed and wind direction. The typical meteorological year data of Tai'an using TRNSYS simulation derived from the latitude and longitude of Tai'an area by using Meteorom7 software. Fig.4 and Fig.5 show the typical meteorological parameters of Tai'an region from the late September to early October (Minaei S.*et al.*, 2016).

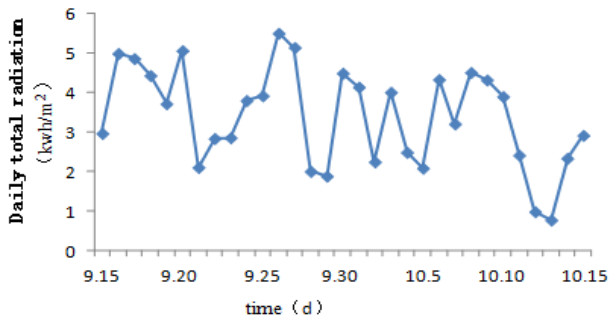


Fig. 4 - Total solar radiation changes

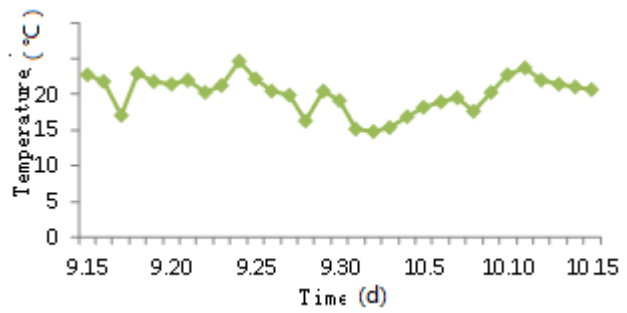


Fig. 5 - September 15th to October 15th temperature change

2.3. Typical weather simulation

In the simulation, we chose September 15th and October 15th from the typical meteorological year data, because the first one is the hottest and the second is the coldest from mid-September and mid-October.

2.3.1 The hottest weather simulation

The weather parameters for September 15th are shown in Fig.6, Fig.7, Fig.8 and Fig.9.

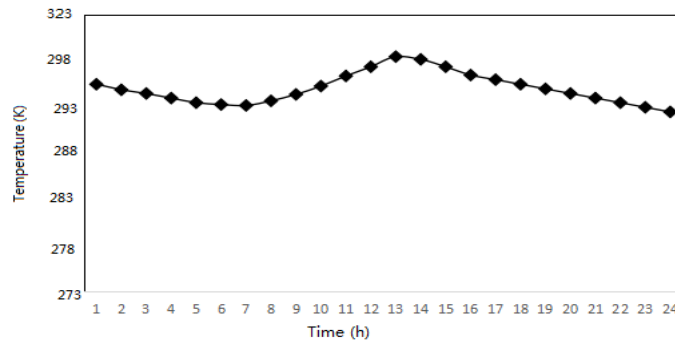


Fig. 6 - September 15th temperature change

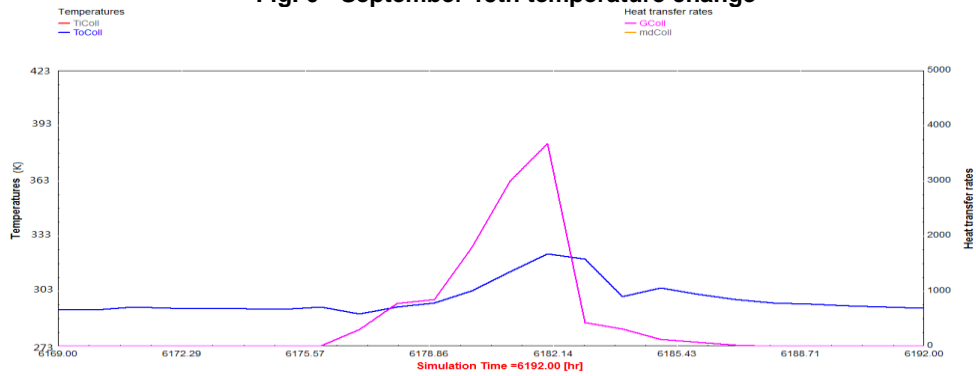


Fig. 7 - Variation of total radiation and outlet temperature of inclined surface of solar collector in September 15th



Fig. 8 - Electric heating rate change in September 15th

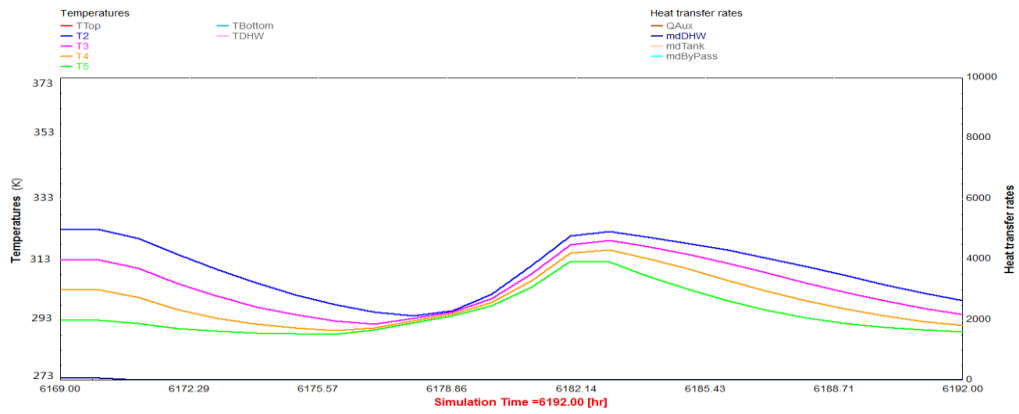


Fig. 9 - Variation of temperature in different layers of water tank in September 15th

2.3.2 The coldest weather simulation

In October 15th the weather parameters is shown in Fig.10, Fig.11, Fig.12 and Fig.13.

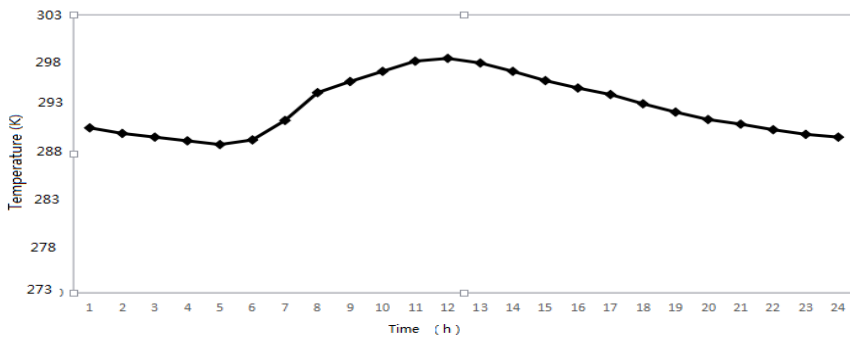


Fig. 10 - October 15th temperature change

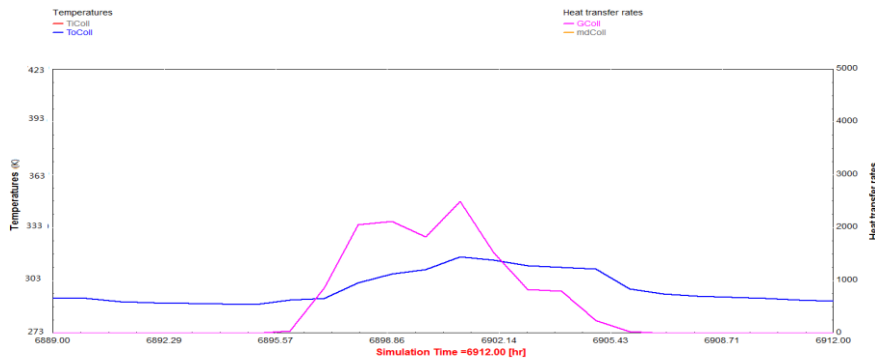


Fig. 11 - Variation of total radiation and outlet temperature of inclined surface of solar collector in October 15th

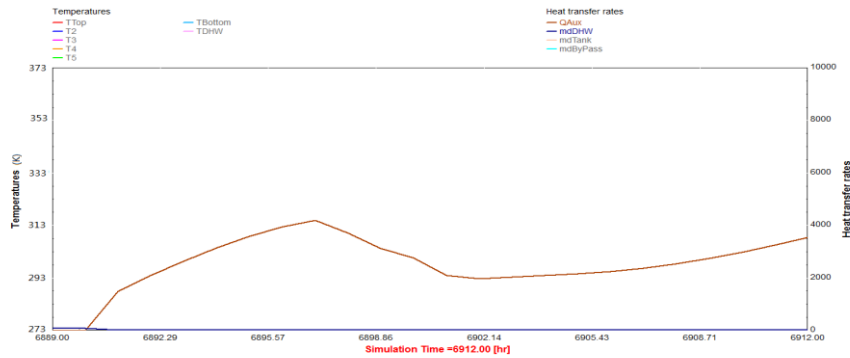


Fig. 12 - Electric heating rate change in October 15th

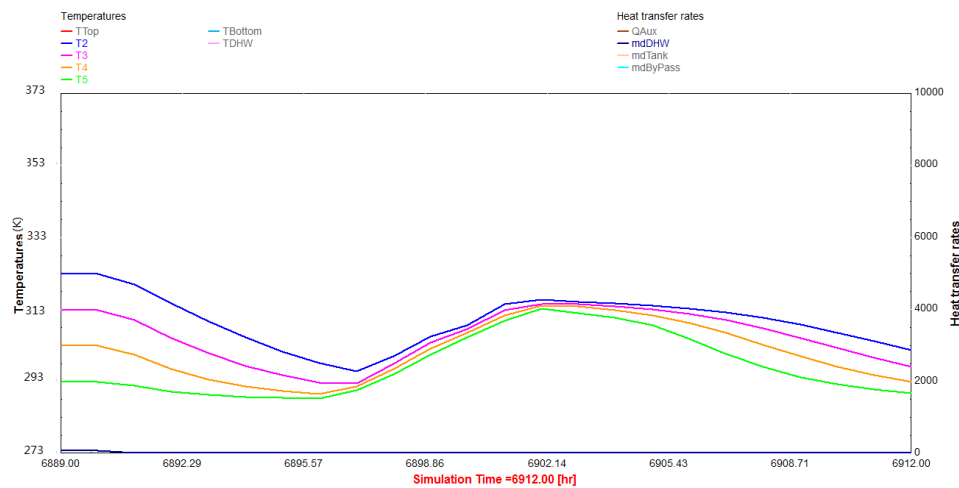


Fig. 13 - Variation of temperature in different layers of water tank in October 15th

3. Test Materials and methods

The test time is September 3, 2016, the test venue for Tai'an city of Shandong Province, P-J-F-80/1.70/0.70-L type flat type test by the collector, water tank and thermometer. The set temperature and simulation results of direct heat exchanger outlet through comparative test analysis of solar energy, solar thermal performance of dry peanut system heat collecting system were performed (Wessapan T and Theerapong B, 2012; Tunde-Akintunde TY 2011; Gan XF 2011). We set the outlet temperature of heat exchanger by measuring the temperature once every hour and the results obtained are shown in Fig.14

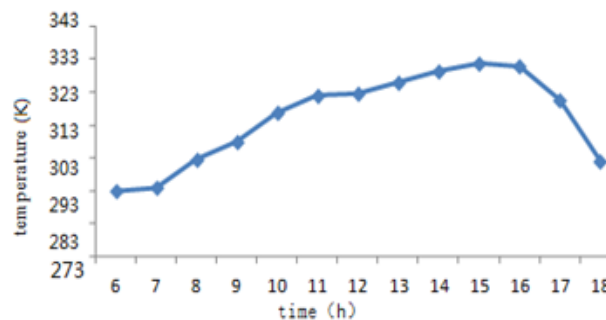


Fig.14 - Variation of outlet temperature of solar collector

CONCLUSIONS

(1) According to the simulation in September 15th, the solar tilt radiation began to increase from zero at 7: 00, the outlet temperature of the collector increases with the increase of radiation of the inclined plane. At 13:00, the maximum amount of solar tilt radiation is reached; the collector outlet temperature reaches the maximum value of 50.3 °C at the same time. At 18:00, the radiation changed to 0, the collector outlet temperature is no longer increased, and it is consistent with the actual situation, which shows that the simulation data is accurate.

(2) According to the simulation in October 15th, the solar tilt radiation began to increase from zero at 7: 08, the outlet temperature of the collector increases with the increase of the radiation of the inclined plane. At 12:00, the maximum amount of solar tilt radiation is reached; the collector outlet temperature reaches the maximum value of 43.4 °C at the same time. At 17:30, the radiation changed to 0, the collector outlet temperature is no longer increased, and it is consistent with the actual situation, which shows that the simulation data is accurate.

(3) With the use of TRNSYS simulation in the outlet temperature of heat exchanger consistent with the outlet temperature of the collector, the temperature is measured. The outlet temperature of the heat exchanger is up to 52°C, indicating that the collector performance of the peanut solar drying device meets well the design requirements.

REFERENCES

- [1] Aktaş M., Şevik S., Amini A., Khanlari A. (2016), Analysis of drying of melon in a solar-heat recovery assisted infrared dryer, *Solar Energy*, Vol.137, pp. 500-515;
- [2] Azizi M., Mohebbi N., Felice FD (2016), Developing a Rating Model for Selection Solar Wood Drying Location, *Agriculture and Agricultural Science Procedia*, Vol.8, pp. 378-386;
- [3] Gan XF, He ZB, Yi SL (2011), Contrast Studies on the Solar Drying Schemes of Eucalypt Timber. *Advanced Materials Research*, Vol.1165, pp.189-193;
- [4] Guan Qiao-Li. (2009), TRNSYS Simulation and Research of Solar Thermal Storage and Ground Source Heat Pump Heating Water System. *Transactions of Tianjin University*, Vol.07, pp.78-82;
- [5] Lahnine L., Idlimam A., Mahrouz M., et al.(2016), Thermo physical characterization by solar convective drying of thyme conserved by an innovative thermal-biochemical process. *Renewable Energy*, Vol.94, pp.72-80;
- [6] Li Bian-Sheng, Shen Xiao-Xi, Liu Wei-Tao. (2011), Drying Experiment and Mathematical Modeling of Solar Drying Equipment, *Journal of South China University of Technology (NATURAL SCIENCE EDITION)*, Vol.04, pp.115-120;
- [7] Liu Mingle, Wang Shuangyan, Li Kerong. (2015), Study of the Solar Energy Drying Device and Its Application in Traditional Chinese Medicine in Drying. *International Journal of Clinical Medicine*, Vol. 06, pp.65-70;
- [8] Liu Sheng-Yong, Zhang Bai-Liang, Yuan Chao, et al. (2001), Study on Drying Corn with Solar collector, *Journal of Agricultural Engineering*, Vol.06, pp. 93-96;
- [9] Tunde-Akintunde Toyosi Y (2011), Mathematical Modelling of Thin Layer Sun and Solar Drying of Cassava Chips, *International Journal of Food Engineering*, Vol.6, pp.98-102;
- [10] Wang An-Jian, Liu Li-Na, Li Shun-Feng (2014), Hot Air Drying Characteristics and Kinetic Model of Peanut, *Journal of Henan Agricultural Sciences*, Vol.08, pp.137-141;
- [11] Wessapan T., Theerapong B.(2012), An Experimental Study on Banana Drying Using a Combined Rejected Heat from Split-Type Air Conditioner and Solar Energy, *Applied Mechanics and Materials*, Vol.1471, pp. 110-115
- [12] Xie Shan-Zhu, Di Nan (2015), Structure Design of Drying Box for Alfalfa Solar Drying System, *Journal of Agricultural Mechanization Research*, Vol.05, pp. 239-241;
- [13] Yan Jian-Chun, Hu Zhi-Chao, Xie Huan-Xiong, Wang Hai-Ou, Yu Shao-Yang (2013), Study on Thin Layer Drying Characteristics and Model of Peanut Pod, *Proceedings of the Chinese Journal of automation*, Vol 06, pp. 205-210;
- [14] Zi Rou, Ti A-Mu, Mao Zhi-Huai, et al. (2011), Design and Test of Solar Drying Unit for Integral Fruit and Vegetable, *Journal of Agricultural Machinery*, Vol. 01, pp. 134-139;
- [15] *** FAOSTAT. Compare data: *Groundnuts, with shell Production*, <http://faostat3.fao.org/home/index.html#COMPARE>, 2012-12-01.

ANALYTICAL RESEARCH RESULTS OF THE COMBINED ROOT DIGGER

РЕЗУЛЬТАТИ АНАЛІТИЧНИХ ДОСЛІДЖЕНЬ КОМБІНОВАНОГО КОПАЧА
КОРЕНЕПЛОДІВ

As. Prof. Ph.D. Eng. Herasymchuk H. A.¹⁾, Prof. Ph.D. Eng. Baranovsky V. M.²⁾,
As. Prof. Ph.D. Eng. Herasymchuk O. O.¹⁾, Ph.D. Eng. Pastushenko A.S.³⁾

¹⁾ Lutsk National Technical University, Lvivska str., 75, Lutsk / Ukraine

²⁾ Ternopil Ivan Puluj National Technical University, Ruska str., 56, Ternopil / Ukraine

³⁾ Mykolayiv National Agrarian University, Georgiy Gongadze str., 9, Mykolaiv / Ukraine

E-mail: baranovskyvm@rambler.ru

Keywords: fodder beets, cleaning shaft, cleaning blade, collision velocity, kinetic energy, damage

ABSTRACT

This paper researches the operation principle structure of a combined root digger that consists of two spherical disks and, above them, a horizontal shaft with cleaning blades. Mechanical and technological justification of structural and kinematic parameters and operating modes of combined digger was carried out based on the analysis of technological process of roots excavation. The dependence of digger operation on the condition of providing complete digging of the root crops is obtained. Deterministic mathematical models of the interaction between the cleaning blade and the root head provided no not dumping and non-damaging of root, were developed.

РЕЗЮМЕ

Наведено будову та принцип роботи комбінованого копача коренеплодів, який складається з двох сферичних дисків і розташований над ними горизонтальний вал з очисними лопатями. На основі аналізу технологічного процесу викопування коренеплодів проведено механіко-технологічне обґрунтування конструктивно-кінематичних параметрів і режимів роботи комбінованого копача. Одержано залежності процесу роботи копача з умови забезпечення повноти викопування коренеплодів. Розроблено детерміновані математичні моделі процесу взаємодії очисної лопаті з голівкою коренеплоду з умови невибивання та непошкодження тіла коренеплоду.

INTRODUCTION

Fodder beet as an important crop is a valuable component for feeding dairy herd. Currently in the country's agricultural sector fodder beets cultivated areas have been decreased due to defects of root harvesting machines and quality inconsistencies of their work concerning agrotechnical requirements (Pogorely and Tatyanko, 2004; Herasymchuk and Baranovsky, 2009). Work analysis of the blade, fork, vibrating and two-disc digging devices revealed that they significantly damage large roots and significant loss of small roots takes place. In addition, the constructive and technological parameters of these types of diggers make impossible to efficiently combine two technological operations of harvesting efficiently – digging of roots with simultaneous separation of residual tops of their heads (Herasymchuk and Baranovsky, 2009; Kozachenko, 2004).

The tests performed on the cleaners that remove residual tops of fodder beets, showed that the cleaning technological process has a number of significant shortcomings. The main shortcomings appear because of the interaction between cleaning blade and the root head. It leads to the dumping of the roots and respectively to the losses during harvesting (Baranovsky, 2006).

The eligibility criteria for modern requirements for the digging tools in the first place are indicators of the completeness of roots (loss) digging, their damage and mass of impurities that come to their cleaning transportation technological systems (Bulgakov et al., 2009).

One of the reserves to increase technological indicators of work quality of root crop machinery is to improve the technological process by application of diggers that combine passive spherical disk system and the shaft set above it that contains the elastic cleaning elements. The intensification of the digging process takes place due to the specific kinematic and dynamic factors arising from the simultaneous interaction between cleaning elements, the roots head and the root heap (Golovach et al., 2012). It can be concluded that the installation of the drive shaft with blades allows digging out roots and separating remained tops

simultaneously, reducing the supply of impurities by the interaction between clearing blades and heap components (Baranovsky and Potapenko, 2017).

MATERIALS AND METHODS

A large number of working tools designs, digging tools assemblies and layout schemes require a differentiated approach in the selection, calculation, design, research and implementation of new outcomes into production. Therefore, classified approach, which takes peculiarities of working bodies, layout schemes and methods of operation into account, gives an opportunity for analysis and synthesis of the necessary structural and technological scheme of combined digger for peculiar work conditions. The variety of root diggers design schemes is connected with the process of harvesting and with structural and technological requirements to digging quality, roots cleaning and transportation.

Based on identification (analysis and synthesis) of digging tools analogues, the advanced designs of combined root diggers were submitted. They combine all the advantages and benefits of spherical single plate digger and usage possibilities in conditions of excessive soil moisture and weed-infested crops. The structural model and construction of a combined digger are shown in Fig. 1.

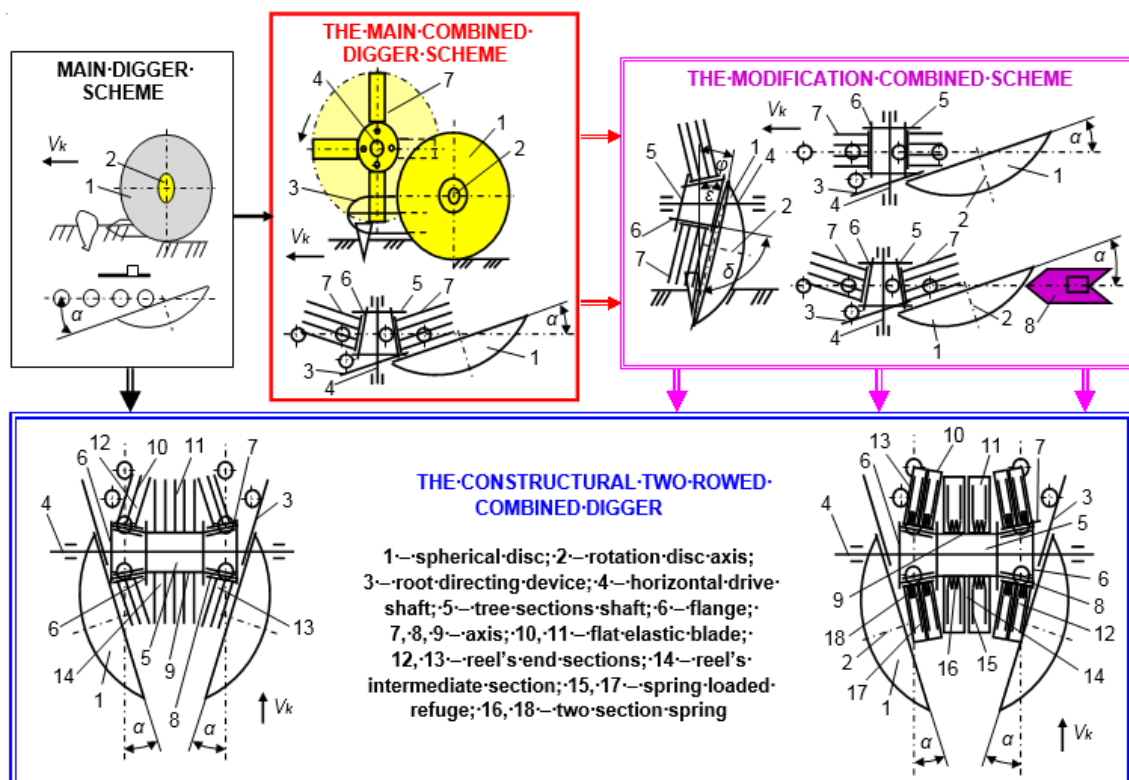


Fig. 1 – The development process identification of the combined digger structural and layout scheme

Combined digger consists of two spherical discs 1 set at an angle α to the axis of root row. Disks 1 are freely planted on their axes of rotation 2. On the front area of the working edge of each spherical disc 1 the root directing device 3 is set. Above the discs, perpendicular to the direction of the digger motion speed V_k , a horizontal drive shaft 4 is set. The horizontal drive shaft includes a reel 5 that bears flanges 6. The reel of the horizontal shaft is made of three sections. The axis 7, 8, 9 are set adherently between the flanges of the reel on its axis range; flat elastic blades 10, 11 are fixed on them. Axis 7 and 8 of two end sections 12, 13 form a truncated cone, the end sections 12, 13 are directed to each other by smaller bases. Axis 9 of the intermediate section 14 forms a cylinder. The planes that pass through the axis 7, 9 or 8, 9 of contiguous sections 12, 14 or 13, 14 are set at an obtuse angle.

When the digger moves, root directing device 3, shifts dumping the row roots to its centre and spherical disc 1 digs roots. Along with digging roots by rotating the drive shaft 4 flat elastic blades 10, 11 of the two end sections 12, 13 interact with the heads of roots, while simultaneously cleaning of heads of roots from residue tops of two adjacent rows and destruction of lumps of soil occur. In addition, flat elastic elements of intermediate section 14 simultaneously interact with roots and lumps of soil, purifying the roots

surface, destroying soil clumps, and pushing the heap, located in the space of spherical disks. Its supply is speeded up to the following transport technology systems of root harvesting machinery.

The installation of the drive shaft with flat blades allows digging out the roots and separating the remained tops. It reduces the flow of impurities due to the contact interaction between the blades and the components of root heap. It also increases the technological reliability of the process of digging out the roots and, as a result, the performance of digger and machinery in general.

The purpose of the research is a further improvement of constructive optimization, kinematic and technological parameters methods of the functioning process of the harvesting machinery combined diggers.

RESULTS

The main structural and kinematic parameters of combined digger describing the technological process of digging out roots 1 (Fig. 2) with simultaneous separation of residual tops from their heads are:

- the speed V_k of the digger 2; angular speed ω_o of the horizontal shaft 5 with cleaning blades 9;
- the installation angle β of clearing blades 9 axle 8 to the axis O_o of cleaning shaft 5 relative to position O ;
- or the length l of cleaning elements 9; placement coordinates (H_o, b_o) of axis O_o of cleaning shaft 5 relative to position O or axis 3 of free rotation of disk 2 with the diameter D , which is set at a depth of stroke h and at the angle α to the axis of root row 1.

The translational speed V_k of the digger is regulated by the requirements of the root harvesting technical process. Current requirements define the harvesting machinery root speed during the harvesting process within 1.8...2.0 m/s.

For the root loss elimination by ensuring the completeness of fodder beet digging, the condition (1) must be provided (Fig. 2):

$$b_e \geq 2\Delta s_{max} + 2\Delta z_{max} + 2r_k \quad (1)$$

where b_e – groove width, formed by the spherical disc, [m];

Δs_{max} – the maximum transverse deviation of the digger during its movement relative to the row axis, [m];

Δz_{max} – the maximum transverse deviation of root centre relative to the row axis, [m];

r_k – the average radius of the root head, [m].

According to Husak and Brychykova (2012) and taking into account (1) it can be written:

$$b_c = 2\sqrt{2hR - h^2}, [m]; \quad b_e = b_c \sin \alpha; \quad (2)$$

$$2 \sin \alpha \sqrt{h(D-h)} \geq 2\Delta s_{max} + 2\Delta z_{max} + 2r_k; \quad \alpha \geq \arcsin \frac{2(\Delta s_{max} + \Delta z_{max}) + d_k}{2\sqrt{h(D-h)}}. \quad (3)$$

Last formulas (2), (3) describe the angle change α of setting of the spherical digging disc relative to the fodder beet longitudinal axes depending on the disk basic parameters and the root head diameter, provided completeness of digging out or losses elimination.

Fig. 3 shows the graphic representation of angle change α according to the dependence (2), (3) at $\Delta s_{max} = 3$ cm, $\Delta z_{max} = 5$ cm, which can be used as a monogram for determining the basic disc parameters, depending on root size characteristics.

The monogram is to be used as follows.

The field roots with the average diameter, such as $d_k = 12...15$ cm (Fig. 3a) and selected spherical discs standard diameters, such as $D = 40$ and 45 cm, determine the angle changing limits. The α of a disc installation is related to the longitudinal axis of the fodder beet location, which satisfies the condition of dependence (3): a disk with the diameter $D = 40$ cm, $0.61 \leq \alpha \leq 0.7$ rad or $34^\circ \leq \alpha \leq 40^\circ$, and with the diameter $D = 45$ cm, $0.57 \leq \alpha \leq 0.66$ rad or $32^\circ \leq \alpha \leq 37^\circ$.

Then, for defined change limits of the disc installation angle $0.61 \leq \alpha \leq 0.7$ rad and $0.57 \leq \alpha \leq 0.66$ rad relative to the longitudinal axis of the roots location, for the diameter of $d_k = 12...15$ cm (Fig. 3b) find out the depth h of disc motion that satisfies the condition (4) and $h \geq 7.8$ and $h \geq 8.6$ cm.

In addition, for the disc spherical diameter $D = 45$ cm and $\alpha \leq 0.66$ rad. (Fig. 3b) the disc stroke depth $h \geq 8.6$ cm and for the diameter $D = 40$ cm and $\alpha \leq 0.7$ rad – $h \geq 9.0$ cm.

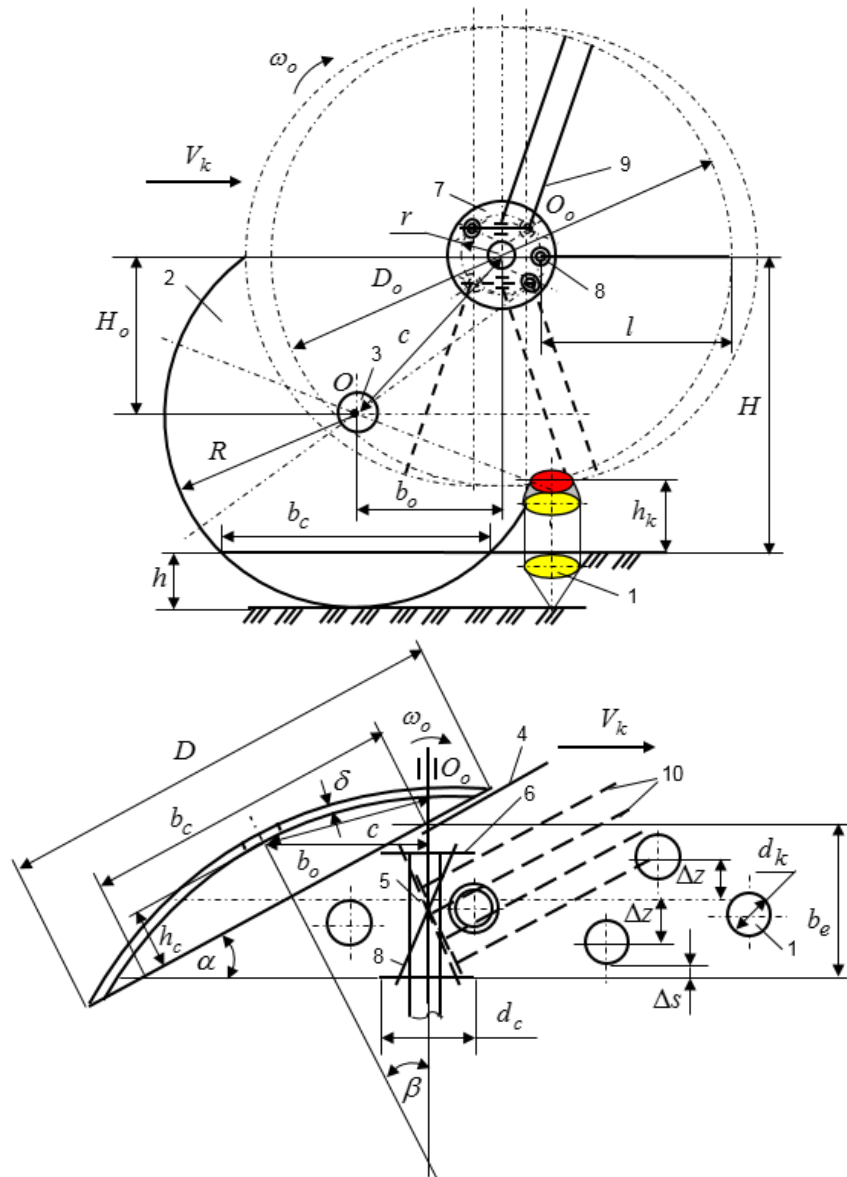


Fig. 2 – The scheme for calculating the parameters of the combined digger

1 – root; 2 – one-sided spherical disc; 3 – axis of disk rotation; 4 – root directing device; 5 – horizontal drive shaft; 6 – flange; 7 – reel; 8 – axis; 9 – cleaning blade; 10 – beater

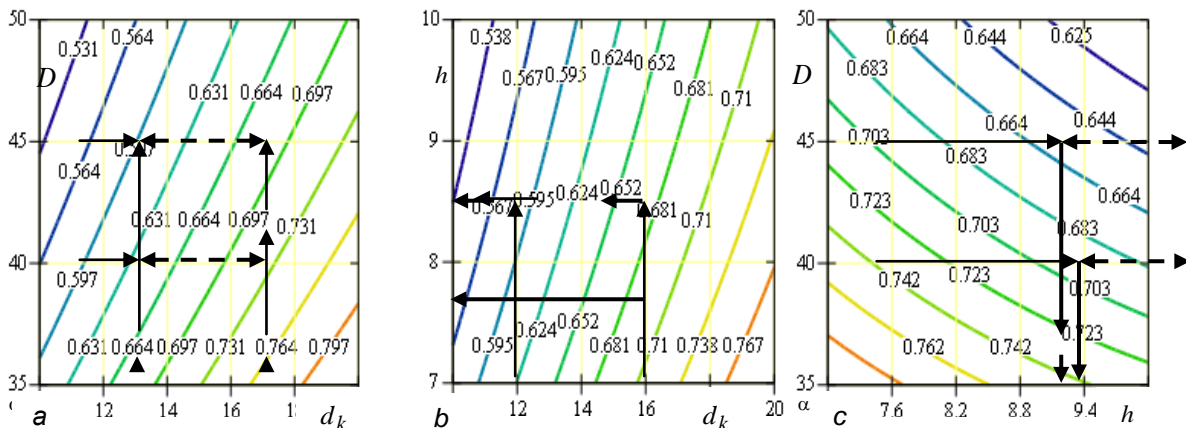


Fig. 3 – Changes dependencies on the angle of installation of the digging disk

a – $\alpha \geq f(d_k, D)$; b – $\alpha \geq f(d_k, h)$; c – $\alpha \geq f(h, D)$

Changes dependencies on the critical angular velocity of the digger drive shaft blade

As the rational (technological) effectiveness of the cleaning shaft is provided due to the blade contact plane on the root head, it is under the direct (or close to it) angle. Being related to the plane which passes through the external cutting edge of the disk, it can be considered the angle β , which characterizes the constructive installation of axes, on which the blades are set, will be equal to the attack angle α of the disk (or close to it), $\beta \cong \alpha$.

According to Fig. 2, it can be considered that the distance $OO_o = c \cong \sqrt{h_c^2 + R^2} + \Delta k \cos \alpha + 0,5d_n \cos \alpha$, where h_c – depth of the disk [m]; Δk – the technological gap between the outer edge of the cutting disc and the outer surface of the cleaning shaft, [m]; $0,5d_n$ – the diameter of the cleaning shaft [m].

Then the horizontal coordinate of the centre O_o of the clearing shaft is determined as:

$$b_o \cong c \cos \alpha \cong \left[\sqrt{h_c^2 + 0,25D^2} + (\Delta k + 0,5d_n) \cos \alpha \right] \cos \alpha \tag{4}$$

The distance H and H_o that define the vertical coordinate of centre placement O_o of the clearing shaft is given by:

$$H = r + l + h_k; \quad H_o = [R_o + (\Delta k' + r_n) \sin \alpha] \sin \alpha \tag{5}$$

To analyse the cleaning blade and the root head interaction, one should consider that the axis O (Fig. 4) of the cleaning shaft is perpendicular to the plane of moving coordinate O_{xyz} and to the row axis and it is above the soil surface at a distance H . The blade AM with the length l is pivotally suspended on the axis A , which is off-centre of the shaft in the value of the rotation radius r and rotated relatively to the axis O at angle β , or relatively to the axis of the row at the angle $90^\circ - \beta$.

The blade end describes a radius circle R_o of the rotation with a constant angular velocity ω_o on the plane Oxz . The blade position AM is determined by the angle φ between the vertical and the described circle radius R_o .

The cleaning blade interaction with a root (the impact centre) is at a point M , located at the distance h_k from the surface. The rotation axis O of the clearing shaft moves with the constant forward speed V_k relatively to fixed coordinates $O_1x_1y_1z_1$.

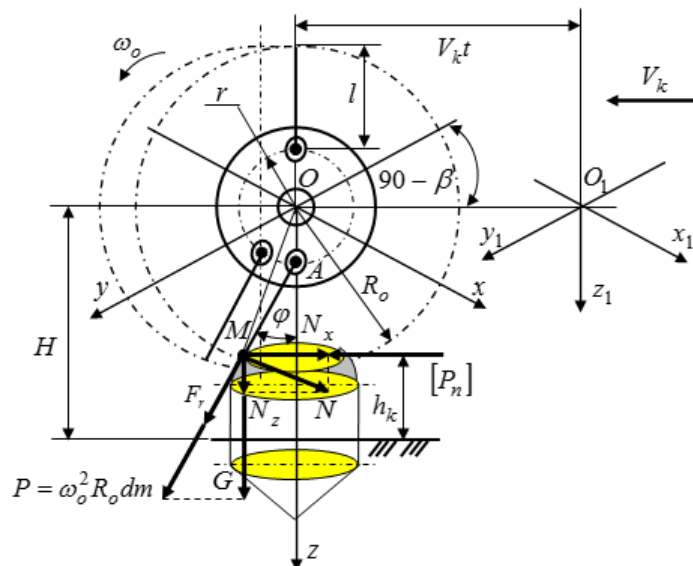


Fig. 4 – Scheme of interaction of the blade with the root crop

In this case there is the blade complex plane motion that is also involved in translational motion with digger speed V_k relatively to the fixed coordinates $O_1x_1y_1z_1$ and rotational motion around a fixed axis Oy .

The blade impact force on the root head at the point M is determined by Newton's Second Law (Landau and Lifshitz, 2012):

$$md / dt = F , \text{ or } md = Fdt \quad (6)$$

where m – blade weight brought in the centre of impact, [kg];

F – impact force, [N];

t – impact time, [s]

The rotation axis A , on which the cleaning shaft blades are fixed, moves relatively to the fixed axes $O_1x_1y_1z_1$ with a constant speed V_o and is equal to:

$$V_o = V_k \cos \beta \quad (7)$$

where β – the angle between the axes directions of the roots row and the rotation axis A of the blades, [deg].

Absolute velocity vector of blade impact \bar{V}_a is the vectors sum of the blade relative velocity \bar{V}_r and transport velocity \bar{V}_o , hence:

$$\bar{V}_a = \bar{V}_r - \bar{V}_o = \bar{V}_r - \bar{V}_k \cos \beta . \quad (8)$$

Detailed research of cleaning root heads from the remained tops is conditionally divided into two stages: the first stage - blade contact with the root body; the second stage - the remained tops removal from a root head. Each stage is divided into three other stages: initial, intermediate and final. The first stage begins with the contact of the blade end with the root body and it ends when the blade takes a vertical position. This stage is characterized by the fact that the blade impact force on the root crop is initially directed upwards, while at the end – horizontally to the ground surface. The second stage finishes when the blade ends the contact first horizontally and then downward. The second stage ends when the root heads cleaning from the remained tops is finished.

For not damaging the roots the following condition should be fulfilled: allowable blade impact forcing on the root should not exceed the permissible specific pressure of compression of root's body. The allowed blade impact force (contact) to the root should not exceed the allowable force of dumping root from the soil (Baranovsky *et al.*, 2010):

$$\frac{F_k}{S_k} < [\sigma_{cm}]; \quad F_k < [P_n] \quad (9)$$

where S_k – contact area, [m²];

F_k – blades contact force (impact), [N];

$[\sigma_{cm}]$ – allowable pressure of root body compression, [N/m²];

$[P_n]$ – allowable power of root dumping from the soil, [N].

During the blade free rotation with angular velocity ω_o inertia centrifugal force F_r occurs, which is directed along the blade and forces the blade to take position along the radius direction r of the hinge A (Bolotyn *et al.*, 2010):

$$F_r = m\omega_o^2 R_o \cos \varphi \quad (10)$$

where F_r – the inertia centrifugal force, [N];

ω_o – blades rotation angular velocity, [rad/s];

R_o – cleaning shaft radius, [m];

φ – the angle between the vertical axis Oz and the radius of the circumscribed circle R_o , [rad].

In addition, during the first stage, the gravity force $G = mg$ has an effect on the blade, which is concentrated in the of blade mass centre, that is located at a distance $r + l$ from the rotation axis and is directed along the Oz -axis. What is more, there is the blades inertia force in the contact point, which is directed perpendicular to the blade in the direction of its rotation and Coriolis inertial force $K = -2mR_o\dot{\varphi}(\omega_o \times V_o)$, directed along the Ox -axis in the direction opposite to the direction of Coriolis acceleration $w_c = 2R_o\dot{\varphi}(\omega_o \times V_o)$, which does not affect the power balance in the $Oxyz$ coordinate system. From these forces action on the root head the reactive force N of coherence of the root with soil occurs, which can be decomposed into two components – horizontal force N_x , which affects the roots dumping from the soil and a vertical force N_z of pulling root from the soil.

The bodies system "the blade of the cleaner – a root" will be in equilibrium at the impact time, with the following condition:

$$\frac{m}{2} \left(\frac{dV_c}{dt} \right)^2 = \frac{d}{dt} (T) < [P_n] \times V_c \quad (11)$$

where T – the kinetic energy of the cleaner blade in the area of impact, [J];

V_c – impact velocity, [m/s].

The kinetic energy of cleaning shaft consists in the mass centre kinetic energy of the blade, which depends on the translational motion speed V_k related inertia axes $O_1x_1y_1z_1$ and kinetic energy of the axes $Oxyz$ that move. The rotation speed of the blade mass centre around the axis of the cleansing shaft at a speed V_r in the distance $(r+l=R_o)$, where r – the axes radius A is related to the shaft centre O , [m]; l – the blade's length, [m].

The speed module of the blade mass centre is relative to the axis of rotation (Bolotyn et al., 2010):

$$V_r = R_o \dot{\varphi} \cos \varphi = (r+l) \omega_o \cos \varphi \quad (12)$$

According to Landau and Lifshitz (2012) the material system kinetic energy is the sum of kinetic energies of all points that are in the bodies system, which is written in general terms:

$$T = \frac{1}{2} \sum_{i=1}^n m (V_c^2 + 2V_c V_r + V_r^2) \quad (13)$$

Considering (8) and after converting the blade kinetic energy, which also rotates around the axis with the tangential speed V_r and moves with forward speed V_k kinetic energy components are (Bolotyn et al., 2010):

$$T = \frac{1}{2} m V_o^2 + m V_o V_r + T_r; \quad T_r = \frac{1}{2} I_n \left(\frac{d\varphi_o}{dt} \right)^2 = \frac{1}{2} I_n \omega_o^2; \quad I_n = \frac{m}{3} (a^2 + l^2) \quad (14)$$

where T_r – the kinetic energy of blade rotation, [J];

I_n – blade inertia moment relative to the rotation axis, that is shaped like a cuboid with sides $2a \times 2b \times 2l$ [kg m²];

φ_o – blade rotation angle, [rad];

a – the blade width, [m].

The blade impact on the roots head that are above the soil is provided by the contact of the blade's free end, that is in the distance of traveling radius-vector $\rho = r+l$ from the axis of blade rotation.

According to the law of change in kinetic energy and considering that the brought blade's mass centre is centered on its free end, the equation (13) will be as follows:

$$T_n = \frac{1}{2} m V_k^2 \cos^2 \beta + m V_k \frac{d\omega_o}{dt} \rho \cos \beta \cos \varphi + \frac{m}{6} \left(\frac{d\omega_o}{dt} \right)^2 (a^2 + l^2). \quad (15)$$

Full time t kinetic energy derivative of a material point is equal to a total elementary work of all active forces that applied to the forces point and a time t derivative of the work A_c [J] is equal to the total capacity of all powers N_c [J/s], that are applied to the system (Landau and Lifshitz, 2012):

$$\frac{d}{dt} \left(\frac{m V_a^2}{2} \right) = \frac{d'}{dt} (A_c) = [P_n] \times dr_k; \quad \frac{d}{dt} (A_c) = N_c = [P_n] \frac{dr_k}{dt} = [P_n] \times V_c; \quad [P_n] \times V_k \sin \beta = N_c = \frac{d}{dt} (T). \quad (16)$$

Considering the operating speed V_k of the combined digger (cleaning shaft) as linear and uniform ($V_k = const$), the first time derivative of equations (16) will look like:

$$\frac{d}{dt} (T_n) = m \left(\frac{dV_k}{dt} \right) V_k \cos^2 \beta + m \left(\frac{dV_k}{dt} \right) \left(\frac{d\varphi_o}{dt} \right) \rho \cos \beta \cos \varphi + \frac{m}{3 \cos \varphi} \left(\frac{d\omega_o}{dt} \right) \omega_o (a^2 + l^2) \quad (17)$$

Thus, for the cleaning shaft with blades that are performed in the form of a cuboid, the condition of not dumping the roots from the soil by the cleaning blades is:

$$[P_{n.n}] \geq m c t g \beta \cos \beta \left(\frac{dV_k}{dt} \right) + \frac{m \rho c t g \beta \cos \varphi}{V_k} \left(\frac{dV_k}{dt} \right) \left(\frac{d\varphi}{dt} \right) + \frac{m a \omega_o (a^2 + l^2)}{3 V_k \sin \beta \cos \varphi} \left(\frac{d\omega_o}{dt} \right) \quad (18)$$

Dependence between the basic structural and kinematic parameters of the combined digger drive shaft, kinematic parameters of the process of residual tops remove from the root heads and the dimensional characteristics of root heads can be represented in the form (Baranovsky et al., 2010):

$$z = \frac{\left(d_k + 2\sqrt{D_o h_k - h_k^2}\right)}{V_k} n_o z_o; \quad V_k = \frac{\left(d_k + 2\sqrt{2\rho h_k - h_k^2}\right)}{2\pi z} \omega_o z_o \quad (19)$$

where z – the blade beats number on the root head for each rotation of the shaft, [pcs.];

h_k – height of the root head above ground, [m];

n_o – the cleaner blade rotational speed, [rpm];

z_o – number of axes, placed on the reel of the shaft, [pcs.].

Substituting the value V_k of equation (19) in equation (18) and taking into account the condition (9) we obtained the mathematical model of the process of cleaning shaft blade interaction combined digger with the root head depending on agro biological characteristics and parameters of the combined digger clearing shaft:

– which describes the condition of not dumping the root from soil by the cleaning shaft blades:

$$F_{k.n} = \frac{2\pi m_o z \rho c t g \beta}{z_o \left(d_k + 2\sqrt{2\rho h_k - h_k^2}\right)} \left(\frac{dV_k}{dt}\right) \left[\frac{z_o \left(d_k + 2\sqrt{2\rho h_k - h_k^2}\right) \cos \beta}{2\pi z \rho} + \frac{\cos \varphi}{\omega_o} \left(\frac{d\varphi}{dt}\right) + \frac{(a^2 + l^2)}{3\rho \cos \beta \cos \varphi} \left(\frac{d\omega_o}{dV_k}\right) \right] \leq [P_n]; \quad (20)$$

– which describes the condition of not damaging the root by the blades of the cleaning shaft:

$$\sigma_{cm.n} = \frac{2\pi m_o z \rho c t g \beta}{S_k z_o \left(d_k + 2\sqrt{2\rho h_k - h_k^2}\right)} \left(\frac{dV_k}{dt}\right) \left[\frac{z_o \left(d_k + 2\sqrt{2\rho h_k - h_k^2}\right) \cos \beta}{2\pi z \rho} + \frac{\cos \varphi}{\omega_o} \left(\frac{d\varphi}{dt}\right) + \frac{(a^2 + l^2)}{3\rho \cos \beta \cos \varphi} \left(\frac{d\omega_o}{dV_k}\right) \right] \leq [\sigma_{cm}]; \quad (21)$$

Accordingly, the blade critical angular velocity ω_o^{kp} of horizontal cleaning shaft, that provides the combined digger rational work of fodder beets can be defined:

– for the condition of not dumping the root by the cleaning shaft blades:

$$\omega_{o.n}^{kp} \leq V_k \frac{\frac{[P_n]}{m \left(\frac{dV_k}{dt}\right)} - c t g \beta \cos \beta}{\frac{(a^2 + l^2)}{3\rho \sin \beta \cos \varphi} + \rho c t g \beta \cos \varphi} \quad (22)$$

– or the condition of non-damaging the root body by the cleaning shaft blades:

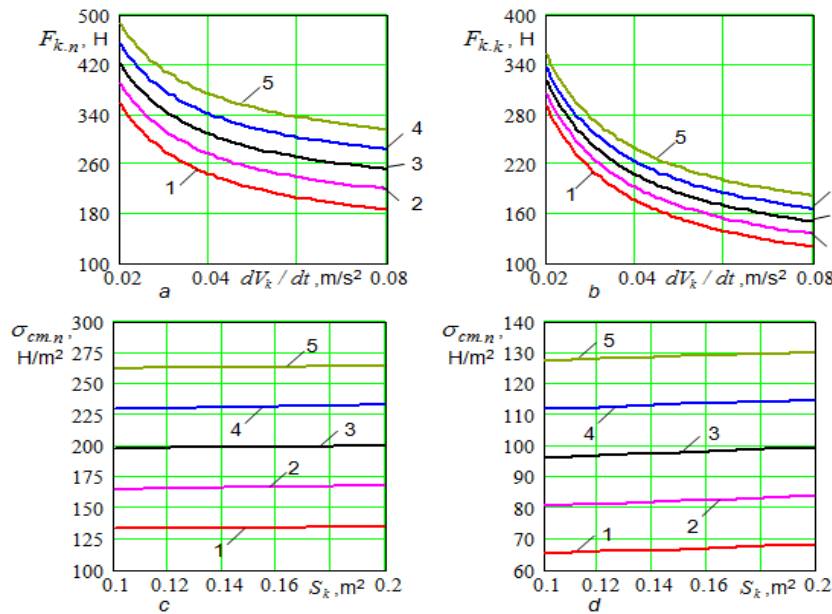
$$\omega_{o.n}^{kp} \leq V_k \frac{\frac{S_k [\sigma_{cm}]}{m \left(\frac{dV_k}{dt}\right)} - c t g \beta \cos \beta}{\frac{(a^2 + l^2)}{3\rho \sin \beta \cos \varphi} + \rho c t g \beta \cos \varphi} \quad (23)$$

According to the obtained mathematical models (20) – (23) there are determined dependencies: force variation of dumping of the roots as a function $F_{k.i} = f(dV_k / dt)$ (Fig. 5a, b), compression pressure of a root as a function $\sigma_{cm.i} = f(S_k)$ (Fig. 5c, d), the blade critical angular velocity as a function $\omega_{o.n}^{kp} = f([P_n], m)$ (Fig. 6a), $\omega_{o.n}^{kp} = f([P_n], \rho)$ (Fig. 6b), $\omega_{o.n}^{kp} = f([\sigma_{cm}], m)$, (Fig. 6c), $\omega_{o.n}^{kp} = f([\sigma_{cm}], \rho)$, (fig. 6d) when $m = 0.5$ kg; $d_k = 0.15$ m; $h_k = 0.07$ m; $\rho = 0,2$ m; $l = 0.15$ m.

Graphic dependences analysis shows that the blades contact (impact) horizontal force with the roots head, in the shape of a cuboid, varies within 180...500 N depending on changes in angular velocity of the cleaning shaft of the combined digger, a specific blade pressure on the root body is in the range of 130...260 N/m². According to experimental studies (Pogorely and Tatyanko, 2004; Herasymchuk and Baranovsky, 2009) the power of root dumping from the soil, depending on the height h_k of the roots above the soil

surface, the root diameter d_k and depth h of its bedding in the soil, is in the range of $[P_n] = 0.15...0,4$ kN, and permissible compression stress – $[\sigma_{cm}] = 140...300$ N/m².

Hence, the critical angular velocity value of the blade with the condition of not dumping the roots from the soil and the digger's speed $V_k = 1.5$ m/s depends on the change of blades mass $m = 0.1...0.5$ kg. It is in the range $\omega_{o,n}^{kp} = 23...100$ rad/s. The value of contact circumference radius of the blade with the root head is $\rho = 0,3$ m; depending on changes of $\rho = 0.1...0.3$ m at $m = 0,25$ kg - 69...82 rad/s (Fig. 6a, b), and accordingly, the condition of the non-damaging of roots - at critical values of angular velocity of $\omega_{o,n}^{kp} =$



33...115 rad/s and $\omega_{o,n}^{kp} = 54...100$ rad/s (Fig. 6c, d).

Fig. 5 – Dependence of change

a, b – $F_{k,i} = f(dV_k / dt)$; c, d – $\sigma_{cm,i} = f(S_k)$; 1, 2, 3, 4, 5 – respectively, $n_o = 7, 8, 9, 10, 11$ rev/s

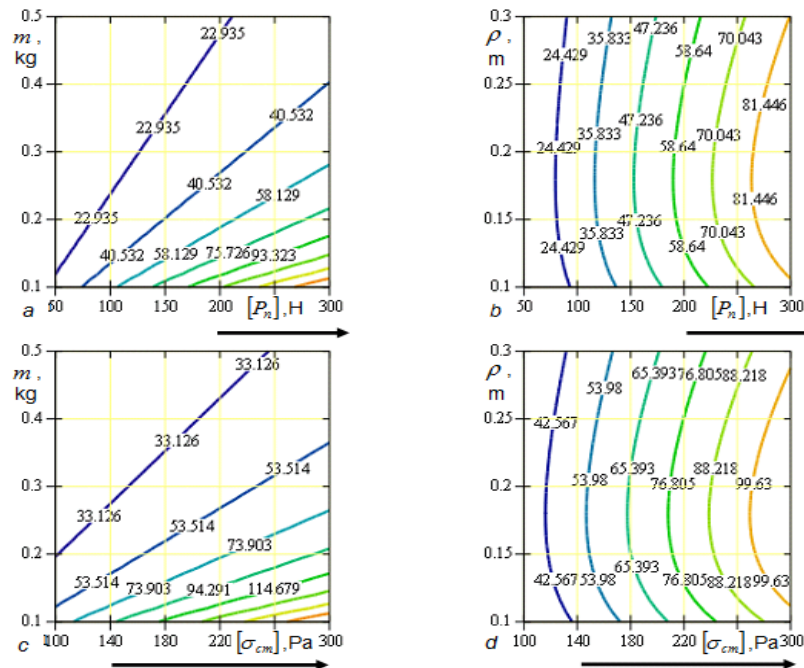


Fig. 6 – Changes dependencies on the critical angular velocity of the digger drive shaft blade

a – $\omega_{o,n}^{kp} = f([P_n], m)$; b – $\omega_{o,n}^{kp} = f([P_n], \rho)$; c – $\omega_{o,n}^{kp} = f([\sigma_{cm}], m)$; d – $\omega_{o,n}^{kp} = f([\sigma_{cm}], \rho)$

CONCLUSIONS

As a result of the technological process of the combined root digger, the following values of its key structural and kinematic parameters were determined: the disc's diameter – $D = 0,45$ m; blades angular velocity – $\omega_o = 60...65$ rad/s; the disc attack angle – $\alpha = 32-37^{\circ}$; the axis setting angle of reel – $\beta \cong 30^{\circ}$; cleaning blade weight – $m = 0,22...0,25$ kg; the reel axles number – 4 pcs.

The method and results obtained in theoretical researches can be used by specialists at design engineering bureaus for development of new or improvement of existing combined cleaning systems of root crop harvesting machinery.

REFERENCES

- [1] Baranovsky V.M., (2006), Basic stages and modern trends in the development of root harvesting machines (Основні етапи та сучасні тенденції розвитку коренезбиральних машин), *Science journal. Journal of TNTU (Науковий журнал. Вісник ТНТУ)*, том 11, no.2, pp.67-75, Ternopil/Ukraine;
- [2] Baranovsky V., Pidhursky M., Herasymchuk H., (2010), Analysis of the residue removal process haulm combined digging working body (Аналіз технологічного процесу видалення залишків гички комбінованим викопуючим робочим органом), *Science journal. Journal of TNTU (Науковий журнал. Вісник ТНТУ)*, том 13, no.4, pp.72-78, Ternopil/Ukraine;
- [3] Baranovsky V.M., Pankiv M.R., Ramsh V.Yu., (2008), Improved Combined Working Body for Digging Roots (Удосконалений комбінований робочий орган для викопування коренеплодів), *Science journal. Journal of TNTU (Науковий журнал. Вісник ТНТУ)*, том 13, no.2, pp.61-73, Ternopil/Ukraine;
- [4] Baranovsky V.M., Potapenko M.V., (2017), Theoretical Analysis of the Technological Feed of Lifted Root Crops, *INMATEH: Agricultural Engineering*, vol. 51. no.1 / 2017, pp. 29-38, Bucharest/Romania;
- [5] Bulgakov V.M., Chernovol, M.I., Sviren N. A., (2009), *Theory beet-lifting machines: monograph (Теория свеклоуборочных машин)*, ISBN 978-966-1508-01-08, Kirovograd/Ukraine;
- [6] Bolotyn S.V., Karapetian A.V., Kuhushev E.Y., Treshchev D.V., (2010), *Theoretical Mechanics (Теоретическая механика)*, Moscow: Academy (Москва: Академия), 432 p, ISBN 978-5-7695-5946-4;
- [7] Herasymchuk H.A., Baranovsky V.M., (2009), Criteria for assessing the technological efficiency of the digging process of root crops (Критерії оцінки технологічної ефективності процесу викопування коренеплодів), *Journal of Lviv National Agrarian University: Agro engineering research (Вісник Львівського національного аграрного університету: агроінженерні дослідження)*, no.14, pp. 163–168, Lviv/Ukraine;
- [8] Holovach I.V., Prysiazhny V., (2012), Development of advanced cleaning of towed root cropping machine (Розробка вдосконаленої очистки причіпної коренезбиральної машини), *Collection of Scientific Papers of Vinnytsia National Agrarian University. Series: Technical Sciences (Збірник наукових праць Вінницького національного аграрного університету. Серія: Технічні науки)*, Issue 11, vol. I (65), pp. 133–141, Vinnytsia/Ukraine;
- [9] Husak A.A., Brichkina E.A., (2012), *Bases of higher mathematics (Основы высшей математики)*, Minsk: TetraSystems (Минск: ТетраСистемс), Minsk/Belarus;
- [10] Kozachenko O.V., (2004), Investigation of the expenditure of mechanical energy by agricultural machinery on the cultivation of crop production (Дослідження затрат механічної енергії машинами сільськогосподарського призначення на вирощуванні продукції рослинництва), *Mechanization and Electrification of Agriculture. Interdepartmental. Collection of Subject Scientific Papers (Механізація та електрифікація сільського господарства. Міжвідомчий тематичний науковий збірник)*, Issue 88, pp. 91–98, Hlevakha/Ukraine;
- [11] Landau L.D., Lyfshyts E.M. (2012), *Mechanics (Theoretical physics, tom 1) (Механика (Теоретическая физика, том 1))*, 5th ed., ISBN 978-5-9221-0819-512, Moscow/Russia;
- [12] Pogorely L.V., Tatianko M.V., (2004), *Beetroot-lifting machine: history, design, theory, forecast (Свеклоуборочные машины: история, конструкция, теория, прогноз)*, K.: Phoenix (К.: Феникс), ISBN 966-651-166-5, Kijv/Ukraine;
- [13] Storozhuk I.M., Pankiv V.R., (2015), Research results of harvesting haulm remnants of root crops, *INMATEH-Agricultural Engineering*, vol. 46. no.2, pp.101-108, Bucharest/Romania.

DESIGN AND TEST OF AN ALL FEED AXIAL FLOW SAME DIAMETER DIFFERENTIAL SPEED THRESHER

/ 全喂入纵轴流同径不同速脱粒分离装置设计与试验

Prof. M.S. Wang Jinshuang¹⁾, Prof. Ph.D. Li Hua²⁾, P.G. Yuan Jianbo³⁾,
Prof. M.S. Ma Guang^{1*)}, Prof. M.S. Xiong Yongsen¹⁾

¹⁾ Jinhua Polytechnic, Jinhua / China; ²⁾ College of Engineering, Nanjing Agricultural University, Nanjing /China;

³⁾ Nanjing Tech University, Nanjing / China

Tel: 13588653962; E-mail: 791228154@qq.com

Keywords: axial flow; differential speed; threshing cylinder

ABSTRACT

Grain harvesting equipment completes cutting, threshing, cleaning and separation work simultaneously, but traditional single-speed all-feed axial-flow threshers cannot adapt to complicated work situations. We put forward a design approach for an all-feed axial-flow with a same-diameter differential-speed thresher to further reduce the grain-crushing rate and threshing loss rate when operating. We test for Xieyou No. 518 rice and obtain the distribution rule of grain mixture after threshed via experimental comparison of a differential-speed thresher versus a single-speed thresher. The results of this research show that the threshing effect of the differential-speed thresher is better than the single-speed thresher and that the first has a lower grain crushing rate and a lower threshing loss rate of 18.0% and 15.8%, respectively. We found this result by analyzing the grain threshed axial distribution, grain crushing rate and threshing loss rate. This study provides a new theoretical and structural reference for the study of separation devices for grain combine harvesters to adapt to the complex harvesting conditions in China.

摘要

谷物联合收获机工作过程一次性完成收割、脱分、筛分、集粮过程。传统单转速纵轴流脱粒滚筒不能适应复杂的工作情况。为降低全喂入谷物联合收获机纵轴流脱粒分离装置谷物破碎率及清选损失率，提出了一种全喂入纵轴流同径不同速脱粒分离装置。选用协优 518 号水稻品种进行同径不同速脱粒滚筒与单速脱粒滚筒的脱分实验，得到了水稻的脱粒分离规律。对比二种脱粒装置脱出物破碎量轴向分布、籽粒破碎率及清选损失率等得到：同径不同速脱粒滚筒的脱分效果优于单速脱粒滚筒，降低了籽粒破碎率和清选损失率，分别下降了 18.0% 和 15.8%。本次研究为适合我国多工况谷物联合收获机脱粒分离装置的研究提供了新的理论及结构参考。

INTRODUCTION

China is the world's largest producer of grain, with a planting area of 94,370.8 km², accounting for 21.98% of the world's grain production (Center A.T.P., 2017). The wide area, the staggered terrain distribution, and the complicated farming system in China have led to a penetration rate of agricultural machinery of only 63% (Li H., 2017). The difference in seasonal conditions for grain harvesting leads to the difficult and uneven separation of straw and grain. In northern harvests, the proportion of dry straw was larger, while in the southern harvests during rainy season the moisture content of straw was relatively high, resulting in the phenomenon of blocking and incomplete threshing during grain combine harvest. The all-feed axial-flow grain combine harvester was developed in the 1980s. It has the advantages of high production efficiency, a high trash content rate, a low threshing loss rate and high adaptability compared with the all-feed horizontal axial-flow grain combine harvester (Watanabe N., 2017). The performance of the grain combine harvester is directly affected by the quality of the threshing during the harvesting process. This topic has been widely studied by scholars in recent years.

Qian *et al.* studied the influence factors of the process of rice flexible tooth threshing and analyzed the multi-friction dynamic contact process of the flexible tooth with the material during operation. The combined effect of the combine harvester was improved and the grain crush rate was reduced by using the multi-correlation matrix and the four-point weighted evaluation method (Qian Z. *et al.*, 2017). Singh *et al.* designed a rice threshing mechanism for the rice harvest of small fields and steep slopes. The influence of the spacing and height of the threshing ring on the separation effect was analyzed by the response surface method and the optimal parameters were obtained, thus reducing production costs (32 kg and INR 3500 or 88 US\$) and increasing the efficiency of the threshing to 94.6% (Singh K P., 2008). Valge as well as Kile *et al.* studied the structure of the grain thresher by the method of multi-evaluation index parameter optimization and obtained the best threshing effect, which improved the complete work efficiency and grain harvest operation (Kile R J., 2013; Valge A.M. *et al.*, 2017; Ye J. *et al.*, 2017). Putri *et al.* redesigned the grain thresher by the method of rapid upper limb assessment (RULA), which effectively reduced injury to farmers and improved the machine's efficiency (Putri N.T. *et al.*, 2016). Dogra *et al.* developed a long nail-toothed threshing mechanism for bean crops, and the multi-level parameter optimization for threshing linear velocity and feeding was studied. The optimal parameters were determined and obtained the threshing break rate, non-collectable losses, the threshing clear rate and threshing efficiency were 0.68%, 0.27%, 98.63% and 99.56% respectively (Dogra B, 2014). Yousif *et al.* developed a threshing device for harvesting sorghum in the event of rain and verified the working and economic efficiency by test experiments (Yousif L.A. *et al.*, 2012). Li *et al.* studied the different threshing structures such as spike tooth cylinder, rectangular tooth cylinder, and combined spike tooth with short-rasp-bar tooth. The results showed that the combined spike tooth with short-rasp-bar tooth has a better threshing effect and lower power consumption by analysis of the multi-indicator assessment factors (Li Y *et al.*, 2009). Soon afterwards, Tang *et al.* studied the influence of different threshing elements in terms of the shear flow and longitudinal axial-flow thresher on operation performance and showed that the shear flow thresher using a blade tooth and the longitudinal axial-flow thresher using a spike tooth have better operational effectiveness when the feed is larger (Tang Z. *et al.*, 2011). Dai *et al.* developed a new type of longitudinal axial-flow thresher device to increase the axial material delivery speed and reduce power consumption, obtaining better efficiency of the grain combine harvester (Dai F., 2011). Tong *et al.* presented a numerical simulation of the mixed flow field in the blower threshing drum and structural improvement method of the axial-flow (Tong S. *et al.*, 2016). They analyzed the influence of vibrating screen surface airflow velocity on the airflow in the thresher cylinder and optimized the parameters by the orthogonal test, and the optimization results were then verified by the field-threshing test.

Although the all-feed axial-flow thresher has been widely used in the threshing system of the grain combine harvester, there are some shortcomings. In the traditional single-speed all-feed axial-flow thresher, the feeding amount is larger, which can cause the feed inlet to block, leading to a higher threshing loss rate and grain crushing rate as well as a poor threshing effect. In this paper, we developed a new type of all-feed axial-flow separation device with same-diameter differential-speed without increasing the length of the threshing cylinder, to overcome the above shortcomings, and more adaptability. The effect of the new thresher is verified by test experiments.

MATERIALS AND METHODS

Materials of experiments

Test for Xieyou No. 518 rice: yield of about 7500 kg/hm², natural plant height of 1200 mm. The average length of the stalk was 855 mm when threshing, the grain thousand-seed weight was 35.89g, the ratio of grass and grains was 1.76, and the water contents of grains and stalks were 14.6% and 58.6%, respectively.

Experimental installation

The experimental installations were the traditional all-feed axial-flow single-speed thresher and the all-feed axial-flow differential-speed thresher designed by our laboratory. The two kinds of threshers had the same total length, diameter of threshing cylinder, and threshing device structure. The speed of the high and low differential-speed threshing cylinders was 799 r/min and 555 r/min, respectively, according to formula (1); the length of the high and low speed threshing cylinders was 430 mm and 1050 mm, respectively, according to formula (2). Moreover, the anti-interference device was designed according to two differential-speed threshing cylinders.

As shown in Figure 1, the coaxial differential-speed threshing drum was made up of a low-speed threshing cylinder with an active bevel gear 3 and a driven bevel gear 6, and a high-speed threshing cylinder with an active bevel gear 4 and a driven bevel gear 5.

According to the design method of bevel gear drive, *Tao Z. (2015)* obtained that the tooth number of the active bevel gear 3 was 21, the tooth number of the driven bevel gear 6 was 32, the transmission ratio was 0.66, the tooth number of the active bevel gear 4 was 18, the tooth number of driven bevel gear 5 was 20 and the transmission ratio was 0.9.

$$n_2 = Kn_1 = \frac{30Kv_1}{\pi r} \quad (1)$$

where, n_2 is the high speed drum speed (r/min); n_1 is the low speed drum speed (r/min); K is the high speed drum and low speed roller linear speed ratio, ($K=26/18=1.44$); v_1 is the low speed drum linear speed (r/min); r is the radius of the threshing drum, ($r=0.31\text{m}$).

$$L_1 = \frac{\varepsilon q}{AR\phi} \quad (2)$$

Where:

L_1 is the length of the grid-type concave plate in the low-speed drum segment (mm);

ε - the percentage of the feeding which has been separated (%); $\varepsilon = 0.55 \sim 0.60$ set 0.60;

q - the feeding amount (kg/s), set 3.5 kg;

A - the unit area productivity of the grid-type concave plate ($\text{kg}/\text{m}^2\cdot\text{s}$), set 1.5;

R - arc radius (mm), set $R=33$ mm (included in the clearance of inlet plate 2 mm);

ϕ - the curved plate Angle ($^\circ$), set $\phi = 220^\circ$.

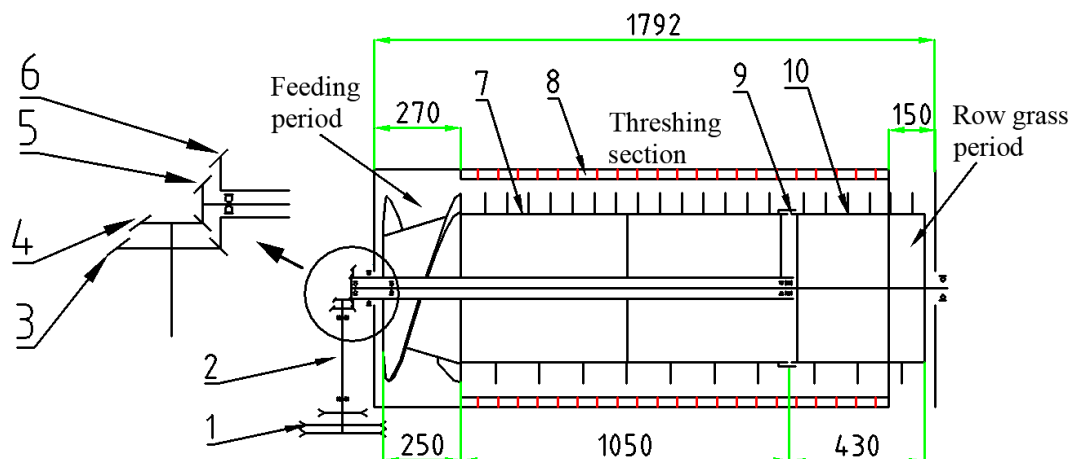


Fig. 1 - All-feed axial-flow same-diameter differential-speed thresher

1-Power pulley; 2- The shaft; 3-Low speed cylinder driving bevel gear; 4-High speed cylinder driving bevel gears;

5-High speed driven bevel gears; 6-Low speed driven bevel gears; 7-Low speed cylinder;

8-Grid concave plate; 9-Transition ring; 10-High speed cylinder

Experiment design

In accordance with the actual harvest process and the feeding amount of 3.0 kg/s, the procedure can be briefly described as follows: the speed of the single rotational speed threshing cylinder is set at 650r/min and the high and low rotational speed cylinders of same-diameter differential-speed thresher are 799 r/min and 555 r/min respectively. Then the materials are put evenly onto the conveyor belt and packing auger transports them into the threshing cylinder. Most of the weeds were expelled from the drain when threshed and other materials fell down from the grid concave plate into the collection box. The material collection box was a total of 60 squares (the square area was axial 140mm x radial 130 mm) (*Dai F et al, 2011; Li Y et al, 2008*), as shown in Table 1. The power consumed was the average value of the sample time beginning with the materials entering the threshing drum to the materials being discharged completely. In order to ensure the accuracy of the measurement results, all the materials in receiving boxes and the loss of the granules were manually treated.

Table 1

The distribution design of test collection										
Feeding mouth	Axial direction(1400mm)									
Radial direction (1040mm)	1-1	2-1	3-1	4-1	5-1	6-1	7-1	8-1	9-1	10-1
	1-2	2-2	3-2	4-2	5-2	6-2	7-2	8-2	9-2	10-2
	1-3	2-3	3-3	4-3	5-3	6-3	7-3	8-3	9-3	10-3
	1-4	2-4	3-4	4-4	5-4	6-4	7-4	8-4	9-4	10-4
	1-5	2-5	3-5	4-5	5-5	6-5	7-5	8-5	9-5	10-5
	1-6	2-6	3-6	4-6	5-6	6-6	7-6	8-6	9-6	10-6
	1-7	2-7	3-7	4-7	5-7	6-7	7-7	8-7	9-7	10-7
	1-8	2-8	3-8	4-8	5-8	6-8	7-8	8-8	9-8	10-8
										Straw outlet

RESULTS

- **The power consumption of the same diameter differential speed thresher**

In the case of continuous feeding, the removal of cylinder consumption power N can be obtained by the following formula (Li Y. *et al*, 2009; Tang Z. 2012)

$$N = N_0 + N_t = A\omega + B\omega^3 + \xi \frac{qv^2}{1-f} \quad (3)$$

where:

N_0 is the consumption power of the empty drum of threshing, (KW);

N_t - the consumption power of threshing, (KW);

A - the resistance coefficient caused by friction of bearing;

B - the resistance coefficient caused by air resistance;

ω - angular velocity of the threshing cylinder, (1/s);

ξ - material elastomer correction coefficient;

q - feeding amount, (kg/s);

v - linear speed of the threshing cylinder (m/s);

f - the friction coefficient of the materials through the gap ($f = 0.75$).

The angular velocity of the high rotational speed cylinder was 1.4 times the angular velocity of the low rotational speed cylinder, according to the calculation results of Section 2.2.

The proportion of materials in the high-speed rotational cylinder was less than 1/3, and the grain was threshed; the consumption power of the high rotational speed cylinder was lower. When the feeding quantity was 2.0 kg/s, the consumption power of the high rotational speed cylinder was about 47% of the low rotational speed cylinder. Therefore, the total consumption power of the differential-speed thresher was lower.

- **Analysis of the distribution of the threshed grain**

Figure 2 shows the sample collection after the test of the single-speed and differential-speed threshers. As shown in Figure 3 (a), the percentage of threshed grain by the differential-speed thresher was higher than that of the single-speed thresher, and the threshing loss rate and grain-crushing rate of the differential-speed thresher were lower than that of the single-speed thresher.

The working efficiency was improved according to the different disposal of materials under the different rotation speeds of the differential-speed thresher, and the weeds were removed while the low rotational speed threshing cylinder was working, reducing the threshing loss rate and grain breakage rate.

As shown in Fig. 3 (b), a materials packing phenomenon could be observed in the feeding end with both kinds of speed threshers, however, the distribution of materials by the differential-speed threshing was uniform. The differential-speed thresher distributed the power evenly with balanced consumption by the threshing cylinder.



Fig. 2 - Single- and differential-speed threshed mixture distribution

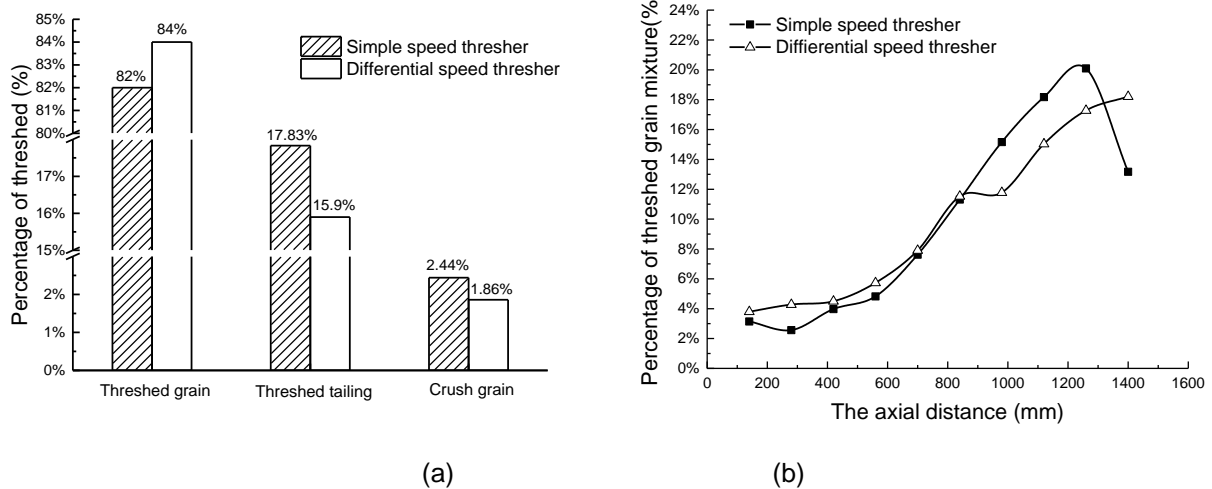


Fig. 3 - Single- and differential-speed threshed mixture distribution

(1) Analysis of the distribution results of the grains threshed

As shown in Fig 4, the distribution trend of the grains was consistent with the distribution trend of the threshed mixture and was mainly concentrated in the first half of the threshing cylinder, because more than 90% of the grain was threshed in the forepart of the thresher (Tang Z, Li Y, Xu L, et al. 2011). The differential-speed thresher was favourable to material flow in the threshing cylinder, which made the distribution of the threshed grains more uniform than was observed in the single-speed thresher.

(2) Analysis of the distribution results of the threshing trash accounts

As shown in Fig 5, the threshing trash accounts distribution of the single speed thresher at the 320 mm-1400 mm section (the front of the axial cylinder), which was significantly higher than that of the 0-320 segment (the posterior segment of the axial cylinder) according to the axial distribution; the trash distribution of the differential speed thresher was more uniform and reasonable than that of the single-speed thresher.

The threshing trash accounts distribution of the forepart of the differential-speed thresher was significantly lower than the forepart of the single-speed thresher, which was beneficial to grain mixture screening.

(3) Analysis of the distribution results of the crushing grains threshed

As shown in Fig. 6, the precursors of the single rotational speed-threshing cylinder (320-1400 segment) are significantly higher than the posterior segment (0-320 segment). Furthermore, the single rotational speed will thresh the grain and strike again, leading to a higher grain fragmentation rate. According to the grain crushing rate statistical result, the differential-speed thresher operation was superior to that of the single-speed thresher, but only by about 5%, meaning that it is able to perform sufficiently during operations.

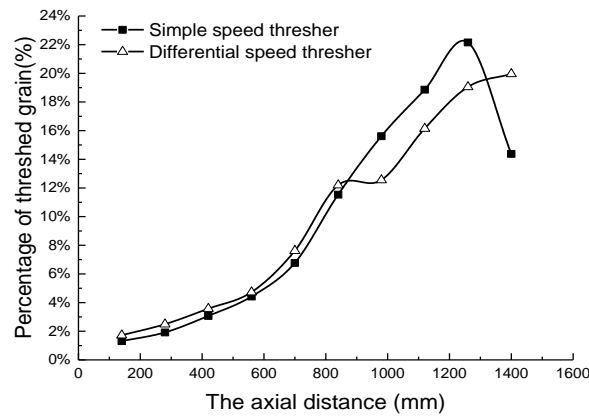


Fig. 4 - Single- and differential-speed threshed grain distribution

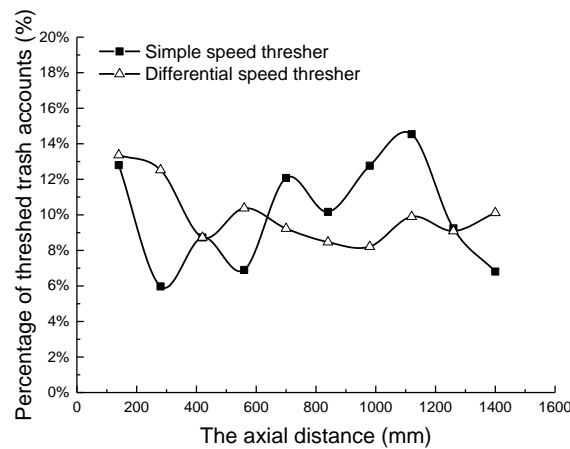


Fig. 5 - Single and differential-speed impurity distribution

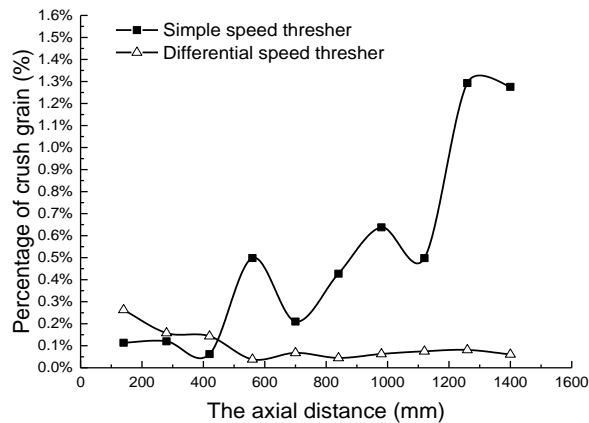


Fig. 6 - Single and differential-speed rice grain crushing distribution

- **Analysis of the grain crushing rate and threshing loss rate**

We selected the rice varieties provided in section 2.1 to carry out the rice threshing comparative test. Under the same working conditions, we calculated the grain crushing rate and threshing loss rate according to the specified calculation method (Dai F, Gao A, Sun W, et al. 2011; Tong S, Shen Q, Tang N, et al. 2016) as shown in Tables 2 and 3. The threshing loss rate of the differential-speed thresher was 15.8% lower than that of the single-speed thresher and had a good threshing effect. The grain crushing rate of the differential-speed thresher was 18% lower than that of the single-speed thresher when harvesting high-yield rice, which is in line with the requirements for high-quality operations.

Table 2

Test of grain threshing loss			
No.	Percentage of cleaning loss (%)		Remark
	Differential speed	Single speed	
1	12	14.4	The accumulation condition of the left side of the front of a single-speed threshing sieve when the feed is larger
2	8.6	9.8	
3	11.8	13.9	
4	13.5	15.1	
5	12.2	15.8	
Average	11.6	13.8	

Table 3

Test of rice grain crushing			
No.	Percentage of crushing (%)		Remark
	Differential speed	Single speed	
1	0.06	0.08	The accumulation condition of the left side of the front of a single speed threshing sieve when the feed is larger
2	0.10	0.12	
3	0.08	0.09	
4	0.05	0.06	
5	0.12	0.15	
Average	0.082	0.10	

CONCLUSIONS

In this paper, we compared the traditional all-feed axial-flow single-speed thresher and the all-feed axial-flow same-diameter differential-speed thresher by grain mixture threshing experiments, and reached the following conclusions:

- (1) We designed an all-feed axial-flow same-diameter differential-speed thresher to improve the comprehensive effect of a grain combine harvester and determined the rotational speed and the length of the high and low rotational speed cylinders according to actual operation conditions.
- (2) The distribution of axial distribution of grain mixture, grains, trash accounts, and crushed grain was obtained by comparing a single-speed thresher and a differential-speed thresher. The results show that the distribution of the threshed grain mixture and the threshed grain gradually decreased from the previous to the latter, and the greatest packing phenomenon occurred closest to the feeding mouth. The distribution of the differential-speed thresher was more uniform than that of the single-speed thresher. The waste distribution of the forepart of the differential-speed thresher was significantly lower than the forepart of the single-speed thresher, which was beneficial to grain mixture screening.
- (3) The experimental results of the two kinds of separation devices were compared and analyzing the grain crushing rate and the threshing loss rate, we found that the grain-crushing rate and the threshing loss rate of the differential-speed thresher were lower than that of the single-speed thresher. This is in line with the demands for high-quality operation of combine harvesters.

REFERENCES

- [1] Center A T P., (2017), The forecast of world agricultural supply and demand forecast for February 2017. *World Agriculture*, vol.04, pp. 215-219;
- [2] Dai F., Gao A., Sun W. et al., (2011), Design and Experiment on Longitudinal Axial Conical Cylinder Threshing Unit. *Transactions of the Chinese Society for Agricultural Machinery*, vol.42, issue 1, pp. 74-78;
- [3] Dogra B., Dogra R., Singh S. et al., (2014), Performance of modified spike tooth thresher for pigeon pea (Cajuns Cajon). *Legume Research*, vol.37, issue 6, pp. 628;
- [4] Kile R.J., (2013), *Threshing bars and combine harvester thresher formed therewith*: US, United States Patent 8602856;

- [5] Ye J., Yan J., Zhang Z. et al., (2017), The effects of threshing and re-drying on bacterial communities that inhabit the surface of tobacco leaves. *Applied Microbiology & Biotechnology*, vol.101, Issue 10, pp. 4279-4287;
- [6] Li H., (2017), New breakthrough in the technological of grain harvest machinery development. *Agricultural Equipment & Vehicle Engineering*, vol.01, pp. 55;
- [7] Li Y, Li H, Xu L., (2008), Comparative experiments on threshing performance between short-rasp-bar tooth cylinder and spike tooth cylinder. *Comparative experiments on threshing performance between short-rasp-bar tooth*, vol.03, pp.139-142;
- [8] Li Y, Qiao M, Xu L. et al., (2009), Development and Performance Experiments on Axial-rethreshing with Axial Feeding. *Transactions of the Chinese Society for Agricultural Machinery*, Vol.11, pp. 50-54;
- [9] Putri N.T., Susanti L., Tito A. et al., (2016), Redesign of thresher machine for farmers using rapid upper limb assessment (RULA) method, *IEEE International Conference on Industrial Engineering and Engineering Management*. IEEE, pp.1304-1309;
- [10] Qian Z., Jin C., Zhang D., (2017), Multiple frictional impact dynamics of threshing process between flexible tooth and grain kernel. *Computers and Electronics in Agriculture*, vol.141, pp. 276-285;
- [11] Singh K.P., Pardeshi I.L., Kumar M. et al., (2008), Optimisation of machine parameters of a pedal-operated paddy thresher using RSM. *Biosystems Engineering*, Vol.100, issue 4, pp.591-600;
- [12] Tang Z., Li Y., Xu L. et al., (2011), Effects of different threshing components on grain threshing and separating by tangential-axial test device. *Transactions of the Chinese Society of Agricultural Engineering*. Vol. 03, pp.93-97;
- [13] Tang Z., Li Y., Xu L. et al., (2012), Experiment and evaluating indicators of wheat threshing and separating on test-bed of longitudinal axial-threshing unit. *Transactions of the Chinese Society of Agricultural Engineering*, vol. 03, pp. 14-19;
- [14] Feng C., (2013), *Dynamics and Reasonable Parameters Matching Research of Gear Transmission System (Thesis)*, Lanzhou Jiaotong University;
- [15] Valge A.M., Lipovskiy M.I., Perekopskiy A.N., (2017), Multicriteria optimization of the combine harvester thresher threshing-separating device parameters. *Bulletin of Russian Agricultural Science*. vol.3, pp. 8-21;
- [16] Watanabe N., (2017), Erratum to: Breeding opportunities for early, free-threshing and semi-dwarf *Triticum monococcum* L., *Euphytica*, vol.213, issue 9, p.211;
- [17] Yousif L A, Elawad S.E.A.G., (2012), Performance evaluation of combine harvester and the P.T.O. tractor operated thresher for stationary threshing of sorghum. *Ama Agricultural Mechanization in Asia Africa & Latin America*, vol.43, issue 1, pp. 52-56.

INFLUENCE OF TECHNOLOGICAL PARAMETERS OF PSEUDOFUIDIZED LAYER GRAIN DRYER ON THE GRAIN DRYING QUALITY

/

ВЛИЯНИЕ ТЕХНОЛОГИЧЕСКИХ ПАРАМЕТРОВ ЗЕРНОСУШИЛКИ ПСЕВДООЖИЖЕННОГО СЛОЯ НА КАЧЕСТВО СУШКИ ЗЕРНА

Prof. PhD. Eng.Sc. Kuznetsov Y.A.¹⁾, Assoc. Prof. D.Eng.Sc. Volzhentsev A.V.¹⁾,
Prof. PhD. Eng.Sc. Kolomeichenko A.V.¹⁾, Prof. PhD. Phil.Sc. Kalashnikova L.V.²⁾

¹⁾Orel State Agrarian University "N.V. Parakhin" / Russia

²⁾Orel State University "I.S. Turgenev" / Russia

Tel: +79208289219; E-mail: kentury@rambler.ru

Keywords: *drying, dryer, grain temperature, pseudofluidization, drying agent*

ABSTRACT

We suggest the construction of pseudofluidized layer grain dryer, which allows carrying out grain recirculation inside the dryer with interchange of heating-cooling cycles and providing the possibility to supply drying agent with high temperature into the drying chamber without risking degradation of grain material quality. The dependence of grain heating temperature on drying duration, drying agent temperature and airflow rate are determined. Experimental investigations allowed establishing the rational values of the factors restricting grain overheating beyond maximum permissible temperature.

РЕЗЮМЕ

Предложена конструкция зерносушилки псевдоожигенного слоя, позволяющая осуществить рециркуляцию зерна внутри сушилки с чередованием циклов нагрева-охлаждения и дающая возможность подавать в сушильную камеру агент сушки с высокой температурой без риска ухудшения качества зернового материала. Определены зависимости температуры нагрева зерна от продолжительности сушки, температуры агента сушки и скорости воздушного потока. Экспериментальные исследования позволили установить рациональные значения данных факторов, позволяющие не перегреть зерно выше предельно допустимой температуры.

INTRODUCTION

New dryer construction is suggested. Its technological process is carried out at the account of grain layer pseudofluidization by drying agent.

The investigations to prove technological parameters of drying installation and determine their possible values providing the preset variation limits of wheat seeds temperature and eliminating grain overheating were carried out. To process experimental results we applied experimental statistics. Regression equation is obtained to determine optimal technological parameters of the dryer.

Grain losses and its quality decrease are caused by many factors, including imperfection of dehydration technique. Safety and improvement of technological qualities of harvested grain is achieved, first, by drying. Drying on the account of using scientifically grounded modes, allows increasing efficiency of the process, resistance of stored grain, improving its seed and food qualities (Tarasenko A.P., 2008; Pilipyuk V.L., 2009; Zhuravlev A.P., 2014).

Nowadays in Russia there is the situation of grain being concentrated at agricultural producer while the technical base of its processing is in the possession of other holders. In this situation, the producer has to sell raw material under very unprofitable conditions. Accordingly, creation of small-sized mobile machinery to organize own grain drying at producer is the most promising direction of agricultural enterprise development (Shhitov S.V., Krivutsa Z.F., Kozlov A.V., 2016; Bibik G.A., 2016; Volkov A.V., 2017).

Based on the comparison of the most effective existing methods of grain drying, providing high process rate and small sizes of drying installations of new types "vibrating fluid bed", "falling bed", "suspension bed", "pseudofluidized layer" (Volzhentsev A.V., 2014; Kalashnikova N.V. u Volzhentsev A.V., 2009; Kuznetsov Y.A., Volzhentsev A.V., Kolomeichenko A.V., Kalashnikova L.V., 2017), it is possible to stress that the utilization of "pseudofluidized layer" type installations prove maximum potential to increase efficiency and intensity of drying process.

MATERIALS AND METHODS

General view and basic constructional units of the developed experimental drying installation are presented in figures 1 and 2.

Alteration and control of the basic parameters of the drying installation were carried out in the following way:

– the air flow pressure adjustment at inlet and outlet from grain layer was provided by alteration of flow section of forced-draught fan VL14-46-2,5-01A. Pressure control is done by digital differential pressure gauge DMT-01M;

– the air flow rate in drying chamber was measured by digital differential pressure gauge DMT-01M. However, the flow rate of drying agent was determined at 9 points: at 6 points along drying chamber walls and at 3 points along symmetry axis of functional area, stretching from loading hole to outlet louver;



Fig. 1 – General view of pseudofluidized layer experimental dryer

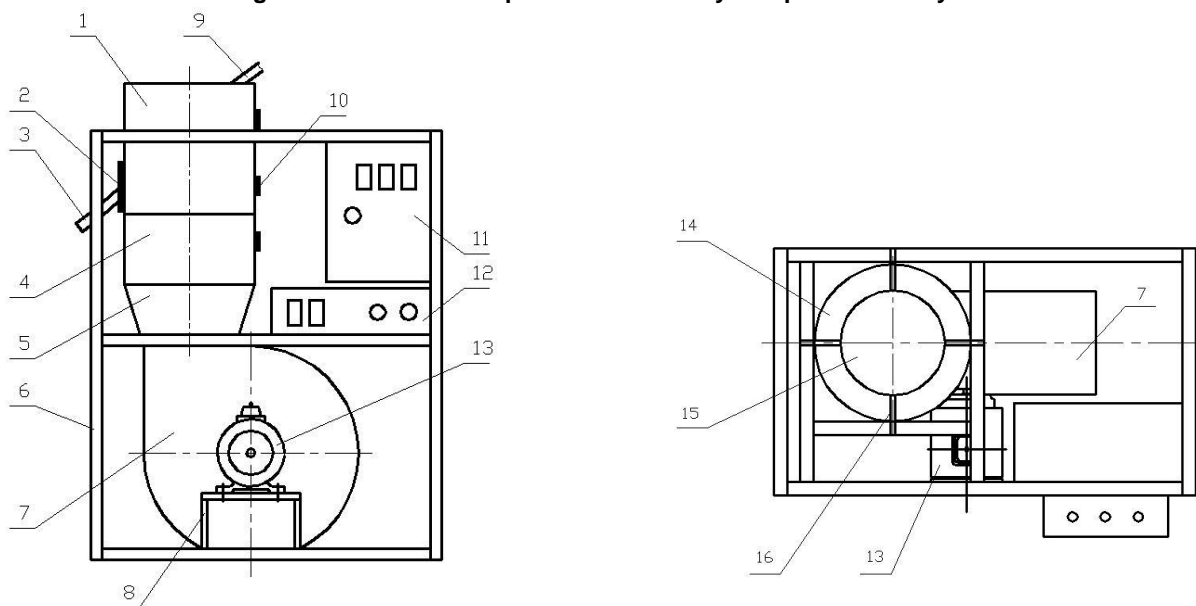


Fig. 2 – Constructional units of drying installation

1 – working chamber; 2 – slider; 3 – unloading sleeve; 4 – electric heater; 5 – diffuser; 6 – frame; 7 – fan; 8 – electric engine frame; 9 – loading sleeve; 10 – plug of technological hole for measurements; 11 – console unit; 12 – measuring instruments; 13 – electric engine; 14 – cooling chamber; 15 – drying chamber; 16 – holder

– the temperature of drying agent in lower turning joint and in drying chamber was controlled according to the data of digital differential pressure gauge DMD-01M. The necessary drying agent temperature was provided with periodical switching off one or more sections of electric heater.

RESULTS

Technological process of experimental dryer operation proved that the main factors determining grain drying quality are drying agent temperature and drying time.

The investigations were carried out to ground technological parameters of drying installation and determining their possible values providing the specified limits of seed wheat temperature variations and eliminating grain overheating. In this regard, it was necessary to study the temperature changes of drying agent t and drying time B_{drying} in the heating temperature T of pseudofluidized grain layer.

Drying agent temperature t , $^{\circ}\text{C}$ was selected with the following values: 60; 80; 100. Temperature variation was done by means of switching on and switching off additional sections of electric heater. Drying time B_{drying} , sec was admitted equal to 100; 200; 300; 400; 500; 600.

The experimental results studying the influence of the mentioned factors on temperature and humidity of pseudofluidized layer of grain material are presented in figures 3, 4, 5.

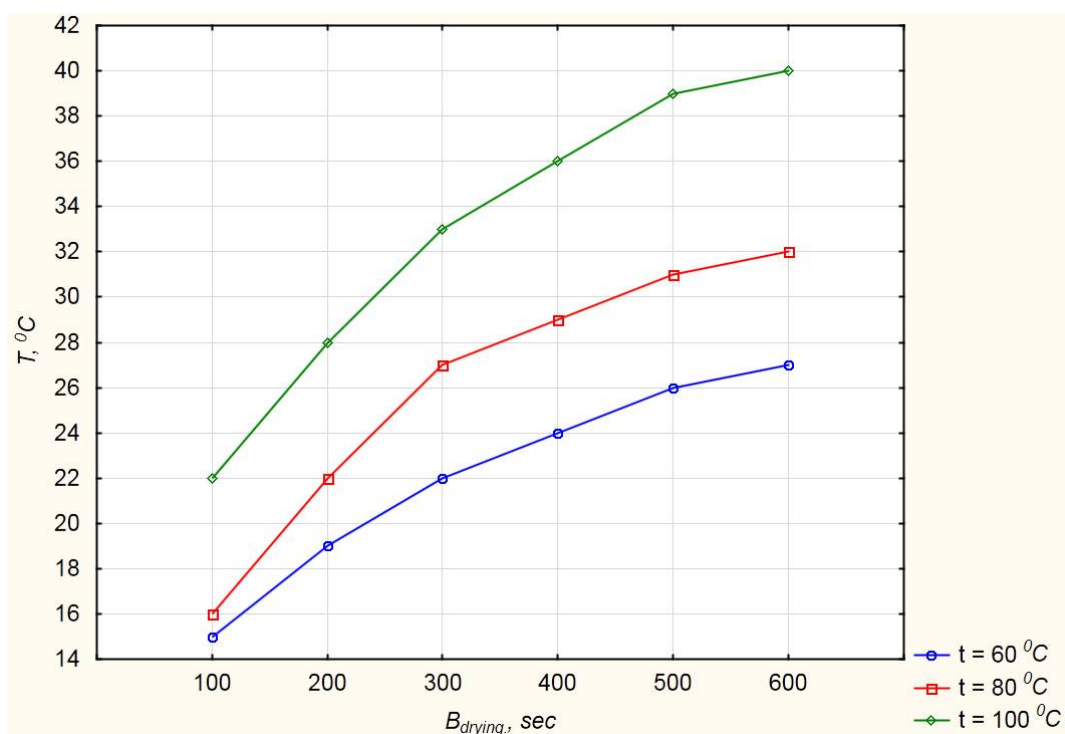


Fig. 3 – Dependence of grain temperature T on drying time B_{drying} at different values of drying agent temperature t

Analyzing the obtained dependences of grain temperature (fig. 3) on drying time B_{drying} at different values of drying agent temperature t , it is possible to conclude that at drying time increase, grain temperature increases and at the end of time limit it does not exceed maximum permitted time. With increase of drying agent temperature grain heating process is intensified sharply and at the meaning of $t = 100^{\circ}\text{C}$ grain temperature T reaches critical value.

Characteristic curves analysis of grain temperature T from drying agent temperature t (fig. 4) displays that with the increase of drying agent temperature, grain temperature increases and reaches ultimate and maximum permitted value at $t = 100^{\circ}\text{C}$.

Grain heating intensity depends also on air flow rate (filtering rate) v penetrating pseudofluidized grain layer. Minimum operating air rate providing sustainable and even layer boiling was admitted equal to 2.2 m/sec. Maximum filtering rate value was 3 m/sec. Further rate increase was inappropriate because it results in non-productive losses of drying agent.

Characteristic curves analysis of grain temperature T from filtering rate v (fig. 5), at different temperatures of drying agent t shows that the process grain heating is significantly intensified with rate

growth v . Grain temperature T reaches its maximum value at drying agent temperature equal to 100°C and air flow rate about 3 m/sec .

Further rate growth v results in overheating and grain technological properties decreasing.

To estimate the effect of the interaction of technological and operating parameters of the experimental dryer on the grain material temperature full factorial experiment was carried out. The regression equation of the following type was obtained:

$$T = 47,729 - 0,899t + 0,0033B_{\text{drying}} - 8,624v + 0,0045t^2 - 0,00004B_{\text{drying}}^2 + 0,1423tv + 0,0003tB_{\text{drying}} + 0,0122B_{\text{drying}}v \quad (1)$$

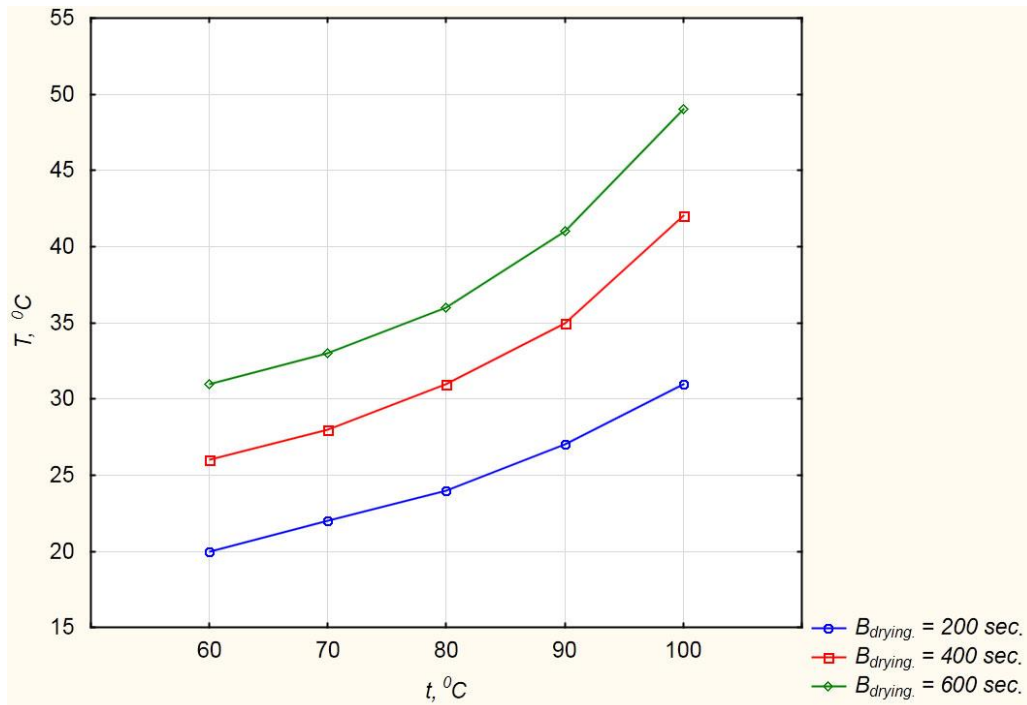


Fig. 4 – Dependence of grain temperature T on drying agent temperature t at different values of drying time B_{drying} .

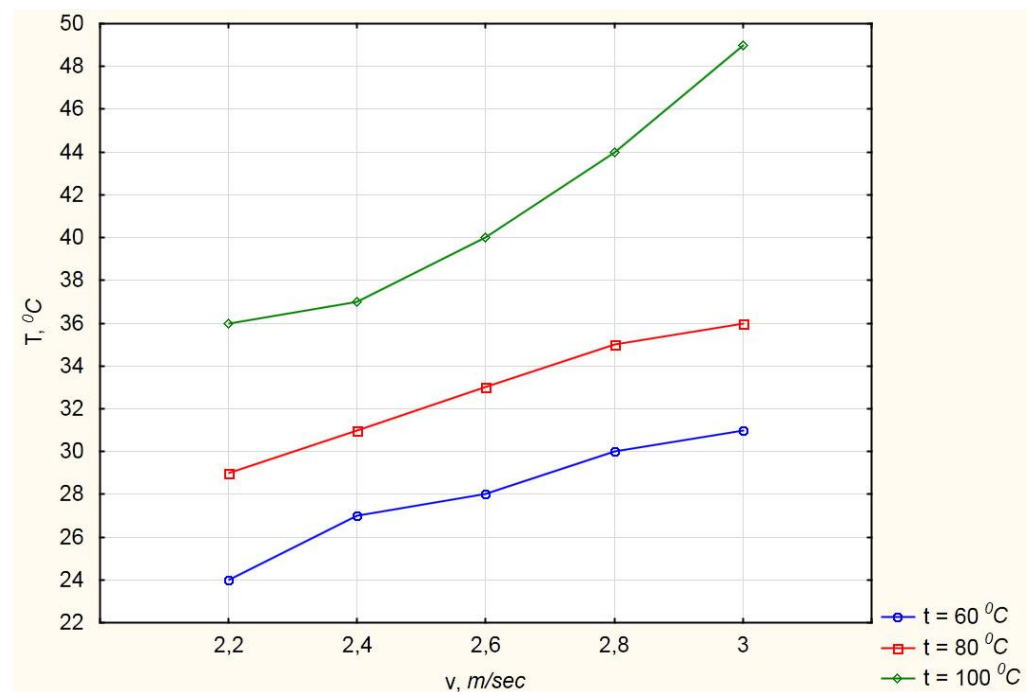


Fig. 2 – Dependence of grain temperature T on filtering rate v

After substitution of the corresponding values of the main factors, factorial dependence of temperature variations of grain T in grain dryer is drawn (fig. 6).

Graphical interpretation analysis of the obtained data suggests that grain heating temperature increases with increase of temperature and drying agent rate. However their marginal values correspond to the following values: $t = 100^{\circ}\text{C}$, $v = 3 \text{ m/sec}$. Maximum drying time at different values is 600 sec. Further increase of the concerned factors is unreasonable, because it will result in grain overheating and its quality deterioration. The experimental dryer due to grain recirculation with oscillation mode permits to prevent overheating of grain material at the expense of heating-cooling cycles interchange. Grain, moving along the complex path, gets into the lower part of the layer, into the active heat exchange area, and receives some heat. Grain, pushed up by airflow, gets into the upper part of the layer where it loses part of the accumulated heat, after touching the colder surface of other grains. As a result, the grain temperature, which is gained at the lower part of the layer, decreases to the moment of getting into the active heat exchange area and receiving another heat impulse. A separate grain temperature increases non-linearly along some wave curve, when maximums are interchanged with minimums, but maximums increase gradually. At the developed boiling, regardless the layer elevation, uniform grain heating is provided and the temperature of the used dryer agent is practically equal to zero.

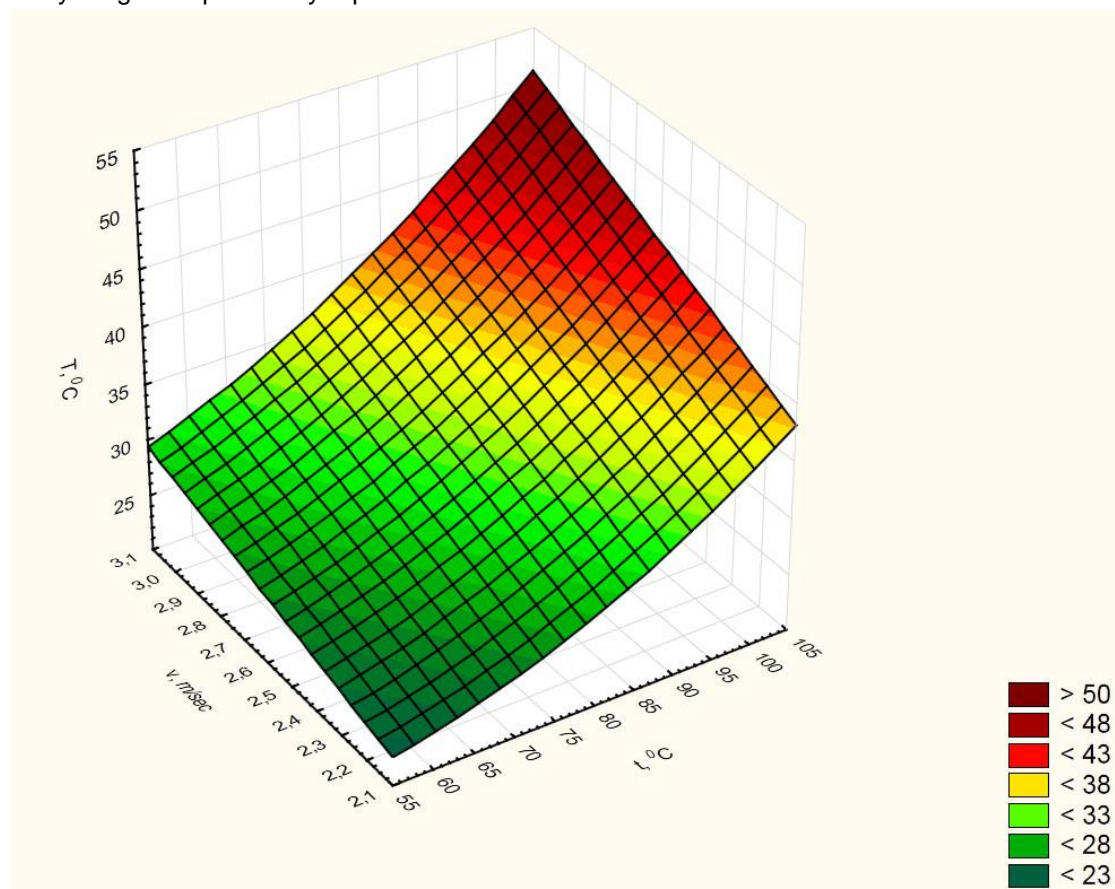


Fig. 6 – Factorial dependence of temperature grain heating within experimental dryer

CONCLUSIONS

1. On the ground of the laboratory research practical guidelines to manufacture are developed: at grain drying in pseudofluidized layer it is recommended to use drying agent with temperature up to 100°C . Further increase of air flow temperature at seed drying for food and especially of seed designation is unreasonable because it will result in grain material overheating.

2. While designing grain dryers of pseudofluidized layer we should limit ourselves with the range of drying agent rates from 2.2 to 3 m/sec. Maximum drying duration to grain material overheating is 600 sec.

3. The developed dryer utilization provides to decrease power demand by over 20% in comparison with serial constructions of small-scale dryers.

ACKNOWLEDGEMENT

The result validity is proved with manufacturing tests based on Research and Education Production Centre «Integratsia» of Federal State Budgetary Educational Establishment of Higher Education “Orel State Agrarian University named after N.V. Parakhin” (Russian Federation). The tests provided drying up to normal amount of moisture and cleaning from light impurities of grain-thrashed heap. The tests were carried out at the place of postharvest treatment of grain material. On completing, the technological process of drying, at unloading grain from dryer, caryopses with changed colour or flavour as the evidence of their damage were not detected. The usage of the developed dryer allowed high quality grain drying after its harvesting, at drying installation efficiency of 180...250 kg/h.

REFERENCES

- [1] Bibik G.A., (2016), Grain drying processes optimization (Оптимизация процесса сушки зерна), *Materials of International science and practice conference “Optimization of electrotechnologies in Agro Industrial Complex”*, Yaroslavl / Russia, pp. 8-12;
- [2] Kalashnikova N.V., Volzhentsev A.V., (2009), Improvement of technological process of wheat grain drying with grounding of parameters of pseudofluidized layer dryer (Совершенствование технологического процесса сушки зерна пшеницы с обоснованием параметров сушилки с псевдооживленным слоем), *Bulletin of Federal State Budgetary Educational Establishment of Higher Education Orel State Agrarian University (Вестник ФГОУ ВПО ОрелГАУ)*, Issue number 1(16), pp. 44-45, Orel / Russia;
- [3] Kalashnikova N.V., Volzhentsev A.V., (2009), Optimal constructional parameters of driers with pseudofluidization of grain material (Оптимальные конструктивные параметры сушилок с псевдооживлением зернового материала), *Mechanization and electrification of agriculture (Механизация и электрификация сельского хозяйства)*, Issue number 3, pp. 6-7, Moscow / Russia;
- [4] Kalashnikova N.V., Volzhentsev A.V., (2009), Grounding of parameters of gas distribution grids in grain driers with pseudofluidized layer (Обоснование параметров газораспределительных решет в зерносушилках с псевдооживленным слоем), *Mechanization and electrification of agriculture (Механизация и электрификация сельского хозяйства)*, Issue number 8, pp. 4-6, Moscow / Russia;
- [5] Kuznetsov Y.A., Volzhentsev A.V., Kolomeichenko A.V., Kalashnikova L.V., (2017), Grounding of construction parameters of pseudofluidized layer dryer working chamber (Обоснование конструктивных параметров рабочей камеры сушилки псевдооживленного слоя), *INMATEH - Agricultural Engineering*, Issue number 2, pp. 33-38, Bucharest / Romania;
- [6] Pilipyuk V.L., (2009), Grain and seeds storage technique (Технология хранения зерна и семян), М.: Vuz. Study book, 457 p., Moscow / Russia;
- [7] Shhitov S.V., Krivutsa Z.F., Kozlov A.V., (2016), Improvement of grain drying technology at the account of het-mass-exchange processes optimization (Совершенствование технологии сушки зерна за счет оптимизации процессов тепломассообмена), *Agroecoinfor (Агроекоинфо)*, Issue number 8, p. 24, Moscow / Russia;
- [8] Tarasenko A.P., (2008), *Modern machines for post-harvest treatment of grain and seeds (Современные машины для послеуборочной обработки зерна и семян)*, М.: KolosS, 232 p., Moscow/ Russia;
- [9] Volzhentsev A.V., (2014), Determination of quality of grain fluidization in dryers (Определение качества оживления зерна в сушилках), *Education, science and production (Образование, наука и производство)*, Issue number 4, pp. 4-7, Moscow / Russia;
- [10] Volkov A.V., (2017), Ways of grain drying intensification (Пути интенсификации сушки зерна), *Materials of VIII International science and practice conference “Agrarian science and education on the modern period of development: experience, problems and ways of their solutions”*, Yaroslavl / Russia, pp. 63-65;
- [11] Zhuravlev A.P., (2014), *Grain drying and grain driers: monograph (Зерносушение и зерносушилки: монография)*, Kinel: RIC Samara State Agricultural Academy, 293 p., Kinel / Russia.

**THEORETICAL RESEARCHES ON COOLING PROCESS REGULARITY OF THE
GRAIN MATERIAL IN THE LAYER**
/

**ТЕОРЕТИЧНІ ДОСЛІДЖЕННЯ ЗАКОНОМІРНОСТЕЙ ПРОЦЕСУ ОХОЛОДЖЕННЯ
ЗЕРНОВОГО МАТЕРІАЛУ В ШАРІ**

Prof. Ph.D. Kotov B.I.¹⁾, Ph.D. Spirin A.B.¹⁾, Ph.D. Tverdokhlib I.V.¹⁾, Ph.D. Polyevoda Y.A.¹⁾,
Ph.D. Hryshchenko V.O.²⁾, Ph.D. Kalinichenko R.A.²⁾

¹⁾ Vinnytsia National Agrarian University / Ukraine;

²⁾ National University of Life and Environmental Sciences of Ukraine / Ukraine;

Tel: 380672152088; E-mail: igor_tverdokhlib@yahoo.com

Keywords: *grain material, cooling, air, heat and mass transfer, venting*

ABSTRACT

The mathematical description of the cooling process dynamics of seed material in a layer, as a method of temporary preservation of grain with cold, before further processing is given.

РЕЗЮМЕ

Наведено математичний опис динаміки процесу охолодження насіннєвого матеріалу в шарі, як способу тимчасової консервації зерна холодом, перед подальшою обробкою.

INTRODUCTION

The urgency to apply artificial cold at the storage of grain materials (food and fodder grain) is defined by different factors. Use of high-efficiency combine harvesters considerably reduces the period of harvesting and makes strict the requirements of processing acceleration and preparation of a grain material for storage. Thus, increasing the amount of units and power capacities for intensive drying, clearing and sorting of grain in most cases is not profitable (Khmelnik M.H., et. al., 2014). The most widespread practice, a method of reduction of grain material humidity in a conditioned state is drying. It is one of the most power-intensive processes in grain production (Gaponjuk O.I., et.al, 2014). The essential factor of reduced price of this process is the add-on of drying machines seasonal loading. As it is known (Voblikov E.M., 2010), the longer the process of grain material drying lasts the more profitable it is. It explains the tendency to extend the drying period in dryers and the use of low-temperature modes (Kotov B., et.al. 2016). Increase in the work period of the machine for drying (Kurhanskyi O. and Kotov B., 2016) is, first of all, a problem of extending the period of safe storage (Paleliulko M.I., 2015). Cooling of the grain mass (Verkholantseva V.O., 2016; Yalpachyk V.F., et.al., 2014) proved to be the most effective method of wet grain time conservation treatment. Conservation treatment of wet grain by cooling supposes the presence of an engineering system which allows to keep it until it is processed and put to constant storage (Kiurchev S.V. and Verkholantseva V.O., 2015; Petrunia B., 2004). Fodder grain can be stored in periodically chilled condition for the entire period of its use. It is possible to use special refrigerating compressor-condenser assemblies (Kozin B., 2014) to cool the grain material during the harvest period at the factories in different grain-cultivated climatic zones. Application efficiency of grain material cooling should be defined (Yalpachyk V.F., et.al., 2014). For this purpose, it is necessary to investigate the cooling process of wet grain by air in stationary volume and to justify the equipment parameters.

Advantages of grain cooling in an embankment or grain tank by artificially cooled air are proved in different works (Petrunia B., 2004; Verkholantseva V.O., 2016) and the limits of grain cooling (Kiurchev S.V. and Verkholantseva V.O., 2015) providing the maximum safety of quality indicators are defined. Perspective use of analytical methods of processes modeling, namely: thermal, biochemical and microbiological at refrigerating storage, is presented by the latest scientific works (Yalpachyk V.F., et.al., 2015, 2016). Many researchers (Kiurchev S.V. and Verkholantseva V.O., 2015; Paleliulko M.I., et.al., 2015; Petrunia B., 2004; Verkholantseva V.O., 2016; Yalpachyk V.F. et.al., 2014) investigated the process of grain cooling during storage. It is possible, by means of mathematical modeling and computer technics, to define cooling process rational parameters and refrigerating storage and the operating conditions of the equipment for its implementation.

The purpose of this work is to create mathematical models for the analysis of grain cooling processes, and to define working process-related parameters.

MATERIALS AND METHODS

The stationary model of the grain material layer, blown through by air (from below-upwards) is object of modelling and research. Air arrives from an air cooler of the refrigerating machine with a constant mass flow rate and constant parameters. To study the object under consideration, we select the analytical method of investigation. For this purpose, we compose the equations of material and energy balance, the conditions for the exchange of heat and the mass of the product with air. This fact makes it possible not to take into account the specific characteristics of the storage, the type of grain material and the equipment parameters.

Let's consider the physical model of the process and the simplifying assumptions for its formalization. Through a layer of dispersed material arranged on a grid, with a thickness H , with the initial grain parameters: humidity u , temperature θ , the air is blown through with parameters constant at the entrance to the layer – temperature t and moisture content d , mass flow G (speed v). The scheme of the process is shown in Fig. 1.

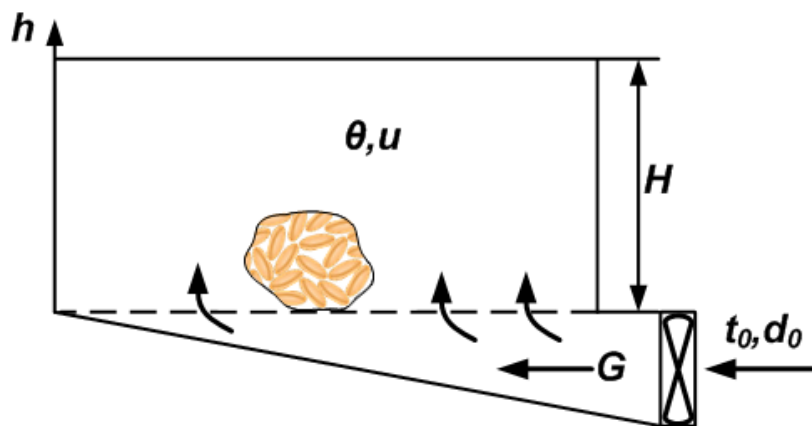


Fig. 1 - The scheme of cooling the grain material in a stack of layers

For a simplified analysis of this process, we made assumptions idealizing the process without distorting the general physical scheme: the thermophysical properties of grain material and air do not depend on temperature; the transfer of heat and mass is convective; other types of heat transfer and mass transfer are accounted for by the coefficients; there are no losses spread to the environment; air movement is unidirectional from the bottom up; the distribution of the temperature and humidity fields is one-dimensional; change in temperature and moisture content of individual grains - without a gradient; contact (conductive) transfer of heat and mass are not taken into account; the coefficients of heat and mass transfer from temperature and humidity are independent and equal to the average values for the process. Heat transfer is carried out according to Newton's law, and mass transfer is described by Merkel's equation.

RESULTS

Let's describe the process of cooling the grain in a layer by differential equations of thermal and a material balance; according to the adopted scheme and the physical model, we introduce the following notation:

$q_h = q/H$ - specific allocation of biological warmth per unit layer altitudes, W/m;

θ, t - temperature of grain material and air, °C;

u, d - moisture content of grain material and air, kg/kg_{dm} and kg/kg_{da};

m_z, m_a - weight of grain and air in layer volume, kg;

c_z, c_a - grain and air specific heat, J/(kg°C);

H - height of a material layer, m;

f, f' - the general surface of grain and transpiration surface, m²;

α, β - heat exchange and mass transfer coefficient, $W/(m^2 \cdot ^\circ C)$ and m/s ;

$d''_n(\theta)$ - saturated air moisture content at temperature of a material surface, kg/kg_{dm} ;

ρ_z, ρ_{z0} - density of wet and absolutely dry grain, kg/m^3 ;

ρ_a - air density, kg/m^3 ;

F_z, F - the square of cross-section of a grain material and air in layer volume, m^2 ;

h - coordinate on layer altitude;

τ - time, s.

Let's write down the differential equations thermal and a material balance for grain and filtrated air.

The equation of thermal balance for an element of disperse material layer in altitude dh which presents change of grain temperature will look like:

$$r_0 F_z \rho_{z0} dh du + c_z F_z \rho_z dh d\theta = q_h dh d\tau - \frac{\alpha f}{H} (\theta - t) dh d\tau \quad (1)$$

The equation of the thermal balance, temperatures of air presenting change for the same element dh like in next equation:

$$\rho_a c_a F dh dt = \frac{\alpha f}{H} (\theta - t) dh d\tau \quad (2)$$

The equation of a material balance presenting change of grain moisture content at surface evaporation for an element dh :

$$-\rho_{z0} F_z dh du = \frac{\beta f'}{H} (d''_n(\theta) - d) dh d\tau. \quad (3)$$

The equation of material balance describing the change in the moisture content of air absorbing the moisture evaporating from the grain, for an element dh will become:

$$\rho_a F dh dd = \frac{\beta f'}{H} (d''_n(\theta) - d) dh d\tau. \quad (4)$$

Opening total differentials of variable quantities $d\theta, dt, du, dd$: $dT = \frac{\partial T}{\partial \tau} d\tau + \frac{\partial T}{\partial h} dh$ (T - the conditional generalized variable) and considering that $\frac{dh}{d\tau} = v$ - speed, m/s ; $m_z = F_z \rho_z H$ - weight of grain, kg ; $m_a = F \rho_a H$ - weight of air in a layer, and also using an obvious relationship $F \rho = \frac{G}{v}$, kg/m we convert the equations (1) - (4) and become:

$$m_z c_z \frac{\partial \theta}{\partial \tau} - m_0 r_0 \frac{\partial u}{\partial \tau} = -\alpha f (\theta - t) - q_h \quad (5)$$

$$m_a c_a \frac{\partial t}{\partial \tau} + c_a G H \frac{\partial t}{\partial h} = \alpha f (\theta - t) \quad (6)$$

$$-m_0 \frac{\partial u}{\partial \tau} = \beta f' (d''_n(\theta) - d) \rho_a \quad (7)$$

$$m_a \frac{\partial d}{\partial \tau} + G H \frac{\partial d}{\partial h} = -m_0 \frac{\partial u}{\partial \tau} \quad (8)$$

The system of the hyperbolic differential equations in a partial derivative (5-8) with sufficient accuracy presents dynamics of processes of a heat and weight exchange at grain layer cooling.

Definition of values θ , u , t , d , as coordinate and time functions is reduced to the following: for any $0 \leq h \leq H$ and $0 < \tau < \infty$ to find the solution of system (5-8) at boundary and entry conditions: $u(h,0) = u_0$; $\theta(h,0) = \theta_0$; $t(0,\tau) = t_0$; $d(0,\tau) = d_0$. The accurate solution of the system can be obtained by numerical methods of calculation. To obtain the approached analytical dependences, we shall make simplifying transformations. Using the definition of Rebinder measure $Rb = \frac{c_z d\theta}{r_0 du}$ (Kotov B., Kalinichenko R., Spirin A., 2015), we get the equation:

$$-\frac{\partial u}{\partial \tau} = \frac{c_z}{r_0 Rb} \frac{\partial \theta}{\partial \tau} \quad (9)$$

Substituting (9) in (5) we will have:

$$m_z c'_z \frac{\partial \theta}{\partial \tau} + q_h = \alpha f(t - \theta) \quad (10)$$

where:

$$c'_z = c_z \left(1 + \frac{1}{r_0 Rb} \right).$$

Rates of derivatives $dt/d\tau$ and $dd/d\tau$ are small enough in comparison with other terms of the equations and they can be neglected. After simple transformations of the equations (6) and (10) we will come to their kind of system:

$$\begin{cases} t - \theta = \frac{1}{B} \frac{\partial \theta}{\partial \tau} - \varepsilon \\ \theta - t = \frac{1}{A} \frac{\partial t}{\partial h} \end{cases} \quad (11, 12)$$

where:

$$A = \frac{\alpha f}{HGc_a}; \quad B = \frac{\alpha f}{m_z c_z}; \quad \varepsilon = \frac{q_h}{\alpha f}.$$

Approximate solution of the system (11-12) (under conditions $\varepsilon = 0$ or $\varepsilon = \varepsilon_0(\theta - t)$ where ε_0 - coefficient of linear approximation of a function $q = f(\theta, t)$) is (Kotov et.al., 2015):

$$\theta = \theta_0 - (\theta_0 - t_0) B e^{-Ah} \int_0^\tau e^{-B\tau} J_0(2\sqrt{ABh\tau}) d\tau \quad (13)$$

$$t = \theta_0 + (t_0 - \theta_0) e^{-Ah} \left(e^{-B\tau} J_0(2\sqrt{ABh\tau}) \right) + B \int_0^\tau e^{-B\tau} J_0(2\sqrt{ABh\tau}) d\tau \quad (14)$$

where:

J_0 - Bessel function of a zero order from imaginary argument.

For the simplified accounts, it is possible to spread out Bessel function abreast and it will be limited to the one first member (solution error less 10%):

$$\theta \approx \theta_0 - (\theta_0 - t_0) e^{-Ah} (1 - e^{-B\tau}) \quad (15)$$

$$t = \theta_0 + (t_0 - \theta_0) e^{-Ah} \quad (16)$$

To determine the humidity reduction rate at cooling, we approximate function $d''_h(\theta)$ by linear dependence:

$$d''_h(\theta) = a\theta + b \quad (17)$$

where

a, b - constant factors, and substituting the solution (15) in the equation (7) taking into account (8) we obtain:

$$T_d \frac{dd}{dh} + d = c' + De^{-Ah} \quad (18)$$

where

$$T_d = \frac{GH}{\beta f \rho_a}; \quad c' = b + a\theta_0; \quad D = a(t_0 - \theta_0)(1 - e^{-B\tau}).$$

The solution of the equation (18) under the condition: $h = 0; d = d_0$ looks like:

$$d(h, \tau) = (d_0 - c'T_d)e^{-\frac{1}{T_d}h} + c'T_d + \frac{e^{-Ah} - e^{-\frac{1}{T_d}h}}{A_1 - A} (a(t_0 - \theta_0)(1 - e^{-B\tau})) \quad (19)$$

From the equations (7) and (8) it is obtained:

$$m_a \frac{\partial d}{\partial \tau} + GH \frac{\partial d}{\partial h} = \beta f' (d''_h(\theta) - d) \rho_a. \quad (20)$$

Taking differential from (19) and substituting the expression obtained in the equation (20) we have:

$$-\frac{m_0}{GH} \frac{du}{d\tau} = \left(\frac{1}{T_d(AT_d - 1)} e^{-\frac{h}{T_d}} - \frac{A}{AT_d - 1} e^{-Ah} \right) D + \frac{d_0 - c'}{T_d} e^{-\frac{h}{T_d}} \quad (21)$$

The solution of the equation (21) under entry conditions: $h = 0; u = u_0$ will have the expression:

$$u(\tau, h) = u_0 + \frac{1}{T_u T_d (A t_d - 1) B} \left(\begin{aligned} & \left(AT_d (\theta_0 - t_0) e^{-Ah} + (t_0 - \theta_0) e^{-\frac{h}{T_d}} \right) e^{-B\tau} + \\ & (ABT_d t (\theta_0 - t_0) + AT_d (t_0 - \theta_0)) e^{-Ah} + \\ & (ABT_d (c't - d_0 t) - Bt (\theta_0 + c' - d_0 - t_0) + \theta_0 - t_0) e^{-\frac{h}{T_d}} \end{aligned} \right) \quad (22)$$

Fig. 2-4 show the examples of calculated graphs of grain temperature change (Fig. 2), cooling air (Fig. 3) and grain moisture content (Fig. 4) in terms of time and height.

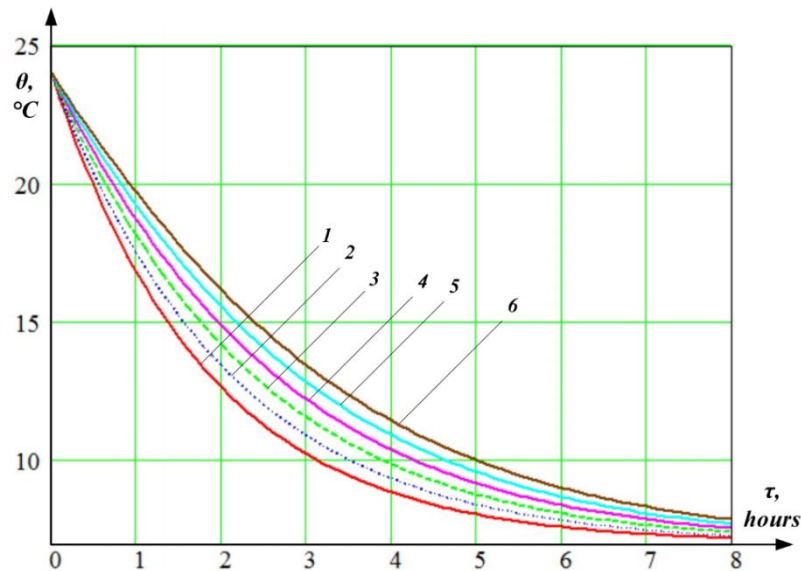


Fig. 2 - Example of graphs of grain temperature variation in time and height ($G=0.205$ kg/s; $t_0=7$ °C; $u_0= 20$ %):
 1 – $h=0.2$ m; 2 – $h=0.4$ m; 3 – $h=0.6$ m; 4 – $h=0.8$ m; 5 – $h=1$ m; 6 – $h=1.2$ m

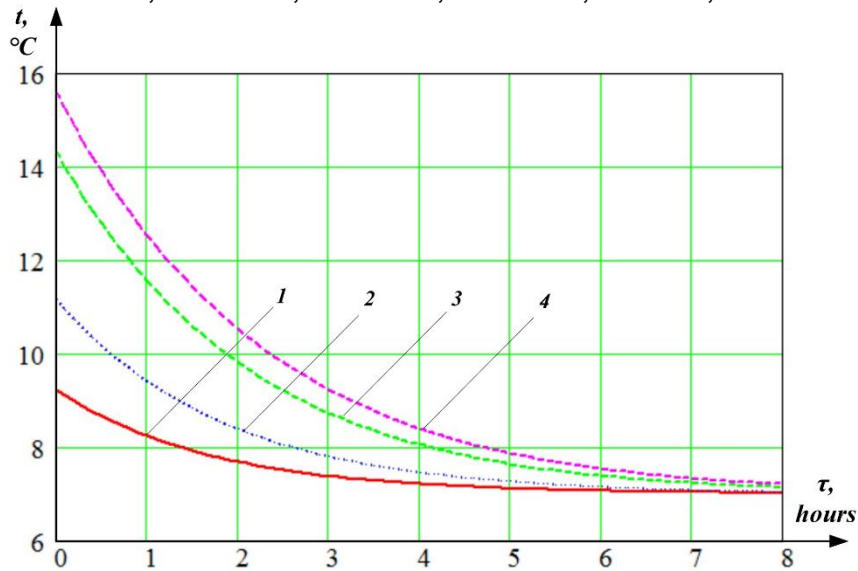


Fig. 3 - Calculated graph of the cooling air temperature in terms of time and height ($G=0.205$ kg/s; $t_0=7$ °C; $u_0= 20$ %): 1 – $h=0.2$ m; 2 – $h=0.4$ m; 3 – $h=0.8$ m; 4 – $h=1$ m

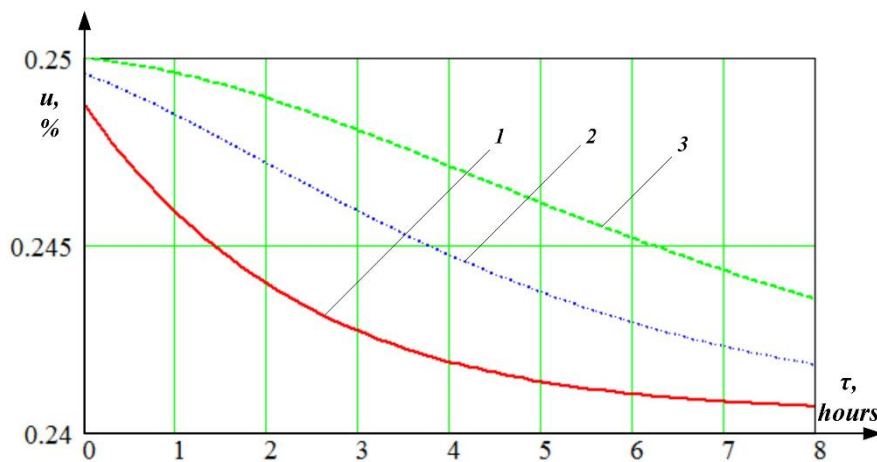


Fig. 4 - Graph of changes in grain moisture content in terms of time and height ($G=0.205$ kg/s; $t_0=7$ °C; $u_0= 20$ %):
 1 – $h=0.6$ m; 2 – $h=2.6$ m; 3 – $h=4.6$ m

Fig. 5 shows the graphs of temperature changes in barley seeds when cooled in field storage.

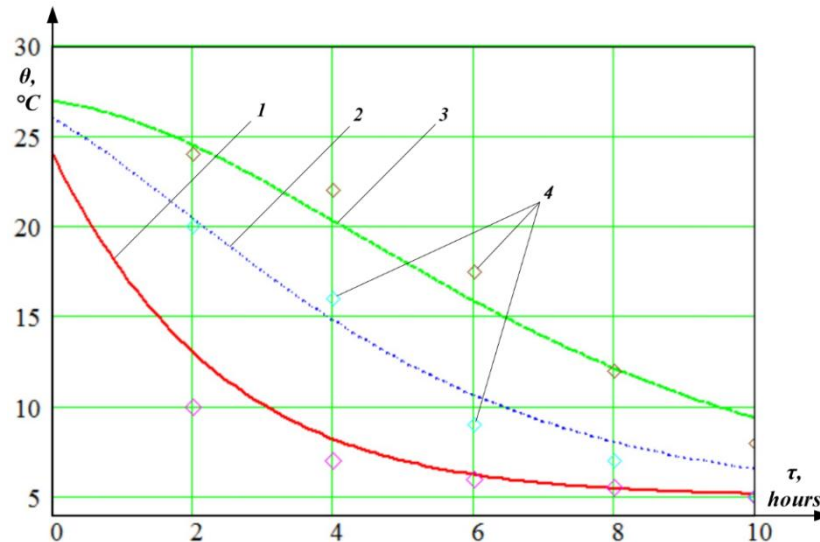


Fig. 5 - Curves of grain temperature changes during cooling in the storage with parameters ($G=0.103$ kg/s; $t_0=5$ °C; $u_0=20.1$ %): 1 – $h=0.6$ m; 2 – $h=2.6$ m; 3 – $h=4.6$ m; 4 – experiment data (for 0.6, 2.6, 4.6 m)

To compare the data obtained theoretically (formula 13) and direct measurements of the grain mass temperature at an altitude (0.6, 2.6, 4.6 m) with the fan turned off, experiments were carried out on the actual object - the grain embankment in the storage (storage section).

CONCLUSIONS

Thus, the gained analytical dependences (13) - (14) and (19) - (22) allow counting change of grain material parameters and chilling air on altitude of a layer at any moment of time; it also allowed defining a cooling time at specified values of the charge of air and its temperature.

The dependence of the cooling duration on the speed of air penetrating the grain layer is in good agreement with the results of the study of heat transfer in a layer of granular materials.

REFERENCES

- [1] Gaponjuk O.I., Ostapchuk M.V., Stankevich G.N., Gaponjuk I.I., (2014), *Active aeration and grain drying (Активное вентилирование и сушка зерна)*, VMV (BMB), ISBN 978-966-413-483-2, 326 p., Odessa;
- [2] Khmelniuk M.H., Lahutin A.Iu., Kochetov V.P., Tomchuk O.M., (2014), Importance of the state of the refrigeration in the food security of Ukraine (Важливість стану холодильного господарства у забезпеченні продовольчої безпеки України), *Scientific works of Odessa National Academy of Food Technologies (Наукові праці Одеської національної академії харчових виробництв)*, Vol.45, Part.1, pp.116-121, Odessa;
- [3] Kiurchev S.V., Verkhohantseva V.O., (2015), Determination of optimization parameters of the process of cooling the grain (Визначення параметрів оптимізації процесу охолодження зерна), *Bulletin of Kharkiv National Technical University of Agriculture named after Petr Vasilenko (Вісник Харківського національного технічного університету сільськогосподарства імені Петра Василенка)*, Vol.163, pp.228-239, Kharkiv;
- [4] Kotov B., Kalinichenko R., Spirin A., (2015), Mathematical modeling of heat and mass transfer process under heat treatment of grain materials in dense layer, *ТЕКА, Commission of Motorization and Energetics in Agriculture*, Vol.17, Issue 5, pp.54-57, Lublin;
- [5] Kotov B., Spirin N., Kalinichenko R., (2016), Heat and mass transfer during the drying of agricultural plant materials in a dense stationary layer (Тепло і масообмін при сушінні сільськогосподарських рослинних матеріалів у щільному нерухомому шарі), *Engineering, power engineering, transport of agroindustrial complexes (Техніка, енергетика, транспорт АПК)*, Issue 2, pp.24-28, Vinnitsa;
- [6] Kozin V.M., Arseniev V.M., Verterov Iu.M., (2014), *Refrigeration technology (Холодильні технології)*, SumDU (СумДУ), 188 p., Sumy;

- [7] Kurhanskyi O., Kotov B., (2016), Use of artificially cooled air during grain storage (Використання штучно охолодженого повітря в процесі зберігання зерна), *Materials of the international scientific conference: Legume crops and soybeans for sustainable development of agrarian production of Ukraine (Матеріали міжнародної наукової конференції: Зернобобові культури та соя для сталого розвитку аграрного виробництва України)*, pp.170-171, Vinnitsa;
- [8] Paleliulko M.I., Pidlisnyi V.V., Tkach O.V., (2015), Justification of the influence of factors on the storage of grain (Обоснование влияния факторов на срок хранения зерна), *MOTROL. Commission of Motorization and Energetics in Agriculture*, Vol.17, Issue 5, pp.54-57, Lublin;
- [9] Petrunia B., Kudashev S., Titlova O., (2004), Prospects for the use of artificial cold for grain storage (Перспективи застосування штучного холоду для збереження зерна), *Scientific works of Odessa National Academy of Food Technologies (Наукові праці Одеської національної академії харчових виробництв)*, Vol.27, pp.26-30, Odessa;
- [10] Verkholtantseva V.O., (2016), *Justification of the regime parameters of grain raw materials cooling during storage (Обґрунтування режимних параметрів охолодження зернової сировини у процесі зберігання)*, Vinnitsa National Agrarian University (Вінницький національний аграрний університет), 22 p., Vinnitsa;
- [11] Voblikov E.M., (2010), *Technology of elevator industry (Технология элеваторной промышленности)*, Lan (Лань), ISBN: 978-5-8114-0971-6, 384 p., St. Petersburg;
- [12] Yalpachuk V. F., Kravets O. V., Verkholtantseva V. O., (2014), Economic evaluation of the efficiency of using the grain cooling method (Економічна оцінка ефективності використання способу охолодження зерна), *Scientific works of Odessa National Academy of Food Technologies (Наукові праці Одеської національної академії харчових виробництв)*, Vol.45, Part.2, pp.199-202, Odessa;
- [13] Yalpachuk V., Kiurchev S., Stuchaiev M., Verkholtantseva V., (2015), Investigation of the heat exchange process in a cooled layer of wheat grain (Дослідження процесу теплообміну при охолодженні шару зерна пшениці), *Bulletin of Kharkiv National University of Agriculture (Вісник Харківського національного університету сільського господарства)*, Vol.166, pp.50-55, Kharkiv;
- [14] Yalpachuk V.F., Kiurchev S.V., Verkholtantseva V.O., (2016), Analytical means of simulation of microbiological and biochemical processes during storage of grain mass (Аналітичні засоби моделювання мікробіологічних та біохімічних процесів при зберіганні зернової маси), *Proceedings of the Tavria State Agrotechnological University (Праці Таврійського державного агротехнологічного університету)*, Vol.16, Part.1, pp.3-8, Melitopol.

MODELING OF MECHANICAL AND TECHNOLOGICAL PROCESSES OF THE AGRICULTURAL INDUSTRY

/

МОДЕЛЮВАННЯ МЕХАНІЧНИХ ТА ТЕХНОЛОГІЧНИХ ПРОЦЕСІВ СІЛЬСЬКОГОСПОДАРСЬКОЇ ПРОМИСЛОВОСТІ**Ph.D. Aliev E.B.¹⁾, Ph.D. Bandura V.M.²⁾, Ph.D. Pryshliak V.M.²⁾,
Ph.D. Yaropud V.M.²⁾, Ph.D. Trukhanska O.O.²⁾**¹⁾Institute of Oilseed Crops of the NAAS / Ukraine, ²⁾Vinnitsa National Agrarian University / Ukraine
Tel: +380978399834; E-mail: yaropud77@gmail.com**Keywords:** *numerical modeling, process, mechanics, manufacture, method, theoretical researches***ABSTRACT**

Modern theoretical researches on the mechanical and technological processes for agricultural industry can be summarized by analytical methods, which lead to the compilation of complex systems of differential equations with boundary and initial conditions. These systems practically cannot be solved by traditional methods, so there is a necessity in their numerical solution via computer modeling. The molecular dynamics method and discrete element method, both of them based on the conception of a discrete structure of a substance, are the most interesting ones among all existing modern computer modeling methods for the mechanical and technological processes of agricultural industry. The purpose of these researches is to carry out the numerical modeling for some mechanical and technological processes for agricultural industry using the Star CCM+ computer software. There have been provided the results of the numerical modeling in the Star CCM+ computer software of the following mechanical and technological processes: mixing of components in a stream-type mixer-feeder, distribution of the straw underlay by the rotor spreader for the non-leash cow maintenance, formation of the pseudo-liquefied seed layer in the hydro-pneumatic seeding machine's intake chamber, transferring of the oil crops seeding material with the air stream power, functioning of the photoelectric seed separators executing mechanism, technological process of the seed separation on an inclined vibrating surface. The given results point about the wide area of implementation of the numerical modeling for theoretical researches of mechanical and technological processes for agronomical manufacturing industry.

РЕЗЮМЕ

Сучасні теоретичні дослідження механічних і технологічних процесів сільськогосподарської обробної промисловості можна підвести до аналітичних методів, що призводить до складання складних систем диференціальних рівнянь з граничними та початковими умовами. Ці системи практично не можуть бути вирішені традиційними методами, тому в їх чисельному вирішенні необхідне використання комп'ютерного моделювання. Метод молекулярної динаміки та метод дискретних елементів, обидва з яких базуються на концепції дискретної структури речовини, є найбільш цікавими серед усіх існуючих сучасних методів комп'ютерного моделювання механічних та технологічних процесів сільськогосподарської обробної промисловості. Метою цих досліджень є проведення чисельного моделювання деяких механічних та технологічних процесів для сільськогосподарської промисловості за допомогою програмного забезпечення Star CCM+. Наведені результати чисельного моделювання в комп'ютерній програмі Star CCM+ наступних механічних та технологічних процесів для аграрної промисловості: змішування компонентів у змішувачі-фідері потокового типу, розподіл соломистої підстилki роторним розкидачем для технологічного обслуговування безприв'язних корів, формування шару псевдозрідженого насіння в гідравлічно-пневматичній впускній камері посівної машини, транспортування посівного матеріалу олійних культур повітряним потоком, функціонування механізму фотоелектричних насінневих сепараторів, технологічний процес сепарації насіння на нахилений вібраційній поверхні. Дані результати свідчать про широку область застосування цифрового моделювання для теоретичних досліджень механічних та технологічних процесів сільськогосподарської промисловості.

INTRODUCTION

Modern theoretical researches on the mechanical and technological processes for agricultural industry can be summarized by analytical methods, which lead to the compilation of complex systems of differential equations with boundary and initial conditions (*Johnson K.L., 1987*). These systems practically cannot be solved by traditional methods, so there is a necessity in their numerical solution via computer modeling.

The molecular dynamics method and discrete element method, both of them based on the conception of a discrete structure of a substance, are the most interesting ones among all existing modern computer modeling methods for the mechanical and technological processes for agricultural manufacturing industry. The molecular dynamics method consists of representing the substance as an aggregation of interacting particles – material points or solid bodies. Their movement is described by the classic mechanics equations. During the particles movement modeling, the molecular dynamics method solves the Cauchy problem on every step with iterative methods – performing an integration of the differential equations with determined initial conditions. The best known software for calculations using the molecular dynamics method is: AMBER, CHARMM, GROMACS, GROMOS and NAMD. The discrete element method can be considered as a generalization of the finite element method. During the modeling with this method the initial locations and velocities of particles must be pre-determined. After this, basing on these initial data of the particles interaction physical laws, the active forces for each particle must be determined. Following this, it's possible to consider various interaction laws; it's sufficient to have a solvable equation for their description. For each particle, the method requires to calculate the resultant force and also to solve the Cauchy problem on the selected time interval. The result for these calculations will be the initial data for the next step. The best known software for the discrete elements method realization is: Chute Maven (Hustrulid Technologies Inc.), PFC2D i PFC3D, EDEM (DEM Solutions Ltd.), GROMOS 96, ELFEN, MIMES, PASSAGE and Star CCM+. The purpose of this research is to perform the numerical modeling for some mechanical and technological processes for agricultural manufacturing industry in the Star CCM+ computer software.

MATERIALS AND METHODS

During the finite elements method modeling process in the Star CCM+ software the initial locations and velocities of the particles and substance stream must be pre-determined. Then, basing on these initial data for the contact interaction physical laws, the forces that act on each particle in each time interval, are being calculated. For each particle, the resultant force is being calculated and the Cauchy problem is solved for a given time interval. The results of this iteration are the initial data for the next step. The following models were selected as physical models for the numerical modeling: k-ε-model of the separated stream turbulence, field of the gravity force, Van-der-Waals real gas model or the non-pressed fluid model, the discrete elements model, the multiphase interaction model. The discrete elements method is based on the momentum conservation law for the Lagrange multiphase stream models.

To perform the research on the particles' movement process under the substance stream affect, it is required to determine the mathematical apparatus that allows obtaining the trajectories, force diagrams and slip values during the particles movement in the substance stream with the velocity gradient.

Let's begin by composing the differential equation for the movement of one particle in the dedicated substance stream area (*Gumerov N., Duraiswami R., 1998*):

$$\left\{ \begin{array}{l} \Omega_p \cdot \rho_p \frac{d_p \overline{V}_p}{dt} = \overline{F} \\ \frac{d_p \overline{S}_p}{dt} = \overline{V}_p \\ \frac{d_p}{dt} = \frac{\partial}{\partial t} + \overline{V}_p \cdot \overline{\nabla} \end{array} \right. \quad (1)$$

Where Ω_p – particle value, m³;

ρ_p – particle density, kg/m³;

\overline{V}_p – particle movement velocity vector, m/s;

\overline{S}_p – particle displacement vector, m;

\overline{F} – vector of the resulting force applied to particles, N.

The effective diameter of the particle is one of its characteristics, which is defined as a diameter of an equal-sized sphere. So, the equivalent particle value can be defined by the equation:

$$\Omega_p = \frac{\pi \cdot D_p^3}{6} \quad (2)$$

Where D_p – particle effective diameter, m.

Attempts to solve this equation system (1) are combined with certain difficulties that can be reduced to the following:

- a) the total number of forces, that affect the particle in the substance stream, are undefined, because the processes of the particle behaviour within the stream are not fully described;
- b) strict analytical expressions for some expressions in the right part of the equation are unknown (for example, an expression for the hydrodynamic air force).

Forces, that affect the particle during its movement in the turbulent stream, can be divided to the following groups, based on the reasons of their emerging:

1. Forces that are caused by the external force fields affect (weight force) (*Dinesh J., 2009*):

$$\overline{F_g} = \Omega_p \rho_p \overline{g} \quad (3)$$

where $\overline{F_g}$ – gravity force vector, N.

2. Forces, that are caused by the uneven balance of the pressure on the particle surface during its movement in the substance stream.

- 2.1 Archimedes force (*Dinesh J., 2009*):

$$\overline{F_A} = \Omega_p \rho_a \overline{g} \quad (4)$$

Where $\overline{F_A}$ – Archimedes force vector, N.

ρ_a – substance density, kg/m³.

- 2.2. Force that is caused by the change of the pressure in the direction of the carrying stream movement due to the acceleration (*Gumerov N., Duraiswami R., 1998*):

$$\overline{F_{ac}} = \Omega_p \rho_a \frac{d_a \overline{V_a}}{dt} \quad (5)$$

$$\frac{d_a}{dt} = \frac{\partial}{\partial t} + \overline{V_a} \cdot \nabla$$

Where $\overline{F_{ac}}$ – force, that is caused by the change of the pressure in the direction of the carrying stream movement, N;

$\overline{V_a}$ – substance movement velocity vector, m/s.

- 2.3. Hydrodynamic Magnus force emerges as a result of an uneven upcoming stream bypassing of the particle. The difference between the stream velocities in different particle perimeter points, which is bypassing, causes the static pressure differential. The reason of the uneven upcoming stream bypassing of the particle can be either its rotating inside the stream, or its persistence in that zones where the stream has a transverse gradient. The value of the Magnus force is proportional to the relative forward velocity and its absolute angular velocity, i.e. (*Kanehl P., 2010*):

$$\overline{F_{Mag}} = \frac{1}{2} \pi D_p^2 \rho_a V_a^2 C_M \frac{\overline{\omega} \times \overline{V_a}}{|\overline{\omega} \times \overline{V_a}|} \quad (6)$$

Where $\overline{F_{Mag}}$ – Magnus force, N; C_M – Magnus empirical coefficient; $\overline{\omega}$ – angular rotational velocity vector, s⁻¹.

3. The viscous resistance force, which is caused during the particle movement with some relative velocity in the substance stream (*Hamzaev H.M., 2007*):

$$\overline{F_D} = \frac{1}{2} \pi D_p^2 \rho_a f_M(Re) (\overline{V_a} - \overline{V_p}) |\overline{V_a} - \overline{V_p}| \quad (7)$$

Where $\overline{F_D}$ – viscous resistance force, N; $f_M(Re)$ – viscous resistance coefficient;

Re_a – Reynolds number.

$$Re_a = \frac{V_a \cdot D_G \cdot \rho_a}{\mu_a}, \quad (8)$$

D_G – hydraulic diameter, m;

To this group we can also add the Basset force, which combines the viscous and inertial impact of the stream to the particle non-stationary movement conditions.

4. Inertial forces, which are caused by the non-stationary particle movement in the substance are:

4.1 Force, which is equivalent to the added mass impact, is presented as:

$$\overline{F}_m = \frac{1}{2} \Omega_p \rho_a \frac{d}{dt} (\overline{V}_a - \overline{V}_p), \quad (9)$$

and expresses the uprising particle inertia during its non-stationary movement (*Hamzaev H.M., 2007*). A moderate increasing of the particle mass is caused by the substance elements inertia, so that particle must transfer an additional acceleration. This additional substance movement is equivalent to the movement of some fictitious mass (additional mass), which moves with the same relevant velocity as the particle.

4.2. Basset force (*Zhang S. and other, 2009*):

$$\overline{F}_B = \frac{6\pi\mu_p^2}{\sqrt{\pi\nu}} \int_{\tau} \frac{d}{dt} (\overline{V}_a - \overline{V}_p) \frac{d\tau}{\sqrt{t-\tau}}, \quad (10)$$

Where \overline{F}_B – Basset force, N;

ν – kinematic viscosity, m²/s;

τ – time, s.

Basset force considers an additional particle movement resistance from the stream, which is caused by the particle relevant velocity configuration. Basset force manifests as a momentum particle movement resistance increasing due to the increasing of its inertia.

5. Forces that are caused by the particle mass changing (Meshchersky force) (*Voronenko B.A., Pelenko V.V., Polyakov S.V., 2013*):

$$\overline{F}_M = \overline{V}_p \frac{dm_p}{dt} \quad (11)$$

Where \overline{F}_M – Meshchersky force, N; m_p – particle mass, kg.

6. Summarized force of the contact interaction between particle and the chamber, which is based on the Hertz-Mindlin spring-dashpot contact model (*Komiwes V., Mege P., Meimon Y., Herrmann H., 2006*):

$$\overline{F}_{Diff} = \beta_p \overline{V}_p \quad (12)$$

Where $F_{contact}$ – force of the interaction between particles and the edge, N;

$$\overline{F}_{contact} = \overline{F}_n + \overline{F}_t \quad (14)$$

\overline{F}_n – normal force component, N;

\overline{F}_t – tangential force component, N.

Normal force component is defined by the following equation:

$$\overline{F}_n = -K_n \overline{d}_n - N_n \overline{V}_n$$

Where K_n – normal coefficient of the spring component rigidity, N/m;

$$K_n = \frac{4}{3} E_{eq} \sqrt{d_n R_{eq}} \quad (16)$$

N_n – normal coefficient of the dashpot component degradation, N/m;

$$N_n = \sqrt{(5K_n M_{eq})} N_{n \text{ damp}} \quad (17)$$

According to the researches (*Johnson K.L., 1987*) tangential component is defined as:

$$\overline{F}_t = -K_t \overline{d}_t - N_t \overline{V}_t \quad (18)$$

if $|\overline{K}_t \overline{d}_t| < |\overline{K}_n \overline{d}_n| C_{fs}$, and C_{fs} – statistic friction coefficient between particles or a chamber wall. In the other

case, the tangential component is defined by the following equation:

$$\bar{F}_t = \frac{|K_n \bar{d}_n| C_{fs} \bar{d}_t}{|\bar{d}_t|} \quad (19)$$

where K_t – tangential coefficient of the spring component rigidity, N/m;

$$K_t = 8G_{eq} \sqrt{d_t R_{eq}} \quad (20)$$

N_t – tangential coefficient of the dashpot component degradation, N/m;

$$N_t = \sqrt{(5K_t M_{eq})} N_{t \text{ damp}} \quad (21)$$

N_{damp} – degradation coefficient

$$N_{damp} = \frac{-\ln(C_{n \text{ rest}})}{\sqrt{\pi^2 + \ln(C_{n \text{ rest}})^2}} \quad (22)$$

R_{eq} – equivalent radius of particles A and B, m;

$$R_{eq} = \frac{1}{\frac{2}{D_A} + \frac{2}{D_B}} \quad (23)$$

M_{eq} – equivalent mass of particles A and B, kg;

$$M_{eq} = \frac{1}{\frac{1}{M_A} + \frac{1}{M_B}} \quad (24)$$

E_{eq} – equivalent Young module of particles A and B, Pa;

$$E_{eq} = \frac{1}{\frac{1-v_A^2}{E_A} + \frac{1-v_B^2}{E_B}} \quad (25)$$

G_{eq} – equivalent module of the particles A and B displacement, Pa;

$$G_{eq} = \frac{1}{\frac{2(2-v_A)(1+v_A)}{E_A} + \frac{2(2-v_B)(1+v_B)}{E_B}} \quad (26)$$

M_A, M_B – particles A and B mass, kg;

d_n, d_t – duplication coefficient for the normal and tangential direction in contact points;

D_A, D_B – particles A and B effective diameters, m;

E_A, E_B – particles A and B Yung module, Pa;

v_A, v_B - particles A and B Poisson coefficients;

\bar{V}_n, \bar{V}_t – normal and tangential components of the particle surface relevant velocity in the contact point, m/s.

For the interaction process between a particle and a wall the (13)-(26) are adequate, but, for the wall, the radius is defined as $D_{wall} = \infty$ and the mass as $M_{wall} = \infty$. As a result, expressions (23)-(24) turn into:

$$\begin{aligned} R_{eq} &= D_p/2 \\ M_{eq} &= M_p \end{aligned} \quad (27)$$

RESULTS

In order to demonstrate the results of the numerical modeling in the Star CCM+ software, let's consider some mechanical and technological processes for agricultural manufacturing industry.

1. The process of the stream-type mixer-feeder operation has been theoretically researched and the mathematical models of the constructive, technological and regime parameters impact on the quality indexes of its operation have been developed (Shevchenko I.A., Aliyev E.B., Doruda S.O., 2013). The physical mathematical models of the streaming feed mixing process, which is used as a base for the mobile mixer-feeder, has been built within the Star CCM+ software (fig. 1). This physical mathematical model of the streaming feed mixing allows defining the constructive and technological parameters for the mobile mixer-feeder depending on the ration and physical mechanical properties of the feeding mix components with optimal quality, quantity and energy indexes of the mixing process.

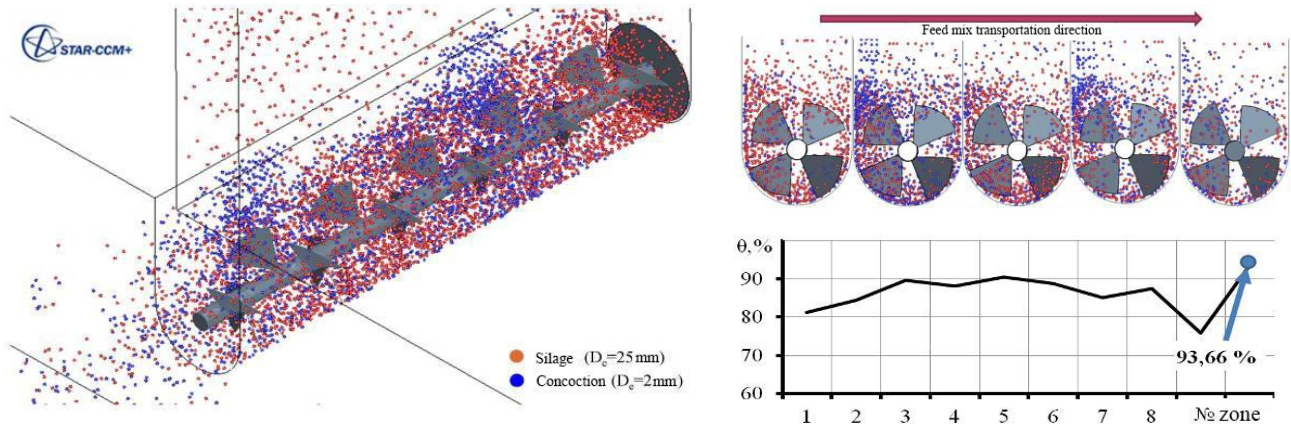


Fig. 1 – Visualization of the mobile mixer-feeder streaming feed mixing process and the dynamic of its homogeneity changing

2. The constructive and technological schemes of the working parts of the rotor straw underlay spreader for the non-leash cow maintenance has been theoretically substantiated (Luts S.M., Aliyev E.B., 2014). The presence and absence of the sealing or directional plate have been used as research objects. The straw particles flight distance and the coefficient of the variation of their even distribution through the box length have been picked as the evaluation criteria. The results of numerical modeling are described in picture 2.

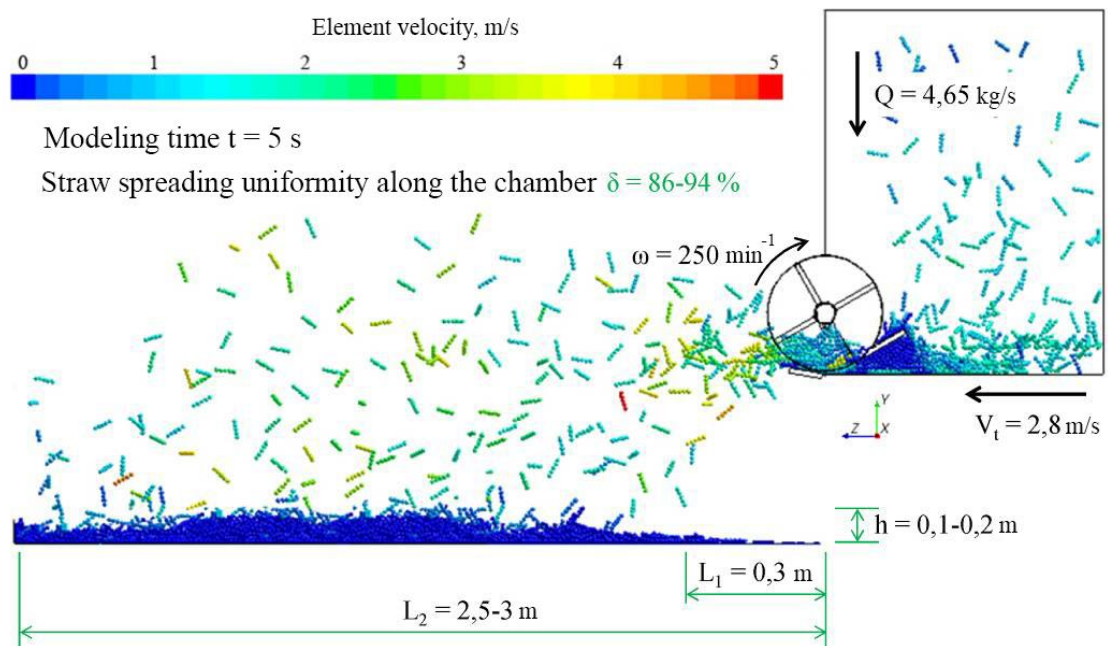


Fig. 2 – Process visualization of the rotor straw underlay spreading with condensing and guiding plates

3. The physical and mathematical model for the formation process of the pseudo-liquefied seed layer in the hydro-pneumatic seeding machine's intake chamber has been developed (Boyko V.B., Aliyev E.B., 2015; Boyko V.B., Aliyev E.B., 2015).

Picture 3 displays the results as a graphical interpretation of the dynamic of the seed spreading in the intake chamber value.

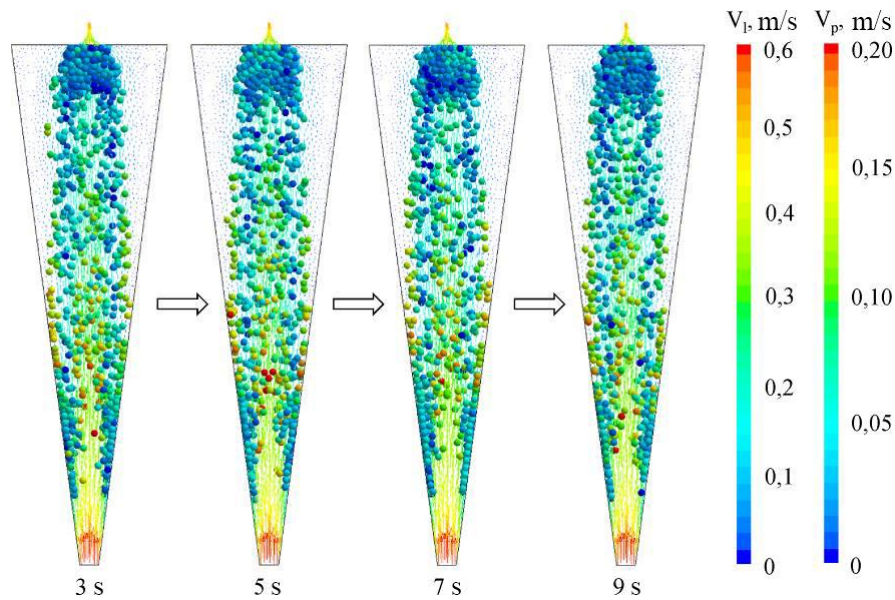


Fig. 3 – Visualization of the dynamic of the seed spreading in the hydro-pneumatic seeding machine's intake chamber value

4. As a result of theoretical researches there has been developed the physical and mathematical model for the process of the oil crops seeding material transferring with the air stream power and presented as visualization of this technological process, as described in picture 5 (Aliyev E.B., Yaropud V.M., 2017; Aliyev E.B., 2017).

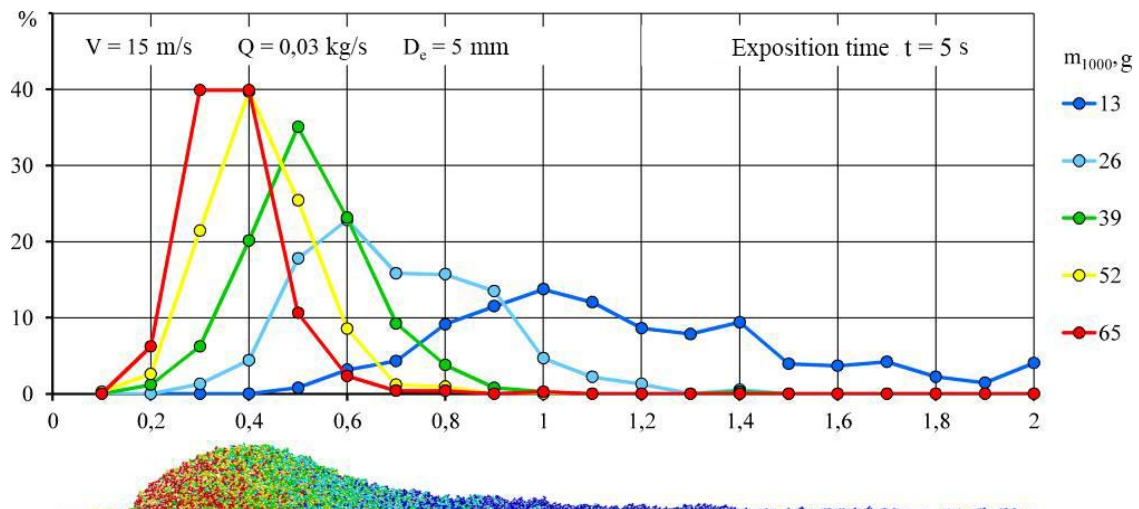


Fig. 4 – Visualization of the distribution of the seed fraction along the area length, which has been created by the air stream impact

5. Numerical modeling of the process of the milk-air mix movement in the milking machine has allowed us to determine a relation between the vacuum pressure fluctuation value and the milk withdrawal velocity, pulsation frequency and the working vacuum pressure value (Linnik Yu.A., Aliyev E.B., Pavlenko S.I. 2014; Pavlenko S.I., Aliyev E.B., Linnik Yu.A., 2014).

Picture 5 describes the spreading of the 1- α liquid content along the milking machine milk hose by the upper milk pipe.

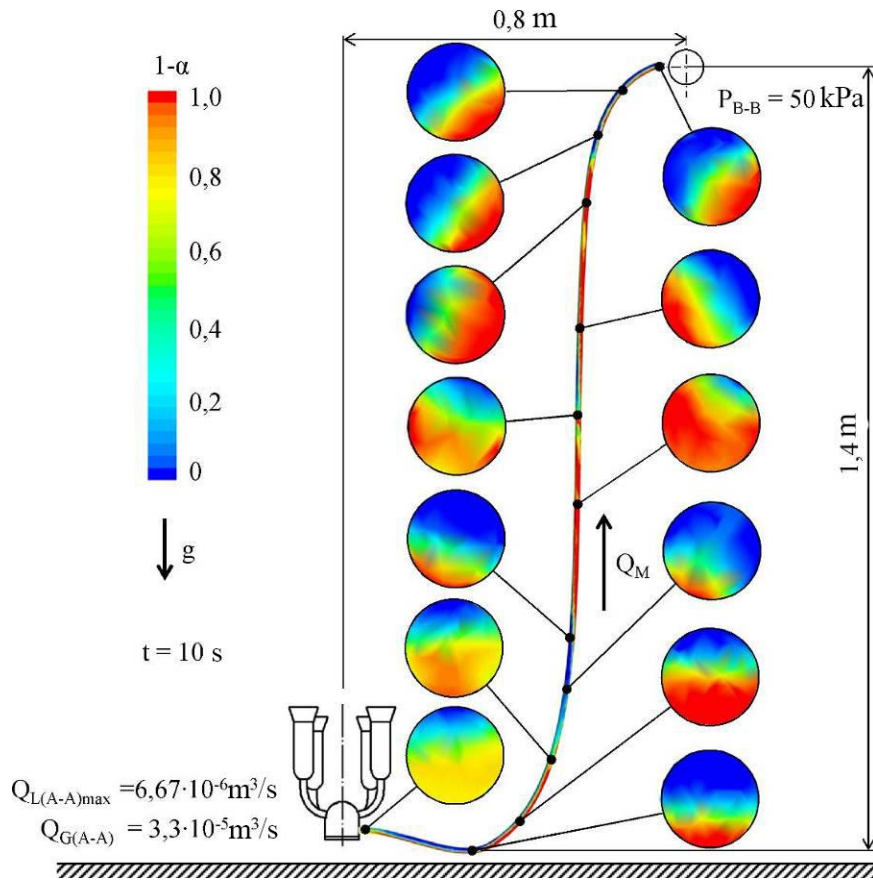


Fig. 5 – Spreading of the 1-α liquid content along the milking machine milk hose by the upper milk pipe

6. As a result of the working process numerical modeling for the photoelectric seed separator executing mechanism, which consists of the falling cylinder and the inclined vibrating roll, there has been determined the timing diagram of the seed transportation in the separate vibration roll canal (picture 6).

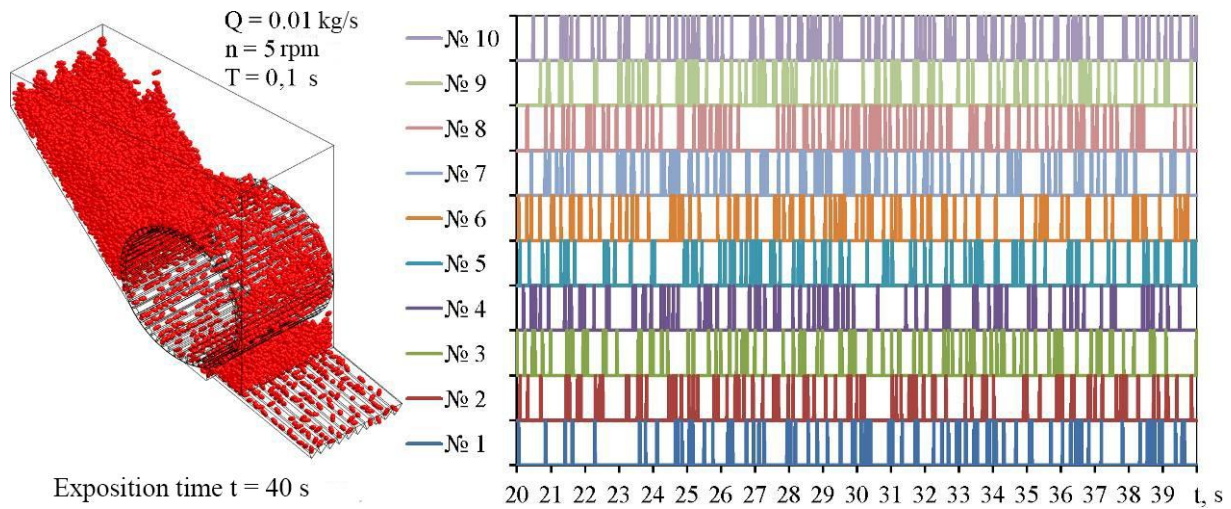


Fig. 6 – Timing diagram of the seed transportation in the separate vibration roll canal of the photoelectric seed separator

7. Through the research on the technological process for the seed separation on the inclined vibrating plate (vibrating separator) in the Star CCM+ software it has become possible to determine the law of its spreading depending on the mass. Picture 7 describes the visualization of this technological process.

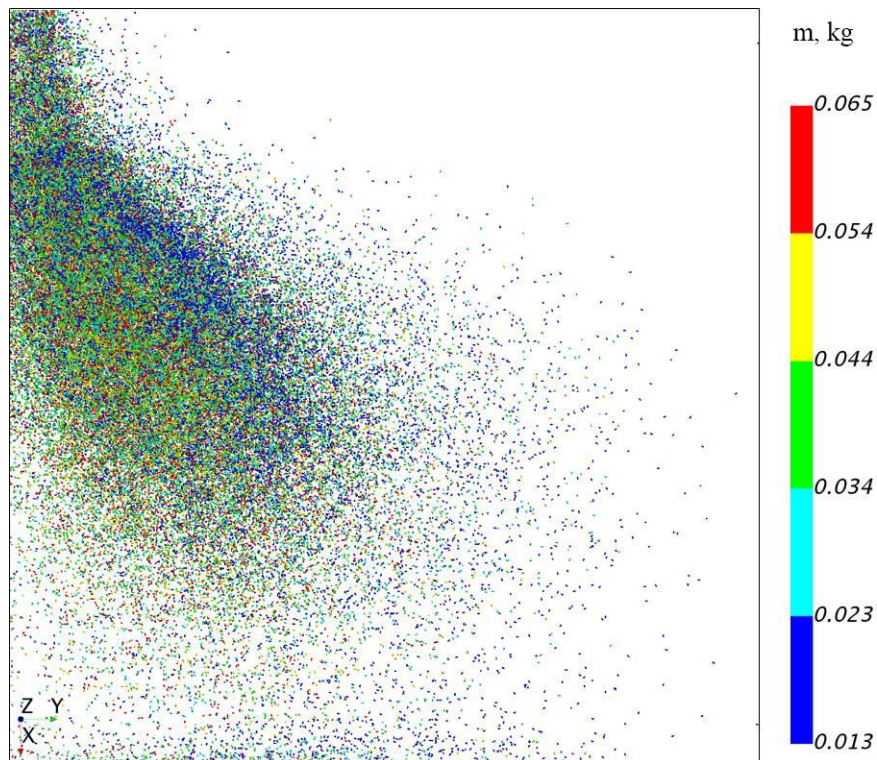


Fig. 7 – Visualization of the technological process of seed separation on the inclined vibrating plate (vibrating separator)

CONCLUSIONS

In this article are given the results of the numerical modeling within the Star CCM+ computer software for some mechanical and technological processes for agricultural manufacturing industry, as the mixing of components in a stream-type mixer-feeder, distribution of the straw underlay by the rotor spreader for the non-leash cow maintenance, formation of the pseudo-liquefied seed layer in the hydro-pneumatic seeding machine's intake chamber, transferring of the oil crops seeding material with the air stream power, functioning of the photoelectronic seed separator's executing mechanism, technological process of the seed separation on an inclined vibrating surface. These results point out the wide area of implementation of the numerical modeling for theoretical researches on mechanical and technological processes for agricultural manufacturing industry.

REFERENCES

- [1] Aliyev E.B., Yaropud V.M., (2017), Physics and mathematical modeling of the movement of seeds in the air flow, *Engineering, power engineering, transport of agro-industrial complexes*, №2 (97), pp.19-23, Ukraine;
- [2] Aliyev E.B., (2017), Results of numerical modeling of mechanical and technological process movement of seed material of oilseed crops under the influence of air flow, *Bulletin of Zhytomyr National Agroecological University*, № 1(1), pp. 173-180, Zhytomyr / Ukraine;
- [3] Boyko V.B., Aliyev E.B., (2015), Theoretical studies of fluid motion in the capacity of a hydro-pneumatic seeding machine, *Engineering of nature use*, №2(4), pp. 78-84, Kharkiv / Ukraine;
- [4] Boyko V.B., Aliyev E.B., (2015). Research of the process of putting the seeds into the pipeline of the hydro-pneumatic sowing machine. *Collection of abstracts of the International scientific Internet conference "Prospects and strategy of adaptive and resource-saving cultivation of oilseeds in conditions of climate change"*, pp. 148-149, Zaporizhzhia / Ukraine;
- [5] Dinesh J., (2009), Modelling and Simulation of a Single Particle in Laminar Flow Regime of a Newtonian Liquid, *Excerpt from the Proceedings of the COMSOL Conference*, pp. 1-9, Bangalore / India;
- [6] Johnson K.L., (1987) Contact Mechanics, *Cambridge University Press*, 434 p., Cambridge / USA;
- [7] Gumerov N., Duraiswami R., (1998), Modeling of particle motion in viscous swirl flow between two porous cylinders, *Proceedings of FEDSM'98 ASME Fluids Engineering Division Summer Meeting*, pp.1-8, USA;

- [8] Hamzaev H.M., (2007), Simulation of the motion of a single particle in the ascending stream of a viscoplastic fluid, *Mat. Modeling*, №3(19), pp. 87-93;
- [9] Kanehl P., (2010), Particle model of the Magnus effect, Bachelor Thesis. *Mathematisch-Naturwissenschaftliche Fakultät Ernst-Moritz-Arndt-Universität*, 35 p., Greifswald/Germany;
- [10] Komiwes V., Mege P., Meimon Y., Herrmann H., (2006), Simulation of granular flow in a fluid applied to sedimentation, *Granular Matter*, Vol. 8 (1), pp. 41-54;
- [11] Linnik Yu.A., Aliyev E.B., Pavlenko S.I., (2014), The mathematical model of the movement of the milk-air mixture on the milk-line of the milking plant, *Scientific and technological progress in agricultural production: materials of the Intern. scientific-techn. conf.: RUE "NPC NAS of Belarus on mechanization of agriculture"*, T3, pp. 181-185, Minsk / Belarus;
- [12] Luts S.M., Aliyev E.B., (2014), Substantiation of the constructive-technological scheme of the universal machine for introducing straw litter on the basis of numerical modeling, *Scientific and technological progress in agricultural production: materials of the Intern. scientific-techn. conf.: RUE "NPC NAS of Belarus on mechanization of agriculture"*, T3, pp. 137-141, Minsk / Belarus;
- [13] Pavlenko S.I., Aliyev E.B., Linnik Yu.A., (2014), Results of numerical modeling of the process of milk-air mixture transfer in a milking machine, *Mechanization, automation and machine technology in animal husbandry*, №4(16), pp. 77-81, Moscow / Russia;
- [14] Shevchenko I.A., Aliyev E.B., Doruda S.O., (2013), Modeling stream mixing forage mixture using discrete element method, *Mechanization and electrification of agriculture*, №97(1), pp. 536-544, Glevaha;
- [15] Voronenko B.A., Pelenko V.V., Polyakov S.V., (2013), On the deposition process of hydro-mechanical solids in a liquid medium, *Processes and devices of food production*, №4, pp. 54-57;
- [16] Zhang S., Kuwabara S., Suzuki T., Kawano Yo., Morita K., Fukuda K., (2009), Simulation of solid–fluid mixture flow using moving particle methods, *Journal of Computational Physics*, №228, pp. 2552-2565.

MODELLING OF THE HYDRO-MECHANICAL MIXER PARAMETERS

/

МОДЕЛЮВАННЯ ПАРАМЕТРІВ ГІДРОМЕХАНІЧНОЇ МІШАЛКИ

Doctor of technical sciences Golub G.A.¹⁾, Doctor of technical sciences Kukharets S.M.²⁾,
Ph.D. Eng. Chuba V.V.¹⁾, Ph.D. Eng. Pavlenko M.Y.¹⁾, Ph.D. Eng. Yarosh Y.D.²⁾

¹⁾National University of Life and Environmental Sciences of Ukraine / Ukraine,

²⁾Zhytomyr National Agroecological University / Ukraine

Tel: +380676653548, E-mail: saveliy_76@ukr.net

Keywords: *biodiesel, reactive power, atomizer, drag, lift force, emulsion*

ABSTRACT

It is determined the reactive power to provide hydro-mechanical rotation of the mixer in the process of biodiesel production. It is established that reactive power depends on the flow and pump speed, the density of the mixture of vegetable oil and potassium methylate, the sectional area of the injector nozzles and their number. It is obtained the value of the resistance moment of hydro mechanical mixer depending on the angular velocity and the maximum radius. It is developed the mathematical model of hydro-mechanical mixer rotation, which allows determining the dynamics of the angular velocity of hydro mechanical mixer rotation and its steady-state value.

РЕЗЮМЕ

Визначено реактивну силу для забезпечення гідромеханічного обертання мішалки в процесі виробництва дизельного біопалива. Встановлено що реактивна сила залежить від подачі та частоти обертання насоса, густини суміші рослинної олії та метилату калію, площі перерізу сопла форсунок та їх кількості. Отримано значення моменту опору гідромеханічної мішалки, який залежать від кутової швидкості та максимального радіуса. Розроблена математична модель обертання гідромеханічної мішалки, яка дозволяє визначити динаміку кутової швидкості обертання гідромеханічної мішалки та її усталене значення.

INTRODUCTION

The mechanized work in the agricultural production is impossible without fuel, as up to 80% of manufacturing operations are diesel fuel operated. Therefore, the economic efficiency of agricultural production depends on the cost of diesel fuel (Golub G. et al 2017). One option to reduce costs in agricultural production is the use of own production bio-diesel (Ivanov B., Stoyanov S., 2016). In addition, the use of diesel fuel for operating diesel engines will significantly reduce CO₂ emissions in the agricultural production process.

In the production of bio-diesel one of the key steps is the process of transesterification (Golub G. et al 2015), taking place due to the mixing of vegetable oil and potassium methylate (Qiu Z. et al, 2010; Ehsan M., Tofajjal H., 2015; Baskar G., Aiswarya R., 2016). Mixing determines the completeness of the process of transesterification, which in turn directly affects the quantitative and qualitative yield of biodiesel. As methyl alcohol, catalyst and oil form a two-phase medium, in which the passage of the reaction is slowed down, to intensify the reaction it is necessary to form an emulsion with increased interphase contact area of the reactants, which is achieved due to the constant mixing (Qiu Z et al 2010; Wulandani D. et al., 2015; Golub G. et al, 2015; Baskar G., Aiswarya R., 2016). It is necessary to avoid too intensive mixing, which can lead to the destruction of the interfacial surface and slow down the reaction of transesterification. In addition, intense mixing requires a considerable amount of energy (Qiu Z. et al, 2010; Golub G. et al, 2015). In this regard, improvement of the equipment for biodiesel production based on the mixing of the emulsion components is important.

For the production of biodiesel, the process of transesterification or methanolysis of oils with an alkaline catalyst has become popular (Golub G. et al, 2015; Ehsan M., Tofajjal H., 2015). Studies have shown that methanolysis proceeds in the temperature range from 20 to 70°C with the use of alkaline catalysts (up to 1.5 % of the total volume of emulsion) (Ehsan M., Tofajjal H., 2015). Most often transesterification process has the following parameters: the processing time up to 40 min, the temperature is about 40°C, ratio of methanol to oil is 6 to 1 in moles, catalyst content is up to 1 % of the emulsion volume

(Golub G. et al, 2015; Baskar G., Aiswarya R., 2016).

It is established that the quality of the methanolysis reaction depends on hydrodynamic conditions (Ehsan M., Tofajjal H., 2015) and requires mixing with a given intensity (Golub G. et al, 2015). It is developed the mathematical model of technological process of transesterification for bio-diesel production on the basis of the possibility theory (Drahniev S., 2010) and it is mathematically modelled the adaptive technological process of transesterification of vegetable oils in batch reactors (Drahniev S., Kukharets S., 2010). It is theoretically studied the mixing efficiency when creating in the emulsion stream of the turbulent regime and grounded the constructive parameters of the hydrodynamic separator in bio-diesel production (Golub G., S. Kukharets, V. Chuba, et al., 2017).

The most widely used have become reactors for carrying out the process of transesterification equipped with mechanical mixers (Drahniev S., 2010). It is known the method of bio-diesel production based on hydraulic mixing using stationary atomizers (Sungwornpatansakul P., Hiroi J., Nigahara Y., et al., 2013; Golub G. et al, 2015). In the works (Drahniev S., Kukharets S., 2010; Drahniev S., 2010; Brásioa A. et al, 2011) it is stated that one of the disadvantages of mechanical mixing is the formation of areas of emulsion stagnation and substantial energy consumption (Sungwornpatansakul P. et al., 2013; Mushtruk M. et al, 2013). Enzymatic reactors of conventional (Poppea J. et al, 2015) and rotating (Xua J. et al., 2017) types are also used, but they have low productivity. Due to lack of the mixing process effectiveness, transesterification doesn't proceed to the full extent, therefore additional operations for flushing (Alamsyah R., Loebis H., 2014) and cleaning (Atadashi I., 2015) are used, which complicates the technological process of bio-diesel production in terms of agricultural production.

Lately, it has become relevant the use of equipment for biodiesel production with the use of hydro-mechanical mixing that occurs due to departure of a mixture of vegetable oil and potassium methylate from atomizers, resulting in a reactive force, which creates the rotational motion of the mixer with blades, and they in turn provide additional mixing (Golub G. et al, 2015). Thus, there is a double mixing of the emulsion components (Pavlenko M., Golub G., 2013).

However, there is currently insufficient research in physical and mechanical properties of bio-diesel and constructive-technological parameters of equipment for the production of bio-diesel, which hinders further enhancement of biodiesel production efficiency. There is also no evidence on the process of biodiesel production using a hydro-mechanical mixing. In this regard, there is the necessity of a theoretical substantiation of the design parameters of the equipment for diesel biofuel production using hydro-mechanical mixing. Determination of the hydro-mechanical mixer parameters in the biodiesel production will allow obtaining data to optimize the operation of complex equipment in vegetable oil transesterification.

MATERIALS AND METHODS

The aim of the research is the development and experimental test of a mathematical model to determine the parameters of hydro mechanical mixer in the production of bio-diesel based on vegetable oils.

Theoretical studies were based on the analysis of the interaction of the blades with the emulsion using the dynamic equations based on Newton's second law. The reactive force of the jet (Kundu P. et al, 2016), which creates a rotary moment of hydro-mechanical blade mixer was determined by the second Newton's law at a constant rate of departure of the jet taking into account the total number of atomizers and parameters of the pump feeding.

To confirm the theoretical studies, the experimental model of the hydro-mechanical mixer was used, the diagram of which is shown in Fig. 1, and the general view – in Fig. 2.

To measure the frequency of rotation of the hydro-mechanical mixer and shaft of hydraulic pump it was used tachometer UT-372. To change the speed of the hydraulic pump shaft, the frequency converter Hitachi-3-G3JX-A4075-EF was used.

RESULTS

To consider the interaction of the hydro-mechanical mixer blades with viscous emulsion medium (components for biodiesel production) the scheme, which is shown in Fig. 3, was used.

The blade of hydro-mechanical mixer, in general case, is set at an angle to the direction of blade movement. The movement of the blade is carried out under the action of reactive force of the jet emitted from atomizers mounted on the ends of the ducts and which are fed with oil mixture with potassium methylate. Viscous medium of the emulsion counteracts the movement of the blade moving under the action of the jet reactive force. As it is known, the blade is influenced by the components of the normal reaction of the

viscous medium resistance. Thus, the horizontal component of the normal resistance reaction of the viscous medium opposes the motion of the blade, and the vertical one creates lifting force influencing the blade.

The total reactive force of all jets when supplying the viscous fluid with the help of the pump of volumetric action will be:

$$F_R = \left(\frac{q_H n_H}{60} 10^{-6} \right)^2 \frac{\rho}{\mu S_\phi n_\phi} \quad (1)$$

where F_R – is the reactive force of the jet, H; q_H – pump supply (for gear-type pumps is considered according to specifications), sm^3/turn ; n_H – rotational speed of the pump, $\text{turn}/\text{min.}$; ρ – the density of the liquid, kg/m^3 ; μ – the reduction ratio of the cross-sectional area of the jet at the expiry of liquid from the atomizer, rel. un. (Kundu P.K. et al, 2016); S_ϕ – the actual cross-sectional area of the atomizer, m^2 ; n_ϕ – number of atomizers, pieces.

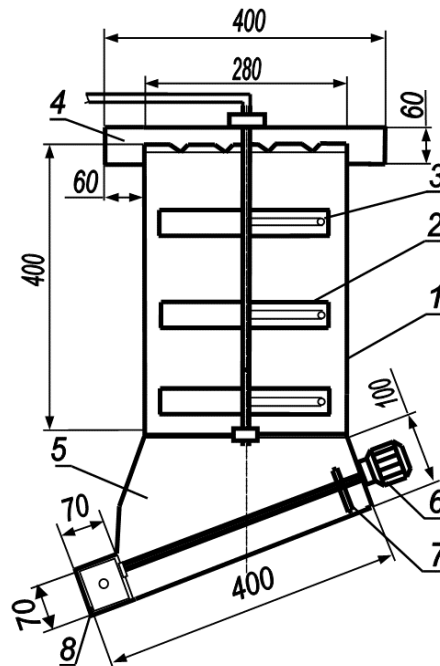


Fig. 1 - Scheme of the experimental model of the hydro-mechanical mixer

1 – the reactor vessel; 2 – hydro-mechanical mixer; 3 – atomizer; 4 – reactor head; 5 – chamber for sediment accumulation; 6 – electric motor; 7 – scraper; 8 – chamber for sediment removal



Fig. 2 - General view of the experimental model of the hydro-mechanical mixer

The resultant of forces of resistance (the total aerodynamic force) is decomposed into two components, the drag (force head) and lifting force. These components help to establish a force that acts in

the fluid flow perpendicular to the plane of the scapula. Viscous medium of the emulsion counteracts the movement of the blades moving under the action of jets reactive forces. When moving the blades in a real fluid, in addition to the pressure force on the blade perpendicular to the blade surface and applied in the centre of pressure, they will act directed along the blade forces of friction and resistance dependent on geometric dimensions of the blade. To account for the action of these forces, as well as other unexplored factors, dimensionless coefficients of the changes in the blade lift k_y and drag force k_x have been introduced. Then, the components of the total aerodynamic force, considering the rotational movement of the blades, can be written as follows:

$$R_{OX} = C_X k_X \frac{\rho \omega^2 r^2}{2} A; \quad (2)$$

$$R_{OY} = C_Y k_Y \frac{\rho \omega^2 r^2}{2} A \quad (3)$$

where C_X, C_Y – accordingly, the coefficients of blade drag and lift force, rel. units; k_Y and k_X – dimensionless coefficients of changes in the blade lift and drag force, rel. units ω – the angular velocity of blades rotation, rad/s; r – the distance from the centre of rotation to the point of force application, m, A – the area of the blade, m^2 .

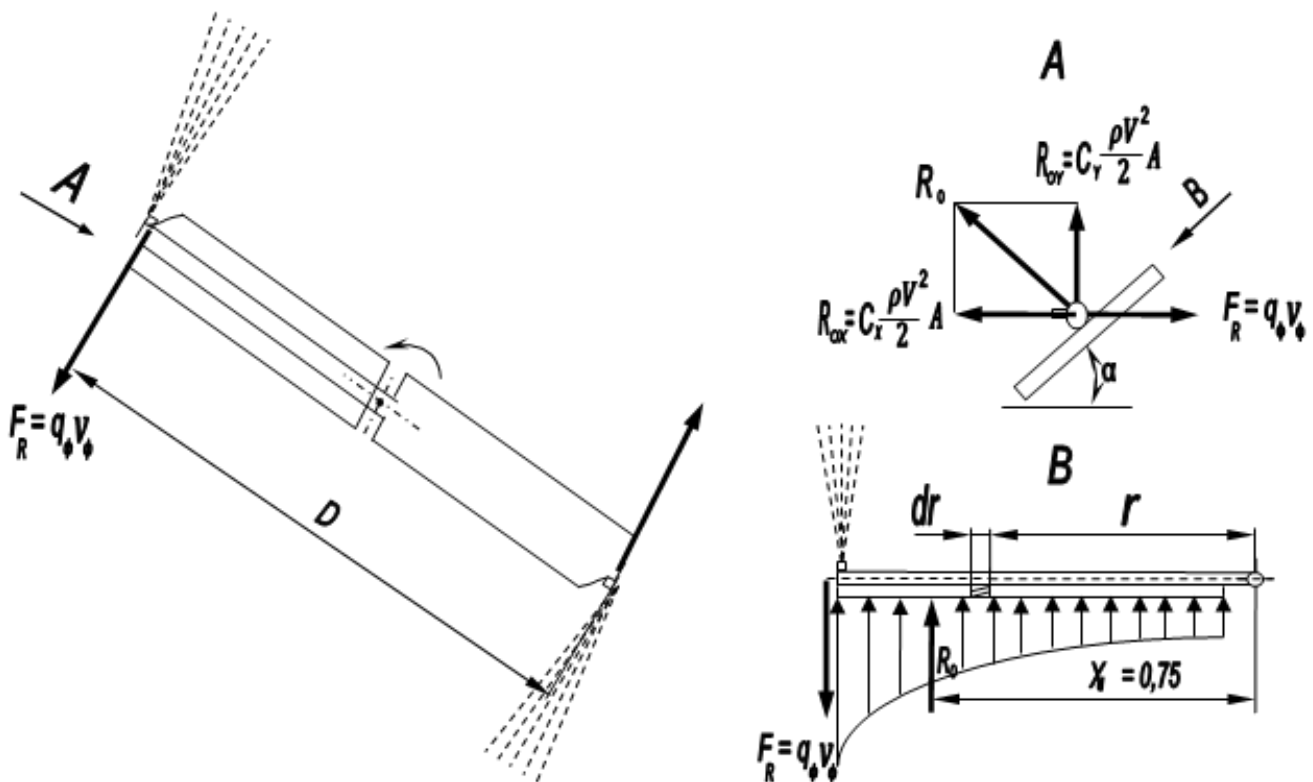


Fig 3 - Interaction scheme of hydro-mechanical mixer blades with the emulsion during the mixing process

During the rotation of the blades the change of drag and lift forces depending on the radius of blade rotation is observed and were determined the elementary drag and lift forces influencing the elementary area of the blade with the length of dr , which is at a distance of r from the axis of rotation. Considering the size of the blade it was determined the elementary moment of resistance dM_R , which is created by the basic drag force on an elementary square of the blade with the length of dr .

Integrating the equation for the elementary moment of resistance due to action of an elementary force of drag, it was obtained the value of the resistance moment depending on the blade rotation radius:

$$M_R = C_X k_X \frac{\rho \omega^2}{8} h r_{\max}^4 \quad (4)$$

where r_{\max} – the maximum radius of the blade, m, h – the width of blades, m.

The resulting equations have given the opportunity to make the differential equation, which describes the dynamics of hydro-mechanical blade mixer and has the following form:

$$J \frac{d\omega}{dt} = \left(\frac{q_H n_H}{60} 10^{-6} \right)^2 \frac{\rho}{\mu S_{\phi} n_{\phi}} \sum_{i=1}^n r_{\phi_i} - C_X k_X \frac{\rho \omega^2}{8} h \sum_{i=1}^n r_{\max i}^4 \quad (5)$$

Where: J – the moment of inertia of the hydro-mechanical blade mixer, kg m^2 ; r_{ϕ_i} – the radius of installation of the i^{th} atomizer, m ; t – mixing time, s .

The differential equation solution allowed us to obtain an equation to determine the dynamics of changes in the angular velocity of hydro-mechanical blade mixer rotation in the following form:

$$\omega = \sqrt{\frac{a}{b} \left[\frac{\sqrt{a} + \sqrt{b} \omega_{\Pi} \exp(2t\sqrt{ab}) - 1}{\sqrt{a} - \sqrt{b} \omega_{\Pi} \exp(2t\sqrt{ab})} \right]} \quad (6)$$

where:

ω_{Π} – the initial angular velocity of rotation of the blades, rad/s ;

$a = \frac{1}{J} \left(\frac{q_H n_H}{60} 10^{-6} \right)^2 \frac{\rho}{\mu S_{\phi} n_{\phi}} \sum_{i=1}^n r_{\phi_i}$ – the ratio of rotational moment to the hydro-mechanical mixer moment of inertia;

$b = \frac{1}{J} C_X k_X \frac{\rho}{8} h \sum_{i=1}^n r_{\max i}^4$ – the ratio of resistance to the hydro-mechanical mixer moment of inertia.

In steady state of hydro-mechanical mixer rotation, its angular speed will be $\omega_{\text{st}} = \sqrt{a/b}$.

According to equation (6), it was designed the graph (Fig. 4) from which it follows that an increase in the frequency of the pump shaft rotation from 700 to 1400 rpm leads to an increase in the steady-state rotation frequency of hydro-mechanical blade mixer from 8.76 to 34 rpm. Steady state of hydro-mechanical mixer rotation begins at time of 0.2-0.4 sec.

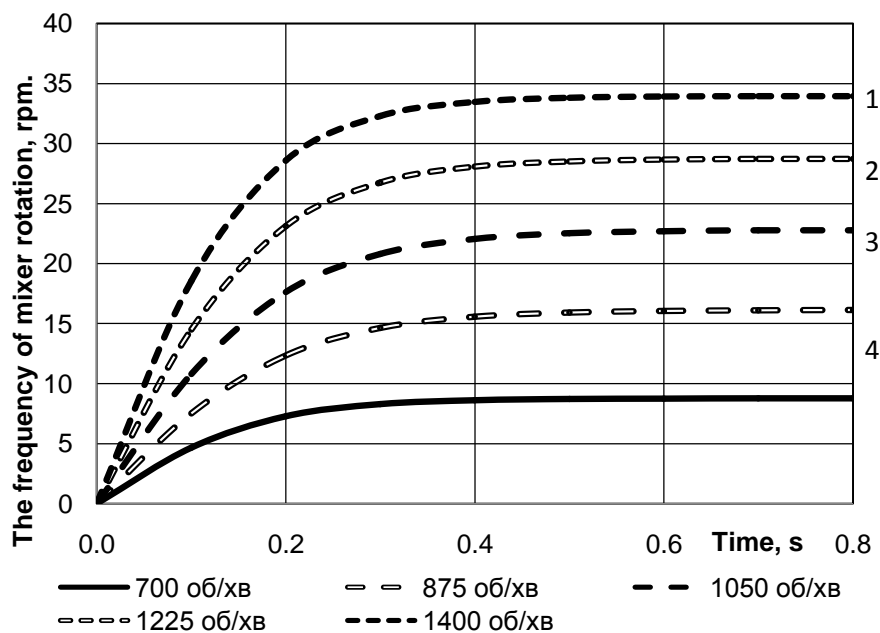


Fig. 4 - Curves of acceleration of hydro-mechanical blade mixer depending on the frequency of pump rotation at an angle of the blades of 60°
 1 – 700 rpm; 2 – 875 rpm; 3 – 1050 rpm; 4 – 1225 rpm; 5 – 1400 rpm

On the basis of experimental studies, the dependence of the drag coefficient on the frequency of pump rotation (Fig. 5) was found, which allowed us to obtain complete coincidence of the experimental data with the theoretical dependence, which relates steady frequency of mixer rotation and the rotational speed of the pump.

For the dependence of the hydro-mechanical mixer established rotation frequency on the angle of the blades, the level of approximation of theoretical and experimental data, estimated by the index of determination is 0.93 rel. units (Fig. 6).

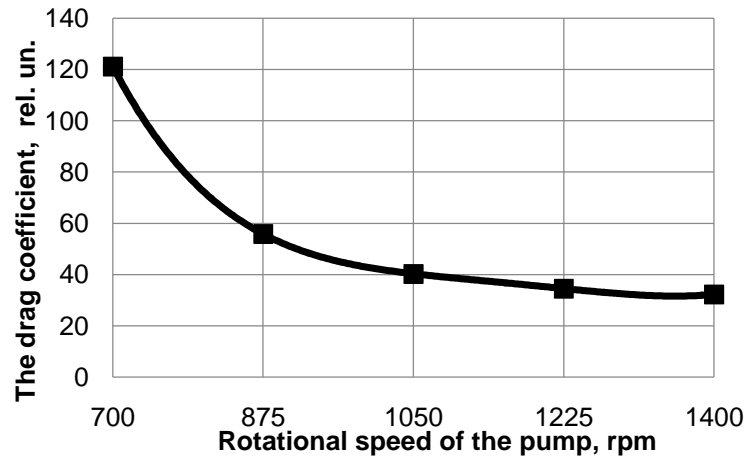


Fig. 5 - The graphical dependence of the drag coefficient on the frequency of pump rotation

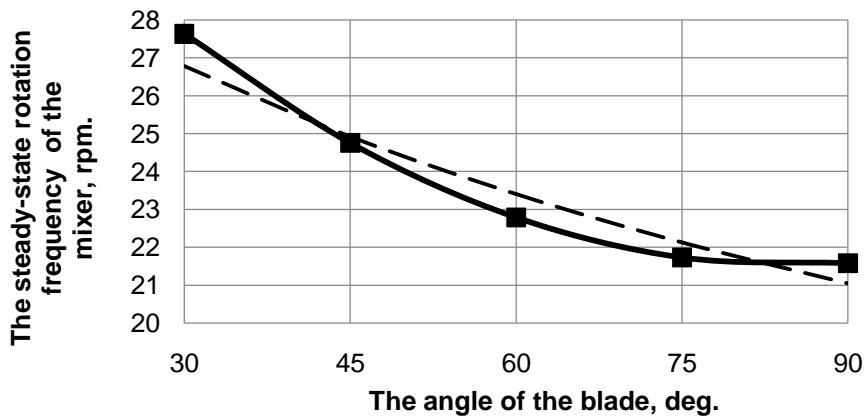


Fig. 6 - The graphical dependence of the mixer steady-state rotation frequency on the angle of the blades

..... – theoretical values; – experimental values

The proposed calculation of equipment for the production of bio-diesel gave the ability to determine the equipment design parameters (Fig. 7) for biodiesel production for agricultural needs. The use of hydro-mechanical mixer for biodiesel production allows obtaining biodiesel according to the simplified technology in agricultural production.

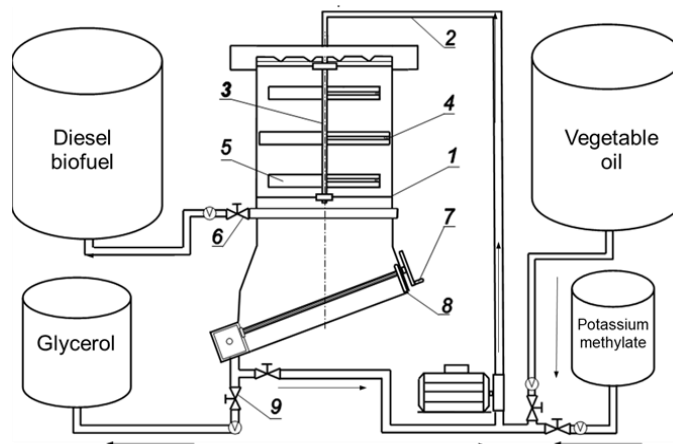


Fig.7 - Diagram of the biodiesel production plant

1 – gravity separator body; 2 – emulsion intake pipe; 3 – hydro jet mixer; 4 – atomizer; 5 – blade; 6 – bio-diesel removal cock; 7 – mechanism for glycerol precipitate removal; 8 – scraper for glycerine precipitate removal; 9 – cock for glycerine precipitate removal

CONCLUSIONS

The developed mathematical model for determining the angular velocity of rotation of hydro-mechanical mixer, depending on the pump parameters, density of vegetable oil, the actual cross-sectional area of the atomizers and their number, as well as the height and radius of the blades allows determining the dynamics of the hydro-mechanical mixer angular velocity of rotation and its steady-state value.

It is established that with increasing pump speed from 700 to 1400 rpm, the rotation frequency of hydro-mechanical mixer changes from 8.76 to 34 rpm and the steady state occurs in 0.2-0.4 sec.

On the basis of experimental studies was found the dependence of the drag coefficient of the pump rotation frequency.

The results of the conducted theoretical and experimental studies of hydro-mechanical mixer for vegetable oil and potassium methylate allowed developing the methods for engineering calculation of the mixer structural and technological parameters.

REFERENCES

- [1] Alamsyah R. Loebis H., (2014), Design and Technical Testing for Crude Biodiesel Reactor Using Dry Methods: Comparison of Energy Analysis, *Energy Procedia*, Sweden, no.47, pp.235-241, ISSN: 1876-6102;
- [2] Atadashi I.M., (2015), Purification of crude biodiesel using dry washing and membrane technologies, *Alexandria Engineering Journal*, Alexandria/Egypt, vol.54(4), pp.1265–1272, ISSN: 1110-0168;
- [3] Baskar G., Aiswarya R., (2016), Trends in catalytic production of biodiesel from various feedstocks, *Renewable and Sustainable Energy Reviews*, Netherlands, vol.57, pp.496–504, ISSN: 1364-0321;
- [4] Brásioa A., Romanenko A., Santosa L., Fernandes N., (2011), Modelling the effect of mixing in biodiesel production, Netherlands, *Bioresource Technology*, vol.102(11), pp.6508–6514, ISSN: 0960-8524;
- [5] Drahnev S., (2010), Experimental researches of technological parameters of the esterification process of vegetable oils (Експериментальні дослідження технологічних показників процесу естерифікації рослинних олій), *Scientific Bulletin of National University of Life and Environmental Sciences of Ukraine (Науковий вісник Національного університету біоресурсів і природокористування України)*, Kyiv/Ukraine, vol.144, no.3, pp.163–172, ISSN 2222-8594;
- [6] Drahnev S., Kukharets S., (2010), Verification of structural parameters of periodic reactor for esterification of vegetable oils (Обґрунтування конструктивних параметрів періодичного реактора естерифікації рослинних олій), *Scientific Bulletin of National University of Life and Environmental Sciences of Ukraine (Науковий вісник Національного університету біоресурсів і природокористування України)*, Kyiv/Ukraine, vol.144, no.4, pp.334-342, ISSN 2222-8594;
- [7] Ehsan M., Tofajjal H., (2015), Production of Biodiesel Using Alkaline Based Catalysts from Waste Cooking Oil: A Case Study, *Procedia Engineering*, vol.105, pp.638–645, ISSN: 1877-7058;
- [8] Golub G.A., Kukharets S.M., Yarosh Y.D., Kukharets V.V., (2017), Integrated use of bioenergy conversion technologies in agroecosystems, *INMATEH – Agricultural Engineering*, Bucharest/Romania, vol.51, no.1, pp.93–100, ISSN 2068–4215;
- [9] Golub G., Kukharets S., Chuba V., et al., (2017), Rationale for the parameters of equipment for production and use of biodiesel in agricultural production, *Eastern-European Journal of Enterprise Technologies*, United Arab Emirates, № 2/1(86), pp.28-33, ISSN 1729-3774;
- [10] Golub G., Kukharets S., Osipchuk O., Kukharets V., (2015), Analysis of the process of biodiesel production and justification of the main parameters of the reactor–separator (Анализ процесса получения биодизельного горючего и обоснование основных параметров реактора–разделителя), *Motrol. Commission of motorization and energetics in agriculture*, Lublin/Poland, vol.17, № 9, pp.149–155, ISSN: 1730-8658;
- [11] Golub G., Kukharets S., Osipchuk O., Pavlenko M., (2015), A study of energy efficiency of the circulating reactors-separators (Дослідження енергетичної ефективності циркуляційних реакторів-розділювачів), *Technical and technological aspects of the development and testing of new equipment and technologies for agriculture of Ukraine (Техніко-технологічні аспекти розвитку та випробування нової техніки і технологій для сільського господарства України)*, Kyiv/Ukraine, vol.19, pp.276–282, ISSN 2305-5987;

- [12] Golub G., Pavlenko M., Chuba V., Kukharets S., (2015)., The production and use of bio-diesel based on vegetable oils (Виробництво та використання дизельного біопалива на основі рослинних олій), *National University of Life and Environmental Sciences of Ukraine*, Kyiv/Ukraine, ISBN 978-617-7189-62-5;
- [13] Ivanov B., Stoyanov S., (2016), A mathematical model formulation for the design of an integrated biodiesel-petroleum diesel blends system, *Energy*, United Kingdom, vol.99, pp.221–236, ISSN: 0360-5442;
- [14] Kundu P.K., Cohen I.M., Dowling D.R., (2016), Fluid Mechanics, *Academic Press*, Boston/USA, ISBN 978-012-4059-35-1;
- [15] Mushtruk M., Sukhenko Y., Sukhenko V., (2013), The production of bio-diesel from technical animal fat (Виробництво дизельного біопалива з технічних тваринних жирів), *Engineering and technology of agroindustrial complex (Техніка та технології АПК)*, Kyiv/Ukraine, no.4(43), pp.17-20, ISSN 2306-1391;
- [16] Pavlenko M., Golub G., (2013), Energy performance of the esterification process of rapeseed oil (Енергетичні показники процесу етерифікації ріпакової олії), *Scientific Bulletin of National University of Life and Environmental Sciences of Ukraine (Науковий вісник Національного університету біоресурсів і природокористування України)*, Kyiv/Ukraine, vol.185, no.3, pp.91-100, ISSN 2222-8594;
- [17] Poppea J., Fernandez-Lafuente R., Rodriguesa R., Ayuba M., (2015), Enzymatic reactors for biodiesel synthesis: Present status and future prospects, *Biotechnology Advances*, Netherlands, no.33(5), pp.511–525), ISSN 0734-9750;
- [18] Sungwornpatansakul P., Hiroi J., Nigahara Y., et al., (2013), Enhancement of biodiesel production reaction employing the static mixing, *Fuel Processing Technology*, Netherlands, vol.116, pp.1–8, ISSN: 0378-3820;
- [19] Qiu Z., Zhao L., Weatherley L., (2010), Process intensification technologies in continuous biodiesel production, *Chemical Engineering and Processing: Process Intensification*, Netherlands, vol.49, no.4, pp.323–330, ISSN: 0255-2701;
- [20] Wulandani D., Ilham F., Fitriyan Y., et al., (2015), Hagiwara Modification of Biodiesel Reactor by using of Triple Obstacle within the Bubble Column Reactor, *Energy Procedia*, Sweden, vol.65, pp.83–89, ISSN: 1876-6102;
- [21] Xua J., Liua C., Wanga M., et al., (2017), Rotating packed bed reactor for enzymatic synthesis of biodiesel, *Bioresource Technology*, Netherlands, no.224, pp.292–297, ISSN: 0960-8524.

THE LONG-TERM ASSESSMENT OF MISCANTHUS× GIGANTHEUS CULTIVATION IN THE FOREST-STEPPE ZONE OF UKRAINE

/

БАГАТОРІЧНА ОЦІНКА ВИРОЩУВАННЯ MISCANTHUS× GIGANTHEUS У ЛІСОСТЕОВІЙ ЗОНІ УКРАЇНИ

Dr. Ph.D. Biol.Sci.Kvak V.¹⁾, Assoc. Prof. Ph.D. Biol.Sci.Stefanovska T.²⁾, Prof. Ph.D. Biol.Sci. Pidlisnyuk V.³⁾,
Ph.D. Stud. Alasmay Z.⁴⁾, Prof. Ph.D. Agri.Sci. Kharytonov M.⁵⁾

¹⁾ Institute of Bioenergy Crops and Sugar Beets of the NAAS of Ukraine ; ²⁾ National University of Life and Environmental Sciences of Ukraine; ³⁾ Jan Evangelista Purkyně University in Ústí nad Labem; ⁴⁾ Kansas State University;

⁵⁾ Dnipro State Agrarian and Economic University

Tel: 0973456227; E-mail: envteam@ukr.net

Keywords: *Miscanthus*, weather, yield, planting density, energy output, prediction

ABSTRACT

Multi-year results of research of *Miscanthus x giganteus* cultivation in several parts of Ukrainian Forest-Steppe zone: western, central, and left parts are presented. The weather conditions at four research sites, based on the meteorological data for years 2011-2015 were analysed. Two subzones of unstable and insufficient rainfall distribution were selected. The influence of climatic conditions to *Miscanthus x giganteus* production was evaluated. The equation of the regression of yield dependence on hydrothermal coefficient and planting density was calculated. It was established that the indexes of environmental conditions in observed climate zones of Ukraine varied from - 0.41 to 0.29 conventional units. The proposed approach provided the opportunity to predict the yield and energy output of *Miscanthus x giganteus* when the data of planting density are known.

РЕЗЮМЕ

Багаторічні результати досліджень вирощування *Miscanthus x giganteus* в декількох частинах лісостепової зони України: Західної, Центральної і лівій частини. Погодні умови в чотирьох науково-дослідних стаціонарах, на основі метеорологічних даних на 2011-2015 роки були проаналізовані. Були обрані дві підзони нестійкого та недостатнього розподілу опадів. Вплив кліматичних умов на вирощування *Міскантуса x giganteus* був оцінений. Рівняння регресії залежності врожайності від гідротермічного коефіцієнта і щільність посадки було розраховано. Було встановлено, що показники екологічної обстановки в спостережуваних кліматичних зонах України коливаються - від 0,41 до 0.29 умовних одиниць. Запропонований підхід надає можливість прогнозувати урожайність і вихід енергії *Miscanthus x giganteus*, коли відомі дані щільності посадки.

INTRODUCTION

The using of perennial grasses biomass and fast growing wood is increasing globally (Pyter et al, 2010; Остерка 2014; Gubišová et al, 2016). It is driven by the climate change phenomena and the obligatory goals to increase sharing of alternative energy by 20% until 2020 forced by European Union countries. Ukraine is an energy-dependent country and for resolving energy consumption issues has to replace exhaustive energy sources by renewable ones, including biomass production. The estimated sharing of renewable energy in country's total primary energy balance is expected to be 8% for year 2020 and 25% for year 2035 (Geletukha et al., 2016). The soil and climatic conditions in the main regions of Ukraine are favourable for energy crops cultivation with high level of biomass energy accumulation. The perennial grass *Miscanthus x giganteus* (M.x *giganteus*) is considered to be one of the most promising bioenergy crops. The plant is a sterile, triploid hybrid, has a C-4 photosynthetic pathway and high conversion efficiency. Besides, it has a good environmental profile with the potential to increase soil carbon, soil fertility and biodiversity, and to reduce nutrient run-off and leaching (Faber et al., 2007; Brosse et al., 2012). These crop first plantations in Ukraine were grown last decade. Since that time the planted areas with *Miscanthus* have been rapidly expanded and currently reach about 1,000 ha. Recently, the several species of herbivorous from six taxonomic orders were recorded at M.x *giganteus* (Stefanovska et al., 2017).

The study of *Miscanthus* crop economic efficiency has a practical usefulness for farmers wanting to invest in energetic crops (Vasylyeva, 2013; Velychko, 2014; Sorică, 2015). The process of achieving the high-yield of *Miscanthus* biomass requires the optimisation of the crop production technologies. In fact, the crop harvest is determined by soil and climatic conditions, planting density, the quality of planting material, soil tillage and fertilization. It is important to determine the optimal parameters of the above-mentioned factors and their interactions (Hastings et al., 2009).

The study conducted by Randall et al. (2016) at two locations in Missouri, USA was focused on assessing the rhizome quality and the soil depth from the surface to claypan affecting the establishment of the crop. Results showed a *M. x giganteus* growth potential in terms of early growth or yield and confirmed earliest obtained results (Christian et al, 2001; 2008). It was shown that propagating larger rhizomes led to the better plantation establishment. However, Randall et al (2016) did not detect the impact of claypan soils to the establishment of the crop.

Another study initiated in 2008 in Iowa, USA (Lok, 2015) was focused on identifying the management practices for *M. x giganteus* to maintain soil resources during the establishment of the crop, which included soil characteristics (soil bulk density, soil aggregate stability, and steady-state infiltration) and the percent plant cover (live plant, mulch, and bare soil). The experiment was carried out with miscanthus and four companion crops: *Secale cereal* (Rye), *Avena sativa* (Oats), *Trifolium incarnatum* (Crimson clover), and *Trifolium repens* (White clover). A little influence of cover crops on soil quality parameters through miscanthus establishment was found. It was mentioned that intermediate aggregate size fractions were the only variables that significantly responded to the addition of cover crops. Thus, the changes in these size fractions were indicative of probable belowground differences that were slowly occurring from bioenergy crop and cover crop root growth. The numerous field studies' results indicated that *M.xgiganteus* had a good tolerance to temperate climate conditions (Anderson et al., 2011).

The analysis of literary sources proved that during the vegetation period the crop required a low amount of mineral fertilizers. The average annual recommended dose of nutrients which applied in practice was the following: 60-100 kg N ha⁻¹; P 7-15 kg P ha⁻¹ and 50-130 kg K ha⁻¹ (Caslin et al., 2011). However, the data about nitrogen impact on plant's yield was rather controversy. Several studies indicated that *M.x giganteus* had the low nitrogen needs for growth. Water available for *Miscanthus* production affected responses to nitrogen. The studies on nitrogen fertilizers impact on *M.x giganteus* biomass yield and plant morphometrical characteristics (Ercoli et al., 1999; Christian & Haase, 2001; Danalatos et al., 2007; Cadoux et al., 2008; Christian et al., 2008) indicated only a little or no effect on that impact. Nitrogen fertilizers were added in the amount of 60-240 kg N ha⁻¹ in non-limiting water conditions. Other studies showed the trend of increasing *M. x giganteus* yield while fertilizing (Lewandowski and Schmidt, 2006; Cosentino et al., 2007). In that research nitrogen fertilizers were applied in ratio of 110 kg N ha⁻¹. The significant positive effect was recorded during the third year of plant's growth in limiting water conditions. The same researchers while investigating two- or three-year-old crops indicated the impact of crop age to the nitrogen properties. However, absence of nitrogen effect was observed in the mature plantation (above 10 years old) of *M.x giganteus* (Lewandowski et al. 2000; Danalatos et al. 2007; Christian et al. 2008). The recent results (Lee et al. 2017) showed that fertilization of the soil increased the yield components and contributed to *M.x giganteus* biomass production.

The annual recirculation of nutritional elements was carried out (Zub and Brancourt-Hulmel, 2010). In that research the outflow of nitrogen and other nutritional substances from the aerial to the earth parts of the plant in an autumn to spring period was monitored. It was shown that nutritional elements were being accumulated in rhizomes and after were reused during new vegetation season. The root system of the plant could penetrate deep enough and used nutritional substances from the deeper soil layers (Tuomisto et al. 2012). The features of this crop allowed providing its cultivation at the marginal lands and ensuring the sustainable energy production.

Just a few study results are available regarding the response of *M.x giganteus* production to the plant density (Danalatos et al. 2007). It was observed that biomass production improved while increasing density from 0.67 to a 1- and 2-plants m⁻².

The crop has rather good productivity when planted at the marginal agricultural (Gopalakrishnan et al. 2011) and moderately contaminated (Pidlisnyuk et al. 2014; Pidlisnyuk et al. 2016) lands. The crop cultivation is not in conflict with the food security requirements (IEA/FAO, 2017). From that stand points the determination of peculiarities of growing plant at the different arable and marginal lands in Ukraine and establishing the impact of climate conditions on the plant productivity have essential scientific and practical

interests (Zhukov and Zadorozhnaya, 2016; Zhukov et al. 2017). A large part of low-yielding, degraded or slightly heavy metals contaminated soils are located at the Forest-Steppe zone of Ukraine. Those soils are a subject to cultivation, and one of the proposed approaches can be growing *M.x giganteus* on them. The study objectives were to examine the effects of climatic/soil conditions and plant density on biomass yield during long-term *M.x giganteus* cultivation in Ukraine. The research was focused on the following main tasks:

- to evaluate impact of climatic conditions and year of growing on miscanthus yield based on calculations of the environmental conditions index (Ij).
- to learn the specificities of yield formation depending on weather conditions for the different parts of forest-steppe zone of Ukraine.
- to analyse the productivity of plant in the third year of vegetation.
- to evaluate the regression equation for the yield and energy output of plant in the third year of vegetation.

MATERIALS AND METHODS

The research was conducted at the four sites located in the following parts of the Forest-Steppe of Ukraine: A, B – Western, C – Central, D - Left part. The sites were assigned to the subzone of sufficient rainfall distribution: the fields of Borshchiv Agricultural College (A, 48°47'13.63''N, 26°02'35.92''E), Yaltushanska (B, 49°00'01.25''N, 27°27'12.12''E) and Bilotserkivska experimental breeding stations (C, 49°43'33.10''N, 30°06'15.20''E), and the subzone of insufficient humidity at Veselo-Podilska (D, 49°36'19.63''N, 33°13'32.79''E) experimental breeding station. *M. x giganteus* autumn star flower variety (the selection breeder of the variety - Institute of bioenergy crops and sugar beets) was planted annually in spring at four sites during 2011-2015 using the similar cultivation scheme. The crop was planted manually on subplots with surface of 75 m² each and the soil loosening and tilling was conducted prior to planting. Mechanical control was used to eliminate weeds. The three planting density rates used were 10, 15, 20 thousand plants ha⁻¹. The experiment was performed in three repetitions.

Sampling, observations and analysis of plant growth

The meteorological indicators: daily air-temperature and precipitation were recorded using the Guide to Agricultural Meteorological Practices (2012). The effective temperatures sum (above 10⁰ C) were calculated. Average decade/monthly meteorological indicators were compared with long-term data.

Agrochemical analysis of soil was performed before and after the experiments; easily hydrolysed nitrogen was analysed by Cornfield's method; phosphorus and potassium were analysed in accordance with Kirsanov's method (Arinushkina, 1970). Biometric characteristics were estimated by measuring plants monthly:

a) the height of the main stem was measured from the soil surface to the top of the longest leaf, and during the phase of panicles - from the base to the top;

b) the number of stems in a stand was determined by calculation of all stems.

4. The yield of dry leaf-stem mass was determined continuously throughout the season.

5. Hydrothermal coefficient (HTC) was calculated as ratio of monthly precipitation ΣP toward total temperatures same month ΣT (reduced for 10 times), $HTC = \Sigma P / 0.1 \Sigma T$

(Radzka et al. 2015).

6. The statistical analysis was performed using computer programs Excel and 'Statistica 6.0'.

The environmental conditions index was calculated using the following formula (Zykin et al., 2005):

$$I_j = \Sigma Y_{ij} / v - \Sigma \Sigma Y_{ij} / vn \quad (1)$$

where:

ΣY_{ij} – the amount of yield for the nth year of research;

$\Sigma \Sigma Y_{ij}$ – the amount of yield for all years of research;

v – the number of planting density studied indicators;

n – the number of researched years.

RESULTS

The data on the climate conditions in the research regions are presented in Table 1. The climate in the research regions is moderate continental with insignificant amplitudes of temperature fluctuations and is characterized by short mild winter, warm damp summer and sufficient precipitation.

Table 1

The climate indicators in the location of the researched plots				
Indicators	A	B	C	D
Climate	moderate continental			
The effective temperatures sum, °C	2500-2600	1942-2059	2500-2800	2600-2900
Precipitation during the vegetation period, mm	370-420	190-380	150-480	280-360
Annual precipitation, mm	570	550	538	457

In order to evaluate annual climate conditions, the index of environmental conditions (I_j) was calculated. The estimation showed that weather conditions had a significant impact on the formation of *M. x giganteus* yield. In particular, the assessment of weather conditions impact during the vegetation period showed that among all years of research, 2013 (A) was the most favourable for the production of biomass, when the environmental conditions index (I_j) was 0.26 conventional units, and the total annual sum of the index values was equal to 0.66. The year 2015 was considered the most unfavourable year, with the index values (I_j) fluctuating from (-0.05) to (-0.41), and the total sum of values was equal to -0.83 conventional units (Table 2).

Table 2

Environmental conditions index (I_j)					
Study years	A	B	C	D	Total value per year
2011	-0.23	-0.22	0.02	-0.02	-0.45
2012	0.03	0.10	-0.11	-0.05	-0.03
2013	0.26	0.18	0.21	0.01	0.66
2014	0.11	0.14	0.29	0.11	0.63
2015	-0.17	-0.20	-0.41	-0.05	-0.83

The divergences between the variants were significant at $P > 0,05$. The analysis of the impact of weather conditions during vegetation period over five years of observations showed that the Western (A, B) and Central (C) parts of the Forest-Steppe of Ukraine were characterized by more favourable and sporadic unfavourable years, while the Left part (D) showed the low amplitude of environmental conditions oscillations. The analysis of dry miscanthus biomass yield in the first year of vegetation is presented in Figure 1.

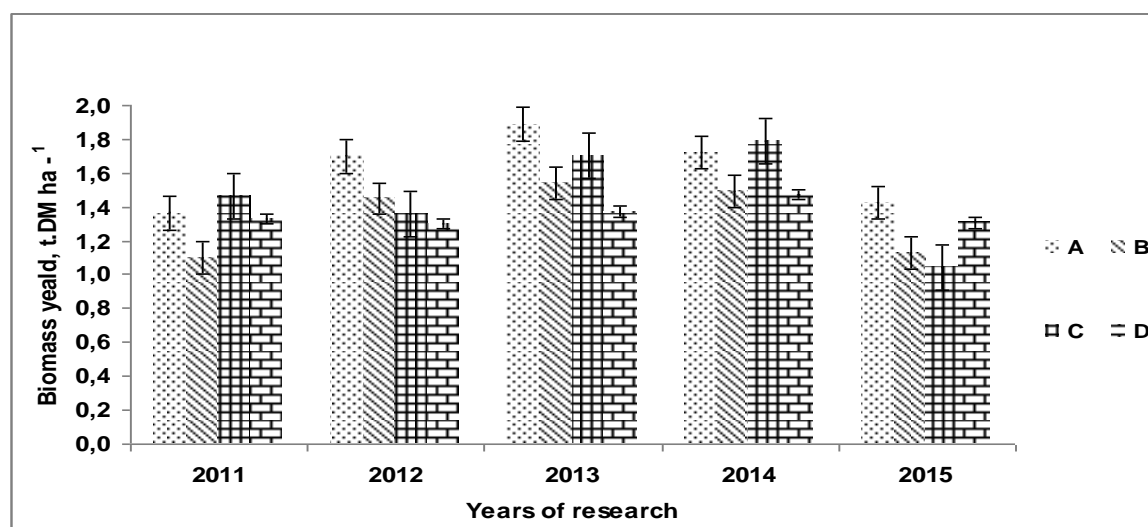


Fig. 1 - Dry Miscanthus biomass yield in the first year of vegetation

The results indicated that crop productivity varied depending on weather conditions and cultivation area. Indeed, the highest yield (1.9 ha^{-1}) was observed in 2013 (A), while the lowest (1.0 ha^{-1}) was obtained in 2015. Over the years of research, the yield of the dry biomass was mostly stable on D, the variation

coefficient for planting density of 10, 15 and 20 thousand plants ha^{-1} was 5.8; 4.6 and 2.9% respectively. The highest fluctuations of the dry biomass yield were observed on C with the variation coefficient 22.1; 18.1 and 11.7%, which were associated with the changes of weather conditions, since in this zone the environmental conditions index (Ij) reached the lowest (-0.41) and the highest (0,29) values. The comparative analysis of the impact of different precipitation and air temperature values represented by the hydrothermal coefficient on miscanthus yield formation proved the existence of the direct close correlation ($r=0.9733$), i.e. increasing of HTC led to the increased yield. In the year 2011 (A) the yield was 1.4 ha^{-1} at the HTC value equal to 0.96, in 2013 the yield was 1.9 ha^{-1} and the HTC value was 1.78 (Fig. 2).

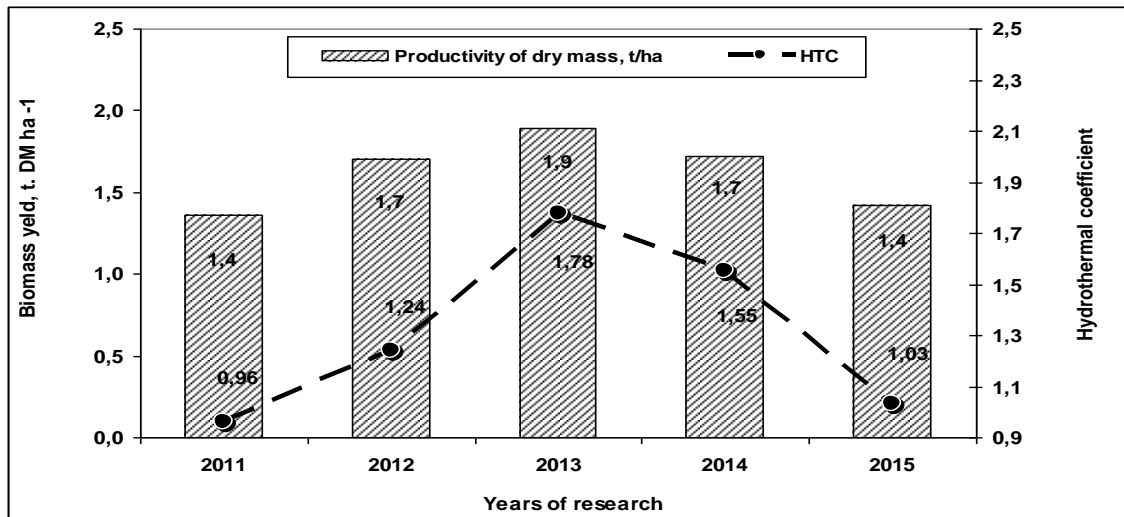


Fig. 2 - The hydrothermal coefficient and Miscanthus yield formation

Regression coefficient at the regression equation $Y = 0.619x + 0.788$ showed how many units the resulting characteristic was down. It was determined that increasing the HTC by 0.1 led to increasing the yield up to 60 kg ha^{-1} . During the first two years, the yield was insignificant and did not have a commercial value. The majority of literature data noted (Christian et al. 2008; Angelini et al. 2009; Maksimović et al. 2016) that under conditions of moderate continental climate, Miscanthus could provide a commercial yield starting from the third year of growth. The maximum yield of the dry biomass (16.3 ha^{-1}) after the third year of vegetation was obtained on field A with the planting density of 20 thousand plants ha^{-1} , whereas the lowest yield (10.4 ha^{-1}) was observed on field C with the planting density of 10 thousand plants ha^{-1} (Fig. 3).

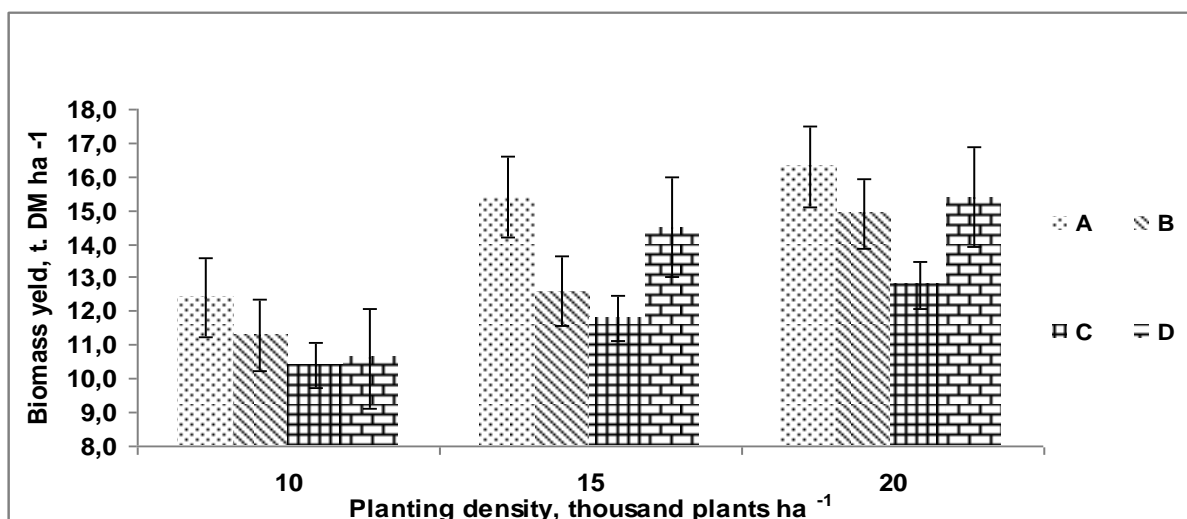


Fig. 3 – Miscanthus biomass yield dependence on planting density in fourth parts of forest-steppe zone

While analysing the yield-producing power of the dry biomass at the planting density of 15 thousand plants ha^{-1} , it can be seen that the highest value was on A, following by 14.5 ha^{-1} on D and 12.6 and 11.8 ha^{-1} on B and C, respectively. That observed order was probably due to the weather conditions. The obtained results demonstrated that the yield of *M.x giganteus* substantially differed depending on the location of the researched fields and years of cultivation. The age of plantations had a significant impact on the yield value,

and the plants themselves were very sensitive to late spring frosts and lack of soil moisture in the middle of the vegetation period. Through the current study there were no late frosts observed on the experimental fields, however, dry summers in years 2011 and 2015 led to the slow development of the aerial parts of plants which was in accordance with the published study of Maksimović *et al.*, (2016). The results presented in Fig. 4 showed that the increased plant density led to the increased yield of miscanthus biomass.

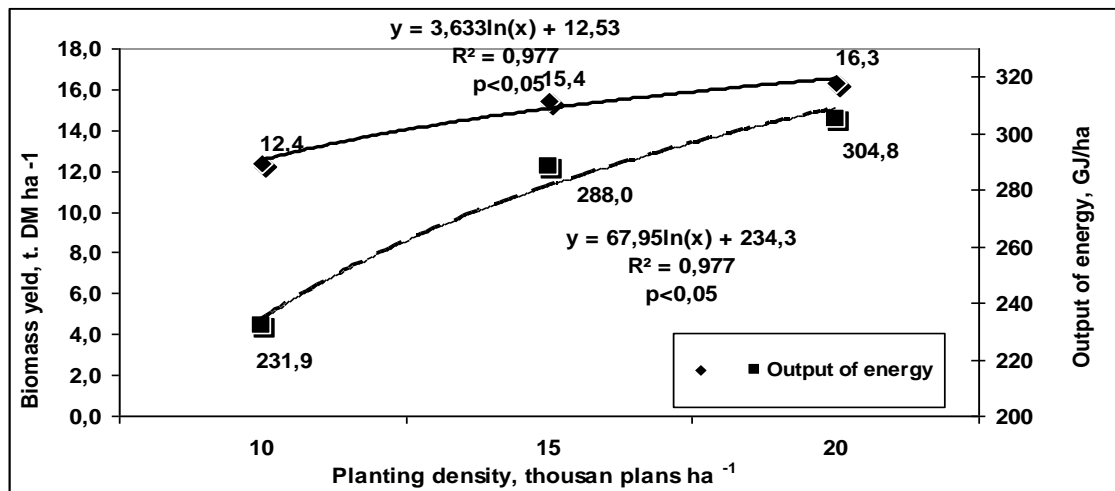


Fig. 4 - Relation between Miscanthus biomass and energy output

Therefore, the output of solid biofuel was going to increase as well. Indeed, at the planting density of 10 thousand plants ha⁻¹ the energy output equalled 231.9 gigajoule ha⁻¹, at the density of 15 thousand plants ha⁻¹ - 288.0 gigajoule ha⁻¹, at the density of 20 thousand plants ha⁻¹ - 304.8 gigajoule ha⁻¹. The highest energy output (288.0-304.8 gigajoule ha⁻¹) was observed at the planting density of 15-20 thousand plants ha⁻¹. The lowest energy output (231.9 gigajoule ha⁻¹) was registered at the planting density of 10 thousand plants ha⁻¹.

Based on the research results the following regression equation was calculated:

$$Y = 3,633 \ln(PD) + 12,53 \quad (2)$$

where Y - the yield of the dry biomass of *M.x giganteus* in the third year of vegetation, ha⁻¹; PD - planting density, thousand plants ha⁻¹; and

$$E = 67.95 \ln(PD) + 234.3 \quad (3)$$

where E - the energy output of the biomass of *M.x giganteus* in the third year of vegetation, gigajoule ha⁻¹; PD - planting density, thousand plants ha⁻¹. The proposed regression equations may be used to predict the yield and energy output when the data of planting density of *M.x giganteus* will be known for another plantation.

CONCLUSIONS

The analysis of weather conditions at the experimental plant-breeding stations during the monitoring years 2011-2015 showed that the temperature regime significantly exceeded the average long-term values for these subzones in Ukraine. Average annual precipitation was within the range of average long-term values. However, their distribution over months was random. The assessment of environmental conditions index (Ij) showed that the Western (A, B) and Central (C) parts of the Forest-Steppe of Ukraine were characterized by more favourable and sporadic unfavourable years, while the left part (D) was regarded as rather neutral, close to zero. The obtained results demonstrated that the yield of *M.x giganteus* substantially differed depending on the location and years of cultivation. The main factors of biomass formation were precipitation and average daily temperature during the vegetation period, represented by a hydrothermal coefficient (HTC). Based on the regression equation $Y = 0.619 \text{ HTC} + 0.788$ it was possible to calculate the yield of the dry biomass during the first year of vegetation. On fields A with planting density of 20 thousand plants ha⁻¹ the yield equal to 16.3 ha⁻¹ of the dry biomass was obtained. Starting from the third year of vegetation, the yield of the Miscanthus ranged from 10.4 to 16.3 ha⁻¹. The yield level also depended on planting density. Based on the data of Miscanthus yield in the third year of vegetation the equations of regression for the yield $Y = 3.633 \ln(PD) + 12.53$ and energy output $E = 67.95 \ln(PD) + 234.3$ were proposed.

These equations provided the opportunity to further predict the yield and energy output when the data of planting density will be known.

ACKNOWLEDGEMENT

The research was partly supported by NATO SPS MYP G4687.

REFERENCES

- [1] Anderson E., Arundale R., Maughan M., Oladeinde A., Wycilso A., Voigt T., (2011), Growth and agronomy of *Miscanthus x giganteus* for biomass production. *Biofuels*, vol.2, no.1, pp.71-87, DOI: 10.4155/bfs.10.80;
- [2] Angelini L.G., Ceccarini L., Di Nasso N., Bonari E., (2009), Comparison of *Arundo donax* L. and *Miscanthus x giganteus* in a long-term field experiment in Central Italy: analysis of productive characteristics and energy balance. *Biomass and Bioenergy*, vol. 33, pp.635–642;
- [3] Arinushkina E. V., (1970), *Manual on chemical analysis of soils*. 2nd ed., M.: MSU, 488 p. (Аринушкина Е.В. Руководство по химическому анализу почв. 2-е изд. М.: МГУ), 488 p;
- [4] Brosse N., Dufour A., Meng X.Z., Sun Q.N., Ragauskas A., (2012), *Miscanthus*: a fast-growing crop for biofuels and chemicals production. *Biofuels Bioproducts & Biorefining*, vol.6, no.5, pp.580-598, DOI: 10.1002/bbb.1353;
- [5] Caslin B., Finnan J., Easson, L., (2011), Crop production, *Miscanthus Best Practice Guidelines*. Teagasc and the Agri-Food and Bioscience Institute: Carlow and Hillsborough, Ireland, pp. 5–26, ISBN 1-84170-567-5;
- [6] Cadoux S., Vanderdriessche V., Machet J.M., Mary Y., B., Beaudouin N., Lemaire G., Gosse G., (2008). Potential yield and main limiting factors of *Miscanthus giganteus* in France. Identification of the needs for further research. *16th European Biomass Conference and Exhibition*, Valence, Spain, 16 p;
- [7] Christian D.G., Haase E., (2001). Agronomy of *Miscanthus*. In Jones M.&Walsh M. (Eds.) *Miscanthus for energy and fibre*, London, UK: James and James Publisher, pp. 21–45;
- [8] Christian D.G., Riche A.B., Yates N.E., (2008). Growth, yield and mineral content of *Miscanthus x giganteus* grown as a biofuel for 14 successive harvests. *Industrial Crops and Products*, vol.28, pp. 320–327;
- [9] Cosentino S.L., Patane C., Sanzone E., Copani V., Foti S., (2007). Effects of soil water content and nitrogen supply on the productivity of *Miscanthus x giganteus* Greef et Deu in a Mediterranean environment, *Ind. Crop. Prod.*, vol.25, pp. 75–88;
- [10] Danalatos N.G., Archontoulis S.V., Mitsios I. (2007). Potential growth and biomass productivity of *Miscanthus x giganteus* as determined by plant density and N-fertilization in Central Greece, In *Biomass Bioenergy*. vol. 31, pp. 145–152;
- [11] Ercoli L., Mariotti M., Masoni A., Bonari E., (1999). Effect of irrigation and nitrogen fertilization on biomass yield and efficiency of energy use in crop production of *Miscanthus*, *Field Crop. Res.*, vol.63, pp. 3–11;
- [12] Faber A., Stasiak M., Kuś J., (2007). Preliminary estimation of the productivity of chosen species of energy plants. *Postępy w Ochronie Roślin*, vol.47, pp. 339-346 (in Polish);
- [13] Geletukha G., Zheliezna T., Tryboi, O., Bashtovyi A., (2016). Analysis of criteria for the sustainable development of bioenergy. *UABio Position Paper*, vol.17, 30 p;
- [14] Gopalakrishnan G., Negri M.C., Snyder S.W., (2011). A novel framework to classify marginal land for sustainable biomass feedstock production. *Journal of Environmental Quality*, vol. 40, no. 5, pp.1593-1600. DOI: 10.2134/jeq2010.0539;
- [15] Gubišová M., Gubiš J., Žofajová A., (2016). Biomass production of gigantic grasses *Arundo donax* and *Miscanthus x giganteus* in the dependence on plant multiplication method. *Agriculture (Polnohospodárstvo)*, vol. 62, no. 2, pp. 43-45. DOI: 10.1515/agri-2016-0005;
- [16] Hastings A., Clifton-Brown J.C., Wattenbach M., Mitchell C.P., Smith P., (2009). The development of MISCANFOR, a new *Miscanthus* crop growth model: towards more robust yield predictions under different climatic and soil conditions. *Glob. Change Biol. Bioenergy*, vol.1, pp.154–170;
- [17] Lee M.S., Wycislo A., Guo J., Lee D.K., Voigt T., (2017). Nitrogen fertilization effects on biomass production and yield components of *Miscanthus x giganteus*. *Front Plant Sci.*, vol.8, article 544, 9 pp.;
- [18] Lewandowski I., Clifton-Brown J.C., Scurlock J.M.O., Huisman W., (2000). *Miscanthus*: European experience with a novel energy crop. *Biomass Bioenergy*, vol. 19, pp. 209-227;

- [19] Lewandowski I., Schmidt U., (2006), Nitrogen, energy and land use efficiencies of miscanthus, reed canary grass and triticale as determined by the boundary line approach. *Agr. Ecosyst. Environ.*, vol. 112, pp. 335–346;
- [20] Lok J.Y.J., (2015). Cover crop impacts on soil quality during *Miscanthus x giganteus* establishment in central Iowa (Order No. 10009252). Available from ProQuest Dissertations & Theses Global. (1765429241). <http://search.proquest.com.er.lib.k-state.edu/docview/1765429241?accountid=11789>;
- [21] Maksimović J., Pivić R., Stanojković-Sebić, A., Vučić-Kišgeci M., Kresović B., Dinić Z., Glamočlija D., (2016). Planting density impact on weed infestation and the yield of *Miscanthus* grown on two soil types. *Plant Soil Environ.*, vol. 62, no.8, pp. 384–388;
- [22] Otepka P. Eds., (2014) *Guidebook on Local Bioenergy Supply Based on Woody Biomass*. USA: Scientific & Academic Publishing, 145 p. ISBN 978-1-938681-99-8;
- [23] Pidlisnyuk V., Stefanovska T., Lewis E.E., Erickson L.E., Davis L.C., (2014). *Miscanthus* as a productive biofuel crop for phytoremediation. *Critical Reviews in Plant Sciences*. vol.33, no.1, pp.1-19. DOI: 10.1080/07352689.2014.847616;
- [24] Pidlisnyuk V., Trögl J., Stefanovska T., Shapoval P., Erickson L., (2016). Preliminary results on growing second generation biofuel crop *miscanthus x giganteus* on the polluted military site in Ukraine. *Nova Biotechnologica et Chimica*, vol.15, no.1, pp.77-84. DOI: 10.1515/nbec-2016-0008;
- [25] Pyter R.J., Dohleman F.G., Voigt T.B., (2010). Effects of rhizome size, depth of planting and cold storage on *Miscanthus x giganteus* establishment in Midwestern USA. *Biomass and Bioenergy*, vol.34, no.10, pp.1466-1470. DOI: 10.1016/j.biombioe.2010.04.014;
- [26] Radzka E., Rymuza K., Lenartowicz T., (2015). Analysis of hydrothermal conditions and their impact on early potato yields. In *Journal of Ecological Engineering*, vol.16, no.2, pp.120-124;
- [27] Randall B.K., Yost M.A., Kitchen N.R., Heaton E.A., Stelzer H.E., Thompson A.L., (2016). Impact of rhizome quality on *miscanthus* establishment in claypan soil landscapes. *Industrial Crops and Products*, vol.85, pp. 331–340. DOI:10.1016/j.indcrop.2015.12.040;
- [28] Sorică E., (2015), Analysis of profitability of implementing the *miscanthus* energetic crop technology for rhizomes capitalization. *INMATEH Agricultural engineering*, Vol.46, No.2, pp.155-164;
- [29] Stefanovska T., Pidlisnyuk V., Lewis E., Gorbatenko A., (2017), Herbivorous insects' diversity at *Miscanthus x giganteus* in Ukraine. *Agriculture (Pol'nohospodárstvo)*, vol. 63, no.1, pp. 23-32. DOI: 10.1515/agri-2017-0003;
- [30] Tuomisto H.L., Hodge I.D., Riordan, P., Macdonald D.W., (2012). Comparing energy balances, greenhouse gas balances and biodiversity impacts of contrasting farming systems with alternative land uses. *UK: Agricultural Systems*, vol. 108, pp. 42-49;
- [31] Vasylieva N. K., (2013), Forecasting of prices in the field of crops-growing in Ukraine and regions, *Economic Annals-XXI*, no.11–12 (2), pp.26-29;
- [32] Velychko, O., (2014), Fundamental basis and connection of modern entrepreneurial logistics and SCM, *Review of European Studies*, Vol. 6, No. 4, pp. 135-146;
- [33] Zhukov, O., Kunah, O., Dubinina, Y., Ganga, D., Zadorozhnaya, G. (2017). Phylogenetic diversity of plant metacommunity of the Dnieper river arena terrace within the "Dnieper-Orilskiy" nature reserve. *Ekológia (Bratislava)*. 36 (4), pp. 352–365. DOI:10.1515/eko-2017-0028
- [34] Zhukov, A., Zadorozhnaya, G. (2016). Spatial heterogeneity of mechanical impedance of a typical chernozem: the ecological approach. *Ekológia (Bratislava)*. 35, pp.263–278;
- [35] Zub H.W., Brancourt-Hulmel M., (2010), Agronomic and physiological performances of different species of *Miscanthus*, a major energy crop. A review. *Agron. Sustain Dev.*, vol. 30(2), pp. 201-214. DOI:10.1051/agro/2009034;
- [36] Zykina V.A., Belan I.A., Yusov V.S., (2005). A method for calculating and evaluating the parameters of ecological plasticity in agricultural plants. *Ufa: Bashkir State University Publishing House*, 100 p;
- [37] *** *Agricultural Meteorological Practices: Guide*, (2012). WMO, no.134, Pub Med database on the World Wide Web: http://www.wmo.int/pages/prog/wcp/agm/gamp/documents/WMO_No134_en.pdf;
- [38] *** IEA/FAO. (2017). How to guide for Bioenergy Road map development and implementation. <https://www.iea.org/publications/freepublications/publication/How2GuideforBioenergyRoadmapDevelopmentandImplementation.pdf>.

OPTIMIZATION OF THE WORKING PERFORMANCE OF HALF-FEEDING PEANUT PICKING DEVICE BASED ON RESPONSE SURFACE METHODOLOGY

基于响应曲面法的半喂入式花生摘果装置作业性能优化

Prof. Ph.D. Hu Z.C.^{*1)}, Prof. Ph.D. LV X.L.²⁾, A.Prof. M.S. Peng B.L.¹⁾,
A.Prof. M.S. Wu F.¹⁾, M.S. Yu Z.Y.¹⁾

¹⁾ Nanjing Research Institute for Agricultural Mechanization Ministry of Agriculture, Nanjing/China

²⁾ Colleges of Machinery and Automotive Engineering, Chuzhou University Anhui/China

Tel: 862584346246; E-mail: nfzhongzi@163.com

Keywords: response surface methodology, picking performance, regression model, parameter optimization

ABSTRACT

The paper researches the effect of structure and operation parameters of the self-developed half-feeding peanut picking device on the picking performance by response surface methodology. Through the response surface optimization test and design principle of Box-Behnken, the cylinder length, roller diameter, the overlap distance of outlet end, the roller speed and the clamping conveying speed are taken as factors; the synthetic weighted mark method is used to obtain the response value that taking the comprehensive index determined by the picking rate of the peanut pods as the test. The paper also makes response surface analysis to the effect of different factor level on the comprehensive index. The quadratic polynomial regression model of each factor to the effect of the comprehensive index is established. The factors are optimized and the optimization results are tested through the picking experiment. The experiment results show that when the picking roller length is 875mm, the roller diameter is 158mm, the overlap distance of roller outlet is 5.6mm, the rotational speed of picking is 302rpm and the clamping conveying speed is 1.1m/s, which is the optimal parameter combination. The quadratic polynomial regression model established can reflect the effect of each index on the working performance optimally. The optimization results based on the quadratic polynomial regression model are consistent with the actual operation. The research provides a technical basis for the improvement of peanut harvesting machinery.

摘要

采用响应曲面法,对自行研制的半喂入式花生摘果装置的结构及作业参数对摘果性能的影响进行了研究。通过响应曲面优化试验,根据 Box-Behnken 试验设计原理,以摘果筒长度、滚筒直径、出口端重叠距离、滚筒转速以及夹持输送速度为因素,采用综合加权评分法获得的由花生荚果摘净率、破碎率确定的综合指标为试验的响应值,对各因素不同水平对综合指标的影响进行响应面试验分析,建立了各因素对综合指标影响的二次多项式回归模型,并对各因素进行了优化,通过摘果试验对优化结果进行了检验。试验结果表明:当摘果辊长度 875mm,辊筒直径 158mm,辊筒出口端重叠距离 5.6mm,摘果辊转速 302rpm,夹持输送速度 1.1m/s 为各因素的最佳参数组合。建立的二次多项式回归模型能较好地反映各参数对作业性能的影响,基于二次多项式回归模型的优化结果与实际作业效果相符,研究为花生收获机械的改进提供了技术依据。

INTRODUCTION

The overall level of peanut harvesting mechanization is low in China. How to improve the level of peanut harvesting mechanization is a big problem faced by the peanut industry in China (Lü X.L. et al, 2012). The half-feeding picking is suitable for dry and wet peanuts, which effectively promotes the marketing time of fresh peanuts in advance. At present, the half-feeding peanut picking device is in the development stage, there are still many problems in the operation process (Lü X.L. et al, 2014; Hu Z.C. et al, 2012; Xu J.K. et al, 2014; Nuti R.C. et al, 2010; Guan M. et al, 2015). Response surface methodology (RSM) is a global function relationship synthesizing test design and mathematical modeling through local experiment to return fitting factor and results. Compared with the traditional optimization test methods, the test group needed by RSM is relatively small, which can use the most economical way and least time to study the experiment comprehensively. It has been widely used in various industries now (Ambati P. and Ayyanna C., 2001; Hu Z.W. et al, 2016; Lee W.C. et al, 2006; Arzu Y. and Adnan D., 2007; Hou X.M. et al, 2013; Zhao H.M. et al,

2011). The paper uses the Box-Behnken pattern of RSM in the Design-Expert to study the effect of half-feeding picking device structure and operation parameters on the picking performance.

MATERIALS AND METHODS

• **Test materials and methods**

The test selects self-developed half-feeding peanut picking device to test the picking performance, as shown in Fig.1. The picking object is spring planting peanuts and the variety is “TaiHua four”. In the experiment, the peanut vines are dug artificially. Twenty plants are fed continuously and uniformly in each test, repeating three times to take the average value of the results. The paper refers to Peanut picker operation quality of Agricultural Industry Standard of the People's Republic of China (NY/T 993-2006) to calculate picking rate and damage rate. The calculation method of each detection index is as follows:

$$\text{Picking rate} = 100\% \times (1 - \text{weight of unpicking}) / (\text{weight of unpicking} + \text{weight of damage} + \text{weight of good})$$

$$\text{Damage rate} = 100\% \times \text{weight of damage} / (\text{weight of unpicking} + \text{weight of damage} + \text{weight of good})$$



Fig.1 - Structure diagram of the peanut picking device

• **Test plan design**

According to the design principle of Box-Behnken (GUO Y et al, 2017), the paper makes response surface test analysis on the picking roller length *L*, the roller diameter *D*, the overlap distance of outlet end *C*, the roller speed *n* and clamping conveying speed *V* in five factors and three levels. These factors are marked as *X*₁- *X*₅, and the test factor codes and level is shown in Table 1. The independent variable coding is calculated according to the following transformation formula:

$$x_i = (X_i - X_{i0}) / \Delta X_i \tag{1}$$

Where, *x*_{*i*} is the code value of independent variable *X*_{*i*}; *X*_{*i0*} is the value of the independent variable *X*_{*i*} in the centre; ΔX_i is the change step of independent variable.

Table 1

Factors level and code of response surface analysis				
Factor	coding	Non- coding	Coding value	level
<i>L</i> /mm	<i>x</i> ₁	<i>X</i> ₁	-1	600
			0	900
			1	1200
<i>D</i> /mm	<i>x</i> ₂	<i>X</i> ₂	-1	150
			0	200
			1	250
<i>C</i> /mm	<i>x</i> ₃	<i>X</i> ₃	-1	5
			0	10
			1	15
<i>n</i> /rpm	<i>x</i> ₄	<i>X</i> ₄	-1	200
			0	350
			1	500

Factor	coding	Non- coding	Coding value	level
V/ m·s ⁻¹	x ₅	X ₅	-1	0.5
			0	1.0
			1	1.5

In order to balance the impact of picking rate and damage rate, the comprehensive indicator determined by synthetic weighted mark method is adopted as the response value of the response surface test. When the comprehensive indexes are determined, according to the importance of each indicator, the total “weight” number is 1 (Wang X.Y. et al, 2008), the damage rate is 50% and the picking rate is 50%. On account of the opposite effect of the damage rate and picking rate on picking quality, the damage rate is negative when the comprehensive indicators are calculated. Additionally, in order to eliminate the effect of difference data measurement scale when the comprehensive marking index is calculated, the calculation is introduced into the average value of each unit data. The comprehensive indicator of each group is expressed as:

$$y_i = \sum_{j=1}^r W_j \frac{y_{ij}}{\bar{y}_j} \quad (2)$$

Where, y_i is the calculation value (weighted score index) obtained by the i test; W_j is the “weight” of the j index; y_{ij} is the j index of the i test; r is the number of factors affecting comprehensive index; \bar{y}_j is the average value the j index in the group of tests.

RESULTS

• Analysis scheme and test results of the response surface

The test is made on the picking test bed according to the response surface. The multiple quadratic regression equation between the factors and response value is established through multiple quadratic regression method. The response surface between response value and variable is used for function analysis. The correlation between the factor and response surface, and the relationship between factors are studied. The response value is optimized for achieving the optimal value with factors combination in the whole region. This test consists of six central point repeat and needs 46 tests, experiment scheme and test results of the response surface are shown in Table 2.

Table 2

Design and results of RSM experimental schemes

Test groups	Variable coding					Response values
	X ₁	X ₂	X ₃	X ₄	X ₅	Composite index Y
1	0	0	-1	-1	0	0.35
2	0	-1	0	1	0	-0.59
3	0	0	0	0	0	0.17
4	0	0	-1	0	1	0.22
5	-1	0	1	0	0	-0.03
6	-1	0	0	-1	0	0.29
7	0	0	0	1	-1	-0.81
8	-1	0	-1	0	0	0.19
9	0	1	1	0	0	0.08
10	1	0	-1	0	0	0.25
11	0	1	0	0	-1	0.17
12	0	0	1	0	1	0.05
13	1	0	0	0	1	0.22
14	-1	-1	0	0	0	0.22
15	0	0	0	0	0	0.17
16	0	0	-1	0	-1	0.14
17	0	0	0	1	1	-0.73
18	0	1	0	0	1	0.14
19	0	0	-1	1	0	-0.64
20	0	0	0	0	0	0.19
21	0	-1	1	0	0	-0.08
22	0	-1	0	-1	0	0.37
23	1	0	1	0	0	0.14

Test groups	Variable coding					Response values
	X ₁	X ₂	X ₃	X ₄	X ₅	Composite index Y
24	1	-1	0	0	0	0.25
25	0	-1	-1	0	0	0.25
26	-1	1	0	0	0	0.08
27	0	1	-1	0	0	0.19
28	0	0	0	-1	-1	0.32
29	0	1	0	-1	0	0.19
30	0	-1	0	0	-1	0.22
31	-1	0	0	0	1	0.11
32	0	1	0	1	0	-1.56
33	0	0	1	-1	0	0.26
34	1	0	0	-1	0	0.33
35	0	0	1	1	0	-1.20
36	1	1	0	0	0	0.11
37	-1	0	0	0	-1	0.14
38	0	0	0	-1	1	0.28
39	0	0	0	0	0	0.17
40	0	0	0	0	0	0.17
41	-1	0	0	1	0	-0.78
42	1	0	0	1	0	-0.75
43	0	-1	0	0	1	0.25
44	0	0	1	0	-1	0.08
45	0	0	0	0	0	0.22
46	1	0	0	0	-1	0.17

• **Picking performance test analysis and the establishment of regression equations**

Design-Expert is used to obtain the response surface model of comprehensive index Y through multiple regressions fitting for the test results, and makes variance analysis on the quadratic equation of the response surface model; it also makes significant testing to the regression equation coefficient. Making regression analysis on the test data in Tab.2, the full-factor quadratic regression model of the comprehensive indicator coding space of the picking is specific to:

$$\begin{aligned}
 Y = & 0.1806 - 0.0316X_1 - 0.0929X_2 - 0.1031X_3 - 0.5905X_4 + 0.0068X_5 - 0.0006X_1X_2 \\
 & + 0.0277X_1X_3 - 0.0029X_1X_4 + 0.0215X_1X_5 + 0.0551X_2X_3 - 0.1969X_2X_4 \\
 & - 0.0138X_2X_5 - 0.1181X_3X_4 - 0.0278X_3X_5 + 0.0302X_4X_5 + 0.0101X_1^2 \\
 & - 0.0428X_2^2 - 0.0453X_3^2 - 0.4558X_4^2 + 0.0145X_5^2
 \end{aligned} \quad (3)$$

The variance analysis of quadratic regression equation model of the comprehensive index for picking (shown in Table 3) shows that the response surface model is significant ($P < 0.001$) with optimal fitting degree. The determination coefficient R^2 of the model is 0.957; the adjustment determination coefficient R_{adj}^2 is 0.9227, which indicates that the credibility and precision of the model is high. From the significance test and analysis of regression coefficient (shown in Table 4), it is known that one degree term X_4 and quadratic term X_4^2 of the roller speed n has an extremely significant influence on the comprehensive indicator of picking. The effect of roller diameter D , the overlap distance C of outlet end and the interactive items (X_2, X_3, X_2X_4) between the roller diameter D and roller speed n on the comprehensive index of picking is quite significant. Picking roller length L and clamping conveying speed V has little influence on the comprehensive index of picking.

Table 3

Variance analysis of quadratic regression equation model Y					
source of variation	Sum of squares	degree of freedom	mean square	Value of F	significance
Model	8.2598	20	0.4130	27.8479	< 0.0001
residual	0.3708	25	0.0148		
error	0.0027	5	0.0005		
total	8.6305	45			
$R^2=95.70\%$					
$R_{adj}^2=92.27\%$					

Table 4

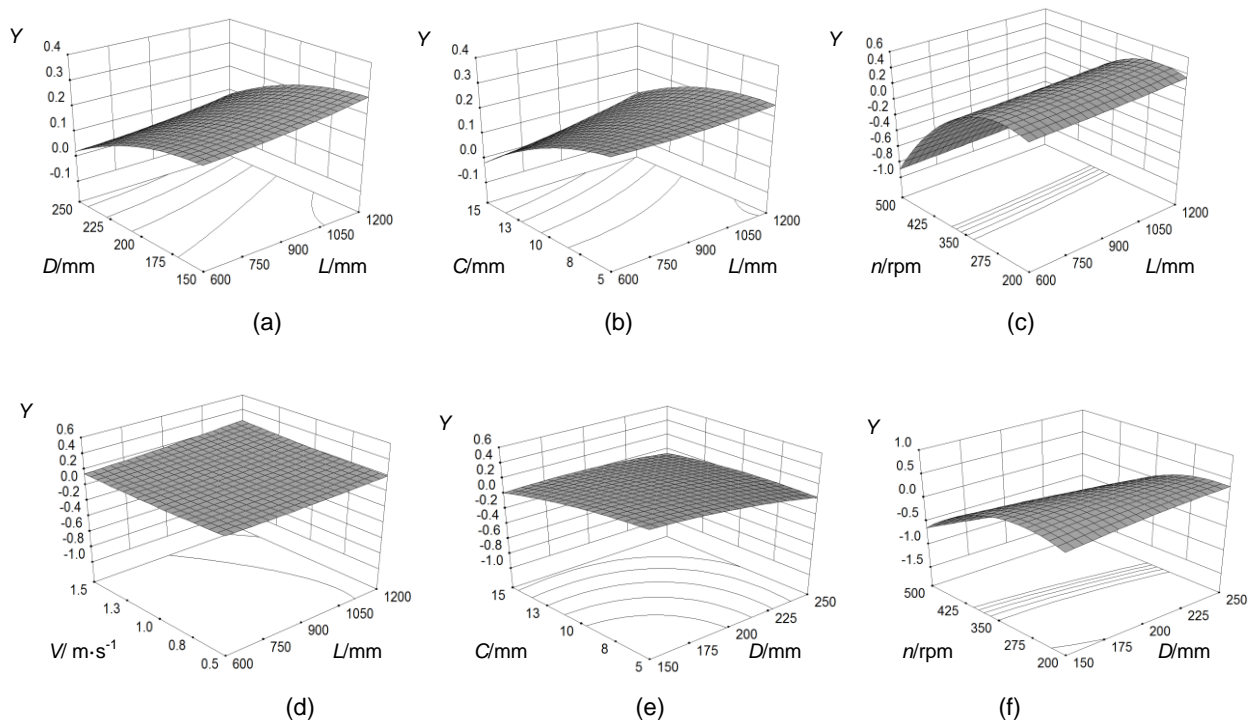
Regression coefficient Y and its significant test

No.	source of variation	regression coefficient	standard error	Value of F	Value of significance P
1	constant term	0.1806	0.0497		
2	X_1	0.0316	0.0304	1.0773	0.3092
3	X_2	-0.0929	0.0304	9.3032	0.0054
4	X_3	-0.1031	0.0304	11.4580	0.0024
5	X_4	-0.5905	0.0304	376.1623	< 0.0001
6	X_5	0.0068	0.0304	0.0494	0.8260
7	$X_1 X_2$	-0.0006	0.0609	0.0001	0.9918
8	$X_1 X_3$	0.0277	0.0609	0.2068	0.6532
9	$X_1 X_4$	-0.0029	0.0609	0.0023	0.9621
10	$X_1 X_5$	0.0215	0.0609	0.1243	0.7274
11	$X_2 X_3$	0.0551	0.0609	0.8198	0.3739
12	$X_2 X_4$	-0.1969	0.0609	10.4570	0.0034
13	$X_2 X_5$	-0.0138	0.0609	0.0517	0.8220
14	$X_3 X_4$	-0.1181	0.0609	3.7645	0.0637
15	$X_3 X_5$	-0.0278	0.0609	0.2088	0.6517
16	$X_4 X_5$	0.0302	0.0609	0.2466	0.6238
17	X_1^2	0.0101	0.0412	0.0599	0.8087
18	X_2^2	-0.0428	0.0412	1.0780	0.3091
19	X_3^2	-0.0453	0.0412	1.2075	0.2823
20	X_4^2	-0.4558	0.0412	122.2492	< 0.0001
21	X_5^2	0.0145	0.0412	0.1236	0.7281

Note: $p < 0.001$ (extremely significant), $p < 0.01$ (quite significant), $p < 0.05$ (significant)

• **Response surface interaction analysis**

The multiple quadratic regression equation can obtain the response surface of picking factors on the interaction of comprehensive index, as shown in Fig.2.



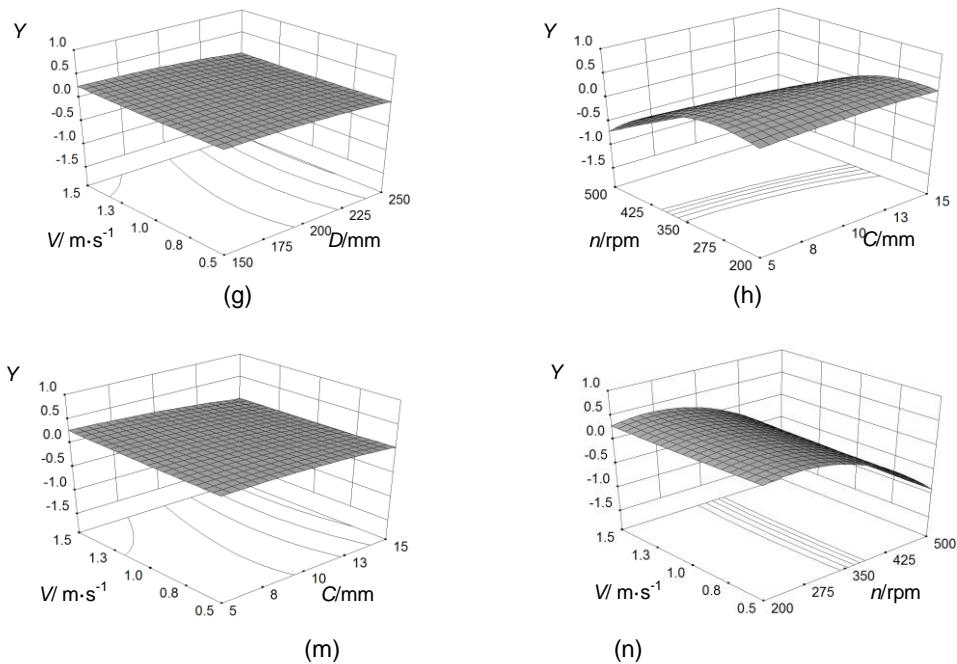


Fig. 2 - The response surface of the interaction of various factors to the comprehensive index

It can be known from Fig.2 and combining the p value of each coefficient that the influence of each factor on picking effect is respectively as the roller speed, the overlap distance of outlet end, the roller diameter, the picking roller length and clamping conveying speed. Improvement of the roller speed increases the picking force and frequency, the larger of picking revolving speed n and the quicker of picking leaf speed, the higher of the picking strength and the higher of picking frequency; the hitting number of picking leave on the peanut pods is more frequently in the same time. The picking rate is gradually increasing with improvement of the roller speed; the growth rate form fast to slow, and the damage rate is also increasing. The growth rate is from slow to fast; the picking rate reaches the maximum without change when the roller speed exceeds a certain limit value and the damage rate increases significantly, reflecting the comprehensive that it increases first and then decreases. With the increase of the roller diameter D and the overlap distance C of outlet end, the larger of the volume of empty picking area, in the whole channel trip from the entrance end to the outlet end, the volume of empty picking area crossed by peanuts. The larger is the available picking area, the better is the effect of picking. The residual space of the blades with staggered configurations of two roller decreases; the damage rate increases and the comprehensive index decreases. With the increase of picking roller length L , the staying time of peanuts in picking is longer, and the hitting time increases. Picking rate and damage rate are both increased, and the comprehensive index has a certain increase and the impact is not obvious. With the increase of clamping conveying speed V , the smaller the time of peanut staying in the picking is, the lower is the picking frequency, and the picking rate and damage rate both decrease. The comprehensive index c has certain decrease, but not an obvious one. In the model, the interaction of the two groups on the comprehensive index is shown in Fig.2. With the increase of roller speed and diameter, the picking rate and damage rate both increase significantly, and the comprehensive index shows a downward trend. As the overlap distance of outlet end and the roller speed is greater, the picking rate and damage rate both increase significantly. The smaller of the comprehensive index, the effect of other interactions on the comprehensive index is small. From the optimized regression model, the interaction of X_2X_4 is quite significant in the model, which indicates that there is interaction between the roller speed and the roller diameter.

- **Optimization of the picking condition and test of the regression model**

The optimization solver of Design Expert is to optimize and solve the above established multiple quadratic regression models, determining the optimal value of the corresponding factors when the comprehensive index Y is the maximum. Where, the selection of clamping conveying speed area needs to consider the productivity of the combined harvester. The suitable walking speed is 0.8-1m/s and the clamping conveying speed is 0.9-1.2m/s when the machine harvests in the field. The optimal parameter combination obtained by optimizing is that the picking roller length is 875mm, the roller diameter is 158mm,

the overlap distance of outlet end is 5.6mm, the roller speed is 302rpm, the clamping conveying speed is 1.1m/s, and the comprehensive index is 0.3731 at this moment. Because the optimal parameter combination obtained by optimizing does not present in the test of the response surface design scheme, the optimization result and prediction model is verified. Three repeated experiments for the optimized parameters combination on the picking test bed are made and the comprehensive index is measured as 0.3238. On account of the small theoretical optimal value and the verification value of Y solved by quadratic regression model, the difference can be ignored in practice. Thus, it is feasible to adopt the optimal combination in the design of machine tool.

CONCLUSIONS

The paper uses Box–Behnken model of the response surface method utilizing Design-Expert software to test the performance of the developed picking device. The weighted mark method is adopted to determine the comprehensive index of damage rate and picking rate. The multiple quadratic polynomial model is established. The paper also uses the response surface of the model to discuss the key factors and its interaction affecting picking performance. The research results show that the influence of each factor on picking effect is respectively as the roller speed, the overlap distance of outlet end, the roller diameter, the picking roller length and clamping conveying speed. With the increase of roller speed and roller diameter, the comprehensive index shows a downward trend. The larger is the roller speed and the overlap distance of outlet end, the smaller is the comprehensive index. The influence of other interactions on the comprehensive index is little. It can be seen from the optimization regression model that there is a significant interaction effect between the roller speed and roller diameter. By optimizing the combination parameters of the picking factors, the optimal combination obtained is that the picking roller length is 875 mm, the roller diameter is 158 mm, the overlap distance of outlet end is 5.6 mm, the roller speed is 302 rpm and the clamping conveying speed is 1.1m/s. The experimental results show that the theoretical optimization value is consistent with the verification value basically and it is feasible to design the test scheme and optimize its structure and operation parameters using the response surface method. It has a guiding role for the development of peanut harvesting machinery.

ACKNOWLEDGEMENT

The study was supported by the National Natural Science Foundation of China (51375247), the Key Laboratory of Modern Agricultural Equipment, Ministry of Agriculture, P.R.China (201602002) and Excellent Talents Training Program by the Ministry of Education (gxfx2017125).

REFERENCES

- [1] Ambati P, Ayyanna C., (2001), Optimizing medium constituents and fermentation conditions for citric acid production from palmyra jaggery using response surface method. *World Journal of Micro-biology & Biotechnology*, vol.17 (4), pp.331- 335;
- [2] Arzu Y, Adnan D., (2007), Optimization of the seed spacing uniformity performance of a vacuum-type precision seeder using response surface methodology. *Biosystems Engineering*, vol.97(3), pp.347-356;
- [3] Guan Meng, Zhao Baoquan, Gao Lianxing et al., (2015), Effect of curing time on moisture content and mechanical properties of peanut pods. *International Agricultural Engineering Journal*, vol.24(2), pp.1-8;
- [4] GUO Ying, CHEN Honghan, ZHANG Huanzhen et al., (2017), Optimization of Fenton pre-treatment of high concentration dye intermediate wastewater based on box-behnken response surface methodology. *Research of Environmental Sciences*, vol.30(5), pp.775-783;
- [5] Hou X M, Li L X, Zhang Z.F. et al., (2013), Optimization of extraction process by response surface methodology and antioxidant activity, *Journal of Food Science*, vol.34(6), pp.124-128;
- [6] Hu Zhichao, Wang Haiou, Peng Baoliang et al., (2012), Optimized design and experiment on semi-feeding peanut picking device. *Transactions of the Chinese Society for Agricultural Machinery*, vol.43(Supp.), pp.131-136;
- [7] Hu Ziwu, Ma Wenpeng, Xing Jinlong, Lai Qinghui, (2016), Performance test of cell wheel not ginseng precision seeding apparatus based on response surface methodology. *Journal of South China Agricultural University*, vol.37(5), pp.109-116.
- [8] Lee W.C., Yusof S., Hamid N.S.A. et al., (2006), Optimizing conditions for enzymatic clarification of banana juice using response surface methodology. *Journal of Food Engineering*, vol.73(1), pp.55-63;

- [9] Lü X.L., Hu Z.C., Peng B.L., (2014), Analysis and Research on the Picking Roller of the Half-feed Peanut Combine Harvester. *Applied Mechanics and Materials*, Vol. 597, pp.502-506.
- [10] Lü X L, Wang H.O., Zhang H.J. et al. (2012), Present Situation and Analysis on Peanut Picking Technology and Equipment. *Hubei Agricultural Sciences*, vol.51(18), pp.4116-4118;
- [11] Nuti R C, Holbrook C.C, Culbreath A., (2010), Peanut peg strength and post-harvest pod scavenging for full phenotypic yield over digging date and variety. *American Peanut Research and Education Society*, vol.42, pp.95-96;
- [12] Wang Xiaoyan, Liang Jie, Shang Shuqi et al., (2008), Design and experiment of half-feeding type peanut picker. *Transactions of the Chinese Society for Agricultural Engineering*, vol.24(9), pp.94-98;
- [13] XU Jikang, Yang Ranbing, Li Ruichuan et al., (2014), Design and experiment of film removing and peanut picking device for half feeding harvester. *Transactions of the Chinese Society for Agricultural Machinery*, vol.45(Supp.), pp.88- 93;
- [14] Zhao H M, Sun J, Xie C Y., (2011), The response surface optimization ultrasonic extraction technology of Hericium polysaccharide. *Farm Prod. Process.* vol.11, pp.73-77.

RESEARCH ON THE PHOTOELECTRONIC SEPARATOR SEED SUPPLY BLOCK FOR OIL CROPS

/

ДОСЛІДЖЕННЯ БЛОКА ПОДАЧІ ФОТОЕЛЕКТРОННОГО СЕПАРАТОРА НАСІННЯ ОЛІЙНИХ КУЛЬТУР

Prof. Ph.D. Eng. Shevchenko I.A, Ph.D. Eng. Aliev E.B.

Institute of Oilseed Crops NAAS, Zaporizhzhia / Ukraine

E-mail: aliev@meta.ua

Keywords: seed, photo separator, research, modeling, supply

ABSTRACT

The results of numerical simulation and experimental research on the seed transfer process under the influence of the working part of the photoelectronic separator seed supply unit are presented. There has been developed physics and mathematical model, which links the productivity of the seed supply unit of the photoelectronic separator, its power consumption and the average time interval between falling seeds from the seeds supply, the frequency of vibroplate oscillations and the rotational speed of the barrel. During research, there has been solved a compromise problem of maximization of the average time interval between falling seeds and the minimization of the power consumed by the seed supply unit, with the maximum value of its productivity, which is comparable to the value of the seed supply.

РЕЗЮМЕ

Представлені результати чисельного моделювання і експериментальних досліджень процесу переміщення насіння під дією робочого органу блока подачі насіння фотоелектронного сепаратора. Наведено розроблену фізико-математичну модель, яка зв'язала продуктивність блоку подачі насіння фотоелектронного сепаратора, його споживаєму потужність і середній інтервал часу між падаючим насінням від подачі насіння, частоти коливань вібрототка і частоти обертання барабана. В процесі досліджень була вирішена компромісна задача, а саме максимізація середнього інтервалу часу між падаючим насінням і мінімізація потужності, що споживається блоком подачі насіння, при максимальному значенні його продуктивності, яка порівняна із значенням подачі насіння.

INTRODUCTION

The unsatisfactory quality of the seeds leads to a significant decline in agricultural productivity and a high over expense of seed material (Aliev E. B., 2016). According to the current standards, oilseed crops varietal and crop yields are determined mainly by their varietal purity, which should be for the elite seed (elite, superelite) – 99.6 - 99.9% depending on the crop.

One of the ways to increase the efficiency of the seed material separation in the seed treatment plant is to fractionate it (Shaforostov V.D., Priropov I.E. 2015) by using a photoelectronic separator (Priropov I.E., 2015) at the final stage of its treatment. Despite the increasing usage of photoelectronic separators in the control and sorting of seed material, their application continues to be rather narrow. In the theses (Clien S., Chiang Y.P., Pomeranz Y., 1994; Thomson W.H., Pomerang Y., 1991; Shazzo A. Y., Usatkov S.V., 2012; Tischenko A. I., 2000) the great prospects of photoelectronic separation in grain-processing industries are described. It is possible to predict the distribution of photoelectronic separation by colour in seed and breeding with a high degree of probability.

However, even in the framework of finished agricultural products processing, the potential of photoelectronic separators is still not fully used up. This is primarily due to the lack of available technical tools and mathematical models and algorithms that are suitable for their operation.

Therefore, in order to solve the problem of oil material separation from oilseed crops, development of a photoelectronic separator design, theoretical and experimental research of its operational process and the substantiation of its rational structural and technological parameters are envisaged.

MATERIALS AND METHODS

The developed photoelectric separator consists of three blocks: a seed supply unit, a seed recognition unit and a seed flow separation unit. The seed feeder of the photoelectric separator (Fig. 1) consists of a bunker 1, a barrel 2 with radially positioned blades 3 and a vibroplate 4 with longitudinal channels 5. The seeds enter the bunker 1 under gravity. Next, the barrel 2 with radially positioned blades 3, executing rotational motion captures the seeds from the bunker 2 and transfers to the vibroplate 4. The vibratoroll 5, while being located angled to the horizon line, performs a periodic transverse movement from one side to another, forcing the seeds to move along longitudinal channels 5. After this the seeds leave the vibratoroll 5 and fall into the next block of the photoelectric separator.

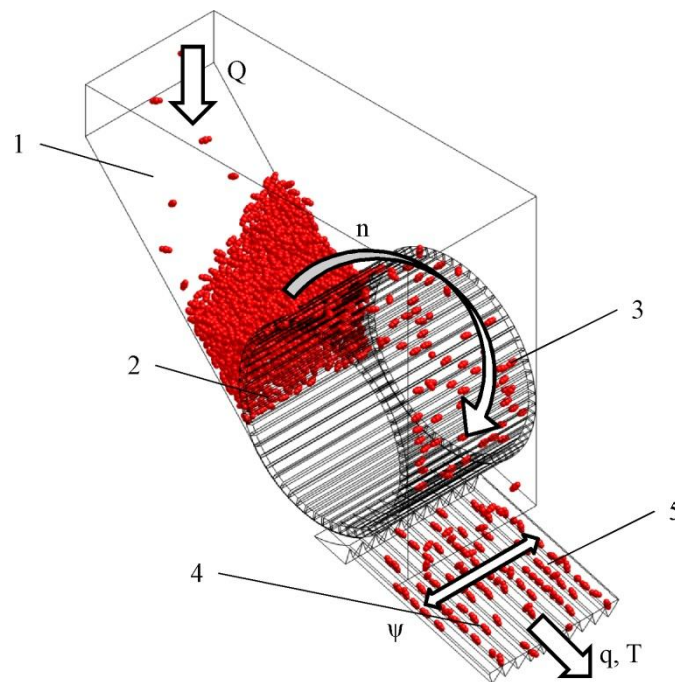


Fig. 1 - Structural and technological scheme of the photoelectric separator seed supply unit

1 – bunker; 2 – barrel; 3 – blades; 4 – vibroplate; 5 – longitudinal channels

The study of the seed supply unit operational process has been conducted in two stages.

The first step for determining the rational regime parameters of the working part of the photoelectric separator seed supply unit is the realization of corresponding physical models in the software package STAR-CCM+. The following physical models were selected for numerical simulation: k- ϵ model of the separated flow turbulence, gravity field, Van der Waals real gas model, model of discrete elements, and model of multiphase interaction. The method of discrete elements is based on the laws of the impulse conservation and impulse momentum for LaGrange models of multiphase environment (Shevchenko I.A., Aliyev E. B., Doruda S.O., 2013; Boyko V.B., Aliyev E. B., 2015; Aliyev EB, Labatyuk Y.M., 2017). However, for the construction of a physics and mathematical model, it must be assumed that the seeds are presented in the form of identical ellipsoids with a defined density and effective diameter. The following physical and mechanical properties of seeds have been determined: Poisson's ratio – 0.5 Young's modulus – 0.2 MPa; density – 800 kg/m³; effective diameter – 0.008 m; coefficient of friction in quiescence – 0.8; normal recovery factor – 0.5; tangential recovery factor – 0.5; coefficient of rolling resistance – 0.3. Properties of the environment have been determined as follows: environment - air; dynamic viscosity – 1.85508 · 10⁻⁵ Pa·s; the Prandtl turbulent numeric is 0.9; free fall acceleration – 9.8 m/s²; temperature – 293 K; pressure – 101325 Pa. The size of the grid cell modeling has been set as 0.001 m. To simplify the mathematical and time operations, the following structural and technological parameters of the seed supply unit have been determined: the fluctuation amplitude of the vibroplate $A = 0.008$ m (corresponding to the size of the vibroplate channel); external barrel radius $r_0 = 0.07$ m; number of blades $N = 38$; the length of the blade is $l = 0.01$ m. It should be noted that the vibratoroll consists of 10 identical longitudinal channels, which are used to transfer seeds. Exposure duration was 100 s.

The second stage has been the conduct of experimental research on the plant, consisting of an experimental sample of the seed supply unit, a laboratory power supply unit with the voltage change option and control equipment (photo-converters connected to an analog-to-digital converter). The design and technological scheme and the general view of the experimental sample of the photoelectronic separator seed supply unit are shown in Fig. 2. The calibrated valve has been used to limit the input performance and to provide a certain level of seeds supply. The frequency and amplitude of the vibroplate vibration has been provided by changing the voltage of the laboratory power unit connected to the wind turbine. The schematic diagram of photoconductors connected to an analog-to-digital converter is shown in Fig. 3. It should be noted that the vibroplate consists of 20 identical longitudinal channels, on which the seeds movement occurs. The control and measuring apparatus works as follows. Falling seed from the longitudinal channel enters between the emitter and the photodetector receiver. As a result, a signal goes to an analog-to-digital converter, which converts the signal to a digital one and displays in a personal computer. There is a measurement of time between falling seeds. In the experimental research course of the experimental sample of the photoelectronic separator seed supply unit, the flax seeds of the Vodogray oilseed grade have been calibrated to a size of 2.5 mm. One experiment has been conducted by passing through a pilot sample of a feed unit of 10 kg of seed.

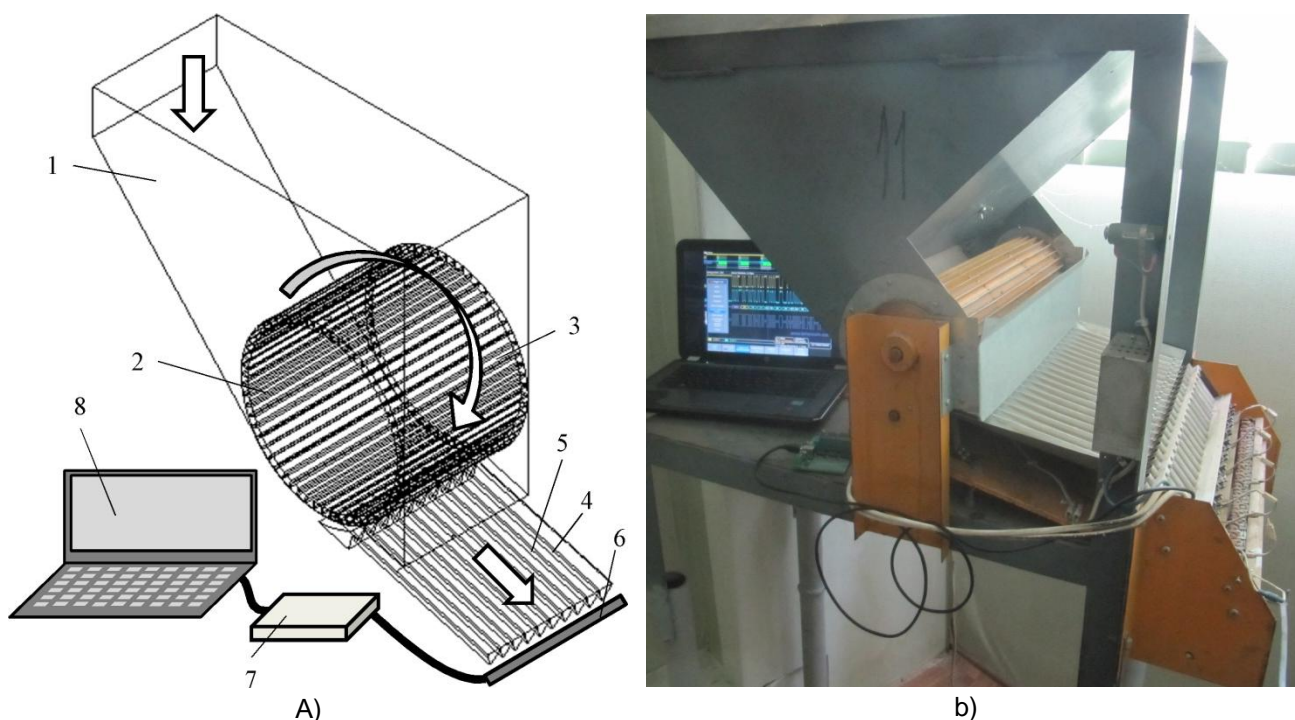


Fig. 2 - Structural-technological scheme (a) and general view (b) of the pilot sample of the photoelectronic separator seed supply unit

1 – bunker; 2 – barrel; 3 – blades; 4 – vibroplate; 5 – longitudinal channels; 6 – photoconductors;
7 – analog-to-digital converter; 8 – personal computer

The variation intervals and levels of factors in theoretical and experimental studies are given in Table 1.

The following optimization criteria have been determined:

- seeds delivery part productivity – q , kg/hr;
- power consumption – P , kW;
- the average time interval between falling seeds is t , s.

The productivity of the seed supply unit q has been determined by measuring the mass of the seed M passing through it and the corresponding time τ . The calculation has been made by the formula:

$$q = \frac{M}{t}. \quad (1)$$

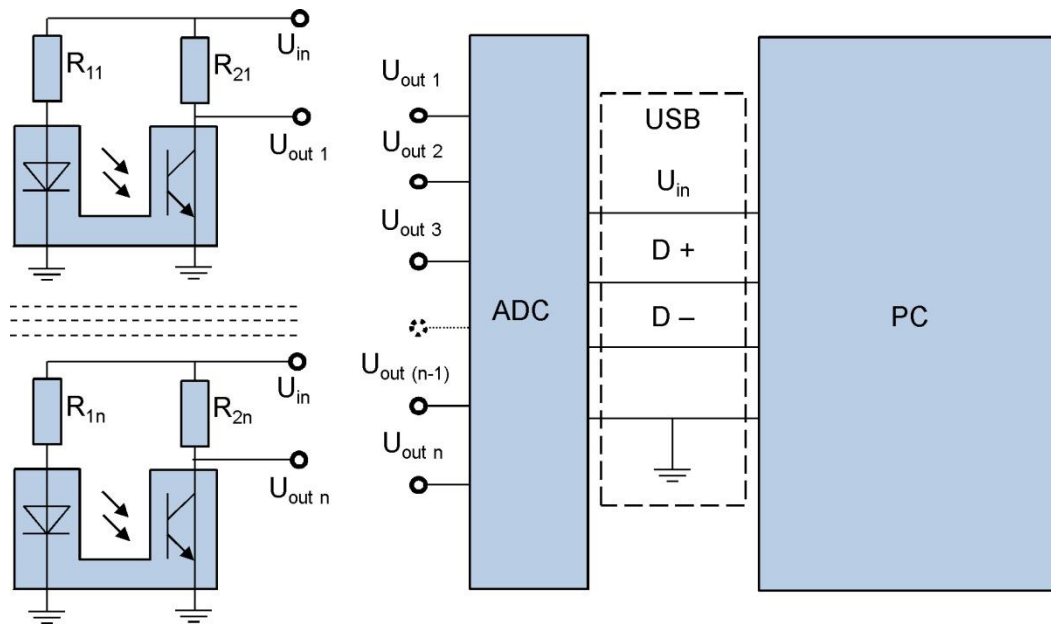


Fig. 3 - Principal electrical circuit of photoconductors
 ADC – analog-to-digital converter; PC – personal computer

Table 1

Variation levels and intervals of factors when conducting researches on the operation process of the photoelectronic separator seed supply unit

Factors variation level	Factors		
	Seed supply Q, kg/hr	Vibroplate oscillations frequency ψ , s ⁻¹	Barrel rotation frequency n, rpm
Upper level (+)	15	10	15
Basic level (0)	9	7.5	10
Lower level (-)	3	5	5
Factors variation interval	6	2.5	5

In experimental studies, the power consumed by the seed supply unit has been measured using an authorized electric meter and calculated using the formula:

$$P = \frac{\Delta E}{\tau}, \tag{2}$$

where: ΔE – meter results, W·hr;
 τ – time of experiment conduction, hr.

The average time interval between falling seeds has been determined in experimental studies using photoconductors connected through an analog-to-digital converter to a personal computer and calculated by the formula:

$$t = \frac{1}{N} \sum_{i=1}^N t_i, \tag{3}$$

where: N – seeds count;
 t_i – the time interval between two falling seeds, s, c.

The first stage, namely numerical simulation, has been conducted on a complete factorial study with a total number of experiments – $3^3 = 27$.

The second stage was conducted in a D-optimal second-order Box-Benkin plan for three factors (15 experiments) in a three-time repetition.

The research results processing have been carried out by the method of mathematical factor planning of experiments, using the computer program Mathematica.

The mathematical model is determined by one optimization criterion.

RESULTS

According to the first stage, as a result of numerical simulation, a visualization of the technological process of moving seeds under the influence of the working part of the photoelectric separator seed supply unit has been obtained (Fig. 4).

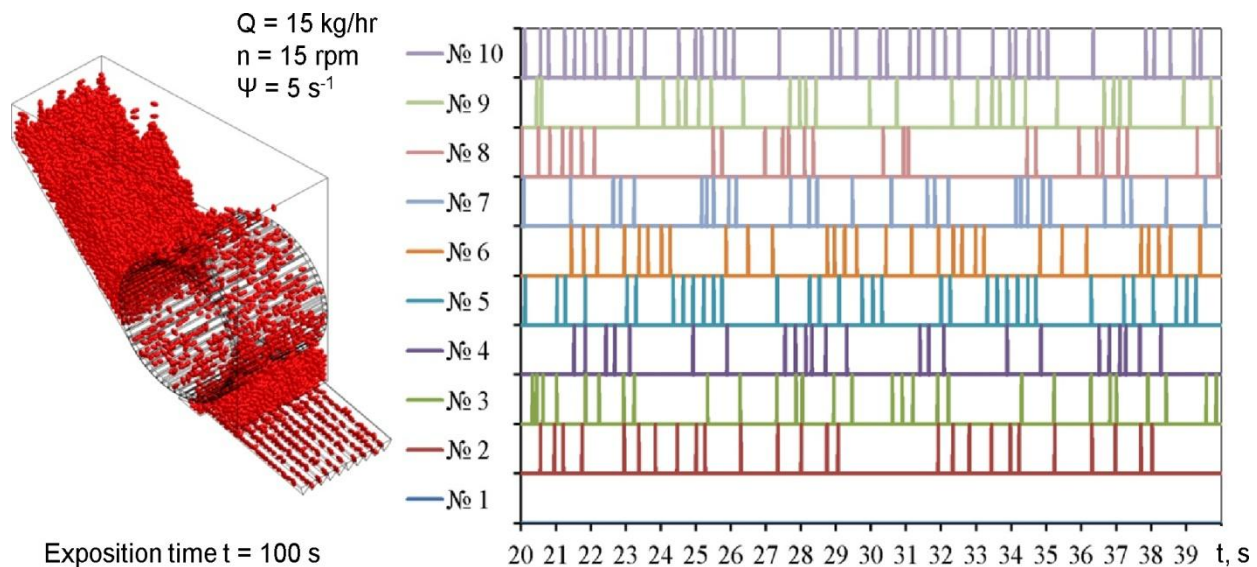


Fig. 4 - Distribution of seedling time intervals from the vibroplate of the photoelectric separator seed supply unit

The approximation of the obtained data has been made using the software package Mathematica. It resulted into the equation of dependence of the seed supply block efficiency of the photoelectric separator q from the above-mentioned factors in the encoded form:

$$q = 4.46961 + 1.50378 x_1 - 1.37183 x_1^2 + 1.94412 x_2 + 1.06579 x_1 x_2 + 0.634078 x_2^2 + 0.150011 x_3 - 0.160614 x_1 x_3 + 0.171217 x_2 x_3 - 0.147393 x_3^2 \quad (4)$$

The calculated coefficients of the correlation coefficient ($R = 0.96$) and Student's criterion $t_{0.05}(27) = 2.05$ are significant at the confidence level of more than 95 %, with coefficients for the following terms of the equation: $x_1, x_2, x_1 x_2, x_1^2, x_2^2$.

In a decoded form, the model (4) after the contraction has the form:

$$q = 3.79771 + 0.403651 Q - 0.0381064 Q^2 - 1.38361 \psi + 0.0710524 Q \psi + 0.101452 \psi^2 \quad (5)$$

Analyzing equation (5), we can conclude that with the increase of the vibroplate oscillations frequency ψ , the productivity of the seed supply unit of the photoelectric separator q increases. In turn, the rotational speed of the barrel practically does not affect the specified criterion. And for the supply of seeds Q there is an optimal value of $Q = 14.4$ kg/hr, in which the maximum value of the seed supply block of the photoelectric separator is observed.

Also, the equation for the time interval between the incident seed t and the factors of research is established:

$$t = 0.058287 - 0.0167361 x_1 + 0.0253472 x_1^2 - 0.0436111 x_2 + 0.00802083 x_1 x_2 + 0.0138889 x_2^2 + 0.00375 x_3 + 0.00239583 x_1 x_3 - 0.00364583 x_2 x_3 - 0.00194444 x_3^2 \quad (6)$$

According to the calculated values of the correlation coefficients ($R = 0.95$) and Student's criterion $t_{0.05}(27) = 2.05$, the coefficients at the level of confidence probability greater than 95% are coefficients for the following terms of the equation: $x_1, x_2, x_3, x_1 x_2, x_1^2, x_2^2$.

In a sketched form, the model (6) after the contraction has the form:

$$t = 0.42485 + 0.00075 n - 0.0194734 Q + 0.00070409 Q^2 - 0.0555903 \psi + 0.000534722 Q \psi + 0.00222222 \psi. \quad (7)$$

From equation (7) it is evident that at low values of the oscillation frequencies of the vibroplate ψ , the rotational speed of the barrel n and the optimum seed supply $Q = 10.31$ kg/hr, there is a minimum of the average time interval between the falling seeds t .

The analysis of the presented dependencies proves the necessity of solving a compromise problem, which is as follows: to ensure the efficient operation of the photoelectronic separator's seed supply unit, it is necessary to provide its productivity q at maximal and equal to the seed supply Q level, with the average time interval between falling seed t being maximum:

$$\begin{cases} q(Q, \psi, n) = Q, \\ t(Q, \psi, n) \rightarrow \max, \\ Q \rightarrow \max. \end{cases} \quad (8)$$

or

$$\begin{cases} q(Q, \psi, n) = Q, \\ Q \times t(Q, \psi, n) \rightarrow \max. \end{cases} \quad (9)$$

Using the software package Mathematica the system of equations (9) solution is

$$\begin{cases} Q = q = 4,7 \text{ kg/hr}, \\ \psi = 10 \text{ s}^{-1}, \\ n = 12 \text{ rpm}, \\ t = 0,047 \text{ s}. \end{cases} \quad (10)$$

The second stage, namely, the experimental research of the operation process of the photoelectronic separator seed supply unit has been carried out using the method of multifactorial experiment mathematical planning, which allows determining mathematical models of processes in the form of regression equations. The obtained mathematical model of the investigated factors influence on the average time interval between the falling seeds has the following form:

$$\begin{aligned} t = & 0.07462 - 0.0171528 x_1 + 0.0253056 x_1^2 - 0.0436112 x_2 + \\ & + 0.0084375 x_1 x_2 + 0.0121805 x_2^2 + 0.00350001 x_3 + \\ & + 0.00197917 x_1 x_3 - 0.00239584 x_2 x_3 - 0.00115278 x_3^2 \end{aligned} \quad (10)$$

For this equation, the 95% dispersion probability level is homogeneous, the value of the Cochran criterion $G = 0.1354 < G_{0.05}(2, 15) = 0.3346$.

Dispersion of the adequacy of the mathematical model $S_{ad}^2 = 3.76 \cdot 10^{-6}$; dispersion of experimental error $S_y^2 = 1.77 \cdot 10^{-6}$; Fisher's criterion $F = 2.12 < F_{0.05}(5, 30) = 2.53$; the model is adequate at any level of confidence probability.

According to calculated values of correlation coefficients and Student's criterion $t_{0.05}(30) = 2.04$ significant at the level of confidence probability greater than 95% are all coefficients. In a sketched form, the model (10) has the form:

$$\begin{aligned} t = & 0.415665 - 0.0000461111 n^2 + 0.000702933 Q^2 + 0.00246598 n + \\ & + 0.0000659722 Q n - 0.000191667 \psi n - 0.0203901 Q + \\ & + 0.0005625 \psi Q - 0.0498236 \psi + 0.00194889 \psi^2. \end{aligned} \quad (12)$$

By analyzing equation (12), it can be stated that all of the above factors are influenced by the average time interval between falling seeds. At the same time, with the increment of the vibroplate fluctuations frequency and the barrel frequency of rotation, the average time interval increases as well. Also, with an increased supply of seeds, the average time interval decreases.

The obtained mathematical model of the investigated factors influence on the productivity of the seed supply unit has the following form:

$$\begin{aligned} q = & 7.58444 + 2.95042 x_1 - 2.87556 x_1^2 + 3.8375 x_2 + 2.49917 x_1 x_2 + \\ & + 1.55361 x_2^2 + 0.157083 x_3 - 0.27 x_1 x_3 + 0.309167 x_2 x_3 - 0.425556 x_3^2 \end{aligned} \quad (13)$$

For this equation, the 95% dispersion probability level is homogeneous, the value of the Cochran criterion $G = 0.1296 < G_{0.05}(2, 15) = 0.3346$.

Dispersion of the adequacy of the mathematical model $S_{ad}^2 = 0.2326$; variance of experimental error $S_y^2 = 0.1170$; Fisher's value $F = 1.98 < F_{0.05}(6, 30) = 2.42$; the model is adequate at any level of confidence probability.

According to the calculated values of the correlation coefficients and Student's criterion $t_{0.05}(30) = 2.04$ significant coefficients at the confidence level greater than 95% are all coefficients. In a sketched form, the model (13) has the form:

$$q = 9.74785 - 0.0170222 n^2 - 0.0798765 Q^2 + 0.235944 n - 0.009 Q n + 0.0247333 \psi n + 0.769931 Q + 0.166611 \psi Q - 3.9405 \psi + 0.248578 \psi^2 \quad (14)$$

Analyzing equation (14), it can be argued that the productivity of the seed supply block is influenced by all the above-mentioned factors. At the same time, with the increase in the frequency of the vibroplate oscillation and the supply of seeds, the productivity of the supply block increases. For the barrel rotation frequency $n = 10.3$ rpm, the optimum is observed.

The obtained mathematical model of the investigated factors influence on the power consumed by the seed supply unit has the following form:

$$P = 222.667 + 48.625 x_1 + 0.625 x_1^2 + 17.5 x_2 - 4.0 x_1 x_2 - 2.29167 x_2^2 + 40.2083 x_3 + 0.0833333 x_1 x_3 - 7.66667 x_2 x_3 + 6.79167 x_3^2 \quad (15)$$

For this equation, the 95% confidence level of the dispersion is homogeneous, the value of the Cochran criterion $G = 0.1977 < G_{0.05}(2, 15) = 0.3346$.

Dispersion of the adequacy of the mathematical model $S_{ad}^2 = 169.24$; variance of experiment error $S_y^2 = 80.33$; Fisher's criterion $F = 2.11 < F_{0.05}(9, 30) = 2.21$; the model is adequate at any level of confidence probability.

According to the calculated values of the correlation coefficients and Student's criterion $t_{0.05}(30) = 2.04$, the coefficients at the confidence level greater than 95% are the coefficients for the following variables: $x_1, x_2, x_3, x_2 x_3, x_3^2$. In a sketched form, the model (15) has the form:

$$P = -2.02083 + 0.271667 n^2 + 8.10417 Q + 7.20833 n - 0.613333 \psi n + 13.1333 \psi. \quad (16)$$

The graphical interpretation of the obtained dependence (16) is presented in Fig. 5.

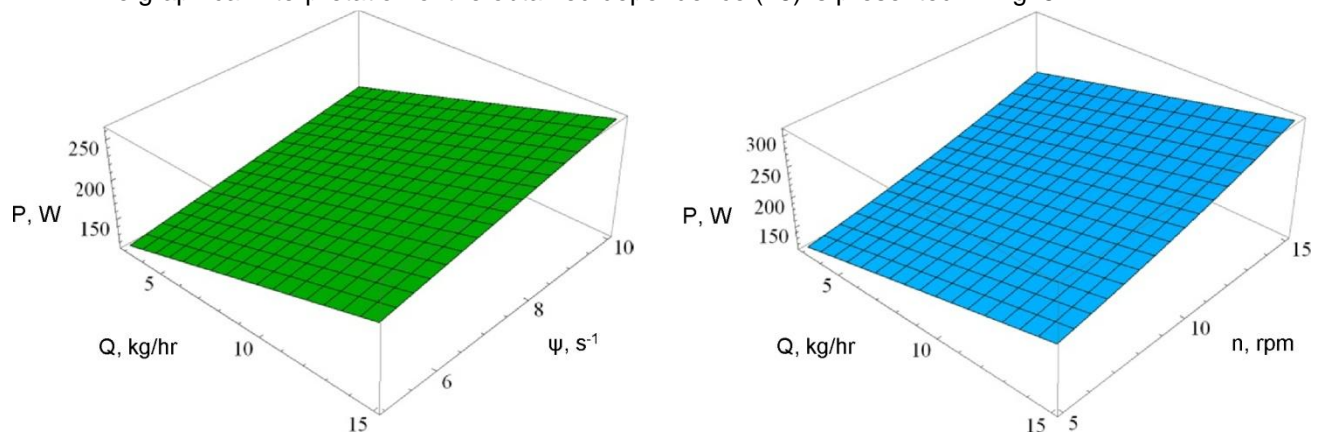


Fig. 5 - The dependence of the power P, consumed by the seed supply unit, on the seed supply Q, the vibroplate frequency oscillation ψ and the barrel rotational speed n

Analyzing equation (16), it can be stated that the power consumed by the seed supply unit is influenced by all the above-mentioned factors. At the same time with their increase, also increases power.

The task of solving a compromise problem was to maximize the average time interval between falling seeds and minimize the power consumed by the seed supply unit, with the maximum value of its productivity, which is comparable to the value of the seed supply, that is:

$$\begin{cases} t(Q, \psi, n) \rightarrow \max, \\ P(Q, \psi, n) \rightarrow \min \\ q(Q, \psi, n) = Q \rightarrow \max. \end{cases} \quad (17)$$

Convert the system of equations (17) to the form:

$$\begin{cases} \frac{q(Q, \psi, n) \times t(Q, \psi, n)}{P(Q, \psi, n)} \rightarrow \max, \\ q(Q, \psi, n) = Q. \end{cases} \quad (18)$$

The solution of the problem (18) using Mathematica software package has resulted in the optimal parameters and operating modes of the photoelectronic separator seed supply unit:

$$\begin{cases} Q = q = 15 \text{ kg/hr}, \\ \psi = 9,9 \text{ s}^{-1}, \\ n = 6,6 \text{ rpm}, \\ t = 0,058 \text{ s}, \\ P = 269 \text{ W}. \end{cases} \quad (19)$$

The comparison of theoretical and experimental data for the productivity functions of the seed supply unit (5) and (14) in the studied range of variation is presented in Fig. 6. Due to the fact that in theoretical research the seed supply block has 10 channels, and in the experimental - 20, the productivity will differ by 2 times, obviously. Statistical analysis has shown that the correlation coefficient between theoretical and experimental data with variation of the factors values is 0.92.

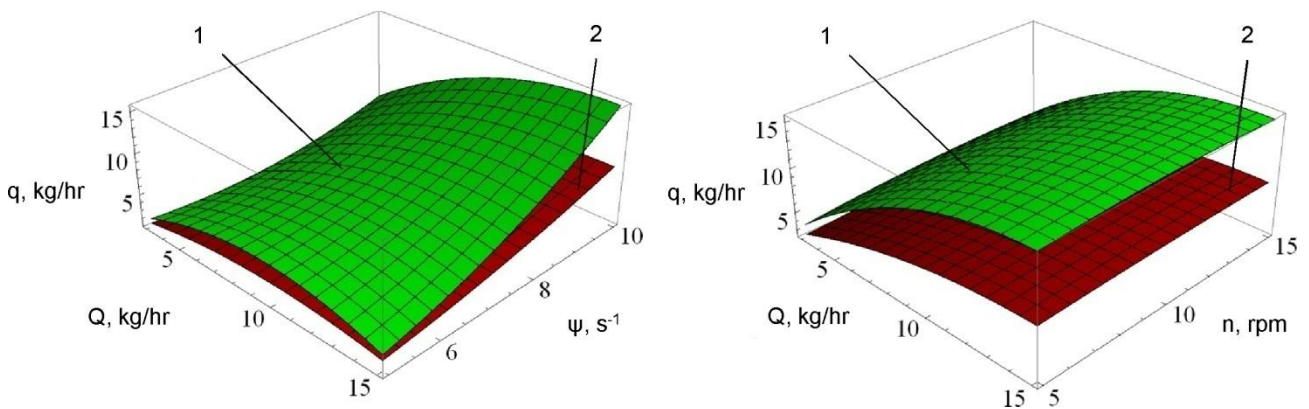


Fig. 6 - Comparison of the experimental (1) and theoretical (2) dependencies of the seed supply unit q

The comparison of theoretical and experimental data for functions of the average time interval between falling seeds (7) and (12) in the studied range of variation is presented in Fig. 7. Statistical analysis showed that the correlation coefficient between the theoretical and experimental data with variation of the factors values is 0.94.

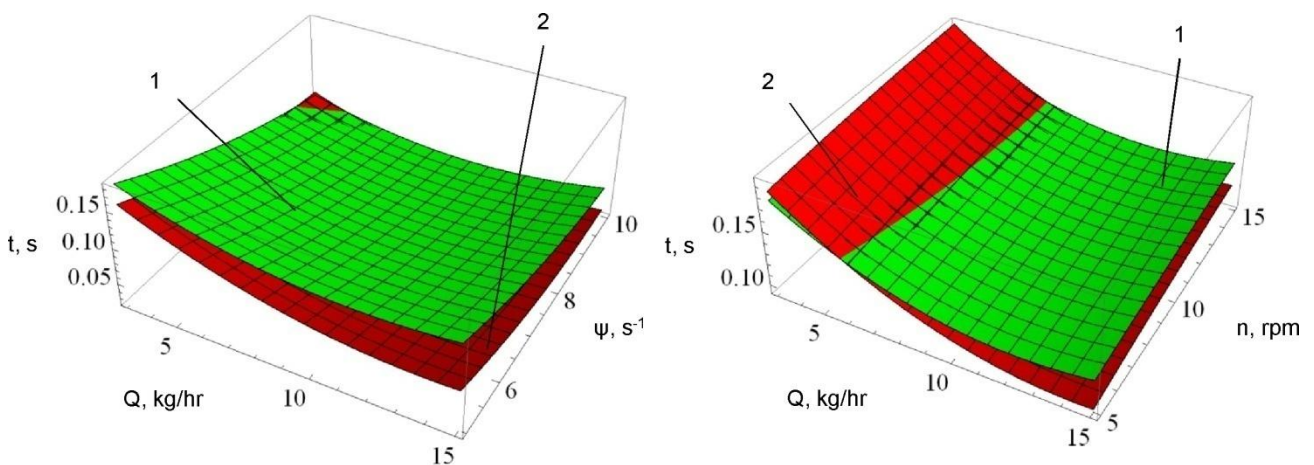


Fig. 7 - Comparison of the experimental (1) and theoretical (2) dependencies of the average time interval between falling seeds t

Due to the fact that in experimental studies the optimal parameters have been determined on the basis of a more extended compromise problem (the function of power dependence was introduced), the actual rational structural and technological parameters of the seed supply unit are taken into account (19).

CONCLUSIONS

As a result of numerical simulation of the seed transfer process under the influence of the working part of the photoelectric separator seed supply unit, a physics and mathematical model that links the productivity of the photoelectric separator seed supply unit q and the average time interval between the falling seeds t from the seed supply Q , the vibroplate oscillation frequency ψ and barrel rotation frequency n has been developed. As a result of solving a compromise problem, which is to ensure the efficient operation of the photoelectric separator seed supply unit, it is necessary for its q efficiency to be maximal and equal to the seed supply Q value, with the average time interval between falling seeds t being the maximum, the rational parameters of the supply unit seeds: $Q = q = 4.7 \text{ kg/hr}$, $\psi = 10 \text{ s}^{-1}$, $n = 12 \text{ rpm}$, $t = 0.047 \text{ s}$.

As a result of experimental studies of the photoelectric separator seed supply unit, the physics and mathematical model, that links the productivity of the photoelectric separator seed supply unit q , its power consumption P , and the average time interval between falling seeds t from the seed Q supply, the vibroplate oscillation frequency ψ and barrel rotation frequency n , has been developed. During research, the following compromise problem has been solved: the maximization of the average time interval between falling seeds t and the minimization of the power P consumed by the seed supply unit at the maximum value of its productivity q , which is comparable to the value of the seed Q . Due to the optimal parameters being determined on the basis of a more extended compromise problem (the function of power dependence has been introduced) in experimental research, the actual rational structural and technological parameters of the seed supply unit are: $Q = q = 15 \text{ kg/hr}$, $\psi = 9.9 \text{ s}^{-1}$, $n = 6.6 \text{ rpm}$, $t = 0.058 \text{ s}$.

REFERENCES

- [1] Aliev E.B., (2016), Technical and technological support of purification and separation processes of oil crops seeds (Техніко-технологічне забезпечення процесів очищення та розділення насіннєвого матеріалу олійних культур). *Records of the Ukrainian Scientific and Practical Conference of Young Scientists and Specialists from May 25-26, 2016 The role of scientific research in providing the processes of the Ukrainian agrarian production innovative development / NAAS, GA ISC NAAS*, pp. 4-5. Vinnytsya/Ukraine;
- [2] Shaforostov V.D., Priporov I.E. (2015), Quality indicators of the photoelectric separator operations on fractional technology for the sunflower seeds separation (Качественные показатели работы фотосепаратора по фракционной технологии при разделении семян подсолнечника). *International Research Journal (Международный научно-исследовательский журнал)*. № 1-3 (32). pp. 23-25. Yekaterinburg / Russia;
- [3] Priporov I.E., (2015), Sorting of sunflower seeds on a photoelectric separator (Сортирование семян подсолнечника на фотосепараторе). *Rural mechanic (Сельский механизатор)*. № 3. pp. 12-13. Moscow/Russia;
- [4] Clieen C., Chiang Y.P., Pomeranz Y., (1989), Image analysis and characterization of cereal grains with a laser range finder and camera contour extractor. *Cereal Ciem*. № 6. pp. 466–470. Minnesota/USA;
- [5] Thomson W.H., Pomerang Y., (1991), Classification of wheal kernels using three-dimensional image analysis. *Cereal Chem*. № 34. pp. 357–361. Minnesota/USA;
- [6] Shazzo A.Y., Usatkov S.V., (2012) Effectiveness of detecting hidden infectivity of grains from images in the infrared spectrum (Ефективність розпізнавання прихованої зараженості зернівок із зображень в інфрачервоному спектрі). OSU periodical. *Food Technology (Вісник ОНУ. Харчова технологія)*. №4. pp.105–108. Odessa / Ukraine;
- [7] Tishchenko A.I. (2000), Improvement of the bulk grain products quality on the basis of the multicriteria photoelectric separators development and application (Повышение качества сыпучих зерновых продуктов на основе разработки и применения многокритериальных фотозлектронных сепараторов). PhD Thesis. 304 p. Barnaul / Russia;
- [8] Aliev E.B., Labatyuk Y.M., (2017), Numerical modeling of mechanical and technological processes of agro-industrial production (Чисельне моделювання механіко-технологічних процесів агропромислового виробництва). *Modern problems of technical systems and technologies improvement in animal husbandry: Periodical of the Kharkov National Technical University of*

Agriculture named after Petr Vasilenko (Сучасні проблеми вдосконалення технічних систем і технологій у тваринництві: Вісник Харківського Національного технічного університету сільського господарства імені Петра Василенка). № 180. pp. 67-71. Kharkiv / Ukraine;

- [9] Boyko V.B., Aliev E.B., (2015), Theoretical studies of fluid motion in the capacity of a hydro-pneumatic seeding machine (Теоретичні дослідження руху рідини в ємності гідропневматичного висівного апарата). *Engineering of nature use (Інженерія природокористування)*. №2(4). pp. 78-84. Kharkiv / Ukraine;
- [10] Shevchenko I.A., Aliev E. B., Doruda S.O., (2013), Simulation of the feed mixes flow mixing process using the discrete elements method (Моделювання процесу потокового змішування кормосумішей з використанням методу дискретних елементів). *Mechanization and electrification of agriculture (Механізація та електрифікація сільського господарства)*. № 97. Vol. 1. pp. 536-544. Glevakha / Ukraine.

RESEARCH ON THE TURNING ABILITY OF A TWO- MACHINE AGGREGATE

/

ИССЛЕДОВАНИЕ РАЗВОРАЧИВАЕМОСТИ ПОСЕВНОГО ДВУХМАШИННОГО АГРЕГАТА

Prof. PhD. Eng. Bulgakov V.¹⁾, PhD. Eng. Ivanovs S.²⁾, Prof. PhD. Eng. Nadykto V.³⁾,
PhD. Eng. Kuvachov V.³⁾, PhD. Eng. Masalabov V.³⁾

¹⁾National University of Life and Environmental Sciences of Ukraine / Ukraine,

²⁾Latvia University of Agriculture / Latvia; ³⁾Tavria State Agrotechnological University / Ukraine

Tel. +380 097-2288-905, E-mail: vbulgakov@meta.ua

Keywords: tractor, two-machine aggregate, coupling, turning

ABSTRACT

On a turning strip of minimum width, a two-machine sowing aggregate can perform loop turns with a mode indicator close to the optimal, and loopless ones – with an indicator almost twice as large. Implementation of both types of turning of the aggregate, studied under optimum conditions, takes place on the turning strip the working width of which is greater than the calculated minimum and the multiple working width of the aggregate. The most efficient solution for the problem of making a turn of such an aggregate is the use of a coupling device that could automatically change the velocity of its movement on the turning strip, depending on the angular velocity of the tractor driven wheels turning.

АНОТАЦІЯ

На поворотній смузі мінімальної ширини двухмашинні посівні агрегат можуть здійснювати петлеві повороти з показником режиму, близьким до оптимального, а безпетлеві – з показником майже удвічі більше. Реалізація обох видів поворотів агрегату, який досліджено, в оптимальному режимі має місце на поворотній смузі, дійсна ширина якої більше мінімально розрахованою і кратна ширині захвату агрегату. Найбільш ефективним рішенням проблеми здійснення повороту даного агрегату з оптимальним значенням показника режиму є застосування зчпного пристрою, який би автоматично змінював швидкість його руху на поворотній смузі залежно від кутової швидкості повороту керованих коліс агрегатуєчого трактора.

INTRODUCTION

The efficiency of the sowing operations is very important both from the economic point of view and in order to meet the optimal agrotechnical terms (Aseeva et al., 2013; Barwicki, 2012; Meca & Cardei, 2012).

One of the directions to increase the efficiency of the machine-and-tractor aggregates is to increase their working width. There are two real ways of implementing this direction: the use of wide-span machines of monoblock (Nadykto, 2009; Kyurchev, 2013, Mitkov, 2010) constructions and the use of couplings.

The first way has both disadvantages and advantages. The monoblock wide-span machine can be aggregated only with one power source of the corresponding traction class. The process of aggregation and adjustment to the working position of a monoblock machine takes less time. At the same time, the transportation complexity of the machine leads to a significant complication of its design and increased price (Moiseenko, 2013; Rubec, 2012, Bulgakov et al., 2017).

The use of couplings makes it possible to use narrow-span machines more efficiently: in the coupling they are aggregated with one tractor, and each separately with the other. To a large extent, this applies to the machine-and-tractor sowing aggregates based on multipurpose cultivating tractors of traction class 1.4.

The conventional use of a coupling in the trailed version is characterised by increased length of the set-off of the sowing aggregate. As a result, this leads to a significant (not less than 38%) increase in the specific time spent on the turns (Karabanicky, 2009; Nadykto, 2005; Smolinsky, 2016).

The most promising option for increasing the operating width of the aggregate is the use of a semi-mounted coupling. Besides, its design should exclude collision of the trailed machines on the turning strip, and the indicator of the turning mode of the machine-and-tractor aggregate should ensure increased technical and economic indicators of its operation. It is the practical solution of exactly this task that determines the topicality of this work.

A significant contribution to the theory and practice of this issue has been made by many scientists (Iofinov, 1986; Bulgakov et al., 2017; Makarenko, 2011). At the same time, the theoretical dependencies developed by them and the obtained practical results cannot be used to justify the design and technological parameters of the machine-and-tractor sowing aggregate developed by us as part of a multipurpose tractor, traction class 1.4 (MTZ-80), two SZ-3 seeders SZ-3.6, and a semi-mounted coupling (Nadykto, 2009; Masalabov, 2012) (such a design was not tackled in the researches, in general).

The known indicators of the aggregate turning mode do not reflect adequately enough the link of its design parameters with its movement mode on the turning strip. As a result, this does not provide an opportunity to achieve essential increase in the technical and economic performance of the sowing aggregate. In this paper, an attempt is made to search for a new scientifically grounded indicator of the turning mode of an aggregate with a semi-mounted coupling, aimed at eliminating these shortcomings.

The aim of the work is to study and determine the optimum turning mode of a two-machine sowing aggregate with a semi-mounted coupling.

MATERIALS AND METHODS

As a research object, a machine-and-tractor sowing aggregate was selected, assembled from a tractor of traction class 1.4 (MTZ-80), a semi-mounted two-machine coupling SS-7.2, developed according to our design, and two trailed grain seeders SZ-3.6 (Fig. 1).



Fig. 1 – An experimental two-machine sowing aggregate with a semi-mounted coupling

When carrying out experimental studies on the turning strip, the actual value of the turning radius (R_a) of the two-machine sowing aggregate was fixed in duplicate repetition, depending on the turning angle of its driven wheels. For this purpose the diameters of the conditional circles, left on the field by the rear wheels of the tractor, were determined (Fig. 2) and R_a was calculated according to the equation:

$$R_a = \frac{(D_1 + D_2)}{4}, \quad (1)$$

where D_1 and D_2 – the diameters of conditional circles, left on the field by the rear left and right wheels of the tractor.

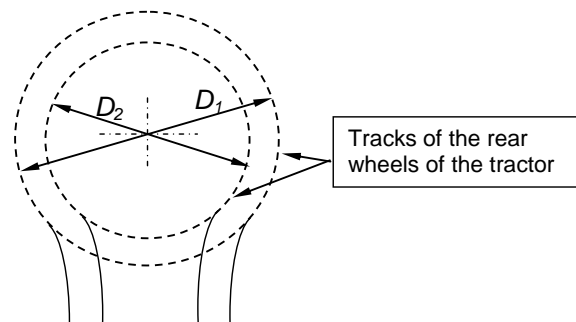


Fig. 2 – A scheme for determination of the turning radius of the sowing aggregate

The actual velocity of the movement of the tractor (V_r) on the turning strip was found as follows. A circle with a diameter of 20 m and, respectively, a length of 62.8 m was drawn on the field. The tractor was moving on a given gear and with full fuel delivery. The driver operated the tractor so that the landmark placed in front moved along the path of the circumscribed circle (Fig.3).

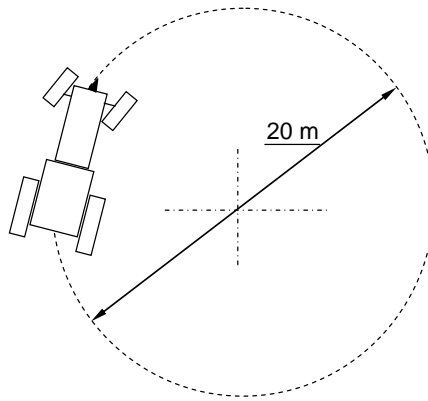


Fig. 3 – A scheme of the section for determination of the real velocity of the aggregating wheeled tractor

The value of V_r was determined from this expression:

$$V_r = \frac{62.8}{t_0}, \quad (2)$$

where t_0 – the time (duration) of the tractor movement along the given circle, s.

The kinematic parameters of the two-machine sowing aggregate were determined according to the scheme in Fig. 4. Here E and d_k are the length of the set-off and the kinematic width of the machine-and-tractor aggregate.

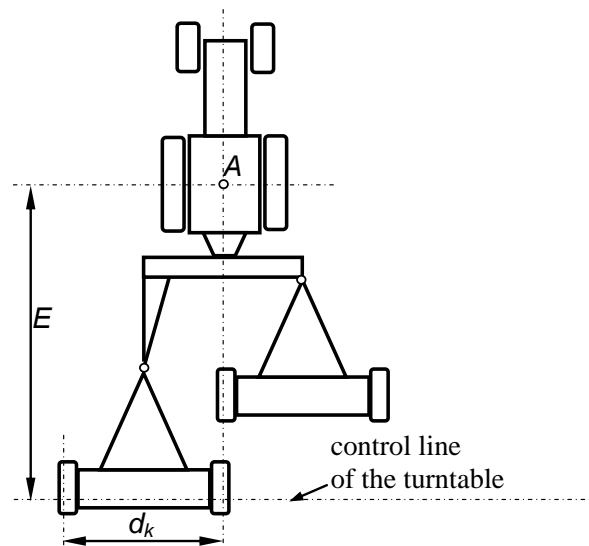


Fig. 4 – Scheme for determining the kinematic parameters of a machine-and-tractor sowing aggregate

A set-off length of the machine-and-tractor aggregate (E) was defined as the rectilinear path on the turning strip passing through the kinematic centre of the aggregate (point A, Fig. 4) until the last row of the working implements of its sowing machines come onto the control line. For the machine-and-tractor aggregate under study the kinematic length is $E = 5.95$ m. The essence of the kinematic width of the aggregate is clear from Fig. 4. For asymmetric aggregates it is, of course, different. In this case, with sufficient accuracy for practice, we can assume that this parameter is equal to the working width of the seeder $d_k = 3.6$ m.

During the experimental field research of the two-machine sowing aggregate on the basis of the MTZ-80 tractor, a specially developed hardware-measuring complex using an analogue-to-digital converter and a PC was used (Fig. 5), on which were synchronously recorded the following:

- the turning angles (α_1, α_2) of the tractor left and the right driven wheels;
- revolutions (n_1, n_2) of the tractor rear wheels.



Fig. 5 – Arrangement of the recording complex in the tractor cab

To record the turning angles of the driven wheels of the tractor, we used rheochord linear sensors SP-3A with the nominal value of 470 Ohm. The stator of this sensor was fixed relative to the frontal semi-axis of the tractor, and the rotary rotor was connected to the axis of the centre pivot of the driven wheel. During the movement of the machine-and-tractor aggregate the driven wheel, under the impact of the control action on the part of the driver, turned in a vertical plane. Together with the centre pivot of the propulsor, the rotor of the SP-3A sensor turned at the same angle. By means of the analogue-to-digital converter the electrical signal from the sensor was recorded on the screen and in the PC memory in the form of a corresponding data file. To register the rotation frequencies of the rear wheels of the MTZ-80 tractor, specially designed current collectors were used, which were mounted on the hubs of these propulsors. During the movement of the machine-and-tractor sowing aggregate the signal from each current collector was displayed via the analogue-to-digital converter on the screen and also mapped in the PC memory in the form of a respective data file.

RESULTS

It is known that the movement of the machine-and-tractor aggregate with an optimum turning radius is possible when the indicator of the mode of this manoeuvre (K_t) appropriately correlates together the design and kinematic parameters of the machine-and-tractor aggregate (Masalabov, 2012):

$$K_t = \frac{V_r}{\omega} = \frac{2\varepsilon_{\max} \left[\frac{l_t}{\tan(\varphi_3)} + \frac{l_{sh}}{\sin(\varphi_3)} - \frac{l_c}{2} \right]^2}{L}, \quad (3)$$

where $\varphi_3 = 90 - \arccos \left[\frac{(l_{sh} - r_{wh})}{R_1} \right]$ – the turning angle of the seeder;

V_r – velocity of the aggregate movement on the turning strip, $\text{m}\cdot\text{s}^{-1}$;

ω – average angular velocity of the tractor driven wheels turning, $\text{rad}\cdot\text{s}^{-1}$;

l_t – distance from the axis of the tractor rear wheels to the coupling frame, m;

l_{sh} – length of the seeder tow bar, m;

l_c – front of the coupling, m;

r_{wh} – radius of the seeder wheel, m;

R_1 – distance from the right wheel of the seeder to the point of its attachment to the coupling extender, m;

ε_{\max} – the maximum turning angle of the aggregate at the moment when it completes "entering into the turn", rad;

L – the base of the tractor, m.

While carrying out experimental studies, the design parameters included in expressions (3) were the following: $l_t = 1.04$ m; $l_{sh} = 2.15$ m; $l_c = 3.6$ m; $L = 2.37$ m; $r_{wh} = 0.59$ m; $R_t = 2.52$ m; $\varepsilon_{\max} = \pi \cdot 2^{-1}$ – for loop turns; $\varepsilon_{\max} = \pi \cdot 4^{-1}$ – for loopless turns of the sowing aggregate.

Substituting these values into (3), we find out that the actual value of the indicator of this machine-and-tractor aggregate turning mode is:

- when performing a loop turn – $11.9 \text{ m} \cdot \text{rad}^{-1}$;
- when performing a loopless turn – $5.9 \text{ m} \cdot \text{rad}^{-1}$.

At the same time, as it was established in the course of mathematical simulation (Masalabov, 2011, Masalabov, 2012), when the frame of the coupling was removed from the rear wheel axis of the tractor to a distance $l_t = 1.95$ m, the true value of the indicator of the machine-and-tractor aggregate turning mode is equal to the optimal value of $11.4 \text{ m} \cdot \text{rad}^{-1}$.

The movement of the experimental two-machine sowing aggregate was carried out on a turning strip the width of which (E_t), for each of the two types of turning (loopless and loop) considered, was found from the expression:

$$E_t = B_w \operatorname{integr} \left(\frac{E_{t \min}}{B_w} \right), \quad (4)$$

where $E_{t \min}$ – the minimum width of the turning strip, m;

B_w – the working width of the aggregate, m.

The minimum width of the turning strip ($E_{t \min}$) was determined by procedure (Bulgakov et al., 2017):

- for the loopless turn

$$E_{t \min} = R_r + E + d_k, \quad (5)$$

- for the loop turn:

$$E_{t \min} = 2.7R_r + E + d_k, \quad (6)$$

where R_r – the conditional turning radius.

According to definition (Iofinov, 1986), R_r is the radius at which the machine-and-tractor aggregate would perform a manoeuvre exclusively along a circle, that is, without transitional sections of the aggregate entering into a turn and leaving it.

By the definition (Iofinov, 1986) the conditional turning radius of the aggregate R_r can be defined as follows:

$$R_r = R_{a \min} + \frac{K_t L}{\pi R_{a \min}}, \quad (7)$$

where $R_{a \min}$ – the minimum turning radius of the machine-and-tractor aggregate.

However, since:

$$R_{a \min} = \sqrt{\frac{K_t L}{2\varepsilon_{\max}}}, \quad (8)$$

then

$$R_r = \sqrt{\frac{K_t L}{2\varepsilon_{\max}}} + \frac{K_t L}{\sqrt{\frac{K_t L}{2\varepsilon_{\max}}}}. \quad (9)$$

Taking into account the concrete value of ε_{\max} , we have:

- for the loopless turn

$$R_r = \sqrt{\frac{2K_t L}{\pi}} + \frac{K_t L}{\sqrt{\frac{2K_t L}{\pi}}}; \quad (10)$$

- for the loop turn:

$$R_r = \sqrt{\frac{\hat{E}_t L}{\pi}} + \frac{\hat{E}_t L}{\sqrt{\frac{\hat{E}_t L}{\pi}}} \quad (11)$$

After carrying out the appropriate calculations it was established that for a loopless mode of rotation $E_{t\min} = 16.15$ m, and for loop mode $E_{t\min} = 27.37$ m.

Considering expression (4) and the fact that $B_w = 7.2$ m, we finally have for the loopless turn $E_t = 21.60$ m, and for the loop turn $E_t = 28.80$ m.

It is on the strips of this width that the experimental machine-and-tractor aggregate must make turns in the process of real operation.

However, under the conditions of experimental studies the manoeuvring of the aggregate was first carried out on strips, where the width of each strip was equal to E_{\min} . Only under such a condition can be tracked the impact upon the turning process of its mode indicator, especially when making a loopless turn.

To make sure of this, we will consider the calculated and the real values of the width of each turning strip. For the loopless turning the difference between $E_t = 28.80$ m and $E_{\min} = 27.37$ m is only 1.43 m. At the same time, for the loopless turn we have $(E_t - E_{\min}) = 5.45$ m. Besides, it can be assumed that the dynamics of the turning process of the experimental machine-and-tractor aggregate on a 16.15 m wide strip can differ significantly from the nature of this process on a strip wider by 5.45 m. As it turned out, during the experimental studies, implementation of a loop (pear-shaped) turning by the experimental aggregate occurred at an average velocity $V_r = 1.88 \text{ m}\cdot\text{s}^{-1}$. The average value of the angular velocity (ω) of turning of the tractor driven wheels was $\omega = 0.155 \text{ rad}\cdot\text{s}^{-1}$.

As a result, the two-machine sowing aggregate made a turn with the real value of the indicator of the turning mode $1.88 / 0.155 = 12.1 \text{ rad}\cdot\text{s}^{-1}$. This is only 1.7% more than the calculated value K_t , which is $11.9 \text{ m}\cdot\text{rad}^{-1}$ for the given type of turning performed by the experimental machine-and-tractor aggregate. Even with respect to the optimal ($11.4 \text{ m}\cdot\text{rad}^{-1}$), the true value of the turning mode indicator is higher only by 6.1%.

When a loopless turn is performed, the situation looks different. In this case, the phases of aggregate entrance into the turn and exit from it are shorter than in the loop manoeuvre. Because of this and also because of the smaller width of the turning strip, the machine operator must exert more intense impact upon the tractor steering wheel at the same velocity of the aggregate movement, which ultimately leads to a lower indicator value of the aggregate turning mode – K_t . Thus, when the velocity of the machine-and-tractor aggregate movement during the turn is $V_r = 1.90 \text{ m}\cdot\text{s}^{-1}$, the value of the angular velocity of turning the steering wheel at the aggregate entrance into the turn and exit from it was $0.30 \text{ rad}\cdot\text{s}^{-1}$. Only such a mode of changing the control impact allowed fitting into the turning strip with a width of 16.15 m. This was the reason for the implementation of a manoeuvre with an indicator of the mode $K_t = 6.3 \text{ m}\cdot\text{rad}^{-1}$. In contrast to the calculated value ($5.9 \text{ m}\cdot\text{rad}^{-1}$), it is higher by 6.8%. At the same time, with respect to the optimum, the true value of K_t is only 55.3%, which is almost twice less.

It should be said that the true value of the angular velocity of turning the tractor driven wheels ($0.30 \text{ rad}\cdot\text{s}^{-1}$) was by 36% higher than the recommended one ($0.22 \text{ rad}\cdot\text{s}^{-1}$). However, otherwise, that is, when the value of ω is decreased, it was not possible to fit into the width of the 16.15 m turning strip. Hence it follows that, in order to reduce value ω of the angular velocity of turning the tractor driven wheels to such a level as to ensure execution of a loopless turn with an optimum value of the indicator of the K_t regime, in practice it is not possible.

You cannot practically achieve this even in case you remove the frame of the coupling from the axis of the tractor rear wheels, that is, you increase the value of parameter l_t . The point is that, according to the results of mathematical simulation (Masalabov, 2012), the increase in the value of this parameter allows reducing the turning radius of the machine-and-tractor aggregate, but only as long as the conditions for manoeuvring the machine-and-tractor aggregate are not violated. In our case, this is topical for the left-side turning of the machine-and-tractor aggregate in which angle φ_3 , and hence the turning radius R_a of the aggregate, can be reduced until there arises a risk that the left wheel of the left seeder comes into contact with the frame of the coupling. In other words, as long as it is possible to increase the turning angle φ_3 of the left seeder until increase in parameter l_t (within certain limits, respectively) helps reducing the turning radius R_a of the machine-and-tractor aggregate.

When the maximum possible values of angles α (the turning angle of the tractor driven wheels, rad) and φ_3 are reached, we obtain the minimum value of the aggregate turning radius. After that, further removal

of the seeder frame from the tractor (increase l_t) causes increase in indicator K_t of the turning mode, as it follows from expression (3). Consequently, execution of the loopless turns by the experimental machine-and-tractor aggregate is possible with a mode index almost twice as high as the optimal value. However, this is only in case the width of the turning strip is really at least of the minimum necessary value. Under real operating conditions it turned out that, in case the actual width of the turning strip, calculated above, is 21.60 m, the experimental machine-and-tractor aggregate can perform even a loopless turn with a mode index close to the optimal one. Thus, during a manoeuvre of the machine-and-tractor aggregate on the strip of the mentioned length at a velocity of $1.92 \text{ m}\cdot\text{s}^{-1}$, the angular turning velocity of the driven wheels of the tractor was $0.185 \text{ rad}\cdot\text{s}^{-1}$. In this case, the actual value of indicator K_t is $10.4 \text{ m}\cdot\text{rad}^{-1}$, which is only by 8.7% lower than the optimal value ($11.4 \text{ m}\cdot\text{rad}^{-1}$). The machine-and-tractor aggregate, performing a manoeuvre, that is, executing a loopless turn, completely fitted into the width of the turning strip, the value of which was 21.60 m.

From the above analysis it follows that there is no practical need to increase the distance between the semi-mounted coupling frame and the axis of the tractor rear wheels (parameter l_t). First, such a solution complicates to a certain extent the design of the machine-and-tractor aggregate. Second, on the one hand, an increase in the value of l_t brings a decrease in the turning radius of the machine-and-tractor aggregate, and, on the other hand, it leads to an increase in the length of its exit on the turning strip. As a result, the time for the manoeuvre may remain almost the same.

On the basis of the research results it can be concluded that, in order to make a two-machine sowing aggregate execute a turn in the optimal mode, it is necessary that the ratio of the velocity of its movement on the turning strip to the angular velocity of tractor driven wheels turning varied within a range of $11\dots 12 \text{ m}\cdot\text{rad}^{-1}$. Such a task can be practically solved by equipping the aggregate with a special automatic device.

CONCLUSIONS

1. As a result of the research, it was established that, in case the two-machine sowing aggregate performs loop turns, the actual value of the indicator of their implementation mode $11.45 \text{ m}\cdot\text{rad}^{-1}$ practically corresponds to the optimal value of $11.40 \text{ m}\cdot\text{rad}^{-1}$. Besides, the loopless turns will be carried out with a mode indicator of $5.7 \text{ m}\cdot\text{rad}^{-1}$, which, although it enters the allowed range of its variations ($4.5\dots 25.0 \text{ m}\cdot\text{rad}^{-1}$), it is still less than the optimal level.

2. On the turning strip of minimum width the two-machine sowing aggregate can perform loop turns with a mode index close to the optimum, and loopless ones with an indicator almost twice as high. Implementation of both types of turning in the optimum mode takes place on a turning strip the actual width of which is greater than the minimal calculated one and multiple working width of the aggregate.

3. The most efficient solution for the problem of performing a turn by a two-machine sowing aggregate with an optimum value of the mode index is to use a device that automatically changes the velocity of its movement on the turning strip, depending on the angular speed of the tractor driven wheels turning.

REFERENCES

- [1] Asejeva A., Kopiks N., Viesturs D., (2013), Optimal distribution of the amount of work among the tractor aggregates considering set agrotechnical terms. *Proceedings of the International scientific conference "Economic science for rural development": Production and cooperation in agriculture. Finance and taxes*, No.30, pp. 38-42., Jelgava / Latvia;
- [2] Barwicki J., Gach St., Ivanovs S. (2012). Proper utilization of soil structure for crops today and conservation for future generations. *Proceedings of 11th International Scientific Conference "Engineering for Rural Development"*, Vol. 11, pp. 10-15, Jelgava / Latvia;
- [3] Bulgakov V., Adamchuk V., Kuvachov V., Ivanovs S. (2017), Theoretical justification of the turn of a wide span tractor (vehicle) for controlled traffic farming, *INMATEH – Agricultural Engineering*, Vol. 53, No 3 / 2017, pp. 159-167, Bucharest / Romania;
- [4] Bulgakov V., Adamchuk V., Arak M., Petrychenko I., Olt J., (2017), Theoretical research into the motion of combined fertilising and sowing tractor-implement unit. *Agronomy Research*, Vol. 15(4), pp. 1498-1516, Tartu / Estonia;
- [5] Bulgakov V., Ivanovs S., Adamchuk V., Petrychenko I., Ruzhylo Z., Nowak J., (2017), Experimental Studies of a Combined Aggregate For Application of Mineral Fertilizers and Sowing. *Proceedings of IX*

International Scientific Symposium “Farm Machinery and Processes Management in Sustainable Agriculture”, pp. 58-63, Lublin / Poland;

- [6] Iofinov S., (1986), *A handbook for the operation of the machine-and-tractor fleet (Справочник по эксплуатации машинно-тракторного парка)*. РН Agropromizdat, 272 p, Moscow / Russia;
- [7] Karabanicky A., (2009), An up-to-date approach to the issue of assembling machine-and-tractor aggregates (Современный подход к вопросу комплектования машинно-тракторных агрегатов), *Proceedings of Kuban University*, vol. 3 (18), pp. 193-196, Krasnodar / Russia;
- [8] Kyurchev V., (2013), Prospects for using combined machine-and-tractor aggregates (Перспективы использования комбинированных машинно-тракторных агрегатов), *Izvestiya of the University of Economics*, Vol. 21 No 5 (142), pp. 104-108, Varna / Bulgaria;
- [9] Makarenko M., (2011) Combined power resources (Комбинированные энергосредства), *Farmer*, No 4, pp. 76-78, Kiev / Ukraine;
- [10] Masalabov V., (2012). (Determination of the turning mode indicator of a two-machine seed machine-and-tractor aggregate, *Proceedings of Tauria Agrarian University*, Vol. 2 (5), pp. 3-7, Melitopol / Ukraine;
- [11] Masalabov V., (2012). A study of the dynamic turning ability of two machines of a machine-and-tractor aggregate. *Proceedings of Tauria Agrarian University*, Vol. 2(3). pp. 15-26, Melitopol / Ukraine;
- [12] Меса V.A., Cârdei P., (2012) Studies and researches for the unification of resistance expression of machines designed to soil tillage with applications in optimization of their working regime, *INMATEH – Agricultural Engineering Journal*, vol. 36, No.1/2012, Bucharest / Romania;
- [13] Mitkov V., Mitkov B., Tylev V., (2010), Combined aggregates are of perspective (Комбинированные агрегаты – это перспективно), *Agroexpert*, No 12, pp. 114-116, Kiev / Ukraine;
- [14] Moiseenko V., (2013), Home-produced combined tillage aggregates (Отечественные комбинированные почвообрабатывающие агрегаты), *Farmer*, No 4, pp. 76-78, Kiev / Ukraine;
- [15] Nadykto V., (2005), New mobile energy resources of Ukraine (Новые мобильные энергетические средства Украины), РН “ММД”, 337 p., Melitopol / Ukraine;
- [16] Nadykto V., (2009), A semi-mounted twin-machine, *Proceedings of Tauria Agrarian University* , Vol. 9 (3), pp. 137-143, Melitopol / Ukraine;
- [17] Rubec A., (2012), Increasing the efficiency of the use of machine-and-tractor aggregates (Повышение эффективности использования машинно-тракторных агрегатов), *Ukrainian Journal of Agribusiness*. No 9, pp. 108-111, Kiev / Ukraine;
- [18] Smolinsky S., (2016), Combined soil tillage aggregates (Комбинированные почвообрабатывающие агрегаты), *Agroexpert*, No 2, pp. 66-69, Kiev / Ukraine.

DEVELOPMENT OF INNOVATIVE TECHNOLOGIES SCIENTIFIC FOUNDATIONS FOR PRODUCING BEST FIBERS FOR SPECIAL PURPOSES

РАЗРАБОТКА НАУЧНЫХ ОСНОВ ИННОВАЦИОННЫХ ТЕХНОЛОГИЙ ДЛЯ ПОЛУЧЕНИЯ ЛУБЯНЫХ ВОЛОКОН ЦЕЛЕВОГО НАЗНАЧЕНИЯ

Ph.D. Researcher Kruglyj D.,¹⁾ Ph.D. doctoral student Boyko G.,²⁾ Prof. Ph.D. Eng. Klevtsov K.²⁾,

¹⁾ Kherson National Technical University, Department of Scientific Research, Kherson / Ukraine;

²⁾ Kherson National Technical University, Faculty of Integrated Technologies and Commodity Science / Ukraine

Tel: +3(08)0508274885; E-mail: galina_boyko_86@ukr.net

Keywords: technological process, flax, hemp, stems, fibre, paper

ABSTRACT

The present work contains the results of theoretical and experimental studies aimed at developing technologies for producing bast fibre retted straw to produce cellulosic semi-finished products in order to expand the scope of oilseed flax fibre in the production of cellulosic consumer goods. It is theoretically and experimentally proved based on comparative studies of the structure and chemical composition of flax stems and hemp, the necessity to create a new technology for the mechanical processing of these crops for the production of fibre with the given qualitative indices.

РЕЗЮМЕ

Представленная работа посвящена развитию научных основ инновационных технологий получения лубяных волокон пригодных для дальнейшей химической переработки и использования его в различных отраслях промышленности. Теоретически обосновано и экспериментально доказано на базе сравнительных исследований строения и химического состава стеблей льна и конопли необходимость создания новой технологии механической переработки этих культур для получения волокна с заданными качественными показателями. На основе установленного механизма штапельирования, выделение костры и разволокнения технических лубяных пучков предложены новые способы обработки стеблей, основанные на процессах управляемого измельчения и очистки, которые способствуют разрушению целостности стеблей и повышению степени разволокнения.

INTRODUCTION

Today, the pulp and paper industry in the world has prospects for development, but it also needs to solve important problems that must be addressed differently in different types of countries (Kocharov S.A. et al., 2002, Vurasco A.V. et al. 2006). Among the numerous problems in the pulp and paper industry of Ukraine, we can distinguish the main one - the search and use of alternative sources of raw materials. The main reason for this problem, which holds back the further development of the pulp and paper industry, is the absence in Ukraine of its own production of primary semi-finished products (Tihosova A.A. et al., 2010, Lyalina N.P. 2015). Thus, the growing shortage of wood raw materials and large foreign exchange costs for the purchase of cellulose abroad make it advisable to use cellulosic materials, in particular, existing bay crops in Ukraine.

It is known that one-year non-woody plants have a high content of cellulose and are widely used both for the production of fabrics and for the production of fibrous semi-finished products intended for the manufacture of cellulosic materials (Myenyaylo-Basistaya I.A. 2013). In many countries of the world, for example in Pakistan, Thailand and Peru, non-hardwood raw materials are the main type of raw material for the production of cellulose. In China, almost 87% of cellulosic products are produced from straw perennials.

Therefore, the manufacture of cellulosic products in Ukraine may be subject to the use of domestic raw materials (hemp and flax), innovative scientifically based technologies for the cultivation and processing of natural fibrous raw materials, increase of investment attractiveness of industrial segments, which will use natural raw materials and coordinated action programs in their products with the government and scientists.

MATERIALS AND METHODS

Materials

According to the prototype, hemp stems of the spring collection, varieties of textile, Victoria, Glance and Nick, were grown in Ukraine. Experimental researches were conducted with varieties of oil flax: Debut, Southern Night and Vira.

Modernized technological process of bast fibres processing

On the basis of the established stapling mechanism, isolation of chaff and garneting of technical bast bunches, new methods of stems processing, based on the processes of controlled crushing and purification, which contribute to the destruction of stems integrity and increase the degree of garneting level, have been proposed.

It was established that the increase in crushing bast fibre complexes at enhancing speed interaction of chopping rollers with the layer of processed material is more intense than with the increase in the number of mechanical actions. In connection with this, forcing the crushing process of technical complexes of bast fibres is more expedient to implement not by increasing the number of mechanical actions, but by increasing the speed of interaction between rasp-bar threshing rollers and fibre strand (*Gilyazetdinov R.N. 2009*).

The composition of the technological line for the production of purified staple fibre from bast crops and the replacement of typical threshing and breaking machines and tow scutcher with the modernized tow scutcher, which includes chopping rollers, is theoretically substantiated.

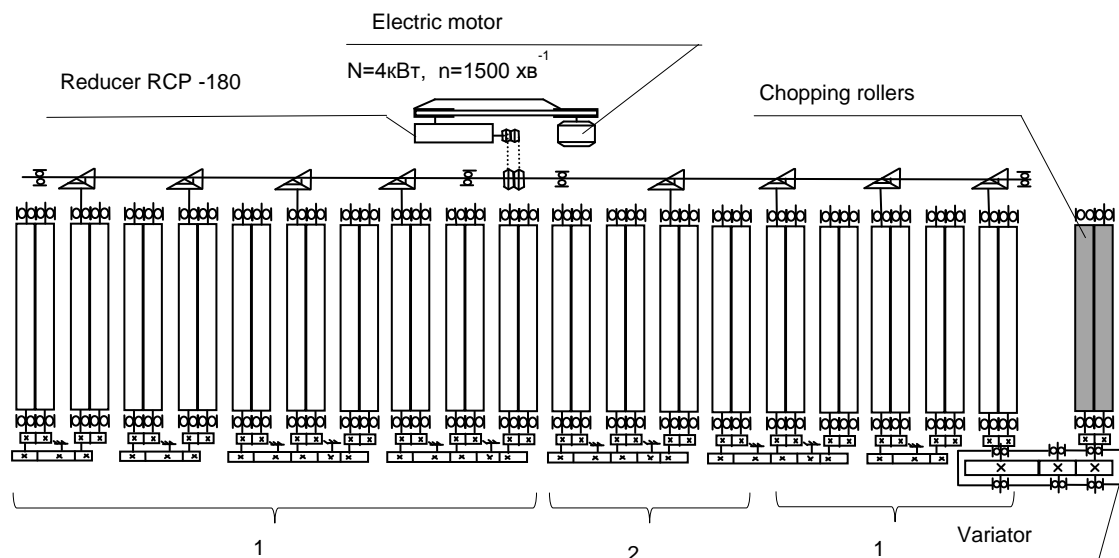


Fig 1 - Kinematic scheme of the experimental installation:

1 - rolls of direct corrugation, 2 - rollers of screw corrosion

The melting part of the plant is driven by an individual electric motor, from which, through a wedge-shift transmission, a worm gear unit RCP-180 and a dual chain drive, two longitudinal shafts receive a rotating moment, which, by means of conical gears, rotate to the lower roller rollers. The velocity of the material being processed in it is 22.4 m/min.

Full-featured installation

To determine the optimal parameters of cleaning plant operation, a full-featured experiment was conducted, in which the staple composition of fibre became an assessment criterion.

The study of mechanical processes theoretical foundations of cleaning and garneting the bast raw materials has shown that due to the differentiation of the conditions of drawing the layer of feedstock and regulating the entering depth, the rotation speed and the grooves step during breaking, it is possible to intensify the separation process of the wood from the fibrous part of the stem.

For bast fibre crushing, it is necessary to change the differentiation conditions of breaking in the last pair of mechanical rollers due to toothed cohesion and regulation of rotation relative speed, which allows to simulate the process of scutching and stapling on the threshing machine. It is also necessary to provide

controlled crushing of broken raw products due to the increase of the processing intensity generated by the introduction of additional forces in the breaking process that characterize threshing process.

For thinning the fibre complexes, it is the most efficient to use devices that provide additional scutching of restrained fibre strand (Novikov E.V. et al., 2014). These devices, in conjunction with additional cleaning plants, should provide a sufficient degree of purification. In order to select rational regimes and parameters of purification, the process of impact interaction of movable operating element with fibre was studied and a model of interaction of roll flute edge with a separable part of chaff and fibre was developed. The analysis of the model showed that the movement of chaff part with fibre strand is influenced, at first, by the speed of roll flute rotation and the frequency of its operations.

The method for determining the impact load on fibre strand, which allows choosing the most rational technological and structural parameters of the installation and process, is proposed.

The impact load on the fibre strand was calculated and a linear model of the impact interaction process of fibre strands with roll flute element was developed.

The analysis of this model and its comparison with experimental data allowed us to establish that fibre strand should be considered as an elastic element that has a restricted mass. Application of the model during the design of equipment for the production and cleaning of short-staple bast fibres will make it possible to determine the rational parameters of equipment and technological process more accurately.

As a result of theoretical study, a nonlinear model of the impact interaction process of fibre strands with roll flute element is created. A methodology that allows estimating nonlinearity of stiffness characteristics of fibre strands on the basis of experimental research results is suggested. The method of calculating the parameters of the impact interaction process is presented. The developed model more fully describes the impact interaction process of fibre strands with movable operating element than linear models.

Increase of bast fibre crushing is characterized by a classic curve of damage accumulation and consists of three stages: the stage of intense damage accumulation, the stage of moderate damage accumulation, the stage of critical destruction.

A new method for determining the physical and mechanical characteristics of staple bast fibres is proposed, based on modern methods of mathematical data processing in the software environment "MATLAB 7.0" (Ostapchuk M.V., et al., 2006).

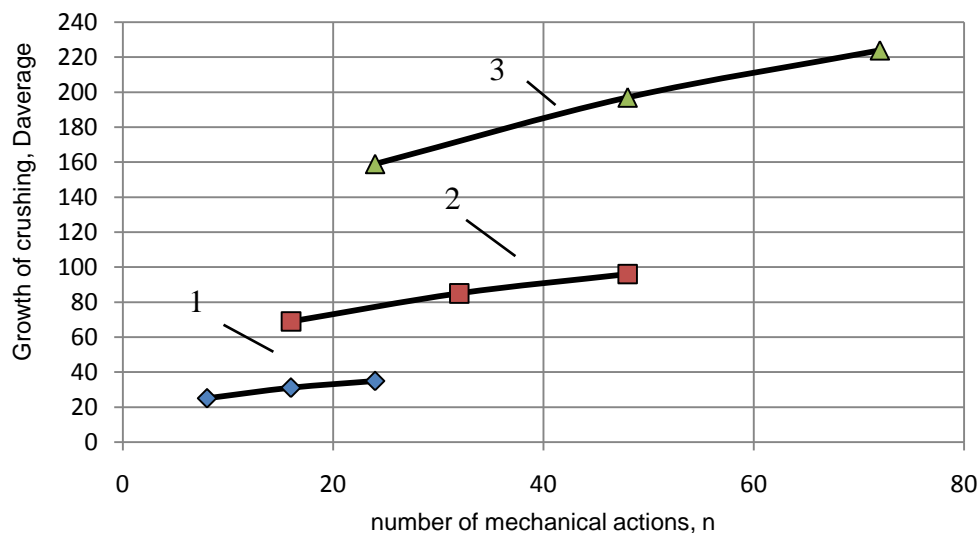


Fig 2- Dependences of the growth of linen complexes fragmentation on the number of mechanical actions at the interaction rate:

1 – 48,98 min^{-1} ; 2 – 97,99 min^{-1} ; 3 – 146,95 min^{-1}

On the basis of the dynamic analysis of fiber strands interaction, which contains the separable part of chaff, with the movable operating element it is shown that the efficiency of garbage impurity extraction during the impact will be increased as the fiber line decomposes, when the mass of wisps of fibers interacting with the movable operating element will come nearer to the mass of separable fibrous parts of chaff.

It was established that the increase in crushing bast fiber complexes with increasing the interaction speed is more intense than with increasing the number of mechanical actions. Consequently, the

intensification of bast fiber complexes crushing process is more expedient to implement not by increasing the number of mechanical actions, but by increasing the interaction speed.

The proposed technology is based on the use of inertial fiber cleanser

The study of theoretical foundations of cleaning and garnetting mechanical processes of bast raw materials has shown that due to the differentiation of the conditions of drawing the layer of feedstock and regulating the entering depth, the rotation speed and the grooves step during passing, it is possible to intensify the separation process of the wood from the fibrous part of the stem (*Virovets V.G., et al., 2011*).

The conducted experimental researches have shown the advantages of the proposed technology, which affirms the expediency of using a fiber cleanser for cleaning and garnetting the technical bast complexes. The optimum values of the nutrient layer density and the rate of its delivery for providing high quality bast fibers obtained on the fiber cleaner have been determined. In addition, crushing of contaminated impurities, which facilitate their easier removal during further processing takes place in pre-treatment process.

Based on the developed mathematical model, the influence of raw materials characteristics and the technological equipment structural specifications on the final qualitative characteristics of the linen fiber was investigated, as well as the most rational modes and parameters of the fiber cleaner operation were selected.

The technological line proposed is based on the use of the modernized breaking part of the tow scutcher unit KPAL and is intended for the mechanical preparation of bast raw materials for further chemical treatment through the use of chipping rollers and additional purification of crushed stalks on a fibercleaner and a fiber-separating machine BOM-2.

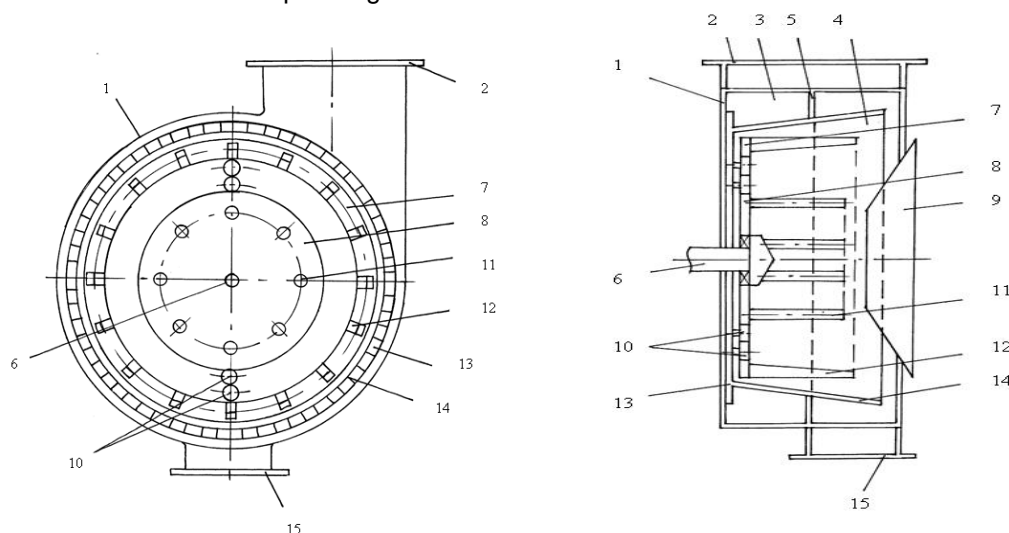


Fig 3 - Fiber cleanser scheme

1 - body; 2 - outlet pipe; 3 - the burning part; 4-fiber-separating part; 5 - separator; 6 - shaft; 7 - external rotating disk; 8 - internal rotating disk; 9 - diffuser loader; 10 - toothed pair; 11 - white rods; 12 - comb; 13 - grate grating; 14 - rods; 15 - outlet pipe

Fibrous processing complexes are not strictly fixed and the process of bonnet separation is intensified by means of centrifugal forces that arise due to the beating rods rotation. In addition, the speed of the external disk drive exceeds the speed of the inner one, creating the effect of additional stretching. Due to the proposed changes in mechanical action, a more efficient cleaning of flaxseed from the derivative (Table 1) is carried out.

Table 1

Variations of the main structural and technological parameters of the fibre cleanser

Variable parameters of working bodies	Numbers of comb combinations							
	1	2	3	4	5	6	7	8
Step of comb fins, mm, (X_1)	120	120	120	150	150	150	120	150
Angle of inclination of comb, degree, (X_2)	55	55	45	55	55	45	45	45
Width of comb ribs, mm (X_2)	100	150	150	100	150	150	100	100

According to the results of theoretical and experimental researches, an innovative technology of bast crops primary processing, which has undergone extensive testing in scientific circles and has found positive feedback from industry experts, has been proposed.

Mathematical description of the technology of stapling and cleaning bast fibers during their processing on the proposed equipment allowed establishing a number of experimental and theoretical dependencies that determine the boundary values of the adjustment parameters of technological equipment separate units and the process of bast crops mechanical treatment in general, which will allow to create an innovative technology for the production of bast fibers for various industries in Ukraine.

RESULTS

On the basis of the conducted research complex the scientific concept of equipment improvement for the innovative technologies of bast crops primary processing has been developed, which ensures the production of bast fibers of the intended purpose. On this ground for the first time:

- it is proposed to use chopping rolls in mechanical processing of bast stems with the aim of intensifying the process of obtaining cellulosic raw material;
- scientific development was given to production theoretical foundations of various intended purpose bast fibers, based on implementing modern technologies for complex mechanical processing of flax stems and hemp;
- a new concept of bast stems mechanical processing is theoretically grounded, based on the garnetting of technical fibers complexes due to the use of new mechanical actions in the initial stages of raw materials primary processing;
- the model of the crushing process of bast fiber complexes has been developed, which made it possible to establish that the increase in crushing of their complexes with increasing interaction speed is much more intense than with increasing the number of mechanical actions;
- the methodology of determining qualitative parameters of bast fibers on the basis of mathematical data processing on the input characteristics of bast crop stems, structural features of the equipment, parameters and modes of mechanical processing has been developed;
- the criterial evaluation methodology of structural parameters of bast crops staple fiber, which will determine its functional purpose has been developed.

As a result, from obtained hemp fiber cellulose, paper was obtained, the qualitative parameters of which are presented in Table 2.

Table 2

Qualitative characteristics of paper obtained from hemp fiber

Quality score name	Quality score value		Divergence $\pm\Delta$
	by standard	received paper	
Weight of paper with an area of 1m ² , g	75,0	97,0	-22,0
Air permeability, at $\Delta p=200$ Pa, S=10 sm ² , l/m ² sec	830	1350	+520
Absolute resistance to dampening, kPa	0,45	0,60	+0,15
Destructive effort, kN / m	2,0	4,5	+2,5
Thickness, mm	0,6	0,8	-0,2

The use of bast crops stems to obtain cellulose materials for various purposes will contribute to a significant reduction of environmental damage from deforestation, eliminate the import dependence of Ukraine in the manufacturing of strategically important products, and an increase in the production of polymeric materials, reinforced with natural vegetable fibres, will provide lower prices for cars, will stimulate the development of farms, reduce soil contamination and improve the composition of the air.

In order to create innovative technologies for the production of bast fibers, practical recommendations for increasing the efficiency of their further chemical treatment, which are aimed at obtaining high-quality fibrous semi-finished products and determining the degree of their suitability for the use in various spheres of industrial production have been developed (*Popadinets N.M, 2011*).

CONCLUSIONS

The theoretical laws and regulations, formulated by the author, are the basis of a new methodology for the creation of both individual processes and the whole technology of bast crops complex processing.

The results of experimental studies indicate that obtaining high-yielding cellulose from flaxseed may be at a temperature of 160-170° C, boiling time of 180-300 minutes, and concentration of NaOH boiling solution of 30-40 g / 1.

Boiling of flax straw untreated stems by the sodium carbonate method makes it possible to increase the yield of cellulose from 60.1% to 90.0%.

If short flax fiber is used as raw material, high yield cellulose can be obtained at a boiling temperature of 170 to 160°C, at boiling time of 180-300 minutes, and concentration of NaON boiling solution of 45-50 g/1.

The analysis of the experimental data obtained shows that, with practically the same strength, the air permeability in paper samples obtained according to the proposed technology is three times higher than the existing standards.

ACKNOWLEDGEMENT

Assistance in obtaining cellulose from bast crops fibers was obtained from the Ukrainian Research Institute of Paper (Kiev, Ukraine).

The evaluation of the physico-mechanical characteristics of paper made from bast fibers was carried out at the production base of the Tsyurupinsk paper company (Kherson region, Ukraine).

REFERENCES

- [1] Gilyazetdinov R.N., (2009), *Development of scientific foundations for the creation of innovative technologies for the primary processing of bast crops (Розвиток наукових основ створення інноваційних технологій первинної переробки луб'яних культур)*, MSc. Dissertation, Kherson National Technical University, Kherson/ Ukraine;
- [2] Kocharov S.A., Zakharov, R.N., Yarullyn A.P., (2002), The main issues of obtaining and using cellulose bast culture (Основные вопросы получения и использования целлюлозы лубяных культур), *International scientific and practical conference*, pp. 29-35, Vologda / Russia;
- [3] Lyalina N.P., (2015), *Development of scientific fundamentals of non-narcotic hemp stems primary processing for obtaining fibres of various functional purposes (Розвиток наукових основ первинної переробки стебел ненаркотичних конопель для отримання волокон різного функціонального призначення)*, MSc dissertation, Kherson National Technical University, Kherson/ Ukraine;
- [4] Myenyaylo-Basistaya I. A., (2013), *Development of technology for processing of oilseed flax retting straw to produce cellulose semi-finished products (Розроблення технології переробки стебел соломки льону олійного з метою одержання целюлозовмісних напівфабрикатів)*, Ph.D. dissertation, Kherson National Technical University, Kherson/ Ukraine
- [5] Novikov E.V., Protalinsky S.E., Bezbabchenko A.V., (2014), Research on technologies for processing cannabis in the same type of fibre of various characteristics (Исследование технологий переработки конопли в однотипное волокно различных характеристик), *Proceedings of high schools. Technology of the textile industry (Известия вузов. Технология текстильной промышленности)*, pp. 42-46;
- [6] Ostapchuk M.V., Stankevich G.M., (2006), *Mathematicians modelling on EOM (Математичне моделювання на EOM)*, "Odesa Druk", p. 313, Odesa / Ukraine;
- [7] Popadinets N.M., (2011), Market of pulp and paper industry: trends, problems and directions of development (Ринок целлюлозно-паперової промисловості: тенденції, проблеми та напрямки розвитку), *Scientific Bulletin of NLTU of Ukraine (Науковий вісник НЛТУ України)*, pp. 278-284;
- [8] Tihosova A. A., Golovenko T.M., (2010), Substantiation of the processing efficiency of flaxen oil stems (Обґрунтування ефективності переробки стебел льону олійного), *Bulletin of Khmelnytsky National University (Вісник Хмельницького національного університету)*, pp. 268 – 274;
- [9] Vurasco A.V., Driker B.N., Mozyrov E.A., (2006), Resource-saving technology for obtaining cellulosic materials in the processing of agricultural waste (Ресурсосберегаюча технологія получения целлюлозных материалов при переработке отходов сельскохозяйственных культур), *Chemistry of plant raw materials (Химия растительного сырья)*, № 4, pp. 5-10;
- [10] Virovets V.G., Gilyazetdinov R.N., Baranik V.G, (2011), *Нетр: Monograph (Коноплі: монографія)* Publishing House "Hellas", p. 384, Sumy / Ukraine.

DEVELOPMENT OF A PNEUMATIC SCREW CONVEYER DESIGN AND SUBSTANTIATION OF ITS PARAMETERS

/

РОЗРОБКА КОНСТРУКЦІЇ ПНЕВМО-ШНЕКОВОГО ТРАНСПОРТЕРА ТА ОБГРУНТУВАННЯ ЙОГО ПАРАМЕТРІВ

Prof. Ph.D. Eng. Hevko R.B.¹⁾, Prof. Ph.D. Eng. Strishenets O.M.²⁾, Prof. Ph.D. Eng. Lyashuk O.L.³⁾,
Assoc. Prof. Ph.D. Eng. Tkachenko I.G.³⁾, Assoc. Ph.D. Eng. Klendii O.M.⁴⁾, Assoc. Prof. Ph.D. Eng. Dzyura V.O.³⁾,

¹⁾Ternopil National Economical University / Ukraine; ²⁾Lesya Ukrainka Eastern European National University / Ukraine;

³⁾Ternopil Ivan Puluj National Technical University / Ukraine; ⁴⁾Separated Subdivision of National University of Life and Environmental Sciences of Ukraine Berezhanly Agrotechnical Institute / Ukraine;

E-mail: sashaklendii@gmail.com

Keywords: *pneumatic screw conveyer, loose material, screw feeder, air pressure.*

ABSTRACT

The paper presents the developed design of a research prototype of a pneumatic screw conveyer and the research methodology aimed at determining power characteristics for moving various types of loose materials depending on the influence of pressure and air volume. The dependences of pneumatic screw conveyer efficiency on the change in the area of a hopper hole, the rotation frequency of a screw feeder and the value of an operating air pressure in a technological line have been determined. The influence of the form and the geometrical parameters of a central replaceable nozzle on the distance of loose materials transportation has been determined.

РЕЗЮМЕ

В статті представлено розроблену конструкцію дослідного взірця пневмо-шнекового транспортера та методу проведення досліджень для визначення силових показників переміщення різних типів сипких матеріалів в залежності від впливу тиску та об'єму повітря. Встановлено залежності продуктивності пневмо-шнекового транспортера від зміни площі отвору бункера, частоти обертання шнекового живильника та величини робочого тиску повітря в технологічній магістралі. Встановлено вплив форми та геометричних параметрів центрального змінного сопла на відстань транспортування сипких матеріалів.

INTRODUCTION

The conducted analysis of recent scientific and patent literature (Lyashuk O.L. et al., 2015; Rogatynska O. et al., 2015; Loveikin V. and Rogatynska L., 2011; Lech M., 2001; Manjula E.V.P.J. et al., 2017; Naveen Tripathi, 2015), which cover the design of operating devices and the ways of loose material transportation in closed casings along both rectilinear and curvilinear routs, shows that they satisfy most of the requirements for the process quality to a certain extend. But the issues connected with the improvement of conveyer efficiency, the reliability of operating elements, the reduction of energy consumption and minimization of loose material damage during its transportation etc. have not been fully investigated yet. This paper presents further investigation of the issues, covered in paper (Hevko R.B. et.al., 2014; Hevko R.B. et al., 2016; Hevko R.B. et al., 2017).

MATERIALS AND METHODS

In order to conduct experimental investigations, a research prototype of a pneumatic screw conveyer (Fig. 1) has been designed and developed. It contains a frame 1, where there is an electric motor 2, which is connected to a V-belt drive 3 with a reducer 4. With the help of a chain drive 5, a take-off shaft of a reducer transmits torque to the shaft of a screw feeder 6. Loose material is loaded into a hopper 7. A center shaft of a screw feeder is connected to a pneumatic system with the help of pneumatic pipelines 8. A splined shaft of a screw feeder is arranged with the possibility of angular displacement in bearing assemblies and is spring biased 9. Pressure of the compressed air is delivered through a pneumatic transmitter 10 to a pneumatic distributor 11 in the central opening of a screw feeder, where there is a replaceable nozzle 12 arranged.

Loose material comes through a hopper into a conveyor body and gets onto a screw feeder, which carries out a rotational motion. If there is an overload, which is caused by the accumulation of a certain amount of loose material in the process chamber of a conveyor body, due to its spiral surface a screw feeder is axially displaced in the direction opposite to the one of loose material transportation with the help of a splined joint and it compresses a spring. Here, air from a pneumatic distributor reaches a central opening of a splined shaft of a screw feeder, which causes further transportation of loose material.

At the first stage of the experimental research, actual efficiency of a pilot plant without air feed has been defined and initial escape of material transportation or steady provision of accelerated material transportation after its rolling off the flights have been determined.

In order to determine the influence of the area of a hopper discharge hole and the frequency of screw rotation on the efficiency of a pilot plant, investigations without high-pressure air feed were conducted based on the implementation of a multi-factor experiment, and searching experiments were conducted based on the implementation of a single-factor classical experiments.

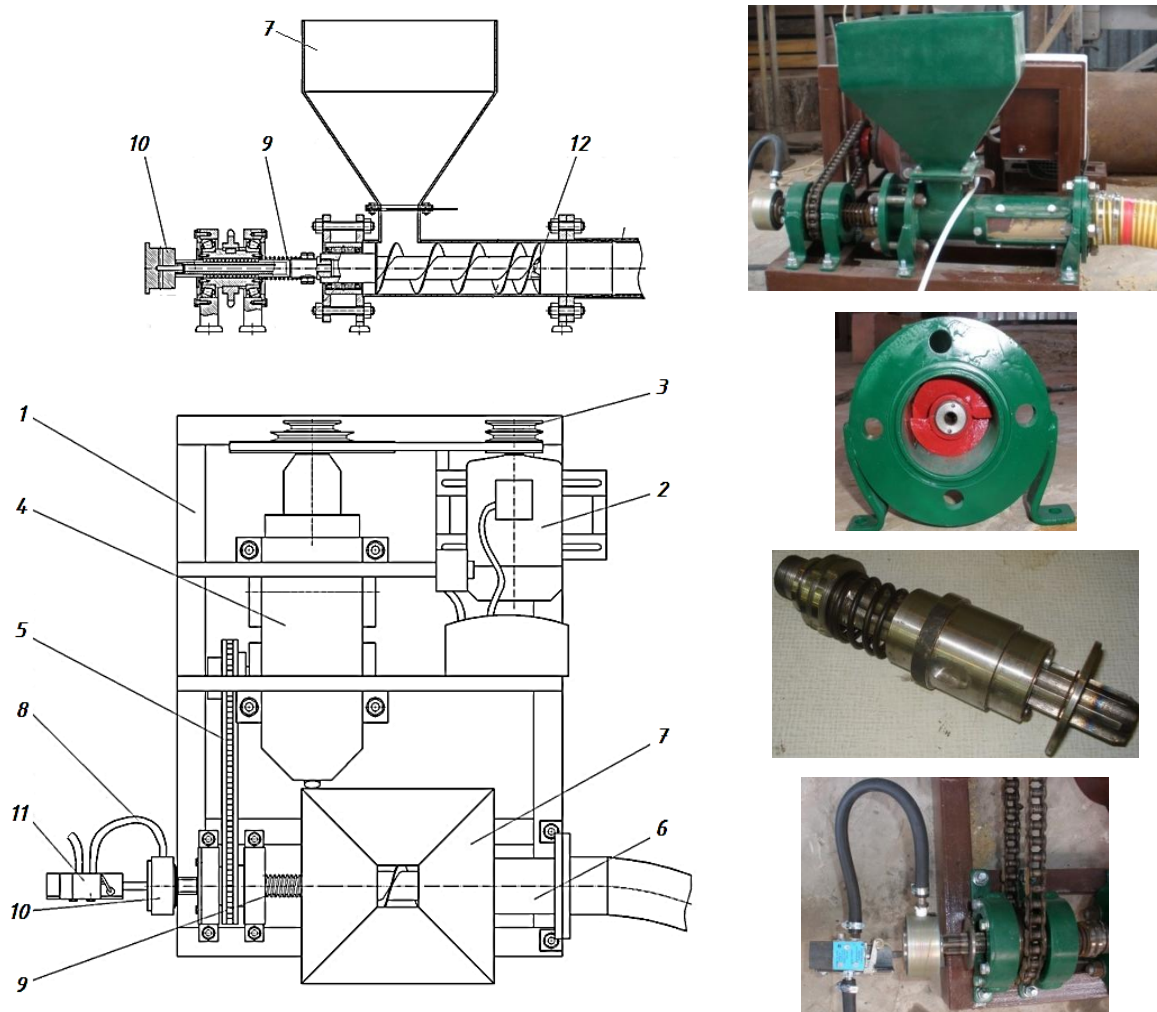


Fig. 1 - Pneumatic Screw Conveyor:

1 – frame; 2 – electric motor; 3 – V-belt drive; 4 – gear box; 5 – chain drive; 6 – feeder housing; 7 – hopper; 8 – pneumatic pipelines; 9 – spring; 10 – pneumatic adapter; 11 – pneumatic distributor; 12 – interchangeable nozzle

A response function or an optimization parameter of the efficiency of a pilot plant Q_1^e without high-pressure air feed, which was determined by an experimental approach, was found in the form of a mathematical model of a logarithmic function

$$Q_1^e = b_0 + b_1 \ln x_1 + b_2 \ln x_2 \quad (1)$$

where Q_1^e – efficiency of a pilot plant without high-pressure air feed, kg/m; b_0 , b_1 , b_2 – coefficients of an

approximate model under orthogonality and symmetry conditions; having made calculations, it has been determined that $b_0 = -27.49$; $b_1 = 5.2$; $b_2 = 2.77$; coded factors according to the area of a hopper discharge hole: $x_1 - S_c \times 10^{-4}$, m^2 ; frequency of screw rotation: $x_2 - n$, rev/m .

According to the results of the conducted multi-factor experiment, the general view of the regression equation of the dependence of the efficiency of a pilot plant Q_1^e without high-pressure air feed on the area of a hopper discharge hole S_c and the frequency of screw rotation n in actual values is the following:

$$Q_1^e = -27.49 + 5.2 \ln(S_c) + 2.77 \ln(n) \quad (2)$$

During the performance of the experiments, the factorial field was determined by the following parameter range: $12 \leq S_c \leq 35$ ($10^{-4} m^2$); $150 \leq n \leq 450$ (rev/m).

The obtained regression equation (2) can be used for determining the efficiency of a pilot plant Q_1^e without high-pressure air feed according to the area of a hopper discharge hole S_c and the frequency of screw rotation n .

Based on the regressional dependences, a response surface with its two-dimensional section of the change in the efficiency of a pilot plant without high-pressure air feed as a functional $Q_1^e = f(S_c, n)$ was constructed, which is represented in Fig. 2.

The pattern of Q_1^e change shows that within the limits of factor variation, the efficiency changes from 0.75 to 9.0 (kg/m). Here, the pattern of Q_1^e change depending on every separate factor is different: the rate of Q_1^e gain depending on the change in the area of a hopper discharge hole S_c is much bigger than the rate of efficiency gain depending on the frequency of screw rotation n and is within the limits of 0.5...2.5 kg/m and 3.5...7.0 kg/m respectively. Thus, the influence of S_c on the efficiency of a plant is much greater than the frequency of screw rotation n .

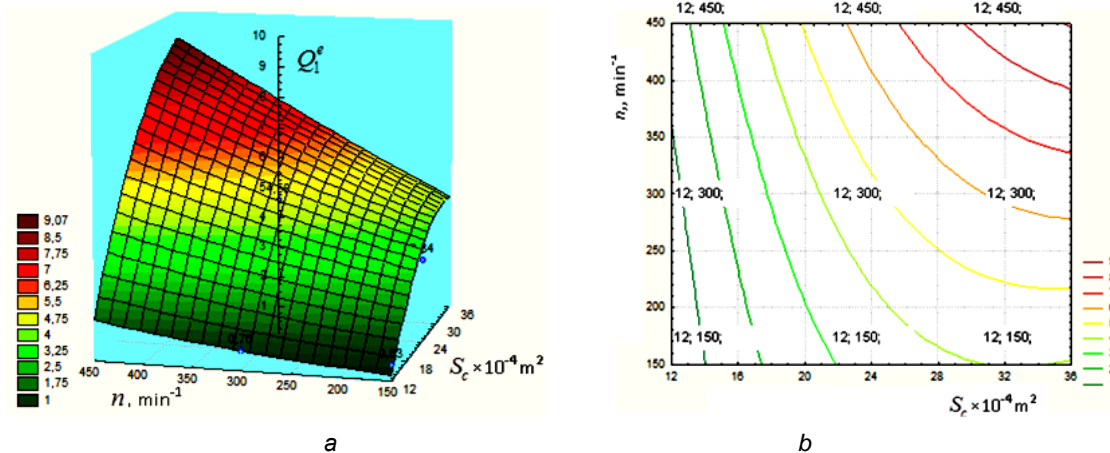


Fig. 2. - Response surface (a) and its two-dimensional section (b) of the change in pilot plant efficiency depending on the area of a hopper discharge hole S_c and the frequency of screw rotation n

The determination of the lower value of the operating pressure P of air feed, at which the beginning of material acceleration (its rolling off) at the discharge end of a flight can be observed, was carried out by means of implementing searching experiments, which were conducted at constant minimum values of the factors $S_c = 12 \cdot 10^{-4} m^2$ and $n = 150 rev/m$.

In order to conduct comparative studies with high pressure air feed P at the take-off shaft of a screw feeder, nozzles of various configurations were made (Fig. 3). When determining maximum distance of free material movement from a nozzle, investigations were conducted at the constant frequency of feeder rotation $n = 450 rev/m$ and air feed pressure $0.8 \cdot 10^6 N/m^2$.

The necessity of conducting searching experiments was based on the fact that a pilot plant is a scaled model, the dimensional specifications of which significantly differ from those of a full-scale pneumatic screw conveyor. The beginning of accelerated material movement was visually observed with the help of screening and comparing high-speed shooting (Fig. 4) at the initial value of $P = 0.05 \cdot 10^6 N/m^2$ and the following level of operating pressure variation $\Delta P = 0.02 \cdot 10^6 N/m^2$.

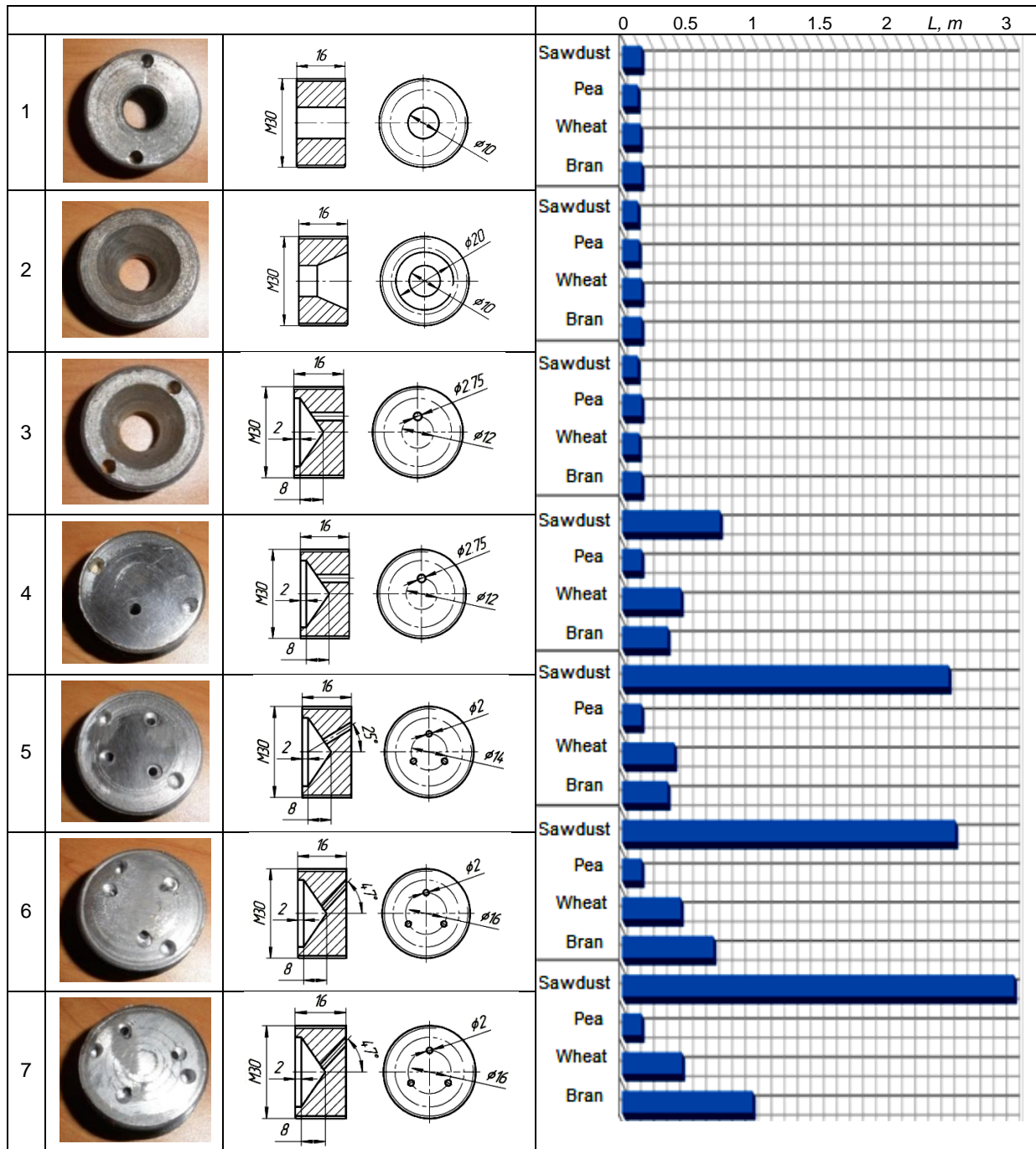


Fig. 3 - The distance of loose material transportation depending on the form and the geometrical parameters of a nozzle of a pneumatic screw conveyor:

1, 2, 3 – with a central opening of various conicity (diameter $D = 10$ mm); 4, – with a non-central opening (diameter $D = 2.75$ mm); 5, 6, 7 – with three openings located at various angles to the axis



Fig. 4 - General view of high-speed shooting of the process of material movement acceleration

RESULTS

The results of the experimental investigations of the change in pneumatic screw conveyer efficiency depending on the initial values of high pressure air feed P are represented by a graphic chart (Fig. 5).

It has been determined that the change of the operating pressure P within the limits of $(0.05...0.2) \cdot 10^6$ N/m² has almost no influence on the efficiency of a pneumatic screw conveyer and material movement acceleration is observed at $P_{\min} \approx 0.2 \cdot 10^6$ N/m².

Experimental investigations of the efficiency of a pilot plant at high pressure air feed were conducted based on the implementation of a multi-factor experiment (three-factor experiment at the levels of variation).

The procedure of planning and conducting experiments and the processing of the obtained experimental data is similar to the previous one, except for the fact that together with engaging the drive of a screw, a compressor unit was simultaneously turned on as well, having the preset necessary value of the operating air pressure P entering the collector.

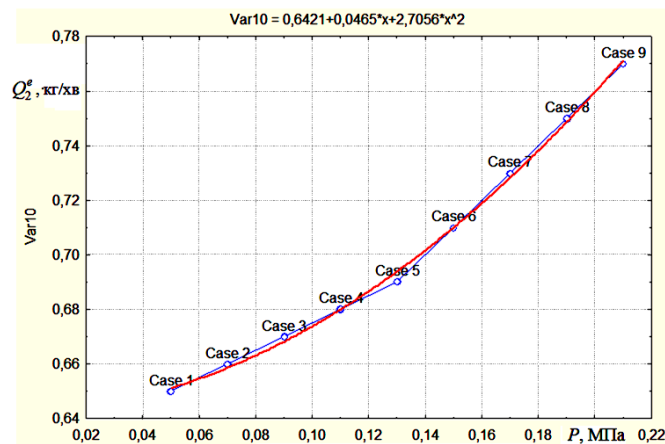


Fig. 5 - Dependence of efficiency as a functional on air pressure $P = (0.5...0.21) \cdot 10^6$ N/m²

The general view of the regression equation, which describes the dependence of pilot plant efficiency Q_1^e at high pressure air feed on the area of a discharge hopper hole S_c , the frequency of screw rotation n and operating pressure P based on the results of the conducted multi-factor experiment in actual values is the following

$$Q_2^e = -25.23 + 7.34 \ln(S_c) + 2.26 \ln(n) + 2.97 \ln(P). \quad (3)$$

During the performance of the experiments, the factorial field was determined by the following parameter range: $12 \leq S_c \leq 35$ (10⁻⁴ m²); $150 \leq n \leq 450$ (rev/m); $0,2 \leq P \leq 0,5$ (10⁶ N/m²).

Based on the regression equation (3), a response surface with its two-dimensional section of the change in the efficiency of a pilot plant Q_2^e at high-pressure air feed as a functional $Q_2^e = f(S_c, P)$ and $Q_2^e = f(n, P)$ at constant values of the relevant third factor, that is to say at $x_2 = n = \text{const}$, $x_1 = S_c = \text{const}$ was constructed. Graphical dependences of functional $Q_2^e = f(S_c, P)$ and $Q_2^e = f(n, P)$ are represented in Fig. 6 and Fig. 7.

It has been determined that efficiency Q_2^e increases with the increase of operative factors and is within the limits of 2...11 kg/s depending on their change. The frequency of screw rotation n and the area of a hopper discharge hole S have the most significant influence on the pattern of efficiency Q_2^e change, here, significant increase of Q_2^e is observed at the increase of the relevant factor value $S_c \geq 24 \cdot 10^{-4}$ m², $n \geq 300$ rev/m. In addition, it has been determined that depending on the change of operating air pressure P within the limits of factor change $0.2 \leq P \leq 0.3$ (10⁶ N/m²), the efficiency of a pneumatic screw conveyer increases rectilinear to the increase of P , here, the gain is about 1.1 kg/m.

The disadvantage of such additional feeding is that air streams, which are coming out of pneumatic system nozzles and directed into a transportation flow, are places at a high angle. Such arrangement of

nozzles is inconsistent with the direction of material movement in a flexible pipe.

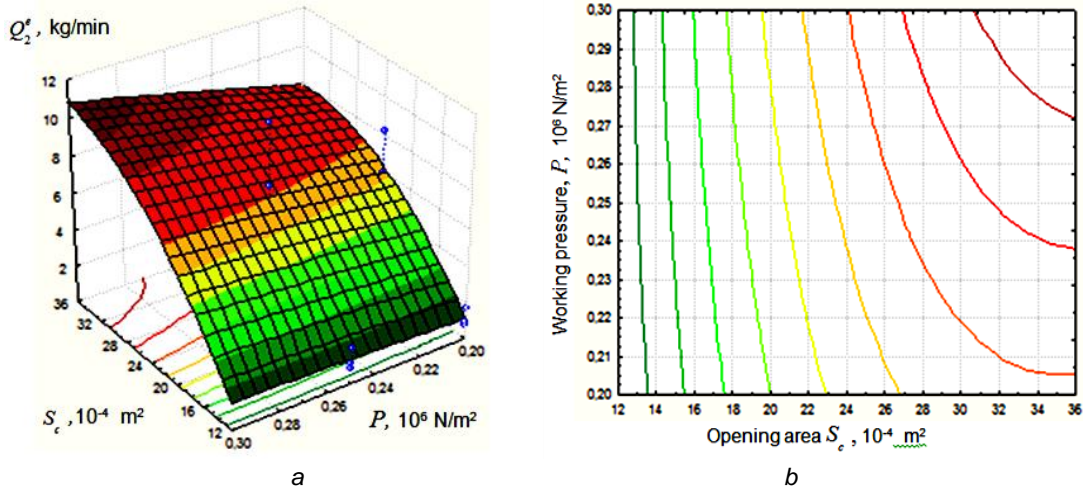


Fig. 6 - A response surface (a) and its two-dimensional section (b) of the efficiency of a pneumatic screw conveyor as a functional $Q_n = f(S_c, P)$ at $n = 300 \text{ rev/m}$

The construction arrangement and the general view of a new technical performance of a pneumatic screw conveyor are represented in Fig. 8. It consists of carriage 1 and 2, where there is a drive 3, a frame 4 with a hopper 5, a screw feeder 6, a pneumatic system 7 and a pneumatic valve 8 arranged. A conveyor pipeline consists of series-connected sections 9 of length l , here, each section contains an elastic casing 10, which, on its right side, is fixed on a coupling cylinder bushing 11 with the help of a ring 12 that is regulated by bolt 13 tightening.

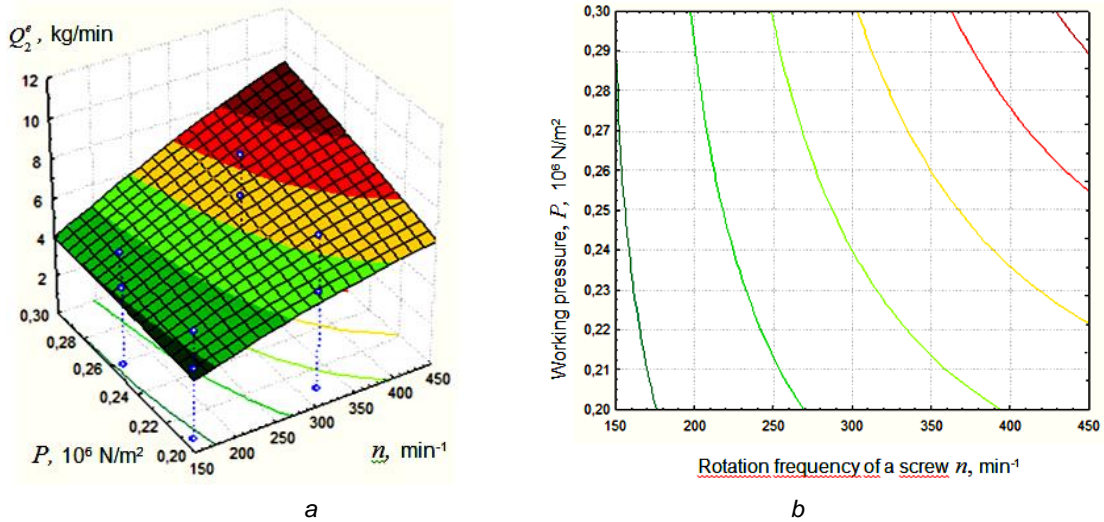


Fig. 7 - Response surface (a) and its two-dimensional section (b) of the efficiency of a pneumatic screw conveyor as a functional $Q_n = f(n, P)$ at $S_c = 24 \cdot \text{m}^2$

In the central part of a cylindrical bushing 11 there are openings 14 inclined in the direction of material transportation, which are arranged in a circle and are caught by a Π -shaped bushing 15, on the outer diameter of which there are connectors 16 arranged at an angle in the direction of material transportation and to which there are air supply hoses 17 attached. On the left side of an elastic casing on air supply hoses there are inlet connectors 18 arranged, which are connected to the common pneumatic system of a conveyor, here, the length of air supply hoses of every next section are twice bigger than those of the previous one and the hoses of the section are displaced in circular direction and fixed along the section length 9 by a clamp 19.

While in operation, material comes through a hopper 5 into a conveyor body 4 on a screw feeder 6. When there is overload caused by the accumulation of a certain amount of loose material in the processing chamber of a conveyor body 4, a screw feeder is displaced axially in the direction opposite to material

transportation. Here, air comes along hoses 17 through holes 14 into the section 9 and dilutes the accumulated material.

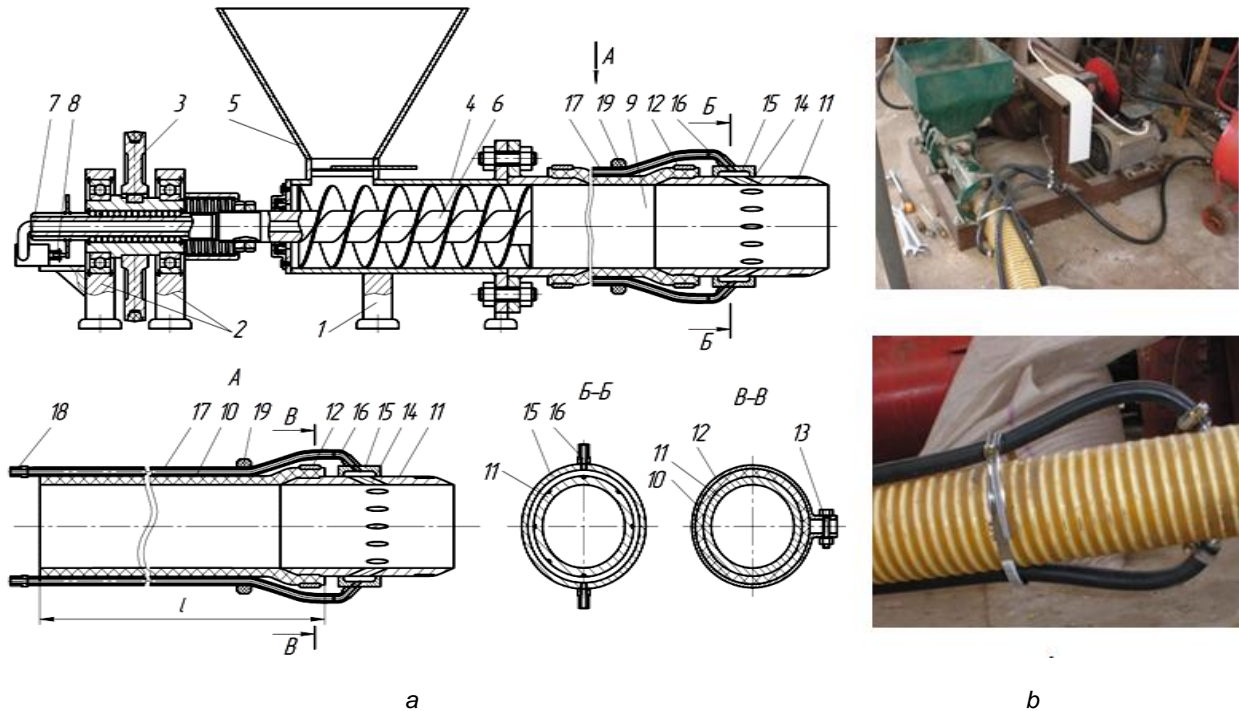


Fig. 8 - Construction arrangement (a) and general view (b) of a pneumatic screw conveyor with feeding hoses connected to a flexible casing

CONCLUSIONS

The paper presents the developed design of a pneumatic screw conveyor and investigation procedure for determining the dependence of pneumatic screw conveyor efficiency on the change in the form and the geometrical parameters of a nozzle, the area of hopper hole, the frequency of screw feeder rotation and the value of operating air pressure in a technological lane.

Response surfaces and their two-dimensional sections have been constructed and their analysis shows that the efficiency Q_n of a pneumatic screw conveyor increases with the increase of the operating factors and is within the limits of 2...11 (kg/s).

The frequency of screw rotation n and the area of a hopper discharge hole S_c have the most significant influence on the pattern of efficiency Q_n change, here, there is significant increase of Q_n with the increase of the value of relevant factors $S_c \geq 24 \cdot 10^{-4} \text{ m}^2$ and $n \geq 300 \text{ rev/m}$.

Based on the results of the conducted investigations, a pneumatic screw conveyor with additional feeding of material flow by means of air streams has been developed and made.

REFERENCES

- [1] Hevko R.B., Dzyura V.O., Romanovsky R.M., (2014), Mathematical model of the pneumatic-screw conveyor screw mechanism operation, *INMATEH: Agricultural Engineering*, vol.44, no.3, pp.103-110, Bucharest / Romania;
- [2] Lech M. (2001) - Mass flow rate measurement in vertical pneumatic conveying of solid, *Powder Technology*, Vol.114, Issues 1–3, pp. 55-58;
- [3] Manjula E.V.P.J., Hiromi W.K. Ariyaratne, Ratnayake Chandana, Morten C. Melaaen (2017) - A review of CFD modelling studies on pneumatic conveying and challenges in modelling offshore drill cuttings transport, *Powder Technology*, Vol.305, pp. 782-793;
- [4] Naveen Tripathi, Atul Sharma, S.S. Mallick, P.W. Wypych (2015) - Energy loss at bends in the pneumatic conveying of fly ash, *Particuology*, vol.21, pp. 65-73;
- [5] Hevko R.B., Klendiy M.B., Klendii O.M., (2016), Investigation of a transfer branch of a flexible screw conveyor, *INMATEH: Agricultural Engineering*, vol.48. no.1, pp.29-34, Bucharest / Romania;
- [6] Hevko R.B., Rozum R.I., Klendiy O.M. (2016), Development of design and investigation of operation

- processes of loading pipes of screw conveyors, *INMATEH: Agricultural engineering*, vol.50, no.3, pp.89-96, Bucharest / Romania;
- [7] Hevko R., Vitrovyi A., Klendii O., Liubezna I., (2017), Design engineering and substantiation of the parameters of sectional tools of flexible screw conveyers, *Bulletin of the Transilvania University of Brasov*, Vol. 10(59), pp. 39-46, Brasov / Romania;
- [8] Hevko R.B., Yazlyuk B.O., Liubin M.V., Tokarchuk O.A., Klendii O.M., Pankiv V.R. Feasibility study of the process of transportation and stirring of mixture in continuous-flow conveyers, *INMATEH: Agricultural engineering*, vol.51, no.1, pp.10-20, Bucharest / Romania;
- [9] Loveikin V., Rogatynska L., (2011), A Model of Loose Material Transportation by Means of High-Speed Conveyers with Elastic Operating Devices (Модель транспортування сипкого вантажу швидкохідними гвинтовими конвеєрами з еластичними робочими органами). *Bulletin of the Ternopil Ivan Puluj National Technical University (Вісник Тернопільського національного технічного університету ім. І.Пулюя)*, Vol.16, pp.66-70, Ternopil / Ukraine;
- [10] Lyashuk O.L., Rogatynska O.R., Serilko D.L., (2015), Modelling of the vertical screw conveyer loading, *INMATEH Agricultural Engineering*, vol.45, no.1, pp.87-94, Bucharest / Romania;
- [11] Rogatynska O., Liashuk O., Peleshok T., Liubachivskyi R., (2015), Investigation of the Process of Loose Material Transportation by Means of Inclined Screw Conveyers (Дослідження процесу транспортування сипкого вантажу похилими гвинтовими конвеєрами), *Bulletin of the Ternopil Ivan Puluj National Technical University (Вісник Тернопільського національного технічного університету ім. І.Пулюя)*, Vol.79, pp.137-143, Ternopil / Ukraine.

JUSTIFICATION OF THE CULTIVATOR SWEEP AND STRENGTHENING ELEMENTS ON THE WORKING SURFACE

ОБГРУНТУВАННЯ ПАРАМЕТРІВ КУЛЬТИВАТОРНОЇ ЛАПИ ТА ЕЛЕМЕНТІВ ЗМІЦНЕННЯ ЇЇ НА РОБОЧІЙ ПОВЕРХНІ

Prof. Ph.D. Eng. Kobets A.S., Lect. Ph.D. Eng., Pugach A.M., Prof. Ph.D. Agri.Sci. Kharytonov M.M.
Dnipro State Agrarian and Economics University, Faculty of Agrarian Engineering / Ukraine;
Tel: 0973456227; E-mail: envteam@ukr.net, S.Yefremova st. 25, Dnipro, Ukraine

Keywords: cultivator, sweep, strengthening elements, working surface, geometric model, substantiated parameters

ABSTRACT

A geometric model and substantiated parameters of the surface of the cultivator sweep, equipped with local strengthening elements have been developed. The minimum inclination angle of the guide is 27° , which was taken into account when designing the sweep construction. The method of designing the cultivator sweep surface, including the formation of the guide curve, the construction of the frame surface, the determination of horizontal, frontal, profile sections and the construction of the scan, was developed. The limits for changing the cultivator sweep parameters with local reinforcement elements are determined.

РЕЗЮМЕ

Обґрунтовані геометрична модель і параметри поверхні культиваторної лапи, оснащеної елементами локального зміцнення. Мінімальним кутом нахилу напрямної є кут 27° , котрий слід приймати при розробці конструкції лапи. Розроблено методику проектування поверхні культиваторної лапи, що включає формування направляючої кривої, побудова каркасу поверхні, визначення горизонтальних, фронтальних, профільних перерізів і побудову розгортки. Встановлено наступні межі зміни параметрів культиваторної лапи з локальними елементами зміцнення.

INTRODUCTION

More than 60% of the Ukraine soils are deep, fertile chernozems (black soil) and more than 75% of them is under cultivation (Slowinska-Jurkiewicz et al, 2013). Tillage tools apply direct energy to the black soil in order to obtain some desired effect such as cutting, breaking, inversion or movement of soil (Biswas, H.S., 1993). Seedbed preparation greatly contributes to the overall cost of farm operations, implying that significant savings are possible through optimized design and development of tillage machinery (Shinde et al., 2011). Modern trends in obtaining environmentally safe products require at least partial refusal of chemical weed control (Dewangan and Rajput, 2017; Vasylieva, 2017; Vasylieva and Velychko, 2017). It is recognized that the use of cultivators is the most effective engineering tool for weed control (Hanna et al., 2000; Sullivan, 2003). There are basically three types of cultivators: field cultivators, row crop cultivators, and rotary cultivators (Srivastava et al., 2008). Consequently, nowadays, requirements for the technical level of cultivators are increasing. It is necessary to emphasize that the soil tillage is a process with high – energy consumption (Gheres, 2014). The objective of mechanical manipulation of the soil designed to agricultural production is to create favourable soil conditions and the environment for crop growth by changing bulk density, soil granulometry size distribution and other characteristics (Ivan and Deac, 2007; Rusu et al., 2013).

The analysis of cultivators' recent developments determines the following main areas of their improvement:

- optimization of the machine overall layout;
- creation of fundamentally new working bodies;
- development of combined assemblies;
- increase of working bodies wear resistance;
- increase of the cultivator sweep cutting capacity;
- improvement of stability process in capture depth and width.

The first three areas require fundamental theoretical and practical research (Kiss and Bellow, 1981; Galat and Ingale, 2016). The remaining approaches are related to solving constructive problems. All methods of extending the cultivator sweeps service life can be divided into two groups. The first group is represented by operational methods including the following ones: sweep restoration by pulling; application of various ways of sharpening the blade (Zhang and Kushwaha, 2004; Wang and He, 2002; Saxena, 2009). The second group is represented by constructive methods: the execution of the sweep of the prefabricated structure, solid alloy blade surfacing, application of local blade strengthening (Badegaonkar et al., 2009), change in the geometry of the sweep surface (Hanna et al, 1993; Gheres M. I., 2014). The geometry of the cutting edge or of the work surface contour of a tool for processing soil shows a particular importance in minimizing the necessary energy for the working process (Tutunaru et al., 2014). The most common way to improve the cultivator wear resistance is for a solid alloy to be applied on the blades. This method of increasing wear resistance has been widely used due to the slight change in the design of cultivator sweeps with a significant increase in service life. It was substantiated that reducing the thickness of the coating and enlargement of the crumbling angle increases the sweeps impact strength (Shafi et al., 2007).

The objective of this study is to develop a geometric model and substantiate the parameters of the cultivator sweep surface equipped with elements of local strengthening.

MATERIALS AND METHODS

The research methodology is based on the shape of the profile, depending on: the direction of the elements orientation and the ratio of high-speed push and static vertical pressure. The main tasks of the study were:

- to obtain the blade profile in the predefined configuration;
- to reveal correlation relations between the profile of the formed teeth and the parameters of the local strengthening strips;
- to study the impact of introduced structural changes on the performance quality in comparison with the standard design cultivator sweep.

Taking into account the cultivator sweep specific operation in the point zone, which occurs along the line curve, on the basis of the deployed surface general model, a surface component has been proposed. Surface parameters are shown in Fig. 1.

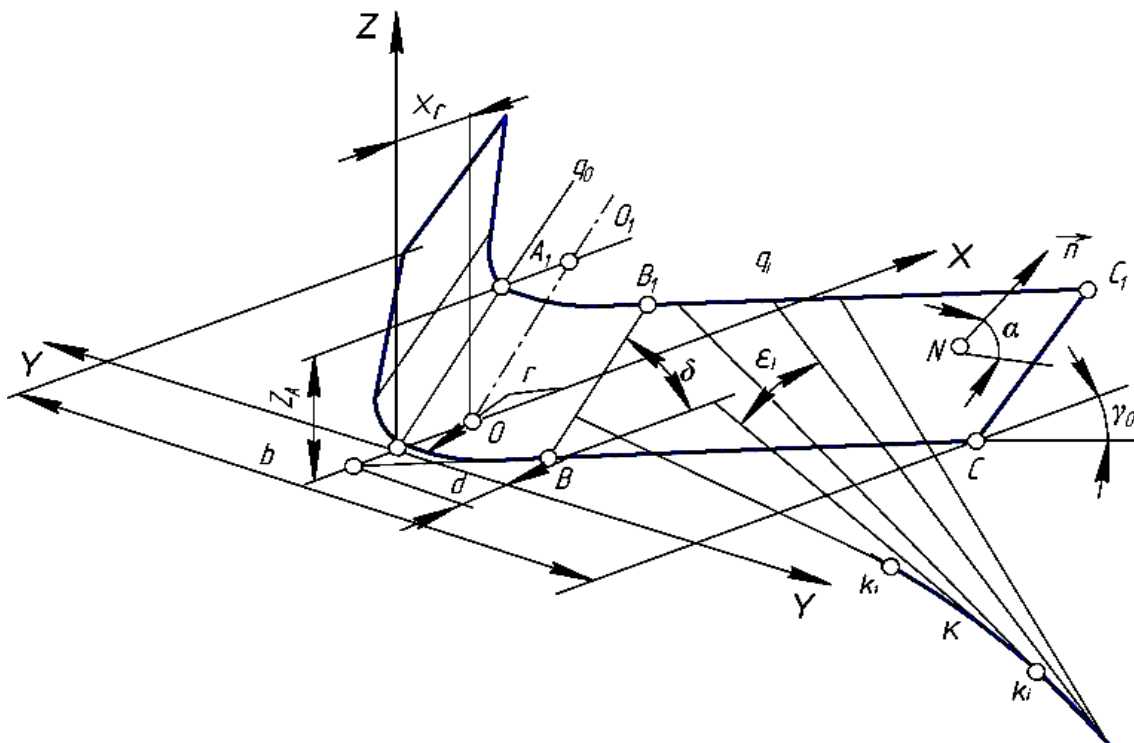


Fig.1 - Scheme of the cultivator sweep surface parameters

(parameter meaning: b - width of sweep grip, mm; Z_a - height of the cultivator sweep surface, mm; k - inclination angle of the generatrix on the projection horizontal plane, mm)

Component of the cultivator sweep surface with local strengthening elements are shown in figure 2.

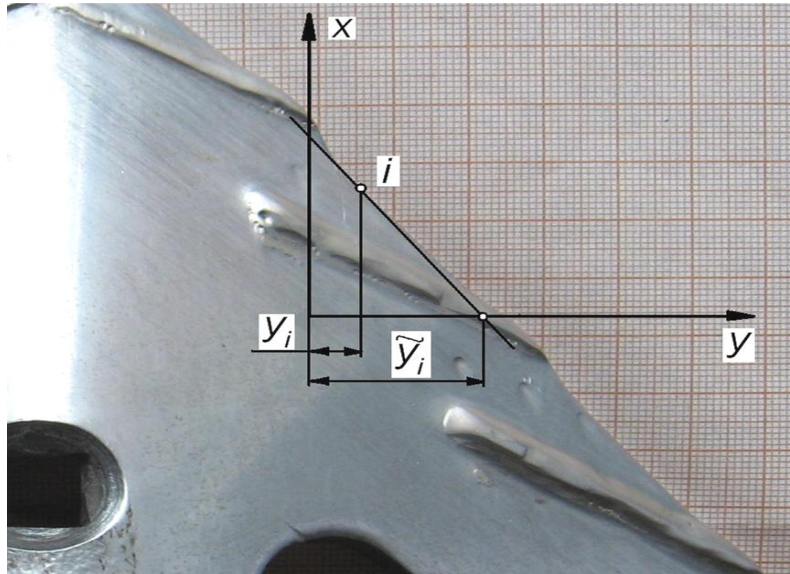


Fig. 2 - Component of the cultivator sweep surface with local strengthening elements

The sweep surface consists of a cylinder surface with an axial line OO_1X and an area BB_1C_1C , which are conjugated to the generatrix of the cylinder BB_1 . The cylinder has a radius r , and the normal \vec{n} area, taken from the point N_o , has a slope to the horizontal area of the projection at an angle α_1 . The angle α_1 is determined by the dependence

$$\alpha_1 = 90^\circ - \alpha \tag{1}$$

where α - the angle of crumbling, degree.

Thus, the scrolling guide surface consists of two lines: the arc of the circle OBB'

$$(x - x_r)^2 + y^2 = r^2 \tag{2}$$

where x_r - the distance from the centre of the circle O_1 to the coordinates; r - the radius of curvature of the sweep point, mm. Straight line BC equation has the form:

$$y = tg\gamma_0 x + d_1 \tag{3}$$

where $d_1 = x_B - y_B \cdot tg\gamma_0$, γ_0 - the angle of guide inclination, degree;

x_B and y_B - coordinates of the point B of a circle transition in a straight line

RESULTS

The coordinates of the transition point B will be determined by differentiating (2) and (3) by x .

$$\frac{dy}{dx} = tg\gamma_0 \quad \text{and} \quad x - r + y \frac{dy}{dx} = 0$$

Substituting in the second equation the expression of the first derivative from the first equation, and taking into account that $x_r = r$, we obtain the first equation for determining the coordinates of the point B

$$x - r + y \cdot tg\gamma_0 = 0 \tag{4}$$

By adding to the equation obtained, the equation of a circle, we obtain a system for determining the coordinates of the point B

$$\left. \begin{aligned} x - r + y \cdot tg \cdot \gamma_0 &= 0 \\ (x - r)^2 + y^2 &= r^2 \end{aligned} \right\} \tag{5}$$

Thus, the guide curve of the cylindrical surface of the sweep point will be the arc of the circle BOB'

$$y = \sqrt{r^2 - (x - r)^2} \quad (6)$$

Generatrix for a cylindrical surface will be a line BB_1 defined by the system:

$$\left. \begin{aligned} z &= tg \delta x + x_\delta, \\ y &= \sqrt{r^2 - (x - r)^2} \end{aligned} \right\} \quad (7)$$

We will write the equation of the sweep wings as an equation of an area passing through three points. Two of them are the point of transition of the guiding point of the sweep $B(x_\delta, y_\delta, z_\delta)$ and the point $C(x_c, y_c, z_c)$ - the extreme point of the sweep blade. These points lie in the horizontal area Oxy . The third point N we define as being arbitrary. The area BB_1C_1C , rotating around the straight line BC , may take any position, which will ultimately be determined by the coordinates of the point N . Thus, fixing two points, B and C , and determining the inclination angle α_1 of the normal to the horizontal projection area, we fix the coordinates x_N, y_N and z_N .

The equation of an area passing through three points B, C, N , looks like a determinant:

$$\begin{vmatrix} x - x_\delta & y - y_\delta & z - z_\delta, \\ x_c - x_\delta & y_c - y_\delta & z_c - z_\delta, \\ x_N - x_\delta & y_N - y_\delta & z_N - z_\delta \end{vmatrix} = 0.$$

Let's expose it to minors and algebraic supplements:

$$\begin{aligned} (x - x_\delta) \begin{vmatrix} y_c - y_\delta & z_c - z_\delta \\ y_N - y_\delta & z_N - z_\delta \end{vmatrix} - (y - y_\delta) \begin{vmatrix} x_c - x_\delta & z_c - z_\delta \\ x_N - x_\delta & z_N - z_\delta \end{vmatrix} + \\ + (z - z_\delta) \begin{vmatrix} x_c - x_\delta & y_c - y_\delta \\ x_N - x_\delta & y_N - y_\delta \end{vmatrix} = 0. \end{aligned}$$

Applying the abbreviated notation for minors, we obtain the area equation from the general form:

$$A_x + B_y + C_z + D = 0 \quad (8)$$

$$\text{where } A = \begin{vmatrix} y_c - y_\delta & z_c - z_\delta \\ y_N - y_\delta & z_N - z_\delta \end{vmatrix}; B = \begin{vmatrix} x_c - x_\delta & z_c - z_\delta \\ x_N - x_\delta & z_N - z_\delta \end{vmatrix}; C = \begin{vmatrix} x_c - x_\delta & y_c - y_\delta \\ x_N - x_\delta & y_N - y_\delta \end{vmatrix}.$$

$$D = B_{y_\delta} - A_{x_\delta} - C_{z_\delta}.$$

where D - the power of the dynamic pressure, N.

The inclination angle of the normal \vec{n} to the bottom of the furrow is $\alpha_1 = 90^\circ - \alpha$,

where α - the inclination angle of the area BB_1C_1C , which is the angle of crumbling.

The angle between two areas α is determined by the dependence

$$\cos \alpha_1 = \frac{AA_2 + BB_2 + CC_2}{\sqrt{(A^2 + B_1^2 + C^2) \cdot (A_2^2 + B_2^2 + C_2^2)}}, \quad (9)$$

where A, B, C - coefficients of the sweep area equation;

A_2, B_2, C_2 - coefficients of another area

Imagine one of the areas as a horizontal area of the furrow bottom. Then, its equation will take the form:

$$C_2 z = 0. \quad (10)$$

Since the area (10) is horizontal, equation (9) will take the form:

$$\cos \alpha_1 = \frac{C}{\sqrt{A^2 + B^2 + C^2}} \quad (11)$$

In order to get rid of the radical in the denominator, we bring the resulting expression to the square:

$$\cos^2 \alpha_1 = \frac{C^2}{A^2 + B^2 + C^2}$$

Taking into account (8), the expression can be written in the form:

$$\cos^2 \alpha_1 = \frac{C^2}{\left| \begin{array}{cc} y_c - y_g & z_c - z_g \\ y_N - y_g & z_N - z_g \end{array} \right|^2 + \left| \begin{array}{cc} x_c - x_g & z_c - z_g \\ x_N - x_g & z_N - z_g \end{array} \right|^2 + C_1^2}$$

Since y_N and x_N can be any positive numbers, then ticking

$$y_c - y_g = R, \quad z_c - z_g = T, \quad y_N - y_g = K, \quad x_c - x_g = E, \quad x_N - x_g = F,$$

it is possible to solve the expression regarding z_N . So, we give the resulting expression in the form:

$$\left| \begin{array}{cc} R & T \\ K & z \end{array} \right|^2 + \left| \begin{array}{cc} E & T \\ F & z \end{array} \right|^2 + C^2 = \frac{C^2}{\cos^2 \alpha},$$

where $z = z_N - z_g$.

Conducting transformations, we come to a quadratic equation:

$$az^2 - 2bz + C^2 \left(1 - \frac{1}{\cos^2 \alpha}\right) = 0 \quad (12)$$

where $a = R^2 + E^2$; $b = T(R \cdot K + E \cdot F)$

As a result of the corresponding transformations, the coordinate z_N will be equal to:

$$z_N = z_g \pm z_{1,2}, \quad (13)$$

where z_1 and z_2 - the roots of the quadratic equation (13).

Forming g , by which the local elements of the strengthening will be located, are determined by the system and simultaneously lie in the area BB_1C_1C . This position imposes to the parameters $k, l, mk, ml + n$, the corresponding connection. To identify the nature of this connection we substitute the equation of the coordinate area y, z , in the expression from the equation of the straight line.

$$A_x + B \cdot (kx + l) + C(mkx + ml + n) + D = 0$$

With known values of the area coefficients A, B, C , which are determined by the coordinates of the points B, C, N we obtain the equation for one of the line parameters as a function of the coordinate x , for example, regarding the angular coefficient k

$$k = -\frac{Ax - B \cdot l - C \cdot m \cdot l - l \cdot n - D}{(B + C \cdot m)}$$

Each generatrix g is tangent to the curve R , which is the edge of the unfolding surface return and has an angle of inclination to the horizontal area \mathcal{E} .

The equation of the return rib is determined by a system of equations:

$$\left. \begin{aligned} x_R &= -\frac{m'l + m'l + n'}{m'k + mk'}, \\ R: y_R &= kx + l, \\ z_R &= mkx + ml + n. \end{aligned} \right\}$$

After removing the dependence of the parameter k from x $k = k(x)$ it is necessary to take the next step. It is essential to determine whether the coordinates of the return ribs fall into an area limited by the wing area BB_1C_1C . If this condition is not met, you need to change one of the functions m , l or n and repeat the calculation. The straight-line guide, which is the initial form of the blade, is located at an angle to the direction γ_i of the cultivator sweep movement. In the process of work, due to the presence of local strengthening elements, some teeth having a profile KE can be formed on the blade, as shown in Fig. 3.

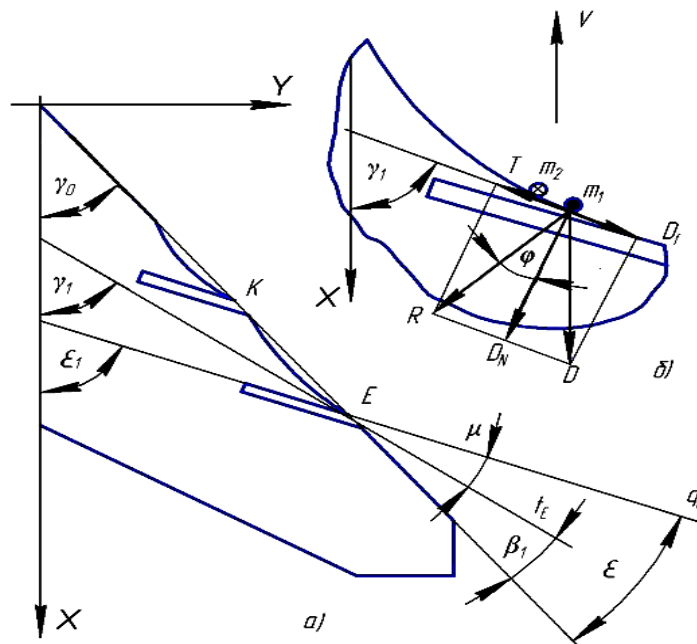


Fig. 3 - Scheme of guide inclination angle substantiation
a - angular parameters of the strengthening elements and the tooth;
b - the forces influencing the particles when moving on the tooth profile

As a result of the sweep operation, the curvature increases, therefore, with the increase in working time, the inclination angle of the tangent γ_1 at the point E will increase and in the limiting sense, it will become equal to the angle of the establishment of the local reinforcement element $\gamma_1 = \epsilon$, where ϵ - inclination angle of the reinforcing element, degree. In accordance with the scheme (fig.3a), we will write the relation of the angles between the tangent to the profile of the blade γ_1 and the establishment of the strengthening element:

$$\mu = \epsilon - \gamma_1 \tag{14}$$

then

$$\gamma_1 = \epsilon - \mu \tag{15}$$

$$\epsilon_2 = \gamma_1 - \mu \tag{16}$$

In its turn, the angle between the generatrix g_E and the guide is equal to:

$$\epsilon_1 = \epsilon - \gamma_o$$

where

$$\gamma_o = \epsilon - \epsilon_1 \tag{17}$$

and taking into account (16)

$$\gamma_o = \gamma_1 - \mu - \varepsilon_1 \quad (18)$$

Laboratory and field experiments have determined that the angle β_1 in the established mode is equal to the difference in the angle of the local reinforcement element installation ε_2 with the inclination angle γ_1 of the tangent t_E at the point E , is equal to:

$$\beta_1 = \gamma_1 - \gamma_o = 7^\circ$$

Therefore, in order to substantiate the inclination angle of the guide γ_o , it is necessary first of all to determine a limiting value γ_1 that ensures movement of plant remains, plant roots or soil on the tooth profile. The justification of the angle γ_o must be divided into two stages: a) initial work of the sweep when the tooth is not formed yet. In this case $\beta_1 = 0$ and $\gamma_1 = \gamma_o$. The angle γ_o is chosen from the condition of weeds cutting, thus $\gamma = 90^\circ - \phi_3$, where ϕ_3 - the angle of weed friction by metal, degree; b) the second stage of the work is that the tooth profile begins to form, the tangent at the point E being at an angle γ_1 different from the inclination angle of the guide to the motion direction. As the tooth profile forms, the angle γ_1 increases and reaches in the established mode, the value equal to the angle ε_2 of the determination of the strengthening elements. To determine the limit value of the angle γ_1 , we take the following assumptions: weed or part of the soil is in a homogeneous moving of soil flow, the mass of the weed or a part of the soil is concentrated at the point.

If you move the sweeps in the soil to any part, whether it is plant residue, plant root or soil aggregate, the following forces will act on the sweep profile: force of a dynamic push, N.

$$D = \rho s v^2 \quad (19)$$

which is decomposed into a tangent component

$$D_t = \rho s v^2 \cos^2 \gamma_1, \quad (20)$$

and normal component:

$$D_N = \rho s v^2 \sin^2 \gamma_1,$$

$$\text{Friction force:} \quad T = f \cdot D_N = f \rho s v^2 \sin^2 \gamma_1, \quad (21)$$

where ρ - soil density, kg / m³; s - cross - section of a particle, m²; v - speed of the working body movement, m / s; f - friction coefficient.

The condition of the particle movement on the tooth profile will look as follows, when the force of the tangent component of the dynamic push is higher than the friction T force $D_t \geq T$, or, having substituted the values of forces, we have:

$$\rho s v^2 \cos^2 \gamma_1 \geq f \rho s v^2 \sin^2 \gamma_1.$$

By reducing on $\rho s v^2$, we get a relation, in which there is only the inclination angle γ_1 and the friction coefficient

$$\cos^2 \gamma_1 \geq f \sin^2 \gamma_1$$

After conversion, we turn to the expression

$$\text{tg} \gamma_1 \leq \sqrt{\frac{1}{f}} \quad (22)$$

Choosing friction coefficient f is quite important. To make this choice, we consider the motion of two particles m_1 and m_2 on the tooth profile KE in accordance with the scheme (fig. 3, b).

Let the particle m_1 moving in front of the particle m_2 be a vegetative remain or the plant root with a friction angle on the steel ϕ_3 and, accordingly, the friction coefficient f_3 . Then the second part m_2 , the proportion of the soil - with the angle of friction on the steel ϕ_1 and, respectively, the friction coefficient f_1 .

There are two possible case studies.

Case 1. The friction angle of the plant remains or the plant root on the metal φ_3 and, accordingly, the friction coefficient f_3 , bigger than the friction angle of the soil on the metal φ_1 .

Then $\varphi_3 > \varphi_1$ and $f_3 > \varphi_1$, which leads to an excess of frictional force of the weed on a steel over the friction force of the ground on the steel. At the same time, the force of the dynamic pressure will influence on the weeds, determined by the formula (20). In this case, the force of the dynamic push D_{t_1} must be higher than the strength of the soil friction on the steel $D_{t_1} \geq T_3$. Therefore, to ensure weed movement, condition (22) should look like:

$$\gamma_1 \leq \arctg\left(\sqrt{\frac{1}{f_{3max}}}\right) \quad (23)$$

where f_{3max} - maximum friction coefficient of weeds on metal.

Case 2. The angle of weed friction on metal φ_3 and, accordingly, the friction coefficient f_3 is smaller than the friction angle of the soil on the metal φ_1 . In this case, $\varphi_3 < \varphi_1$ and $f_3 < \varphi_1$ and, accordingly, the soil friction strength on the steel exceeds the friction force of the plant remain on the steel $T_1 > T_3$. Such values of the friction angles lead to the fact that the force of the dynamic push will perceive the proportion of the soil, while $D_{t_1} \geq T_1$. In this case, the condition that ensures the movement of the weed and the soil, should look like:

$$\gamma_1 \leq \arctg\left(\sqrt{\frac{1}{f_{1max}}}\right) \quad (24)$$

where f_{1max} - the maximum friction coefficient of the soil on the metal.

For a general-purpose cultivator sweep it is necessary to take friction coefficient with highest meaning.

Defining the angle γ_0 by the expression

$$\gamma_0 = \gamma_1 - 7^\circ \quad (25)$$

find the inclination angle of the guide.

The values of the friction angles of the soil on steel are presented in Table. 1

Table 1

The boundaries of changing the friction angle of the soil on the steel

Soil texture	The friction angle of the soil on a steel, φ_1 [degree]	The coefficient of soil friction on a steel, f_1
Sandy	26°30'...35°	0,499...0,7
Light and medium loam	19°30'...26°30'	0,354...0,499
Heavy loam and clay	31°...42°	0,601...0,9

Heavy loam and clay have the largest angle of friction $\varphi_1 = 42^\circ$. The maximum friction angle of the plant roots on the steel is $\varphi_3 = 44^\circ 40'$. The values of the inclination angles are determined based on the data given and in accordance with formula (25).

The results are shown in Table. 2. As it can be seen from Table 2, the minimum inclination angle of the guide is 27° , which was taken into account when designing the sweep construction.

The experimental samples of the sweeps installed KPS-4, which were aggregated with a tractor DT-75M, are shown in fig. 4.

Table 2

The variation range of the inclination angle of the generatrix depending on the soil texture

Soil texture	The friction angle of the soil on a steel, φ_1 [degree]	Maximum friction angle of crop residues on steel, φ_3 [degree]	Inclination angle of generatrix γ_0 , [degree]
Sandy	26°30' ... 35°	37°	27°
Light and medium loam	19°30' ... 26°30'	37°	27°
Heavy loam and clay	31° ... 42°	37°	31°



Fig. 4 - Experimental samples of sweeps

Conditions of conducting experiments: speed up to 2.3 m / s, soil – ordinary molisol, soil texture – medium loam, relief - smooth, microrelief - levelled, background on the field - remains of corn stalks with length from 4 ... 7 cm to 24 cm, in quantities from 1-2 to 3-6 p / m². The soil moisture is 19.1% and the hardness of the soil is 529 kPa.

CONCLUSIONS

1. A geometric model and substantiated parameters of the surface of the cultivator sweep, equipped with elements of local strengthening, have been developed.
2. The method of designing the surface of the cultivator sweep, including the formation of the guide curve, the construction of the frame surface, the determination of horizontal, frontal, profile sections and the construction of the scan, has been developed.
3. The following limits for changing the parameters of the cultivator sweep with local reinforcement elements are determined: the width of the capture $b = 230, 270, 330$ mm; radius of sweep point $r = 20...40$ mm; angle of deflection of wings $2\gamma = 70...73^\circ$; angle of deflection $\alpha = 27...30^\circ$; angle of application of reinforcement elements to the blade $\varepsilon = 20 \dots 30^\circ$; step of reinforcing elements along the blade $h_e = 30...40$ mm; reinforcement elements length $l_e = 40...50$ mm; reinforcement elements overlap $\Delta_a = 10...15$ mm; reinforcement elements width $S_e = 3...5$ mm; reinforcement elements thickness $s = 1...2$ mm.

ACKNOWLEDGEMENT

The work has been funded by the Ukrainian Ministry of Education and Science.

REFERENCES

- [1] Badegaonkar U.R., Dixit G. Pathak K.K., (2010), An experimental investigation of cultivator shank shape on draft requirement. *Archives of Applied Science Research*, 2 (6) pp.246-255;
- [2] Biswas, H.S., (1993), Performance Evaluation and optimization of straight blades for shallow tillage and weeding in black soils, *Agric. Mech. in Asia, Africa and Latin America*, 24(4) pp.19-22;
- [3] Dewangan A., Singh Rajput N., (2017), Stress Analysis of Cultivator: A Survey Approach. Crop cultivation. *International Research Journal of Engineering and Technology*. vol.04 Issue: 01. pp.692-696;
- [4] Galat U.N., Ingale A.N., (2016), Failure Investigation & Analysis of Agricultural 9 Tyne Cultivator Used In Various Soil Condition. *International Journal on Recent and Innovation Trends in Computing and Communication*. Volume: 4 Issue: 1, pp. 173–179;
- [5] Gheres M.I., (2014), Mathematical model for studying the influence of tillage tool geometry on energy consumption. *INMATEH – Agricultural Engineering*, vol. 42, No.1, pp.5-12;
- [6] Hanna H.M., Hartzler R.G., Erbach D. C., (2000), High-speed Cultivation and Banding for Weed Management in No-Tillage Corn, *Applied Engineering in Agriculture*, vol.16, pp.359-365;
- [7] Hanna H. M., Marley S. J., Erbach D. C., Melvin S. W., (1993), Change in soil microtopography by tillage with a sweep. *Agricultural and Biosystems Engineering*. vol. 36(2), pp.301-307;
- [8] Ivan I., Deac T., (2007), Analysis of the possibilities to increase agricultural yields in Romania, Acta Technica Napocensis Series: *Applied Mathematics and Mechanics*, vol. V, Nr. 50, pp.457-460;
- [9] Kiss G.C., Bellow D.G., (1981), An analysis of forces on cultivator sweeps and spikes. *Can. Agric. Eng.* 23. pp.77-83;
- [10] Rusu T., Păcurar I., Dîrja M., Păcurar H.M., Oroian I., Cosma S.A., Ghereş M., (2013). Effects of soil tillage systems on soil, humus and water conservation properties, *Agricultural science*, Nr.4/2013, pp.35-40;
- [11] Saxena, A.C., (2003), Status report on abrasive wear of rotavator blades” CIAE, *Bhopal*, pp.1-9;
- [12] Shafi A., Sial J., Iqbal M., Hussain K.A., (2007), Development and testing of sweep shovels in field. *Pak. Journal of Agricultural Science*, vol. 44(4), pp.684-688;
- [13] Shinde G.U., Kjaale S.R., Potekar J.M., Nadre R.G., (2011), Computer Aided Design Optimization of Flexible Cultivator. *Journal of Agricultural Machinery' Science*. 7 (1), pp.77-83;
- [14] Slowinska-Jurkiewicz A., Bryk M., Medvedev V.V., (2013), Long-term organic fertilization effect on chernozem structure. *Int. Agrophys.*, 2013, 27, pp.81-87 DOI: 10.2478/v10247-012-0071-1;
- [15] Srivastava A. K., Goering C. E., Rohrbach R. P., Buckmaster D.R., (2006), Soil tillage. Chapter 8, *Engineering Principles of Agricultural Machines*, 2nd ed., St. Joseph, Michigan: ASABE. Copyright American Society of Agricultural and Biological Engineers, pp.169-230;
- [16] Sullivan P., (2003), Principles of Sustainable Weed Management for Croplands. *ATTRA Publication #IP039*, available at: <http://attra.ncat.org/attraa-pub/PDF/weed.pdf> ;
- [17] Tutunaru L.F., Nagy E.M., Coța C., (2014), Influence of tillage tools cutting edge wear over technical and economic indicators. *INMATEH – Agricultural Engineering*, vol.44, No.3/ pp.5-12;
- [18] Vasylieva N., (2017), Economic aspects of food security in Ukrainian meat and milk clusters, *Agris On-line Papers in Economics and Informatics*, vol.9, No.3, pp.81-92, ISSN 1804-1930. DOI: 10.7160/aol.2017.090308;
- [19] Vasylieva N., Velychko O., (2017), Development of the controlling system in the management of dairy clusters, *Eastern-European Journal of Enterprise Technologies*, vol. 4, No. 3 (88): Control Processes, pp. 20-26. ISSN 1729-3774 (Print), 1729-4061 (Online). DOI: 10.15587/1729-4061.2017.108591;
- [20] Wang X.M., He, X.L., (2002), Effect of Boron addition on structure and properties of low carbon bainitic steels, *ISIJ International*, 42, pp. 538-546;
- [21] Zhang J., Kushwaha R.L., (2004), Wear and draft of cultivator sweeps with hardened edges. *Canadian Agricultural Engineering*, 37 (1), pp.41- 47.

WRITING NORMS

Article Types

Three types of manuscripts may be submitted:

1. **Regular articles:** These should describe new and carefully confirmed findings, and experimental procedures should be given in sufficient detail for others to verify the work. The length of a full paper should be the minimum required to describe and interpret the work clearly (max.10 pages, even number);
2. **Short Communications:** A Short Communication is suitable for recording the results of complete small investigations or giving details of new models or hypotheses, innovative methods, techniques or apparatus. The style of main sections has not necessarily to be in accordance with that of full-length papers (max. 6 pages, even number);
3. **Reviews:** Submissions of reviews and perspectives covering topics of current interest are welcome and encouraged (max.10 pages, even number).

Manuscripts should be written in English (American or British usage is accepted, but not a mixture of these) and submitted **electronically** at the following e-mail addresses: ***inmatehjournal@gmail.com***

Please be sure to include your full affiliation and e-mail address (see Sample manuscript)

The authors are responsible for the accuracy of the whole paper and references.

There are allowed 2 papers by each first author.

The text layout should be in single-column format. To avoid unnecessary errors it is strongly advised to use the “spell-check” and “grammar check” functions of your word processor.

Review Process

All manuscripts are reviewed by 2 members of the Scientifically Review Office. Decisions will be made as rapidly as possible and the journal strives to return reviewers' comments to authors in approx.3 weeks.

The editorial board will re-review manuscripts that are accepted pending revision.

NOTE:

Submission of a manuscript implies: that the work described has not been published before (excepting as an abstract or as part of a published lecture or thesis) that it is not under consideration for publication elsewhere.

1. REGULAR ARTICLES

- Manuscripts should be concise, in **1.15 line spacing**, and should have 2 cm all over margins. The font should be **Arial 10 pt.** Ensure that each new paragraph is clearly indicated, using **TAB at 1 cm.**
- Title will be **Arial 12 pt.** and explicit figures will be **Arial 9 pt.**
- Text will be written in English.
- Chapters' titles are written by **Arial 10 pt, Bold, Uppercase** (e.g. **INTRODUCTION, MATERIAL AND METHODS**), between chapters is left a space for 10 pt. At the beginning of each paragraph, TAB of 1 cm.
- The paper body will be written in **Arial 10 pt., Justify alignment.**

TITLE **Arial 12 pt., Uppercase, Bold, Center** (in English language) and **Bold Italic** (in native language).

Should be a brief phrase describing the contents of the paper. Avoid long titles; a running title of no more than 100 characters is encouraged (without spaces).

AUTHORS **ARIAL 9, Bold, Centre alignment**

Under the paper's title, after a space (enter) 9 pt., write **authors' names** and **affiliations (Arial 8 pt.-Regular)**

When the paper has more than one author, their name will be followed by a mark (Arabic numeral) as superscript if their affiliation is different. **Less than 6 authors.**

Corresponding author's name (next row), **(Arial 8 pt.)**. Should be added also: phone, fax and e-mail information, for the paper corresponding author (**font: 8 pt., Italic**).

KEYWORDS **(In English)** about 4 to 7 words that will provide indexing references should be listed (**title: Arial 10pt, bold italic, text Arial 10 pt., italic**).

A list of non-standard **Abbreviations** should be added. In general, non-standard abbreviations should be used only when the full term is very long and used often. Each abbreviation should be spelled out and introduced in parentheses the first time it is used in the text. Standard abbreviations (such as ATP and DNA) need not to be defined.

ABSTRACT (*in English and Native language, Arial 10 pt.*), the title *bold*; the text of abstract: *italic*) should be informative and completely self-explanatory, briefly present the topic, state the scope of the experiments, indicate significant data, and point out major findings and conclusions. The Abstract should be max.250 words. Complete sentences, active verbs, and the third person should be used, and the abstract should be written in the past tense. Standard nomenclature should be used and abbreviations should be avoided. No literature should be cited.

INTRODUCTION (*Arial 10 pt.*) should provide a clear statement of the problem, the relevant literature on the subject, and the proposed approach or solution. It should be understandable to colleagues from a broad range of scientific subjects. We should refer to the current stage of researches performed in the field of the paper to be published, by quoting up-to-date specialty studies, preferably published after 2006, excepting certain referential specialty books/studies, especially papers issued in magazines/journals/conferences/ISI quoted symposia or in other international data bases, which are well known and available.

MATERIALS AND METHODS (*Arial 10 pt.*) should be complete enough to allow experiments to be reproduced. However, only truly new procedures should be described in detail; previously published procedures should be cited, and important modifications of published procedures should be mentioned briefly. Methods in general use need not be described in detail.

RESULTS (*Arial 10 pt.*) should be clarity presented. The results should be written in the past tense when describing findings in the authors' experiments. Results should be explained, but largely, without referring to the literature. Discussion, speculation and detailed interpretation of data should not be included in the Results, but should be put into the Conclusions section.

CONCLUSIONS (*Arial 10 pt.*) The main conclusions drawn from results should be presented in a short Conclusions section. Do not include citations in this section.

Formulae, symbols and abbreviations: Formulae will be typeset in Italics (preferable with the Equation Editor of Microsoft Office 2003) and should be written or marked as such in the manuscript, unless they require a different styling. They should be referred to in the text as Equation (4) or e.g. (4). The formulae should be numbered on the right side, between brackets (*Arial 10 pt.*):

$$P = F \cdot v \quad (1)$$

Terms of the equation and the unit measure should be explained, e.g.

P is the power, [W];

F – force, [N];

v – speed, [m/s]

SI units must be used throughout.

Tables should be self-explanatory without reference to the text. The details of the methods used in the experiments should preferably be described in the legend instead of in the text. [The same data should not be presented both in table and graph form or repeated in the text.](#)

Table's title will be typed *Arial 9 pt, Bold, Centered*

In the table, each row will be written Arial 9 pt, single-spaced throughout, including headings and footnotes.

The table should be numbered on the right side, between brackets (*Arial 10 pt*):

Figure (*Arial 9 pt., Bold, Center*) should be typed in numerical order (Arabic numerals). Graphics should be high resolution (e.g.JPEG).Figure number is followed by what represent the figure or graph e.g.:

Fig.1 – Test stand

Legend: *Arial 8 pt, Italic, Center, e.g.*

1 - plansifter compartments; 2- break rolls; 3 – semolina machines; 4 – reduction rolls; 5 – flour

ACKNOWLEDGMENTS (*Arial 10 pt.*) of people, grants, funds etc should be brief (*if necessarily*).

REFERENCES (*Arial 10 pt.*)

(In alphabetical order, in English and in the original publication language).

Minimum 10 references, last 10 years, minimum 3 references from the last 2 years

It can be used "References" tool from the *Word Editor*.

References should be cited in the text in brackets as in the following examples:

(Babiciu P., Scripnic V., 2000)

All references must be provided in English with a specification of original language in round brackets.

Authors are fully responsible for the accuracy of the references.

References should be alphabetically, with complete details, as follows:

Examples:

Books: Names and initials of authors, year (between brackets), title of the book (Italic), volume number, publisher, place, pages number or chapter, ISSN/ISBN:

[1] Vlăduț V., (2009), *Study of threshing process in axial flow apparatus (Studiul procesului de treier la aparatele cu flux axial)*, vol.1, ISSN/ISBN, "Terra Nostra" Publishing House, Iași/Romania;

Journal Article: Names and initials of authors, year (between brackets), full title of the paper, full name of the journal (Italic), volume number, publisher, place, ISSN, page numbers:

[1] Lizhi Wu, Yan Di., (2005), *Demonstrational study on the land consolidation and rehabilitation (LCR) project of saline-alkali soil in arid areas: a case study of Lubotan LCR project in Pucheng County, Shaanxi Province (干旱区盐碱化土地整理工程实证研究-以陕西蒲城县卤泊滩土地整理项目为例)*, *Transactions of the Chinese Society of Agricultural Engineering*, vol.21, no.1, pp.179-182, Madison/Wisconsin;

[2] Leonov I.P., (1973), *Basic machine theory for tobacco stringing. Post-harvest care of tobacco and rustic tobacco (Основы теории машин для закрепления табака на шнуры. Послеуборочная обработка табака и махорки)*, *Collection of scientific articles (сборник научно-исследовательских работ)*, pp.37-45;

Conference or Symposium: Names and initials of authors, year (between brackets), full title of the paper (Regular), full name of the conference/symposium (Italic), volume number, publisher, place, ISSN, page numbers

[1] Bungescu S., Stahli W., Biriș S., Vlăduț V., Imbrea F., Petroman C., (2009), *Cosmos program used for the strength calculus of the nozzles from the sprayers (Program Cosmos folosit pentru calculul de rezistență la zgomot al aparatelor de distribuție)*, *Proceedings of the 35 International Symposium on Agricultural Engineering "Actual Tasks on Agricultural Engineering"*, pp.177-184, Opatija / Croatia;

Dissertation / Thesis: Names and initials of authors, year (between brackets), full name of the thesis (Italic), specification (PhD Thesis, MSc Thesis), institution, place;

[1] Popa L., (2004), *Research on the influence of structural and functional parameters of the braking system on the braking performance of agricultural trailers (Cercetări privind influența caracteristicilor constructive și funcționale ale sistemelor de frânare asupra performanțelor de frânare ale remorcilor agricole)*, PhD dissertation, Transylvania University of Brașov, Brașov / Romania.

Patents: Names and initials of authors, year (between brackets), patent title (Italic), patent number, country:

[1] Grant P., (1989), *Device for Elementary Analyses*. Patent, No.123456, USA.

Legal regulations and laws, organizations: Abbreviated name, year (between brackets), full name of the referred text, document title/type (Italic), author, place:

[1] *** EC Directive, (2000), *Directive 2000/76/EC of the European Parliament and of the Council of 4 December 2000, on the incineration of waste, Annex V, Official Journal of the European Communities, L332/91, 28.12.2000, Brussels.*

Web references: The full URL should be given in text as a citation, if no other data are known. If the authors, year, and title of the documents are known and the reference is taken from a website, the URL address has to be mentioned after these data:

The title of the book, journal and conference must be written in Italic, the title of the article, chapter of the book, must be written Regular.

Citation in text

Please ensure that every reference cited in the text is also present in the reference list (and vice versa). Do not cite references in the abstract and conclusions. Unpublished results, personal communications as well as URL addresses are not recommended in the references list.

Making personal quotations (one, at most) should not be allowed, unless the paper proposed to be published is a sequel of the cited paper. Articles in preparation or articles submitted for publication, unpublished, personal communications etc. should not be included in the references list.

Citations style

Text: All citations in the text may be made directly (or parenthetically) and should refer to:

- **single author:** the author's name (without initials, unless there is ambiguity) and the year of publication:

"as previously demonstrated (Brown, 2010)".

- **two authors:** both authors' names and the year of publication: (Adam and Brown, 2008; Smith and Hansel, 2006; Stern and Lars, 2009)

- **three or more authors**: first author's name followed by "et al." and the year of publication: "As has recently been shown (*Werner et al., 2005; Kramer et al., 2000*) have recently shown"

Citations of groups of references should be listed first alphabetically, then chronologically.

Units, Abbreviations, Acronyms

- Units should be metric, generally SI, and expressed in standard abbreviated form.
- Acronyms may be acceptable, but must be defined at first usage.



Edited by: INMA Bucharest

6 Ion Ionescu de la Brad Blvd., sect. 1, Bucharest, ROMANIA

Tel: +4021.269.32.60; Fax: +4021.269.32.73

<http://www.inmateh.eu>

e-mail: inmatehjournal@gmail.com